Glasgow Theses Service
http://theses.gla.ac.uk/
theses@gla.ac.uk

AN ANALYTICAL AND EXPERIMENTAL STUDY
OF REINFORCED EARTH RETAINING WALLS

by

M. A. OSMAN, B.Sc.

A thesis submitted for the degree of
Doctor of Philosophy

Department of Civil Engineering
University of Glasgow

March, 1977

PAGE NUMBERS ARE CUT

OFF IN THE ORIGINAL

ABBREVIATED TABLE OF CONTENTS

TABLE OF CONTENTS

ACKNOWLEDGEMENTS

SUMMARY

This thesis is concerned with a theoretical and experimental study of rectangular reinforced earth retaining walls built on a rigid foundation.

Previous design methods based on conventional earth pressure theory, the theory of elasticity and the finite element method have been reviewed along with the results of laboratory and field tests made by other investigators.

A new Energy theory has been proposed for reinforced earth wall design in an attempt to overcome the disadvantages of previous approaches based on Rankine theory. This new theory takes account of a non-linear tension distribution over the length of the reinforcing ties, the deflected shape of the wall and of the effect of tie length on the tension developed. Simplified assumptions were made to obtain expressions for the tie tension and the factor of safety against pull out failure.

Apparatus was constructed to enable model walls to be tested. Free field strain coils were developed to measure soil strains and the horizontal deflections of the front face of the walls. Strain gauges and pressure cells were calibrated for the measurement of tie tensions and the vertical soil stresses.

The model tests conducted were:

(a) Tests to failure with the main observations being made on conditions at failure. In some of these walls, the tie tensions were also obtained.

(b) Instrumented walls not tested to failure. In these tests the stresses and deformations of the ties and the soil were observed during wall construction and after completion of the walls.

The tests to failure were conducted on walls failing by tie breaking or tie pull out modes of failure, and using

perspex panel skin elements.   In the tie breaking tests,
aluminium foil ties were used.   The results from these
tests were compared with theoretical predictions and previous
relevant tie breaking failure tests.

The conventional design approaches based on the Rankine,
Meyerhof and the Trapezoidal methods were found to predict
practically the same critical wall heights but were only
about 28 per cent to 39 per cent of the experimental results.
Various expressions designated T.L.L.A., T.L.L.D., T.P.P.D.,
LO.L.A., and LO.L.D. were obtained from the Energy theory,
depending on different assumptions.   Each of these *energy*
expressions predicted a range of critical heights which were
slightly lower than, ~~but closer to~~ the experimental results,
than the values predicted by the existing theories.   The
maximum discrepancy between the experimental results and the
Energy theories predictions was about 37 per cent of the
observed values.

The tie breaking test results were found to be consistent
with other similar model tests conducted in France[7] and
in the U.S.A.[45]

The pull out tests were conducted using either aluminium
foil ties or perspex ties.   The walls built with the perspex
ties were instrumented to measure the tie tensions.   The
results from these tests indicated that the maximum tie tension
decreased with increasing tie length.   The existing theories
were found to predict different patterns and magnitudes from
the observed values while the Energy theory (T.L.L.D.) and
(T.L.P.D.) reasonably took account of the effect of tie length
on the maximum tie tension.

On comparing the observed adherence lengths and the
corresponding predicted adherence lengths, the theoretical
values were found to be larger than the experimental results,
hence further tests were undertaken to check the internal
wall stability on a non-ultimate strength concept.

Thirty-five walls were built to a maximum height of 500mm.
The walls were instrumented to obtain:

(i)   The tie tensions at various wall levels.

(ii) The wall deflections.

(iii)The strains in the soil.

(iv) The stresses in the soil.

From the results of these tests the following relation-
ships were   established:

(1)   The tie tension distribution over the tie length
and at various levels in the walls.

(2)   The maximum tension envelopes.

(3)   The tension versus fill height curves.

(4)   The horizontal strains over vertical and horizontal
sections in the wall.

(5)   The wall deflection curves.

(6)   The vertical stress variation over a horizontal
section in the wall.

The comparison between the observed tensions and the
theoretical predictions revealed closer agreement with the
Energy theory (LO.L.A.) than with the existing theories.

The experimental safety factors against tie pull out
failure were evaluated by assuming either the total tie
length to be effective, or the tie length beyond the maximum
tension position effective, and using either the maximum or
average tie tensions.   Experimental safety factors against
pull out were calculated from the slope of the tie tension
distribution curves, using a computer programme developed
for this purpose.   The experimental safety factor against
tie pull out was found to be a minimum at the top of the
wall and increased towards the bottom of the wall.
Comparison with the existing and the Energy theories
indicated that none of the existing theories gave a general

agreement with the observed results.   The Energy theory
(LO.L.A.) appeared to follow the general pattern of the
observed points and agreement in magnitude was reached in
some cases.

Test results reported[29] on a full scale wall built
at Grànton, were analysed.   This was the first example of
the use of reinforced earth in the U.K. ·

It was found that the pattern of the tie tension
distribution curves was, generally similar to the tension
distributions observed in the model.   In addition, it was
found that the full scale wall behaviour was affected by
the construction procedure, especially the compaction
operation.   Analysis of tie tensions showed that compaction
effects on tie tensions were more pronounced at low ($\doteq$ 1.5m)
fill heights above tie level.   A simplified theoretical
model gave a similar trend to the observed results and
indicated that probably compaction did influence the tie
tension.

The observed tie tensions were noted as generally higher
than the theoretical predictions, especially when a coefficient
of earth pressure corresponding to the fill condition as
placed was used.   The Energy theory (LO.L.A.) was found to
give a pattern of the maximum tie tension distribution with
wall height, which was similar to the general pattern of the
observed results.

The completed full scale wall had an adequate safety
factor against pull out and tie breaking failures.   Analysis
also showed that a critical stage may occur during the wall
construction, since at low fill heights, above the tie level,
the safety factor against pull out tended to be less than one.
This was shown to be mainly due to compaction stresses.

An established plane strain finite element programme was
used to analyse both the model and the full scale walls.
The analysis was mainly intended to investigate the
magnitude and patterns of the various stresses and strains

acting in the soil, and the tie tension development. The programme uses a non-linear, stress dependent model for the soil behaviour and takes into account the incremental wall construction. It was found that the results of the finite element analysis were sensitive to the soil properties and other simplifying assumptions adopted in the programme.

Comparison between the finite element solution and the model wall behaviour showed similarities in pattern between the predicted and the observed wall deflections although they did not correspond completely with each other in magnitude. The predicted tie tensions were generally greater than the observed tie tensions.

In the knowledge that the actual full scale wall behaviour was affected by the construction procedure, the finite element analysis showed that the stresses and deformations of a full scale wall can also be affected by foundations and skin element conditions.

It was finally recommended that the Energy theory be extended to take account of the skin element and foundation conditions and the compaction stresses.

NOTATION

a,b,c	General constants
A	Factor for comparison between existing theories
A_i	Factor for comparison between Energy theories
A_r	Tie X-sectional area
b	Tie width
B	Factor for comparison between critical wall height expressions
c	Unit cohesion of soil
C_i	Distribution factor
C_1 to C_5	Coefficients in the Energy theories (Total equilibrium)
d	Depth of uniformly distributed surcharge load
D_1 to D_5	Coefficient in the Energy theories (Local equilibrium)
Dr	Relative density
e	Eccentricity
E	Modulus of elasticity (Young's modulus)
E_r	Modulus of elasticity of tie material
E^{so}	Modulus of elasticity of soil
E_t	Tangent modulus of elasticity
E_i	Initial tangent modulus of elasticity
E_q	Equivalent modulus of elasticity of reinforced earth material
f	Tie/soil coefficient of friction
Fr	Total tie resistance against pull out
h	Fill height above tie level
H	Total fill height above base of a wall
H_c	Critical height of a wall
ΔH	Vertical tie spacing
i	Subscript denoting the number of a reinforced earth layer from top of the wall
K	Ratio of horizontal to vertical stress
K_a	Coefficient of active earth pressure
K_o	Coefficient of at rest earth pressure
L, L_a	Tie length & adherence length
ΔL	Increment of tie length
M	Moment of earth pressure about the toe of the wall.

n	Total number of reinforced layers in a wall
N	Number of ties from top of the wall to the level where the first tie crosses the theoretical Coulomb plane
P	Earth pressure force
P_r	Total resisting force
P_s	Total sliding force
P_w	Wheel load
p(Z)	Earth pressure at depth Z below surface of the wall
R	Reaction
RM	Resisting moment
R_t	Tensile strength of tie material
S	Horizontal tie spacing
SF	Factor of safety
t	Thickness of tie
T	Tie tension
T_{max}	Maximum tie tension over wall height H
T_m	Maximum tension along a tie of length L.
ΣT	Total tension in ties over wall height H.
U_{ext}	Total external work
U_1	Strain energy stored in a tie
ΔU_{ext}	Increment of external work
W	Weight of soil
x,y,z, X,Y,Z	Cartesian coordinates
y(z)	Deflected shape of wall
$\propto$	Banerjee's empirical coefficient
$\hat{\propto}, \hat{\beta}$	Coefficients used to define the shape of the tie tension distribution over tie length curves
θ, β	Angles of inclination of the Coulomb failure plane with the horizontal and vertical respectively
ϵ_1, ϵ_v	Axial and volumetric soil strains respectively
ϵ_x, ϵ_y	Horizontal strain and vertical soil strains respectively
σ_{y1}	Yield stress of tie material
σ_x, σ_y	Horizontal and vertical soil stresses respectively
σ_1, σ_3	Major and minor principal stresses

τ_{xy}, γ_{xy}	Shear stress and strain respectively
δ	Wall deflection
ϕ	Angle of internal friction of soil
γ	Density of soil
χ	Non-dimensional tension factor
χ_o	Non-dimensional factor in Banerjee's equation
ν	Poisson's ratio

CHAPTER ONE

INTRODUCTION

1.1 General Introduction

A rational method of reinforced earth design has recently been introduced by H. Vidal, a French architect and engineer. However, the soil reinforcement technique itself is probably an old practice. Lee et al[45] and Chang et al[15] described some forms of earth reinforcements occurring naturally or used by man. The stabilization of soil by plants' roots is well known. Man, throughout his history, has used various forms of soil reinforcement, e.g. in the construction of roads on swampy areas using tree trunks and branches, in the construction of low dykes from mud and sticks, the stabilizing of river bank soil by fagotting and in other applications.

Reinforced earth can be defined as an association of earth with reinforcements whereby the frictional forces between the two materials are mobilized.

The term "earth" applies generally to all soil types. In practice, only soils which are predominantly granular are used. The reinforcements have to be of high tensile strength, corrosion resistant and offering a satisfactory angle of friction on soil.

It was shown by Vidal[77,79] that reinforced earth could be used for the construction of different works such as quay walls, raft foundations, swimming pools, arches and other structures varying in shape and function. This reflects the flexibility of reinforced earth, although at present reinforced earth is used essentially in the construction of retaining walls, bridge abutments and earth embankments.

A retaining wall with rectangular cross section, Fig (1.1) is constructed by alternating layers of compacted granular soil and metal ties which are distributed at convenient horizontal and vertical intervals. The ties
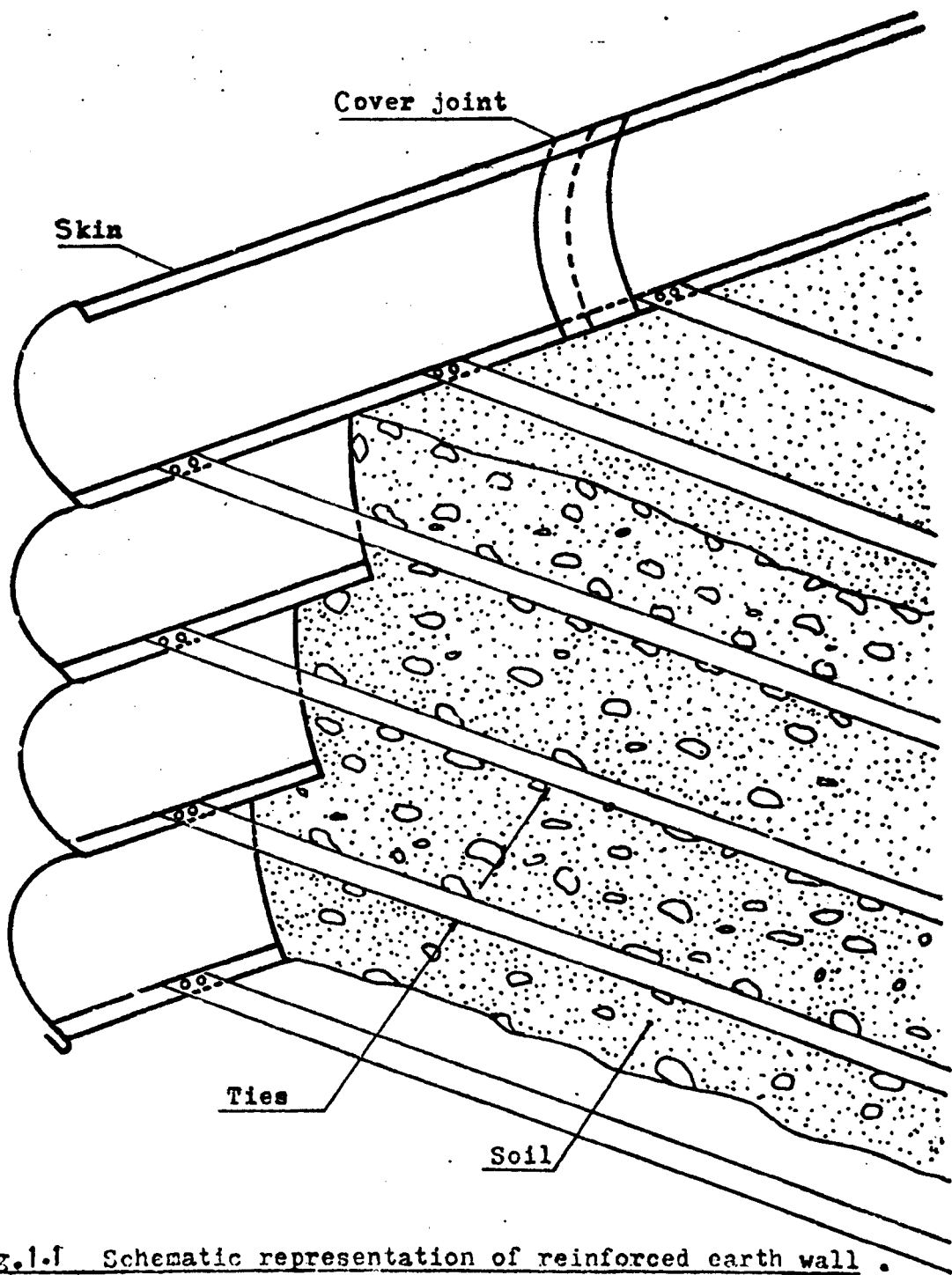
Fig.1.1 Schematic representation of reinforced earth wall .

are attached at one end to a thin membrane known as the skin which provides stability of the soil in direct contact with it and also maintains the life of the structure. Two types of skin elements are used in practice:

(1) Semi-elliptical skin elements of non-corrosive metal (Fig 1.2.a).

(2) Concrete panel skin elements (Fig 1.2.b).

The use of reinforced earth material in retaining structures is known to possess certain advantages which make it preferable in most cases to conventional retaining walls. These advantages were described by Schlosser and Vidal, [67] Barclay, [6] Darbin [23] and Gedney et al. [30] The main advantages are:

(1) Economy in the total cost of the job.
A cost analysis of four types of retaining walls is shown in Fig (1.3) and demonstrates that reinforced earth is the cheapest.

(2) The material can withstand large differential settlements, and has been used at sites with poor foundations and also in highway construction on steep slopes in mountainous areas.

(3) The material is suitable for the construction of temporary retaining structures.

The external and internal stability of reinforced earth walls has to be checked when the design of these walls is considered. The external stability of this type of retaining wall requires checking against:

(i) Overturning of the wall as a solid mass.

(ii) Failure of the wall by horizontal shearing along the base or at any horizontal plane, parallel to the direction of the ties.

(iii) Foundation failure.

Thickness ÷ 1.5-4.0 mm

Tie

Soil

250-330 mm
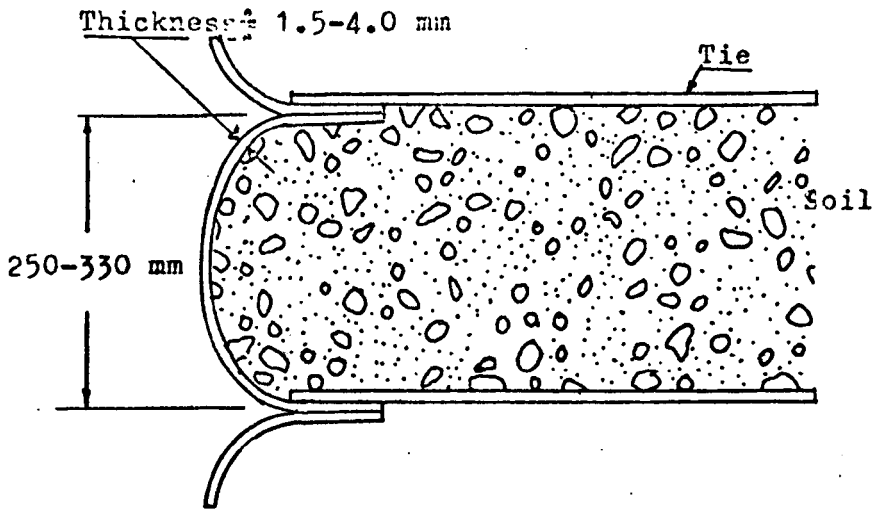
Fig 1.2.a   Elliptical metal skin element.

375

1335

730

1505

25

180

190

100

750
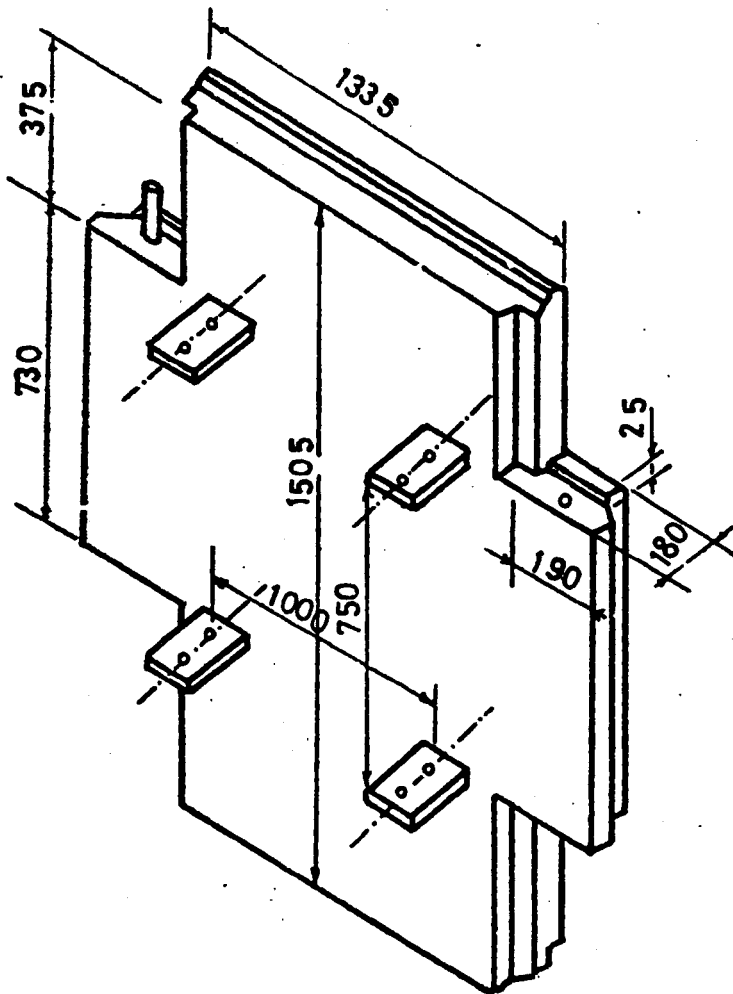
Fig.1.2.b Concrete panel skin element(dimensions in mm).

Fig.(1.2) Types of skin elements
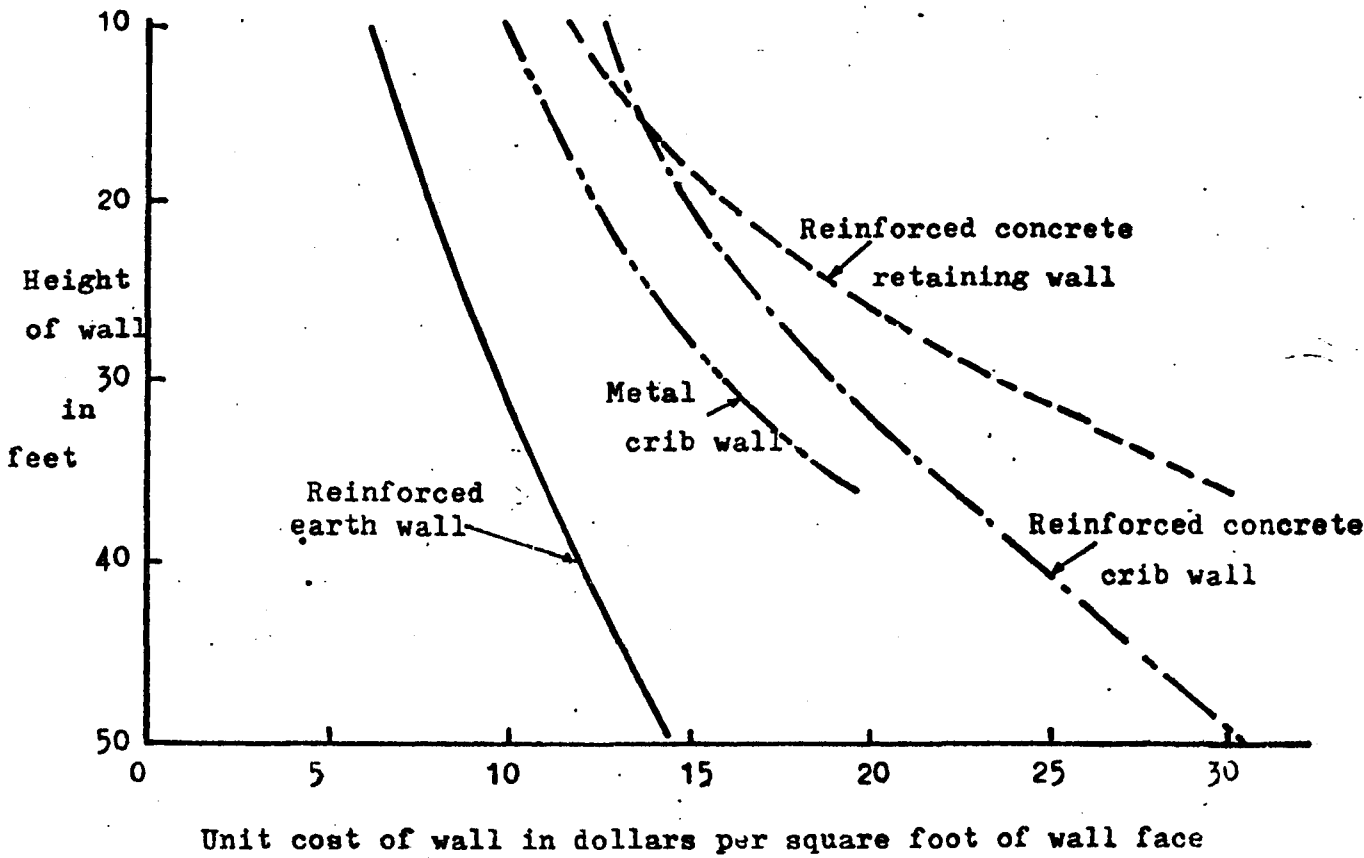
Fig.4.3 Cost comparison between four types of walls

(After Chang[14]   )

These aspects of reinforced earth wall design can be dealt with, within the context of conventional soil mechanics approaches.

(iv) An external failure can also occur due to tearing or buckling of the skin elements.

The internal stability of a reinforced earth wall is mainly dependent on the tie forces. These forces are a function of various factors such as the wall geometry, the type of foundation, type of loading and the properties of materials used within and beyond the reinforced earth wall.

Simple analytical methods, based on the conventional Rankine and Coulomb earth pressure theories, have been suggested for the design of the internal stability of reinforced earth walls. These methods are mainly based on the assumption of homogeneity and isotropy of the wall backfill. Reinforced earth, being essentially a composite material, deviates from these assumptions.

Closed form solutions based on the theory of elasticity and the finite element method have also been applied to the analysis of reinforced earth material by Harrison et al[32] and to Romstad et al[54] respectively.

Most of the model tests conducted to study the internal stability of reinforced earth walls, have been based on an ultimate strength concept and the main observations made were for conditions at failure. Existing design methods based on the conventional earth pressure theory, were tested on the basis of these model tests and a discrepancy was found[3,7,63] between the Rankine theory and the model test results.

Although results from full scale walls have been found[29,63] to be affected considerably by the construction procedure, they are valuable in understanding reinforced earth behaviour and in evaluating the internal stability of a particular structure. Full scale walls have also been found[63] to behave in a different manner from the assumptions on which conventional design methods, such as the Rankine theory were based.

This thesis is concerned with the theoretical and experimental investigation of the internal stability of rectangular reinforced earth retaining walls built on rigid foundations , the purpose being to evaluate existing and new theories against the actual performance of model and full scale reinforced earth walls.

1.2.   Scope of Thesis

A review of literature pertaining to theoretical and experimental studies on reinforced earth retaining walls is presented.   The simple analytical design approaches are compared and discussed.

An Energy theory based on the principle of elastic strain energy of ties and the external work done due to elastic deformation of the wall is developed to overcome the shortcomings of the simple linear Rankine design method which is currently accepted as a basis for reinforced earth wall design.

Model reinforced earth retaining walls built on rigid foundations, using a cohesionless material are studied for ultimate and non-ultimate strength concepts.   Some walls were instrumented to obtain the tie tension distribution the strains in the soil, the wall deflections, and the stresses in the soil.   The observations fitted reasonably with the proposed new theoretical approach.

Actual field data taken from the instrumented section in a full scale reinforced earth retaining wall are evaluated in terms of the existing and the Energy theories.   The full scale wall and model wall results were compared.

Because of the complexity of reinforced earth wall behaviour and the various factors that could affect the wall performance, an established finite element programme is used to analyse the model and the full scale walls.   The results of the analyses are presented and compared with observed wall behaviour.

Finally conclusions are drawn from various approaches used to study reinforced earth retaining walls, and recommendations for future studies on these walls are made.

CHAPTER TWO

LITERATURE REVIEW

The aim of this chapter is to give a brief account of the theoretical and experimental studies which have been carried out on reinforced earth walls by previous investigators.

These studies will only be outlined at this stage and will be referred to in detail where necessary in later chapters.

The theory of reinforced earth was presented by Vidal in a series of papers[77,78,79,80] in which he gave the basic concepts underlying the principle of reinforced earth.

Schlosser and Vidal[67] made further contributions to design methods for reinforced walls. Simple equations, based on the Rankine and Coulomb earth pressure theories were given for the evaluation of the internal stability of these walls. Methods of determining the tension in the ties were discussed and later modified by Schlosser[60,61] on the basis of a different distribution of vertical pressure on horizontal sections suggested by Meyerhof. Schlosser also suggested methods of evaluating the resistance of ties to failure by pullout.

Using similar methods to Schlosser and Vidal, Lee et al[45] developed simple equations for checking the internal stability of walls and Schlosser et al[63] incorporated a reduction factor to design methods using the Rankine theory of earth pressure, partly to account for the difference noted between Rankine theory and the model test results and also to give an expression which agrees with the wall behaviour suggested by the tension distribution mechanism shown in Fig (2.1).

Banerjee[5] envisaged a design method for the internal stability of reinforced earth retaining walls, based on a failure surface which is similar to the Coulomb failure plane. This method uses an empirical coefficient in the derivation of the expressions and takes account of the soil cohesion which is neglected in the other design approaches.

Symons[72] gave a comprehensive review of most of the fore-

Curve of

maximum tie tension position

T

(I)
Active
zone

T_m

(II)
Passive zone

Fill

$\tau = \dfrac{dT}{dl} \cdot \dfrac{1}{2b}$

$\dfrac{\pi}{4} + \dfrac{\phi}{2}$
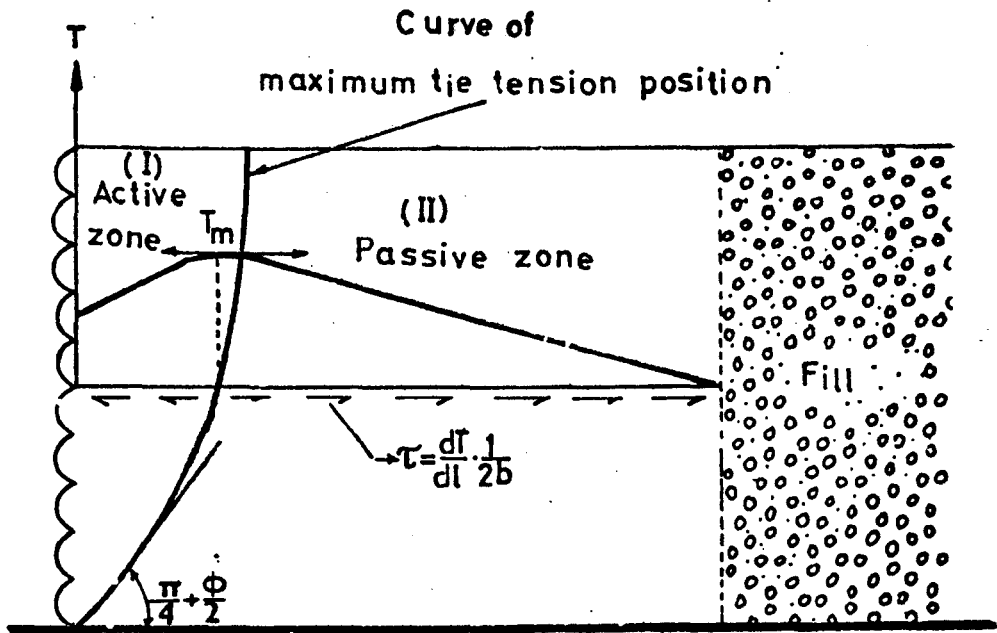
Fig(2.1) <u>Reinforced earth wall behaviour based on tie tension</u>
<u>distribution along the tie length(Schlosser et al[63])</u>

going design methods.

Harrison and Gerrard[32] presented a mathematical model for reinforced earth which is not of direct applicability to the reinforced earth retaining wall problem.

Finite element methods have been applied to the analysis of reinforced earth retaining walls by Vauloup[76] Yziquel[81] and Corte[21] working in France. Banerjee[5] and Romstad et al[54] have also investigated this method in the U.K. and U.S.A. respectively.

Model studies on reinforced earth retaining walls have been carrried out in Laboratoire Central des Ponts et Chaussées by several investigators[7,47,61,64 to 67] in the University of Lyon[3,9,17,46] in California[44,45] and also in Japan.[75]

Fewer observations have been made on actual wall behaviour in the field. Schlosser and Vidal[67] and Schlosser[62] presented results of observations on a wall at Incarville. Baguelin et al[4] reported surveys of the geometry, the site conditions and the theoretical safety factors against slippage at the base on Vigna (I) Viga (II) and Peyronnet walls. Marec et al [48] published information of wall geometry, soil and tie material properties and the sizes and statistics of the ties and the skin elements adopted in La Giraude, Bava, Menieri and Ricard walls. Tests from walls at Dunkirk in France were reported by different authors[6,47,61]. Chang[14] published the final report on a wall in Los Angeles County, which was built by the Department of Transportation of the State of California, U.S.A. . Finlay and Sutherland[29] published the test results observed on a wall at Granton in the U.K.

CHAPTER THREE
THEORY AND DESIGN OF REINFORCED EARTH RETAINING WALLS

3.1 Introduction

In this chapter the conventional analytical approaches to the design of reinforced earth walls are first considered. Methods of assessing the internal stability are compared as are the resultant expressions for the calculation of:

(i) The tension in the ties.

(ii) The critical wall height for walls failing by the ties breaking.

(iii) The adherence length of a tie to prevent wall failure by tie pull out.

The original methods of analysis were based on earth pressure theories such as Rankine and Coulomb. The Rankine theory is mainly used in designing full scale reinforced earth retaining walls. The shear stresses which can develop at the soil/tie interface are neglected and this gives a linear tension distribution with wall depth which is at variance with reality.[67] The Rankine theory was found to give an overestimate of the tie tension when compared with observations on models and to imply a wall behaviour which is different from the wall behaviour observed on full scale walls.[63]

A new energy theory has therefore been advanced in this chapter. This theory is based on the equilibrium of the

external work done and the internal energy stored in the tie and takes into account:

(i)   The effect of tie length on the tension magnitude.

(ii) The non-linear tension variation along the tie length and with the wall height.

(iii) The deflected shape of the wall.

Some attempt will be made in this chapter to indicate which of the theories is most appropriate for the general problem.   This can be done for most of the theories only by comparing the results with those obtained from model or full scale tests, and this approach will be followed up in Chapters Five and Six.

Conclusions drawn are given at the end of this chapter.

3.2 Factors Influencing Stresses in Reinforcing Ties

The level of tie tension in a reinforced earth wall and its mode of variation along a tie length is dependent on the following parameters:

(1) Type of the soil used as the backfill material.

(2) Type of the reinforcing tie material.

(3) The spacing of the ties.

(4) The tie position within the height of the reinforced earth wall.

(5) The tie geometry (length, width and thickness).

(6) The flexibility of the skin elements.

(7) The geometry of the reinforced earth wall.

(8) The method of wall construction.

(9) The properties of soil underlying the reinforced earth wall.

(10) The frictional characteristics of the interfaces between the soil and the ties and also between the backfill and the skin elements.

(11) The density of the backfill.

(12) The moisture content of the backfill.

(13) The type of loading on the reinforced earth wall.

(14) The elastic properties of the backfill material.

(15) Time effects.

Hence it is rather difficult to formulate a theory which takes all these parameters into account. In the theories outlined in this chapter, various simplifying assumptions have been made and are noted.

3.3 Theoretical Expressions For Tie Tension

The analytical expressions derived by previous authors to determine the tie tension at various tie levels in a reinforced earth wall will be outlined at this stage.

3.3.1 Rankine Theory

The design of reinforced earth retaining walls, using the Rankine theory was discussed by Schlosser and Vidal.[67] The reinforced earth mass was assumed to be isotropic and homogeneous, and the wall facing smooth. If these conditions are satisfied, then the vertical direction will be a principal direction for the vertical stress. The expression for the tension in the ties using this method is obtained by considering the equilibrium of the horizontal pressure force acting on the wall face and the tension in the tie.

From Fig (3.1a) the vertical stress at any depth h is

$$\sigma_y = \gamma.h \qquad \dots\dots\dots\dots\dots\dots\dots\dots (3.1)$$

and the horizontal stress is related to it by the coefficient of the earth pressure K

$$\sigma_x = K.\gamma.h \qquad \dots\dots\dots\dots\dots\dots\dots\dots (3.2)$$

This coefficient depends on the soil type, the wall deflection and geometry of the wall. For granular, dense backfills a very small deflection of the wall causes the value of K to drop to the minimum active state[73] and K will be equal to the coefficient of active earth pressure K_a.

Considering local equilibrium of the tie and the skin
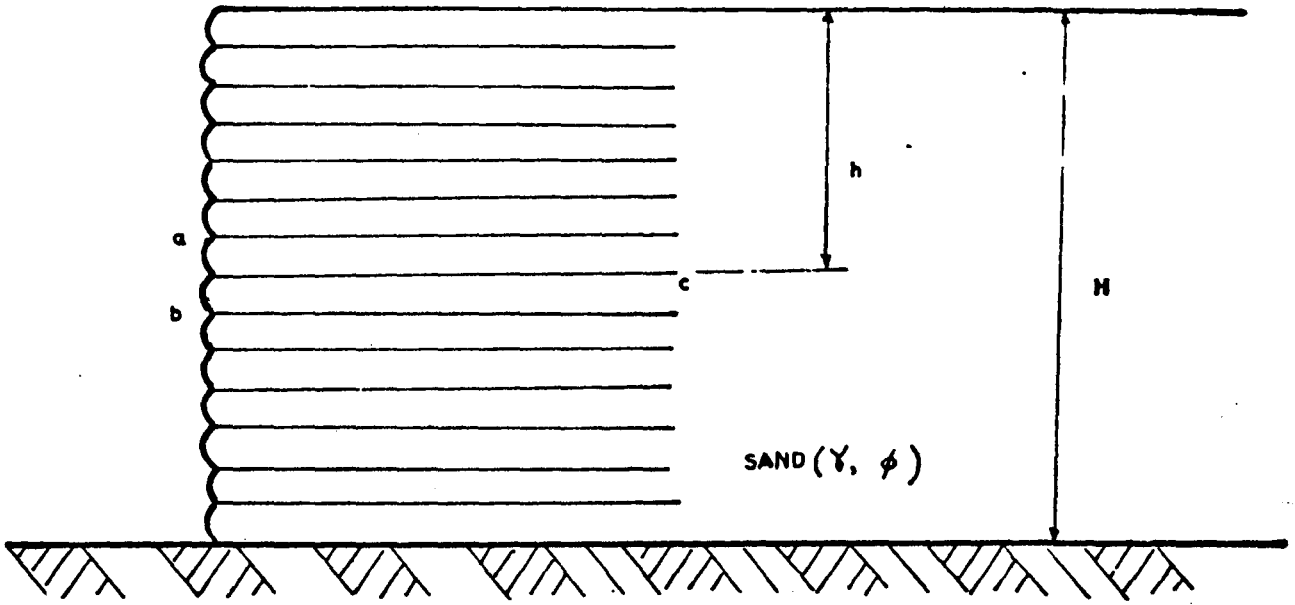
Fig(3-1a) The Rankine theory parameters.
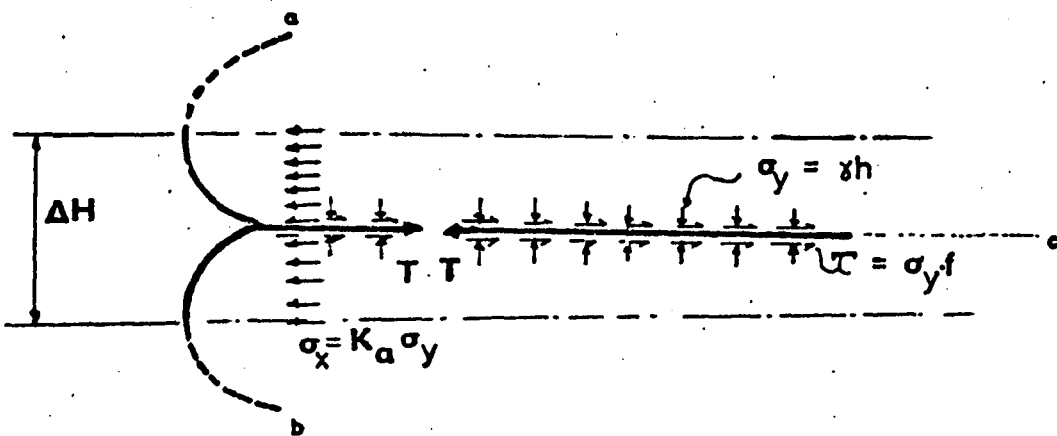
$$T = \sigma_x \Delta H = K_a \sigma_y \Delta H$$

Fig(3-1b) System of forces on section a,b,c.

Fig.(3-1) The Rankine theory.

elements Fig (3.1b), the tie tension per unit width of the wall is

$$T = \sigma_x . \Delta H$$

substituting for $\sigma_x = K_a . \gamma . h$

The tension expression is

$$T = K_a . \gamma . h . \Delta H \quad \ldots\ldots\ldots\ldots\ldots\ldots\ldots\ldots\ldots\ldots\ldots \quad (3.3)$$

and the maximum tension at the bottom of the wall is

$$T_{max} = K_a . \gamma . H . \Delta H. \quad \ldots\ldots\ldots\ldots\ldots\ldots\ldots\ldots\ldots \quad (3.4)$$

By adopting an approach which is similar to Rankine, Schlosser and Vidal[67] and Schlosser[60] derived tension expressions based on a Trapezoidal and Meyerhof's vertical stress distributions respectively. The derivations of the tension expressions using these methods are as follows:

3.3.1.1 The Trapezoidal vertical stress distribution

A trapezoidal vertical stress distribution due to the combined effect of vertical and horizontal thrusts is often assumed on horizontal planes within conventional retaining walls.

In considering this vertical stress distribution in the reinforced earth wall design, the wall is assumed rigid and capable of transferring the moment produced by the thrust on the back of the wall to the sections near to the wall face Fig (3.2).

The moment M due to the horizontal thrust P on a wall of height H is:
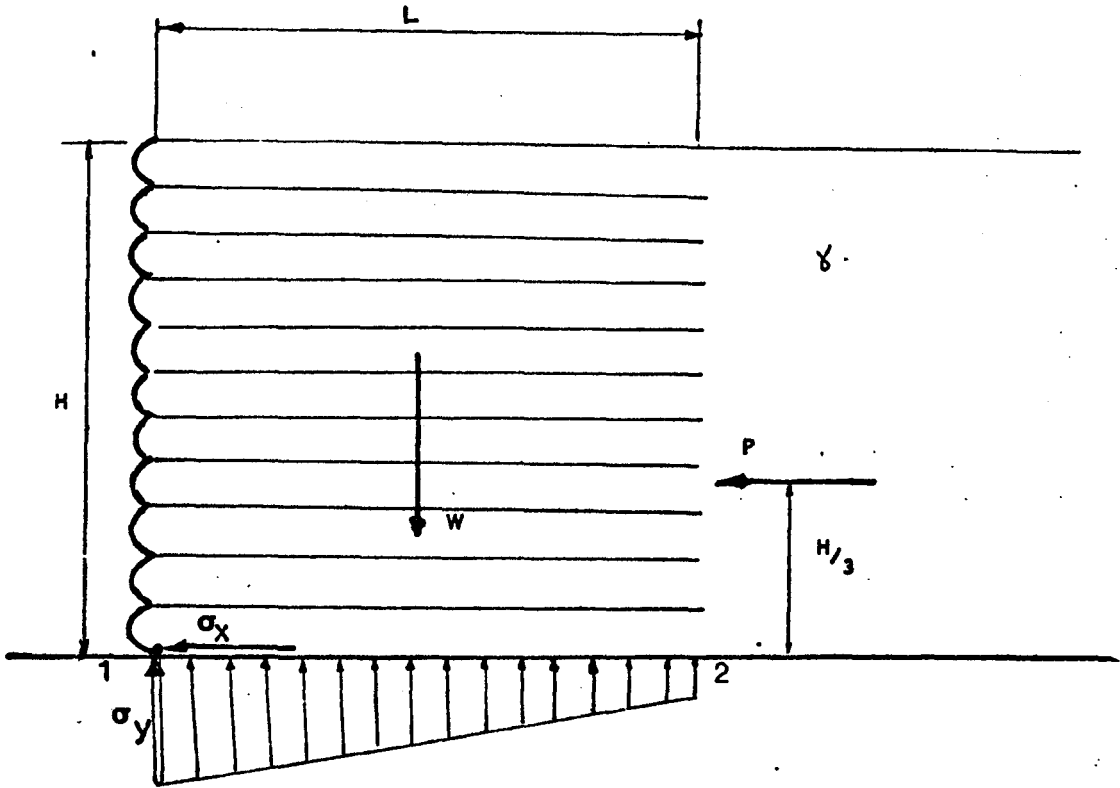
Fig.(3-2) The Trapezoidal vertical stress distribution.
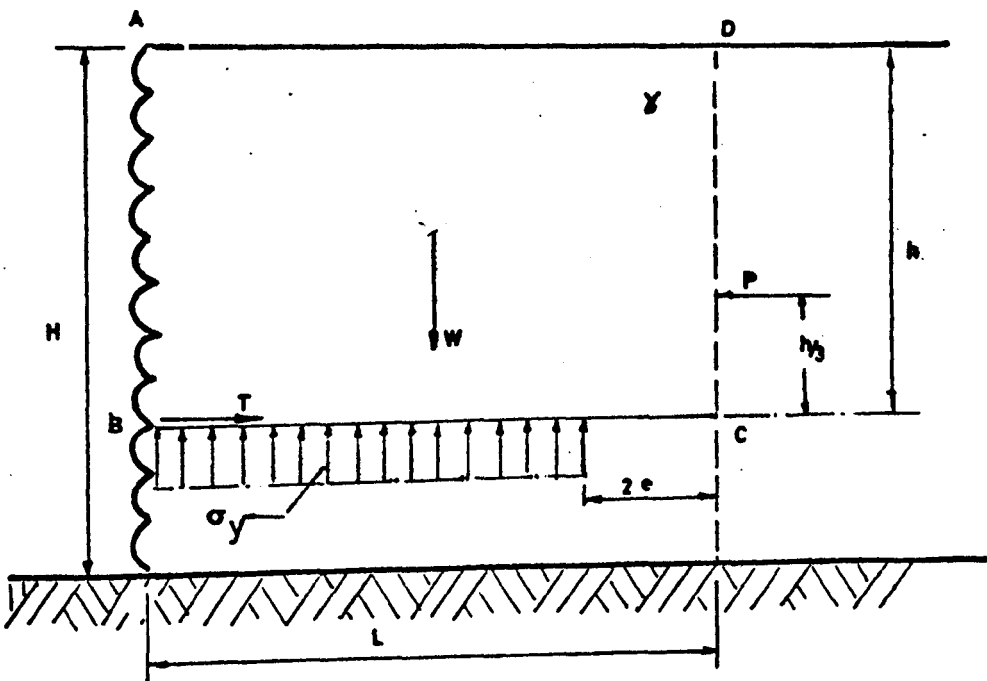
Fig.(3-3) Meyerhof's vertical stress distribution.

$$M = P \cdot \frac{H}{3}$$

where $\quad P = \frac{1}{2} \cdot K_a \cdot \gamma \cdot H^2$

$\therefore \qquad M = \frac{1}{6} K_a \cdot \gamma \cdot H^3$

The vertical stress at sections 1 and 2, Fig (3.2) is given as

$$\sigma_{y_{1,2}} = \frac{W}{L} \pm \frac{M}{Z}$$

where $\quad \bar{Z} = L^2/6$ and $W = \gamma \cdot H \cdot L$

$\therefore \qquad \sigma_{y_{1,2}} = \gamma H \left(1 \pm K_a \left(\frac{H}{L}\right)^2 \right)$

The maximum tension per unit wall width

$$T_{max} = K_a \cdot \sigma_{y_1} \cdot \Delta H$$

or $\quad T_{max} = K_a \gamma H \cdot \Delta H \left(1 + K_a \left(\frac{H}{L}\right)^2 \right) \dots\dots\dots\dots$ (3.5)

3.3.1.2 Meyerhof's vertical stress distribution

By adopting Meyerhof's vertical stress distribution the effect of the thrust acting at the back of the wall in increasing the vertical stress is approximated by assuming a uniform stress distribution over a base length equal to L - 2e where e is the eccentricity of the reaction, Fig (3.3).

The vertical stress $\quad \sigma_y = \dfrac{W}{L - 2e}$

where $\qquad e = \dfrac{h}{3} \cdot \dfrac{P}{W} = \dfrac{1}{6} \cdot K_a \dfrac{h^2}{L}$

$\therefore \qquad \sigma_y = \dfrac{\gamma \cdot L \cdot h}{L - \frac{1}{3} K_a \dfrac{h^2}{L}}$

By taking the equilibrium of the horizontal stress acting over a wall height h and the force in the tie, the tie tension per unit wall width is given as

$$T = K_a \, \sigma_y \cdot \Delta H$$

$$\text{or} \quad T = K_a \, \frac{\gamma h}{1 - \frac{1}{3} \cdot K_a \left(\frac{h}{L} \right)^2} \cdot \Delta H \quad \ldots\ldots\ldots\ldots \quad (3.6a)$$

The maximum tension at the bottom of the wall is

$$T_{max} = K_a \, \frac{\gamma H}{1 - \frac{1}{3} K_a \left(\frac{H}{L} \right)^2} \cdot \Delta H \quad \ldots\ldots\ldots\ldots \quad (3.6b)$$

3.3.2 Coulomb Theory

The use of the Coulomb earth pressure theory in the design of the internal stability of reinforced earth retaining walls was first advanced by Schlosser & Vidal[67] who derived an expression for tie tension based on the assumption that the active earth pressure thrust was resisted by the tension in the ties.

In the special case of a retaining wall with smooth vertical face and horizontal backfill, the resultant total tension in the ties lying in plane AB, Fig (3.4a) may be computed by considering the equilibrium of a failure wedge ABC. The forces acting on this wedge are:

    (i)   The weight W of the soil contained in the wedge ABC.

    (ii) The reaction R of the earth acting on plane AC. This is inclined at an angle ϕ with the normal

Given .

1- Density of backfill γ

.2- Angle of internal friction of soil ϕ

3- The friction angle between soil & wall facing = 0

4- The total wall height   H

5- The vertical tie spacing ΔH

6- The coefficient of active earth pressure. K_a
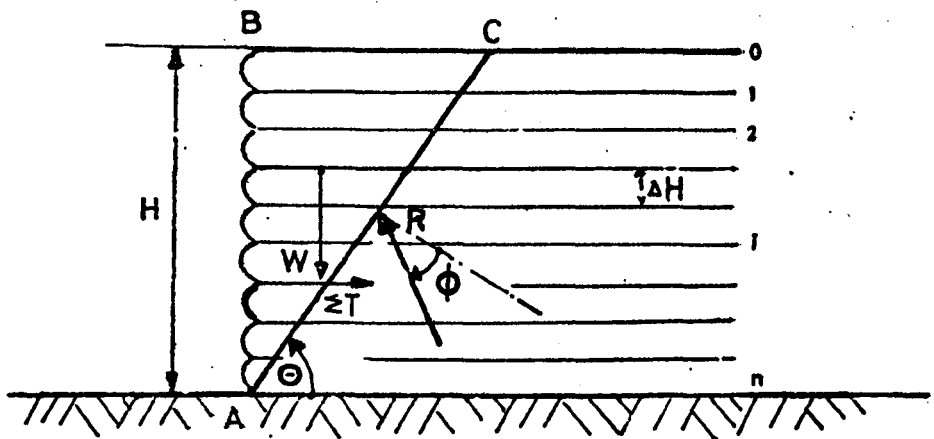
Fig.(3-4a)
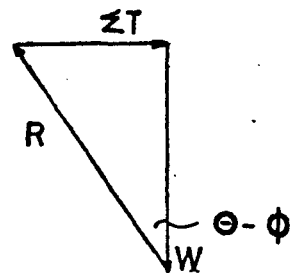
Fig.(3-4b)

Fig.(3-4) Coulomb theory parameters .

to this plane, since the soil is assumed to be in a failure state.

(iii)   The total tension ΣT which is the sum of the forces in the ties lying in the plane AC.

From triangle of forces   Fig (3.4b)

$$\Sigma T = W.\tan(\Theta - \phi)$$

substituting $W = 0.5.\gamma H^2.\text{Cotg}\,\theta$

$$\Sigma T = 0.5.\gamma.H^2\text{Cotg}\,\theta \;.\tan(\Theta - \phi)$$

The maximum value of the total tension ΣT is given when

$$\frac{d\Sigma T}{d\Theta} = 0. \qquad \text{This gives}$$

$$\Theta = (\frac{\pi}{4} + \frac{\phi}{2})$$

$\therefore$ $\Sigma T = 0.5.K_a.\gamma.H^2$ (per unit wall width)

Assuming a linear tension distribution with wall height, the tie tension at the ith layer, is   given by

$$T_i = \frac{i}{(n + 1)} \;.\; K_a.\gamma.H.\Delta H$$

The maximum tension T_{max} per unit wall width, is obtained where $i = n$ as

$$T_{max} = \frac{n}{n + 1}.K_a.\gamma.H.\Delta H \;\ldots\ldots\ldots\ldots\ldots\ldots (3.7)$$

Lee et al[45]   also derived a tie tension expression using the Coulomb method but equated the moments about the toe of the wall, of the earth pressure thrust and the tension

in the ties.   A linear tension distribution over the wall
height has been assumed.   The maxiumum tie tension per
unit wall width T_{max} was given as

$$T_{max} = \frac{n^2}{n^2 - 1} \cdot K_a \cdot \gamma \cdot H \cdot \Delta H \quad \ldots\ldots\ldots\ldots\ldots\ldots (3.8)$$

For walls in which n is large, the coefficients
$\frac{n}{n+1}$ and $\frac{n^2}{n^2-1}$ in equations (3.7) and (3.8) approach unity.
Therefore the maximum tension per unit wall width, given
by these equations can be written as

$$T_{max} = K_a \cdot \gamma \cdot H \cdot \Delta H \quad \ldots\ldots\ldots\ldots\ldots\ldots\ldots (3.9)$$

Equation (3.9) is identical to equation (3.4).   Therefore
in the particular case of a rectangular wall with a large
number of reinforced layers and a smooth back, in which the
tie tension is assumed linearly varying with the wall height
the Rankine and Coulomb theories give identical tension
expressions.

Generally the Coulomb theory has the advantage that it
can be adopted for walls with irregular geometry and rough
back.

3.3.3 Comparison between the maximum tension expressions

The Rankine tie tension expression is mainly adopted in
practice.   The other design methods, mentioned in the
previous section, give identical or slightly higher tie

tension than the Rankine theory. In order to show the differences between the Rankine, Coulomb, the Trapezoidal and Meyerhof tie tension expressions, the maximum tie tension expression given by these methods can be presented in the general form

$$T_{max} = A.K_a \gamma \, H. \, \Delta H \text{ per unit wall width} \quad \ldots\ldots\ldots \quad (3.10)$$

where A is a factor depending on the ratio of the wall height to tie length $\frac{H}{L}$ and also on the angle of the internal friction of the soil ϕ. In the cases of the Rankine and Coulomb theories, A = 1.0 for all $\frac{H}{L}$ ratios and ϕ values.

Considering the Trapezoidal and Meyerhof Methods the coefficient A is given by

$$A = (1 + K_a \, (\frac{H}{L})^2) \qquad \text{Trapezoidal} \quad \ldots\ldots\ldots \quad (3.11)$$

$$A = 1 / (1 - \frac{1}{3} K_a (\frac{H}{L})^2) \qquad \text{Meyerhof} \quad \ldots\ldots\ldots \quad (3.12)$$

Values of A have been calculated for values of ϕ and $\frac{H}{L}$ ratios ranging between $25^\circ - 50^\circ$ and $0.5 - 1.5$ respectively and plotted against ϕ values as shown in Fig (3.5).

It can be seen that the maximum tension predicted from the Trapezoidal and Meyerhof vertical stress distributions increases with increasing $\frac{H}{L}$ ratio and decreases with increasing ϕ values. These methods always predict larger tensions than the Rankine theory depending on the $\frac{H}{L}$ ratio and ϕ values used in the design of the wall.

$$T_{max} = A \cdot K_a \cdot \gamma \cdot \Delta H \cdot H$$

——————— Trapezoidal

—— · —— · — Meyerhof.

Coulomb=Rankine A= 1.0, All ϕ, All H/L
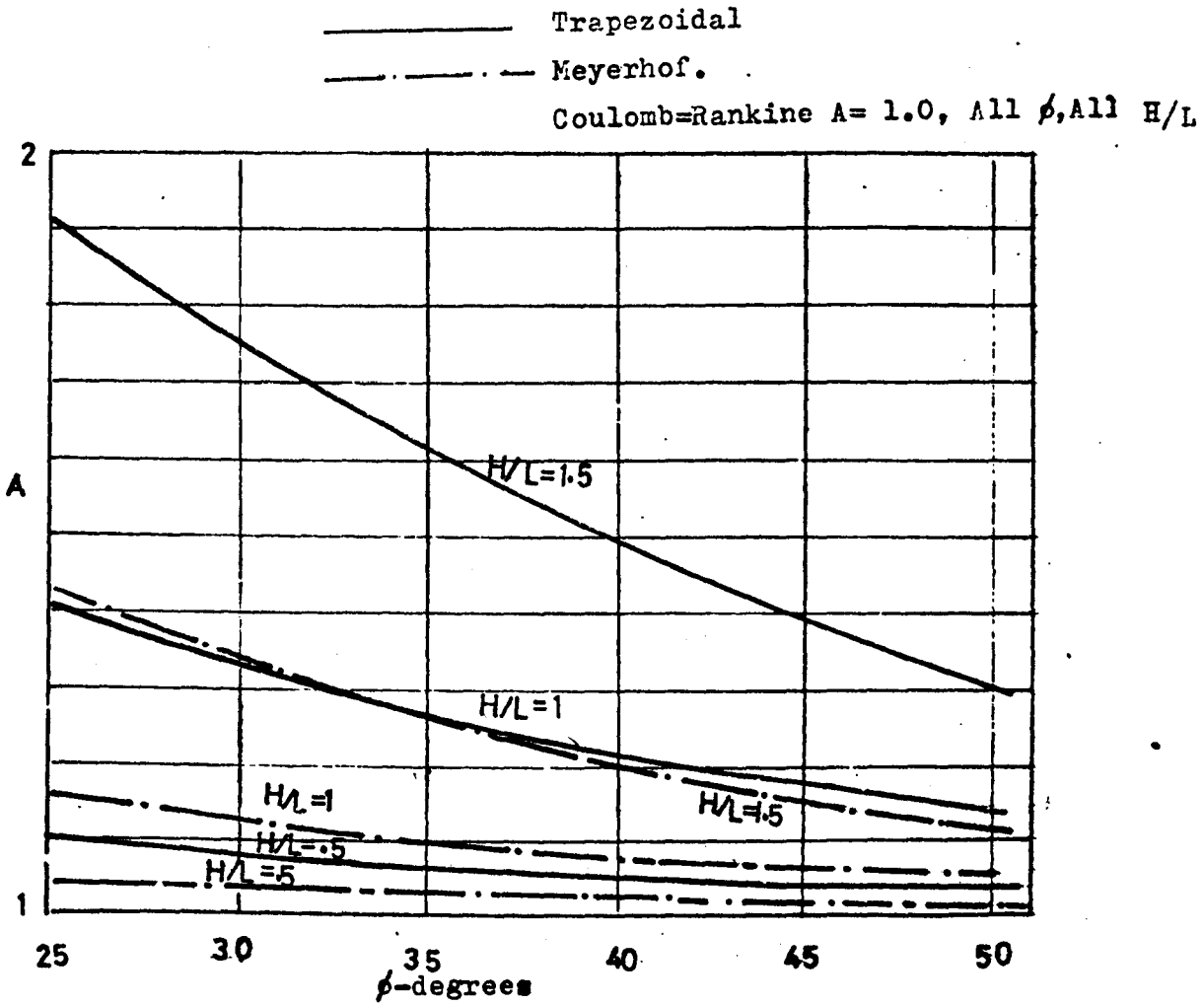
Fig(3.5)Comparison between Coulomb,Rankine, Trapezoidal & Meyerhof maximum tension expressions.

3.4 Banerjee's[5] Analysis of Reinforced Earth Retaining Walls

This approach is basically similar to Coulomb theory, but instead of resolving the forces in the vertical and the horizontal directions to get the total tension in the ties as a function of the angle of inclination of the failure plane, forces are resolved along the inclined plane and compared to get the safety factor against sliding of the wedge. In his analysis the soil is assumed to have a cohesion c which increases the wedge resistance against sliding.

Considering the equilibrium of the plane A-C, Fig (3.6), inclined at angle β with the vertical, the total sliding and resisting forces per unit wall width are calculated as

The sliding force $\quad P_s = 0.5 \gamma H^2 . \sin\beta$

The resisting force $\quad P_r = 0.5 \gamma H^2 . \sin\beta . \tan\beta . \tan\phi$
$$\Sigma T(\tan\phi . \cos\beta + \sin\beta) + c.H.\sec\beta$$

where c = unit cohesion of the soil

The safety factor is given by

$$SF = \frac{P_r}{P_s} \quad \dots\dots\dots\dots\dots\dots\dots\dots\dots\dots \quad (3.13)$$

Assigning,

$$A_w = 0.5 \gamma H^2 \qquad X = \frac{\Sigma T}{A_w} \quad \text{and} \quad X_0 = \frac{2cH}{A_w}$$

The safety factor is given as:

$$SF = \tan\beta . \tan\phi + X(\tan\phi \cot\beta + 1) + X_0 . \mathrm{cosec}\, 2\beta \dots (3.14)$$

This expression is a function of the non-dimensional tension parameter X and the angle of the failure plane inclination with the vertical β.   These two factors vary dependently (Appendix(I)). In order to get the value of β corresponding to the minimum safety factor, Banerjee assumed that X and β were independent.

By differentiating equation (3.14) with respect to β and equating it to zero, the value of β corresponding to the minimum safety factor was given as

$$\beta = \tan^{-1} \left(\frac{2\,X\tan\phi + X_o}{2\tan\phi + X_o} \right)^{\frac{1}{2}} \quad \dots\dots\dots\dots\dots\dots \quad (3.15)$$

In the case of granular soil $X_o = 0$ and

$$\beta = \tan^{-1}(\ X\ )^{\frac{1}{2}} \quad \dots\dots\dots\dots\dots\dots\dots\dots \quad (3.16)$$

Fig.(3.6) Parameters of Banerjee's equation.

3.5 Theoretical Expressions for Critical Height of Walls Failing by Tie Breaking

The concept of the critical wall height was introduced by Schlosser and Vidal[67] in studying model walls failing by tie breaking. This concept made it possible to examine the theories against model test results without measuring the tension in the tie, by assuming that the maximum tie tension T_{max} was equal to the tensile strength of the tie material R_t when failure occurred.

In this section the different critical wall height expressions based on the conventional approaches and Banerjee's analysis will be presented and compared.

3.5.1 The Rankine and Coulomb Methods

The maximum tie tension over a wall width S is given by

$$T_{max} = K_a \, \gamma.H. \Delta H.S$$

substituting

$$R_t = T_{max}$$

and $H_c = H$

$$H_c = \frac{R_t}{K_a.\gamma.\Delta H.S} \quad \ldots\ldots \ldots\ldots\ldots\ldots\ldots\ldots\ldots\ldots \quad (3.17)$$

It is possible to get two expressions of the critical wall height by proceeding as in the Rankine and Coulomb cases and using the Trapezoidal and Meyerhof's vertical pressure distributions.

3.5.2 The Trapezoidal Method

$$H_c = \frac{R_t}{K_a \cdot \gamma \cdot \Delta H.S \left(1 + K_a \left(\frac{H_c}{L}\right)^2 \right)} \quad \ldots\ldots\ldots\ldots \quad (3.18)$$

3.5.3. Meyerhof Method

$$H_c = \frac{R_t}{K_a \cdot \gamma \cdot \Delta H.S} \left(1 - \frac{1}{3} K_a \left(\frac{H_c}{L}\right)^2 \right) \quad \ldots\ldots\ldots \quad (3.19)$$

3.5.4 Banerjee's[5] Method

He considered two cases:

(a) Failure of the first tie at the bottom of the wall in tension. For this case it was assumed that the non-dimensional tension factor X was given by

$$\frac{T}{\gamma h \Delta HS} = 0.35 \quad \text{(as found from a finite element analysis)}.$$

Proceeding as before, the critical wall height was given as

$$H_c = \frac{R_t}{0.35 \cdot \gamma \cdot \Delta H.S} \quad \ldots\ldots\ldots\ldots\ldots\ldots\ldots \quad (3.20a)$$

(b) The failure of all the ties in tension.
The total non-dimensional factor X was given by Banerjee as

$$X = \frac{\Sigma T}{0.5 \gamma H_c^2} = \frac{n \cdot R_t}{0.5 \gamma H_c^2}$$

where n is the number of ties per unit wall width

$$n = \frac{H_c}{\Delta H.S}$$

$$\therefore H_c = \left(\frac{n.R_t}{0.5\gamma X}\right)^{\frac{1}{2}} \quad \ldots\ldots\ldots\ldots\ldots\ldots\ldots (3.20b)$$

The assumption of all the ties breaking simultaneously is only valid if the ties have a constant safety factor against tie breaking failure, which is not fulfilled for rectangular walls with constant strip density. In model studies Schlosser and Vidal[67] noticed that failure of rectangular reinforced earth walls with uniform strip distribution, starts at the toe of the wall. Therefore, equation (3.20a) given by Banerjee will be considered for comparison with other theories.

3.5.5 Comparison between the expressions for critical wall height for cohesionless backfill

In a similar manner to the comparison made between the tension expressions the author has expressed the critical wall height as

$$H_c = B \frac{R_t}{K_a \gamma . \Delta H.S} \quad \ldots\ldots\ldots\ldots\ldots\ldots\ldots (3.21)$$

where B = 1.0 for the Rankine theory,

$$B = \frac{1}{1 + K_a \left(\frac{H_c}{L}\right)^2} \quad \text{Trapezoidal} \ldots\ldots\ldots\ldots (3.22)$$

$$B = 1 - \frac{1}{3} K_a \left(\frac{H_c}{L}\right)^2 \quad \text{Meyerhof} \ldots\ldots\ldots\ldots (3.23)$$

$$B = \frac{K_a}{0.35} \quad \text{Banerjee} \ldots\ldots\ldots\ldots (3.24)$$

The variation of the coefficient B with the angle of internal friction ϕ of the soil and different $\frac{H_c}{L}$ ratios

is shown in Fig (3.7).   The Trapezoidal and Meyerhof's
pressure distributions predict critical wall heights which
increase with decreasing $\frac{H_c}{L}$ ratio and increase with increas-
ing ϕ value, but are always less than the critical wall
height predicted by the Rankine theory.

Banerjee's expression predicts lower critical wall
heights than the Rankine theory for ϕ values greater than
28° for all $\frac{H_c}{L}$ ratios.

Further discussion of these methods will be made in the
next chapter in terms of model test results.
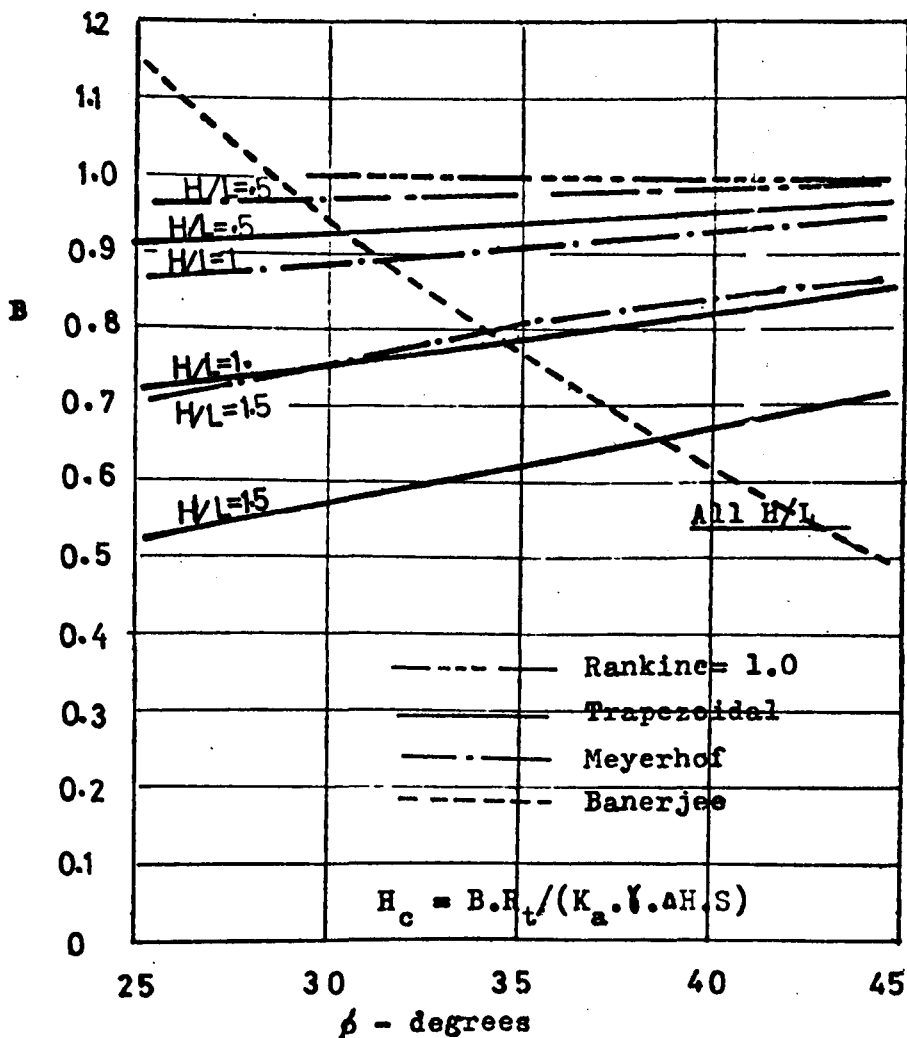
Fig(3.7) Comparison between Rankine, Trapezoidal, Meyerhof & Banerjee
critical height expressions .

3.6   Theoretical Design Methods Assuming Tie Pull Out Failure

3.6.1   Introduction

In order to calculate the tie length which provides stability for walls failing by tie pull out, estimates of tie pull out resistance and the tension in a tie are required.   The latter quantity may be calculated by one of the previous methods.   The tie pull out resistance is a function of the tie surface area, its depth below the wall surface and the tie/soil coefficient of friction.   Simplifying assumptions have been made in calculating this force[60]. The coefficient of friction f , is normally assumed constant and the vertical stress distribution is constant and identical on opposite faces of the tie.

3.6.2   The Rankine and Meyerhof methods 'Schlosser[60,61] ,

Schlosser[60] derived expressions for the adherence length by assuming that all the tie length was effective in providing resistance against pull out failure.   For a tie of length L and width b and under an overburden pressure γh, the tie resistance against pull out failure F_r is

$$F_r = 2bL\gamma h f \quad \dots\dots\dots\dots\dots\dots\dots\dots\dots\dots\dots (3.25)$$

where f is the soil/tie coefficient of friction.   The tension per unit wall width in a tie at a given depth. h below the surface of a reinforced earth wall can be calculated from the Rankine theory by equation (3.3).   By equating equations (3.25) and (3.3) and considering a wall of width S, the adherence length was given as:

$$L_a = \frac{K_a . \Delta H . S.}{2.b.f.} \quad \dots\dots\dots\dots\dots\dots\dots\dots\dots\dots (3.26)$$

In a similar manner Schlosser[60,61] derived an expression for the adherence length by assuming the Meyerhof method for the tie tension calculation, and equation (3.25) for estimating the tie resistance against pull out failure.

The adherence length was given as:

$$L_a = \frac{h^2 . K_a}{3L} + \frac{K_a \Delta H . S}{2bf \left(1 - \frac{K_a}{3} \left(\frac{h}{L}\right)^2\right)} \quad \dots\dots\dots\dots (3.27)$$

Equation (3.27) gives an adherence length which increases with wall depth. At the top of the wall, i.e. when $h = 0$, this equation gives an identical result to equation (3.26). Schlosser[60] compared both equations for a full scale wall and found that for practical purposes, the results from the two equations can be taken as similar. Equation (3.26) is mainly used in practice for the design of reinforced earth retaining walls.

3.6.3 The Rankine Method using Lee's assumption (Lee et al[45])

Lee et al[45] derived an expression for the adherence length by assuming that the tie tension is given by the Rankine theory, but that only the tie length extending beyond the Coulomb failure plane was effective in providing resistance against tie pull out failure.

Considering Fig (3.8) the tension in the tie at a depth h_i below the wall surface, using Rankine theory is

$$T_i = K_a . \gamma . h_i . \Delta H . S$$

The tie resistance against pull out at   level i below
the wall surface is

$$Fr_i = 2.b\gamma.h_i.f \ (L - (H - h_i)\tan\beta)$$

The safety factor against pull out

$$SF = \frac{Fr_i}{T_i}$$ substituting for Fr_i and T_i from the
above equations

$$SF = \frac{2bf}{K_a \ \Delta H.S} . \ (L - (H - h_i)\tan\beta) \dots\dots\dots\dots\dots\dots(3.28)$$

The adherence length can be obtained by substituting SF = 1
and $\beta = (45 - \frac{\phi}{2})$ in equation (3.28).   This gives

$$L_a = \frac{K_a \ \Delta H \ S}{2bf} + (H - h_i). \sqrt{K_a} \quad \dots\dots\dots\dots(3.29)$$

Equation (3.29) predicts an adherence length which
increases with increasing wall height.   It gives a minimum
adherence length at the base of the wall (i.e. when $h_i = H$)
which is identical to the adherence length predicted by
equation (3.26).

3.6.4   The Coulomb force method

Lee et al[45]   envisaged a method of design for tie
pull out failure based on the Coulomb theory.   He assumed
that the reinforced earth wall behaves monolithically and
that only the tie length extending beyond the Coulomb failure
plane is effective in preventing tie pull out failure.

An expression for the safety factor against tie pull
out failure was obtained by comparing the total tie resisting

<u>force</u> against pull out and the earth pressure force as follows:

The earth pressure force P for a wall height H and width S is

$$P = 0.5 \, K_a \, \gamma \cdot H^2 S$$

The pull out resistance of a tie at level i Fig (3.8) is

$$Fr_i = 2bf \gamma \cdot h_i L_i$$

or $Fr_i = 2bf \gamma \cdot h_i \, (L - (H - h_i) \tan\beta)$

By summing all tie resistances and comparing them to the earth pressure force P, the safety factor against tie pull out was given as

$$SF = \frac{4bf}{K_a H^2 S} \sum_{i=N}^{n} [\, h_i \, (L - H \tan\beta) + h_i^2 \cdot \tan\beta \,] \quad \dots \quad (3.30)$$

N is the number of ties from top of the wall to the level where the first tie crosses the theoretical Coulomb failure plane.

Substituting for $h_i = i\Delta H$ and $H = n\Delta H$ in equation (3.30) we get

$$SF = \frac{4 \cdot b \cdot f \cdot \Delta H}{K_a H^2 \, S} \sum_{i=N}^{n} i \, (L - \Delta H(n-i) \sqrt{K_a} \,) \quad \dots \dots \quad (3.31)$$

The adherence length can be calculated from equation (3.31) by assigning the safety factor equal one.
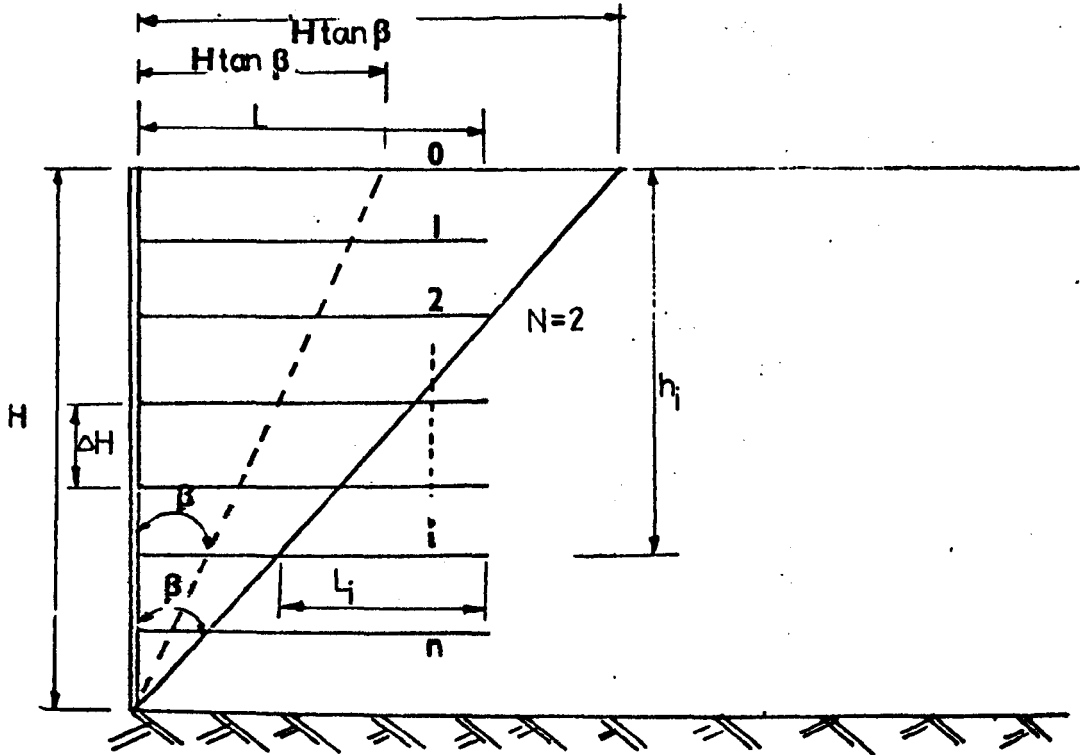
Fig.(3.8) Parameters in the Coulomb & Banerjee design methods against tie pullout failure.

3.6.5 The Coulomb moment method

In this method Lee et al[45] adopted the same assumptions previously made in the Coulomb force method.

The expression of the safety factor against tie pull out was obtained by comparing the total resisting moment of the tie frictional force, and the earth pressure moment about the toe of the wall as follows:

The tie resisting moment RM, at level i, Fig (3.8) is

$$RM_i = 2bf \gamma h_i L_i (H - h_i)$$

The total resisting moment is

$$RM = \sum_{i=N}^{n} 2b \cdot f \cdot \gamma \cdot h_i L_i (H - h_i)$$

$$RM = \sum_{i=N}^{n} 2bf \cdot \gamma \cdot h_i (L - (H - h_i) \tan\beta)(H - h_i)$$

The total moment due to the earth pressure force is

$$M = \frac{K_a \gamma H^3 . S}{6}$$

$$SF = RM/M$$

$$\therefore SF = \frac{12bf}{K_a H^3 S} \sum_{i=N}^{n} h_i (L - (H - h_i) \tan\beta)(H - h_i)$$

substituting for $h_i = i . \Delta H$ and $H = n . \Delta H$.

$$SF = \frac{12bf . \Delta H^2}{K_a H^3 S} \sum_{i=N}^{n} i(n - i) [L - \Delta H(n - i) \sqrt{K_a}] \dots \quad (3.32)$$

The adherence length corresponding to the safety factor against pull out equal one can be calculated from equation (3.32).

3.6.6 Banerjee's[5] expression of the adherence length for cohesionless backfill

For a soil with an angle of internal friction ϕ and a unit cohesion c, according to Banerjee[5] the sum of tension forces in the ties is given by

$$\Sigma T = \sum_{i=1}^{n} 2 \alpha b L_i (c + \gamma.h_i \tan\phi) \quad \ldots\ldots\ldots\ldots (3.33)$$

L_i and h_i are shown in Fig (3.8) and α is an empirical coefficient, suggested to be in the range $0.4 \leq \alpha \leq 0.60$. For a wall of width S, Banerjee's non-dimensional tension parameter χ is given by

$$\chi = \frac{\Sigma T}{0.5 \gamma H^2 S}$$

From equation (3.14), in the case of granular soil and a safety factor equal one, the non-dimensional tension X is equal to the coefficient of active earth pressure K_a. Hence,

$$\Sigma T = 0.5 K_a \cdot \gamma \cdot H^2 . S \quad \ldots\ldots\ldots\ldots\ldots\ldots\ldots (3.34)$$

For granular soil c = 0. The expression for the adherence can be derived by equating equations (3.33) and (3.34), substituting

$$L_i = L - (H - h_i \tan\beta) \quad \text{and}$$

carrying out the summation we get

$$L_a = \frac{K_a H_c^2 S}{2 \alpha b \Delta H (n^2 + n) \tan\phi} + H_c \tan\beta - \frac{\Delta H}{3} (2n + 1) \tan\beta$$

$$\ldots\ldots (3.35)$$

where $\tan\beta = \sqrt{K_a}$.

3.6.7. Comparison between the theoretical design methods assuming tie pull out failure

The foregoing theoretical design methods assuming tie pull out failure do not lend themselves to a simple comparative analysis as has been done for the tie tension and critical wall height expressions in sections (3.3.3) and (3.5.5) respectively. This is because the final expressions contain terms which are directly comparable only for particular cases and cannot easily be compared in a general way.

However, comparisons will be made in Chapter Five based on results of model tests.

3.7 Comments on existing theories

In the foregoing sections the methods of analysis of reinforced earth walls have been presented. Basically these methods were derived from the Rankine and Coulomb earth pressure theories, which assume that the backfill of a retaining wall is homogeneous and isotropic. The reinforced earth material being essentially a composite material, deviated from these assumptions. When the Rankine theory was applied to the reinforced earth wall design it neglected the shear stresses developing at the soil/tie interface, which is a basic requirement for the internal stability of a reinforced earth wall. As a result, this theory gave a linear tension distribution with wall height, which was at variance with observations made on full scale walls.[67,14] The Rankine method implied a maximum tension near the wall face and the Coulomb theory implied a constant tension along the tie length. Both implied assumptions were not in agreement with the tension variation along a tie observed on full scale walls.[67,29,14] These methods do not take into account the tie length effect on the tie tension which has been indicated in model tests.[3,17] The Rankine theory has been found to overestimate the tie tension when compared with model test results.[63,7]

The Trapezoidal and Meyehof design methods were derived on similar bases to Rankine theory and differ from it only by considering the effect of the thrust on the back of the wall on the vertical stress distribution. Thus these methods

resulted in a higher tie tension than the Rankine theory and therefore will lead to a more conservative reinforced earth wall design.

The methods of designing reinforced earth retaining walls based on failure surfaces, such as Banerjee's method, have been reported to be unsuitable for reinforced earth wall design.[63]

It is therefore necessary to derive a theory which takes into account the nonlinear tie tension variation along a tie length observed on full scale walls, the non -linear tie tension distribution with wall height, the deflected shape of wall and the tie length effect on the tension in a tie. The author has developed a theory based on an energy approach which attempts to take these factors into account. The assumptions and derivations of this theory will be presented in the next section.

3.8 Strain Energy Theory

3.8.1 Introduction and general statement of approach

The strain energy theory obtains expressions for the reinforced earth wall design by establishing energy relations from elastic deformations of the reinforced earth wall facing and the ties, under the action of the earth pressure and the tension forces respectively.

The external work done is calculated first by assuming that the wall yields to a stable position given by the general function y(Z) under the action of the earth pressure force p(Z) which varies in the general manner shown in Fig (3.9).

The incremental external work over a height dZ and wall width S is given by

$$U_{ext} = S.p(Z).y(Z).dZ \quad \dots\dots\dots\dots\dots\dots\dots \quad (3.36)$$

and the total external work can be calculated by summing these increments over the total wall height H and width S as

$$U_{ext} = S \int_{0}^{H} p(Z).y(Z).dZ \quad \dots\dots\dots\dots\dots \quad (3.37)$$

The external work done is assumed to be stored in the reinforcing ties as an elastic strain energy and the strain energy stored in the skin elements is assumed to be negligible. Provided that the tension distribution along the tie length is specified, the strain energy stored in the
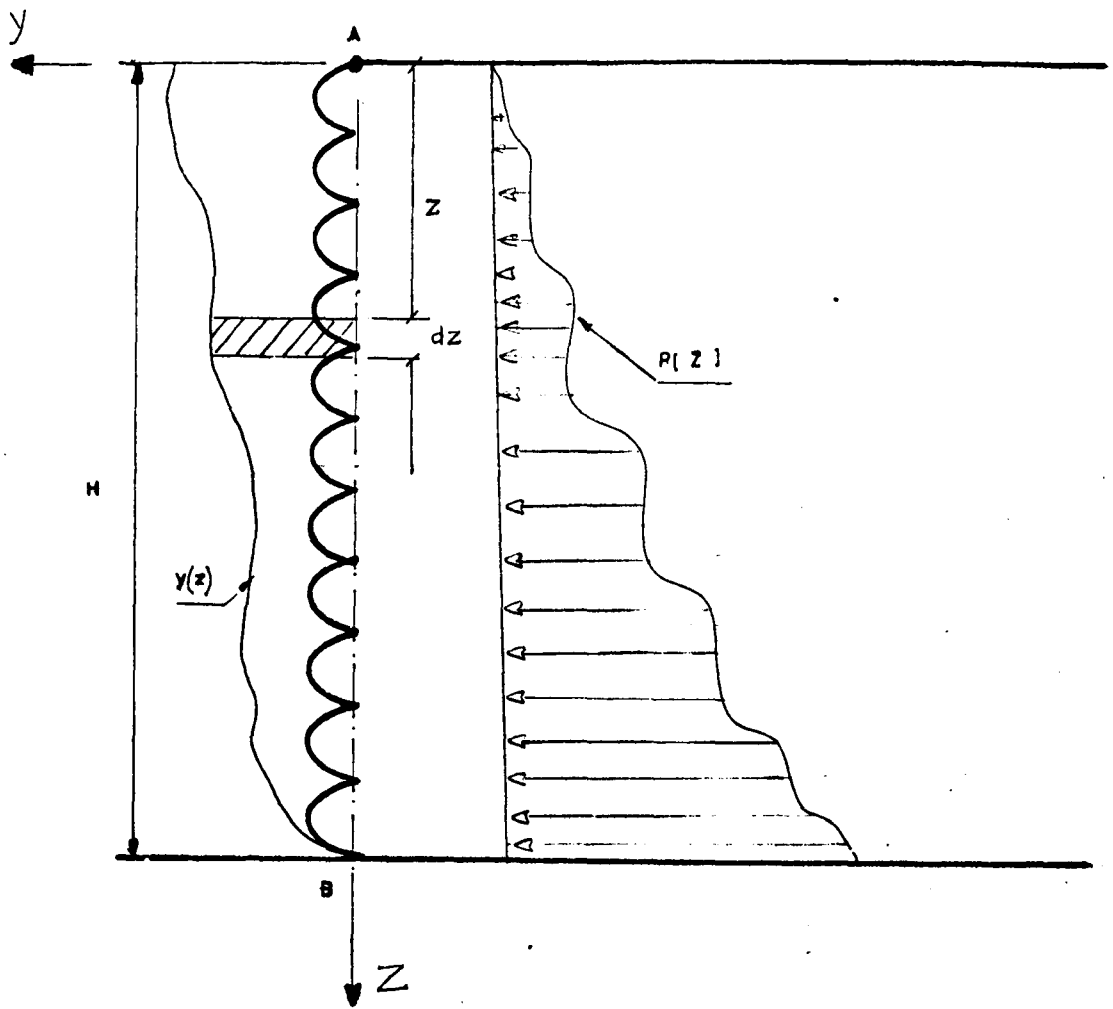
Fig.(3-9) The Energy theory parameters

$$U_{ext.} = s \int_0^H p(Z).y(Z).dZ$$

Fig.(3-10b) Idealized deflected shape of wall.
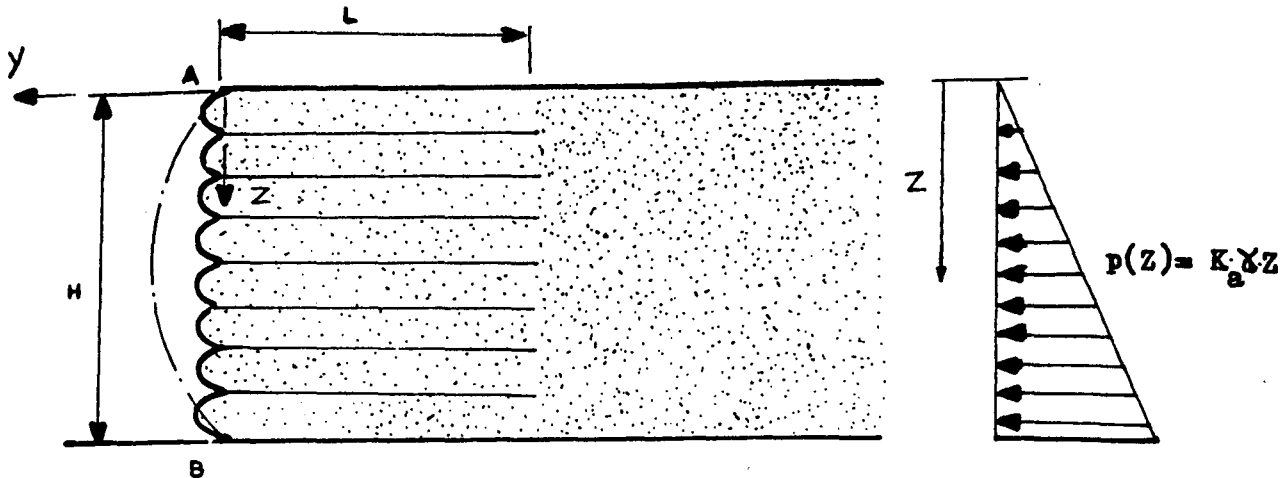
Fig(3-10a) Earth pressure distribution @ section A-B.

tie can be calculated by equation ($II.1$) derived in
Appendix(II)   which gives the internal work done as

$$U_i = \int_0^L \frac{T(x) \; dx}{2 \; A_r \; E_r} \quad \dots\dots\dots\dots\dots\dots\dots\dots\dots\dots \quad (3.38)$$

where

$T(x)$ =   function which gives the tension variation
along the tie

A_r =   cross-sectional area of the tie

E_r =   the Young's modulus of the tie material

By equating the external work done at a given tie level
and the strain energy stored in the tie, it is possible to
obtain an expression for the tie tension.

3.8.2.   Assumptions

To produce an analytical solution, assumptions regarding
the earth pressure distribution with the wall height, the
tension variation along the tie length and the deflected
shape of the wall have to be made.

3.8.2.1.   Pressure distribution over wall height

Different   pressure distributions with wall height can
be incorporated in equation (3.37) to calculate the external
work.   In the present study hydrostatic pressure distribution
is assumed Fig (3.10a) mainly to simplify the solution of the
equation.

For a wall without a surcharge the pressure at depth Z

below the wall surface is given by

$$p(Z) = K_a \cdot \gamma \cdot Z \quad \dots\dots\dots\dots\dots\dots\dots\dots (3.39)$$

3.8.2.2. Tension variation along a tie length

Observations on field structures[63,29] showed that the tension variation along the tie length may have the following characteristics:

(1)   The maximum tension occurs at a distance $(\hat{\beta}L)$ from the wall face Fig (3.11).   This distance varies according to the tie position in the reinforced earth wall.   It is small for ties lying at the bottom of the wall and increases with increasing wall height.   Therefore $\hat{\beta}$ may be assumed to vary between zero and 0.50 for real walls and $0 \leq \hat{\alpha} \leq 1$.

(2)   The tension decreases to zero at the free end of the tie.

In view of these observations two assumptions have been made regarding the tension distribution along the tie length. These are a linear distribution and a parabolic distribution as shown in Fig (3.11).   The strain energy stored in the tie was calculated from these tension distributions using equation (3.38).   For the assumed linear and parabolic tension variations, the strain energy stored in the tie was found to be

Linear $\qquad U_i = \dfrac{Tm^2 \cdot L}{6 \, A_r E_r} \quad \dots\dots\dots (3.40\ a)$

Parabolic $\qquad U_i = \dfrac{4}{15} \cdot \dfrac{Tm^2 L}{A_r E_r} \quad \dots\dots (3.40\ b)$
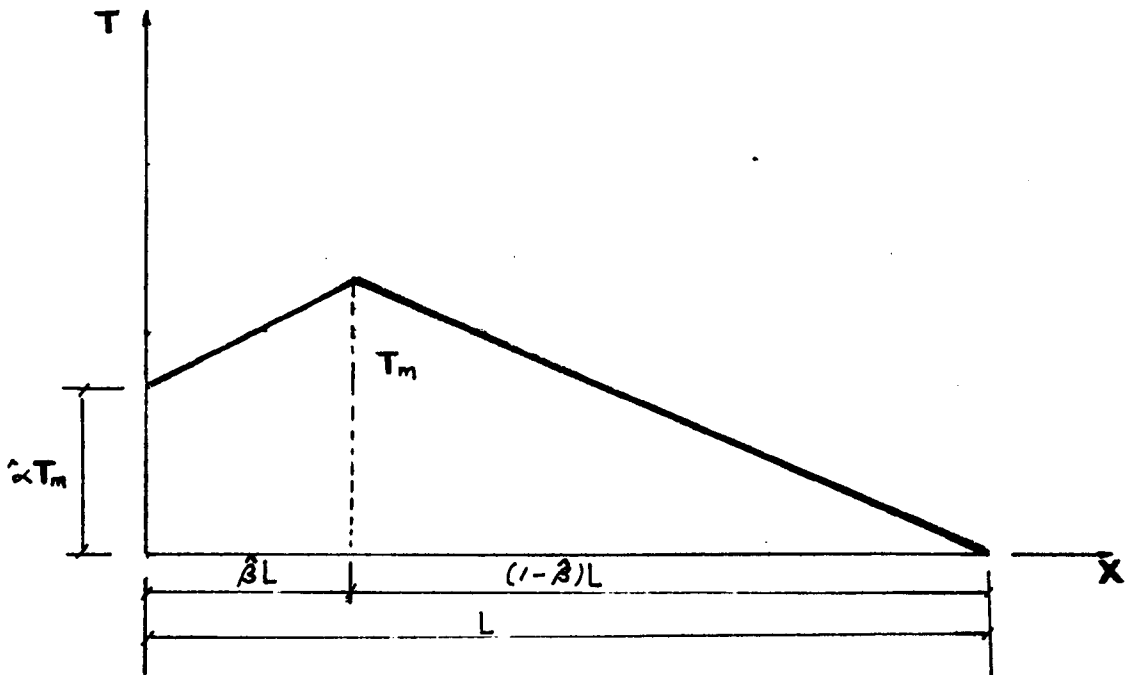
Fig.(3-11a) Linearly varying tension along a tie length.
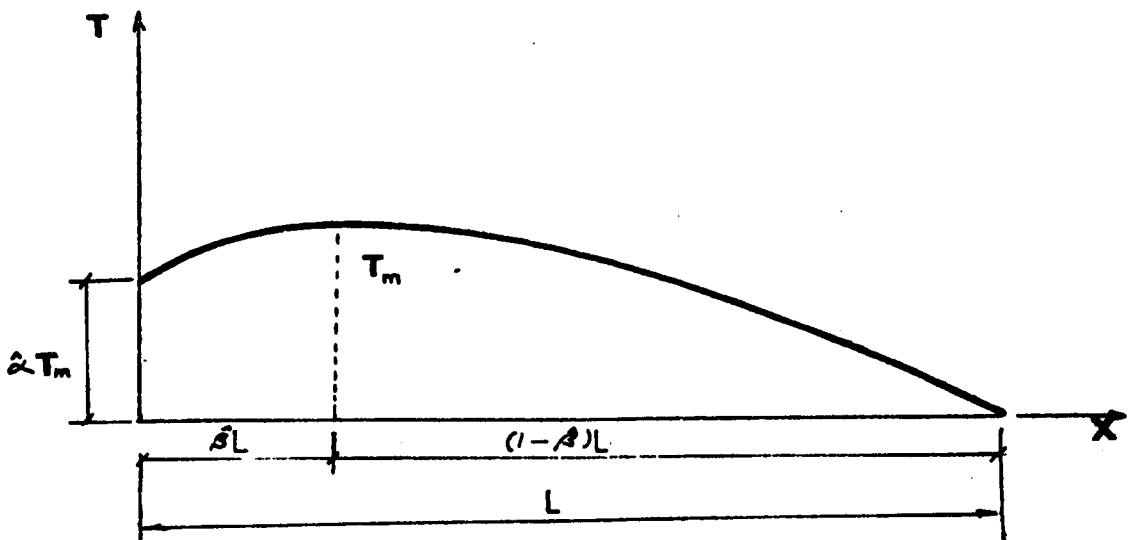
Fig.(3-11b) Parabolic variation of tension along a tie length.

Fig.(3-11) Assumed tension distribution along a tie length used in the derivation of the energy theory expressions.

respectively as shown in Appendix(III) ·

Tm is the maximum tension along the tie Fig(3.11).

3.8.2.3. Deflected shape of wall

The reinforced earth wall is assumed to behave as a
composite material with a constant elastic modulus E_q
, which is a function of the elastic modulus of the
tie material E_r, cross-sectional area A_r and the area of
the soil bounding the tie A^{so} and is given by

$$E_q = \frac{E_r . A_r}{A^{so}} \quad \text{Schlosser and Vidal[67]} \quad \ldots\ldots\ldots\ldots (3.41)$$

The deflected shape of the wall was approximated by
an approach similar to Jakobson[35] Fig (3.12). The
soil backfill was assumed to be initially in an at rest
condition and the horizontal pressure at depth Z below the
wall surface is given by

$$K_o . \gamma . Z. \quad \ldots\ldots\ldots\ldots\ldots\ldots\ldots\ldots\ldots\ldots\ldots\ldots (3.42)$$

As the wall deflects the pressure changes from an
at rest state to an active state characterized by the co-
efficient of active earth pressure K_a, the decrease in
pressure will be

$$(K_o - K_a) . \gamma . Z \quad \ldots\ldots\ldots\ldots\ldots\ldots\ldots\ldots (3.43)$$

As the pressure changes the zone near the wall face will tend
to fail. As a first approximation this zone is assumed to
be a wedge bounded by a plane inclined at $(45 + \phi/2)$ with the
horizontal. Assuming that the skin elements do not inter-

fere in the wall deflection, the displacement at depth Z is given by

$$y(Z)_1 = \frac{K_o - K_a}{E_q} \cdot \gamma \cdot Z \; \frac{H - Z}{\tan(45 + \Phi/2)} \quad \ldots\ldots\ldots\ldots (3.44a)$$

Since this equation includes the term $(K_o - K_a)$ it is referred to as the <u>pressure difference equation</u>. Or, if only the active earth pressure is assumed to cause this deformation, then the deflected shape of the wall is given as

$$y(Z)_2 = \frac{K_a}{E_q} \cdot \gamma \cdot Z \cdot \frac{H - Z}{\tan(45 + \Phi/2)} \quad \ldots\ldots\ldots\ldots (3.44b)$$

Since this equation is derived in terms of the active earth pressure coefficient K_a, it is referred to as <u>the active earth pressure equation.</u>

Equations (3.44a) and (3.44b) give a parabolic deflected shape of wall which is similar to the idealized deflected shape of wall shown in Fig (3.10b).
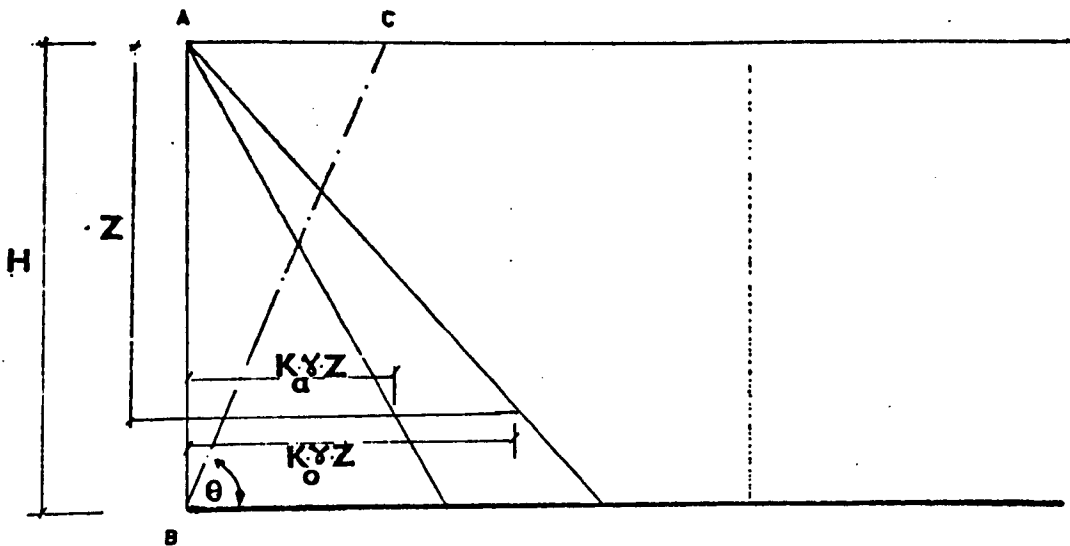
Fig.(3-12) Wall deflection parameters(After Jakobson(35)).

3.8.3 The Energy Theory

3.8.3.1. Introduction

Two approaches were used to obtain expressions for the tie tension, critical height of the wall failing by tie breaking, the safety factor against pull out failure and the adherence lengths of the ties from the energy theory. These methods are:

(1) A Total equilibrium energy approach in which the the external work is calculated first and then a distribution factor C_i is assumed in order to obtain the external work at each tie level. The strain energy stored at that wall level is equated to the external work. The governing equation is

$$U_i = C_i U_{ext} \dots\dots\dots\dots\dots\dots\dots\dots\dots\dots\dots\dots\dots\dots (3.45)$$

(2) A Local equilibrium energy approach in which the incremental external work at a depth h below the wall surface, over a small wall height ΔH, is equated to the strain energy of the tie calculated from the tie tension distribution. The governing equation is

$$U_i = \Delta U_{ext.} \quad \dots\dots\dots\dots\dots\dots\dots\dots\dots\dots\dots\dots (3.46)$$

3.8.3.2. Method 1: Total equilibrium energy approach

The total external work is calculated by adopting the general equation (3.37) and assuming a linear earth pressure distribution and equation (3.44a) for the wall deflection, i.e.

$$U_{ext} = S \int_{o}^{H} p(Z) . y(Z) . dZ$$

$$U_{ext} = S \int_{o}^{H} \frac{K_a . \gamma Z (K_o - K_a) \gamma Z . (H - Z) \; dZ}{E_q . \tan(45 + \phi/2)}$$

substituting for $E_q = \dfrac{E_r A_r}{A^{so}}$, $K_a = \dfrac{1 - \sin\phi}{1 + \sin\phi}$

and $K_o = (1 - \sin\phi)$ Jaky's [36] expression and simplifying, we get:

$$U_{ext} = \frac{\sin\phi \, K_a^{2.5} . \; S^2 \quad . \; \Delta H . \gamma^2 . H^4}{12 . A_r . E_r} \quad \dots\dots\dots (3.47a)$$

when the wall deflection equation (3.44b) is used instead of equation (3.44a). The external work expression will be

$$U_{ext} = \frac{K_a^{2.5} . S^2 . \Delta H \; \gamma^2 H^4}{12 . A_r . E_r} \quad \dots\dots\dots\dots (3.47b)$$

This work is assumed to be stored as an elastic strain energy in the ties. To get the external work done at each tie level, a certain distribution of the total work has to be assumed. This may be achieved by adopting a distribution factor C_i which must satisfy the condition $\sum_{i=1}^{n} C_i = 1$.

Linear, parabolic and sinusoidal modes of the external work distribution were considered.

The linear distribution factor, first advanced by Schlosser and Vidal [67] is of the form

$$C_i = \frac{2i}{n(n+1)} \qquad \dots\dots\dots\dots\dots\dots\dots\dots\dots\dots (3.48a)$$

The parabolic and sinusoidal distribution factors suggested by the author are

$$C_i = \frac{6i(n-i)}{n(n^2-1)} \qquad \text{parabolic} \quad \dots\dots\dots (3.48b)$$

$$C_i = \sin\frac{i\pi}{n}.\tan\frac{\pi}{2n} \qquad \text{sinusoidal} \quad \dots\dots\dots (3.48c)$$

These latter two variations are almost identical Fig (3.13), therefore either of them may be assumed for nonlinear energy variation with wall depth.

Using Equation (3.45) and substituting for U_i, U_{ext} and C_i from equations (3.40), (3.47) and (3.48), the expressions for the tension in the ties from the total energy equilibrium are obtained.

3.8.3.2.1. <u>Expressions from the total equilibrium energy approach</u>

The assumptions used in the derivation of the energy expressions are summarized in Table (3.1) . It is possible to get eight sets of expressions by combining the tension variation along the tie length, the energy distribution with wall depth and the wall deflection assumptions. The general form of these equations are:

(i) The tie tension is given by

$$T_i = \sqrt{[C_1.K_a^{2.5}.\frac{\Delta H}{L}]} \ . \ S.\Upsilon.H^2 \dots\dots\dots (3.49)$$

(ii)   The maximum tension

$$T_{max} = \sqrt{\left[C_2 . K_a^{2.5} . \frac{\Delta H}{L} \right]} \ S. \gamma . H^2 \ \ldots\ldots\ldots (3.50)$$

(iii)   The critical wall height for wall failing by tie breaking

$$H_c = \left[\frac{R_t}{S.\gamma} \sqrt{\frac{C_3 L}{\Delta H . K_a^{2.5}}} \right]^{\frac{1}{2}} \ldots\ldots\ldots\ldots (3.51)$$

(iv)   The safety factor against pull out

$$SF = \frac{2b \ L^{3/2} \ f}{SH^2} . \sqrt{\frac{C_4 \ \Delta H.}{K_a^{2.5}}} \ \ldots\ldots (3.52)$$

(v)   The adherence length

$$L_a = \left[\sqrt{\left(\frac{C_5 . K_a^{2.5}}{\Delta H} \right)} . \frac{SH^2}{2 \ b \ f} \right]^{\frac{2}{3}} \ldots (3.53)$$

where C_1, C_2, C_3, C_4 and C_5 are coefficients. Their values depend on the assumptions adopted in the derivation of each equation. The values of these coefficients are shown in Table (3.2) for each set of assumptions.
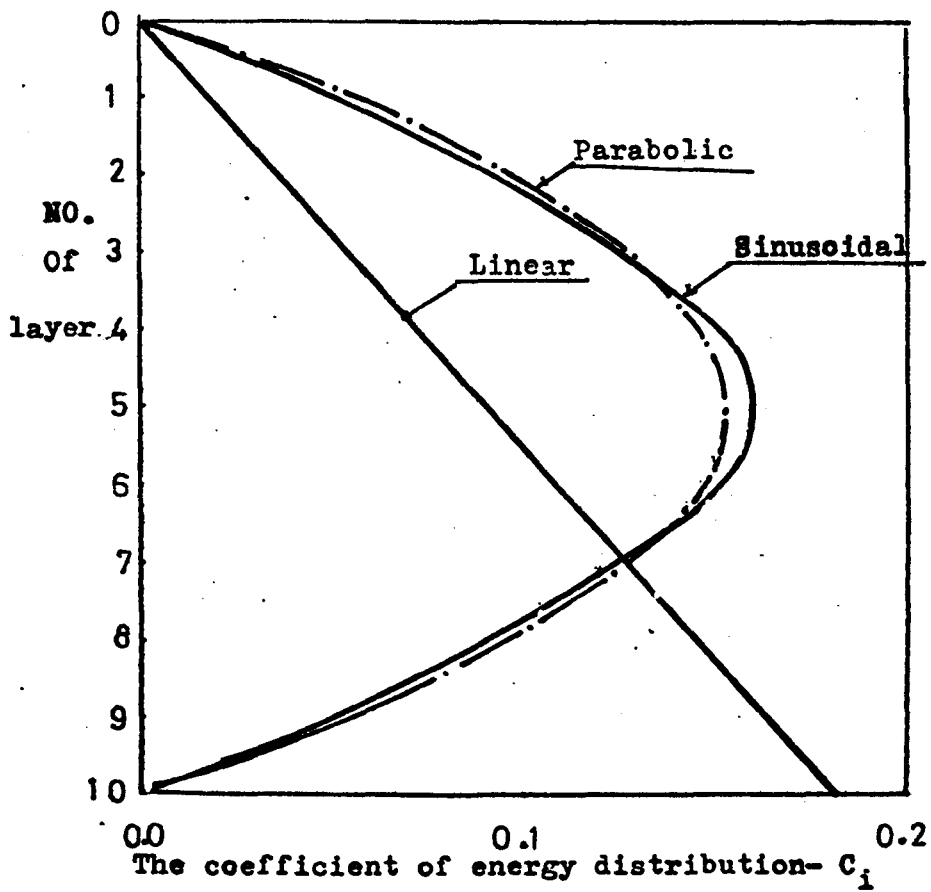
Fig(3;3) Assumptions of strain energy distribution with wall depth

Approaches \ Assumptions	Tension distribution over the tie length	The strain energy distribution with wall height	The deflected shape of the wall
Total equilibrium	Linear Fig (3.11a)	Linear, i.e. $c_i = \dfrac{2i}{n(n+1)}$	Using Eq.(3.44a) derived by assuming pressure difference
	Parabolic Fig(3.11b)	Parabolic, i.e. $c_i = \dfrac{6i(n-i)}{n(n+1)(n-i)}$	Using Eq.(3.44b) derived by assuming active earth pressure
Local equilibrium	Linear Fig (3.11a)		Using Eq.(3.44a) derived by assuming pressure difference
	Parabolic Fig(3.11b)		Using Eq.(3.44b) derived by assuming active earth pressure

TABLE (3.1)   Summary of the approaches and assumptions used in the derivation of the energy theory expressions.

Coefficients / Assumptions	C_1	C_2	C_3	C_4	C_5
T.L.L.D.	$\dfrac{i\,\sin\phi}{n(n+1)}$	$\dfrac{\sin\phi}{(n+1)}$	$\dfrac{(n+1)}{\sin\phi}$	$\dfrac{in(n+1)}{\sin\phi}$	$\dfrac{\sin\phi}{in(n+1)}$
T.L.L.A.	$\dfrac{i}{n(n+1)}$	$\dfrac{1}{n+1}$	$(n+1)$	$in(n+1)$	$\dfrac{1}{in(n+1)}$
T.L.P.D.	$\dfrac{3i(n-i)\sin\phi}{n(n^2-1)}$	$\dfrac{3n.\sin\phi}{4(n^2-1)}$	$\dfrac{4}{3}\dfrac{(n^2-1)}{n.\sin\phi}$	$\dfrac{in(n^2-1)}{3(n-i)\sin\phi}$	$\dfrac{3(n-i)\sin\phi}{in\,(n^2-1)}$
T.L.P.A.	$\dfrac{3i(n-i)}{n(n^2-1)}$	$\dfrac{3n}{4(n^2-1)}$	$\dfrac{4}{3}\dfrac{(n^2-1)}{n}$	$\dfrac{in(n^2-1)}{3(n-i)}$	$\dfrac{3(n-i)}{in(n^2-1)}$
T.P.L.D.	$\dfrac{i\sin\phi}{1.6n(n+1)}$	$\dfrac{\sin\phi}{1.6(n+1)}$	$\dfrac{1.6(n+1)}{\sin\phi}$	$\dfrac{1.6.i.n(n+1)}{\sin\phi}$	$\dfrac{\sin\phi}{1.6in(n+1)}$
T.P.L.A.	$\dfrac{i}{1.6n(n+1)}$	$\dfrac{1}{1.6(n+1)}$	$1.6(n+1)$	$1.6in(n+1)$	$\dfrac{1}{1.6in(n+1)}$
T.P.P.D.	$\dfrac{15i(n-i)\sin\phi}{8n\,(n^2-1)}$	$\dfrac{15}{32}\dfrac{n\,\sin\phi}{(n^2-1)}$	$\dfrac{32}{15}\dfrac{(n^2-1)}{n\,\sin\phi}$	$\dfrac{8}{15}\dfrac{in(n^2-1)}{(n-i)\sin\phi}$	$\dfrac{15}{8}\dfrac{(n-i)\sin\phi}{i.n(n^2-1)}$
T.P.P.A.	$\dfrac{15i(n-i)}{8n\,(n^2-1)}$	$\dfrac{15}{32}\dfrac{n}{(n^2-1)}$	$\dfrac{32}{15}\dfrac{(n^2-1)}{n}$	$\dfrac{8}{15}\dfrac{i.n(n^2-1)}{(n-i)}$	$\dfrac{15}{8}\dfrac{(n-i)}{i\,n\,(n^2-1)}$

TABLE (3.2). The values of the Coefficients C_1, C_2, C_3, C_4 and C_5 corresponding to the different assumptions in the total equilibrium energy equations.

Abbreviations: The abbreviations shown in Table (3.2) stand for the assumptions adopted in the derivation of the tie tension expressions as indicated in Table (3.3).

TABLE(3.3) <u>Abbreviations adopted in the designation of the</u>

<u>expressions derived by the total equilibrium energy approach</u>

Energy Approach	Tie tension variation	Energy distribution over wall height	Earth pressure in wall deflection
<u>T</u>otal	<u>L</u>inear or <u>P</u>arabolic	<u>L</u>inear or <u>P</u>arabolic	<u>A</u>ctive or <u>D</u>ifference

3.8.3.3. <u>Method 2: Local equilibrium energy approach</u>

Using the local equilibrium energy approach based on equation (3.46), four sets of equations are obtained from different combinations of assumptions shown on Table (3.1). These equations are of the form:

(i) Tension in the tie

$$T = \left(D_1 \cdot \frac{K_a^{2.5}}{L} \right)^{\frac{1}{2}} \cdot \gamma \cdot h \cdot \Delta H.S \cdot \sqrt{H-h} \quad \ldots (3.54)$$

(ii) The maximum tension in the tie

$$T_{max} = \left(D_2 \frac{K_a^{2.5}}{L} \right)^{\frac{1}{2}} \cdot \gamma \Delta H.S.H.^{3/2} \quad \ldots (3.55)$$

(iii) The critical wall height

$$H_c = \left(\frac{R_t}{\gamma \cdot \Delta HS} \cdot \sqrt{\frac{D_3 L}{K_a^{2.5}}} \right)^{\frac{2}{3}} \quad \ldots (3.56)$$

(iv)   The safety factor against tie pull out

$$SF = \frac{2b \, f \, L^{3/2}}{S. \Delta H} \cdot \frac{1}{\sqrt{(D_4 K_a^{2.5} \, (H - h)}} \quad \ldots\ldots\ldots (3.57)$$

(v)   The adherence length

$$L_a = \left(\left(D_5 \cdot K_a^{2.5} \, (H - h) \right)^{\frac{1}{2}} \frac{S \Delta H}{2 \, b \, f} \right)^{2/3} \quad \ldots\ldots (3.58)$$

where D_1, D_2, D_3, D_4 and D_5 are coefficients.   Their values depend on the assumptions adopted in the derivation of the particular equation.   A list of the values of these coefficients is shown on Table (3.4) for each set of assumptions.

TABLE (3.4) The values of the coefficients D_1, D_2, D_3, D_4 and D_5 corresponding to the different assumptions in the local equilibrium energy approach

Coefficient / Assumptions	D_1	D_2	D_3	D_4	D_5
LO.L.D	$6.\sin\phi$	$\frac{8}{9}\sin\phi$	$\frac{9}{8\sin\phi}$	$6\sin\phi$	$6\sin\phi$
LO.L.A.	6	$\frac{8}{9}$	$\frac{9}{8}$	6	6
LO.P.D.	$\frac{15}{4}\sin\phi$	$\frac{5}{9}\sin\phi$	$\frac{9}{5\sin\phi}$	$\frac{15}{4}\sin\phi$	$\frac{15}{4}\sin\phi$
LO.P.A.	$\frac{15}{4}$	$\frac{5}{9}$	$\frac{9}{5}$	$\frac{15}{4}$	$\frac{15}{4}$

Abbreviations

The abbreviations stand for the assumptions adopted in the derivation of a particular equation as indicated in Table (3.5)

TABLE (3.5)   Assumptions adopted in the local equilibrium
               approach

Energy Approach	Tie tension variation	Earth pressure in wall deflection
LOcal	Linear or Parabolic	Active or Difference

3.8.4 Comparison between the energy theory tie tension expressions

Twelve tie tension expressions have been obtained by adopting different assumptions in the energy theory.   It is necessary to choose only some of these equations to facilitate further comparative analysis with the other theories and test results.

To help in visualizing the effect of the different assumptions, a wall comprising 15 layers and a $\emptyset$ value of 40° was assumed.   The tie tension expressions given by the energy theory were expressed in the general form

$$T = A_i \sqrt{\left(\frac{\sin\phi \cdot \Delta H \cdot K_a^{2.5}}{L} \right)} \cdot S \cdot \gamma \cdot H^2 \quad \ldots\ldots\ldots(3.59)$$

where A_i is coefficient which is different for different assumptions and its values are shown in Table (3.6) against the corresponding assumptions:

TABLE(3.6)   The values of the coefficient A_i corresponding to different assumptions

Assumption	Coefficient A_i
T.L.L.D.	$\sqrt{\dfrac{i}{n(n+1)}}$
T.L.P.D.	$\sqrt{\dfrac{3i(n-i)}{n(n^2-1)}}$
T.P.L.D.	$\sqrt{\dfrac{i}{1.6n(n+1)}}$
T.P.P.D.	$\sqrt{\dfrac{15i(n-i)}{8n(n^2-1)}}$
T.L.L.A.	$\sqrt{\dfrac{i}{n(n+1)\sin\emptyset}}$
T.L.P.A.	$\sqrt{\dfrac{3i(n-i)}{n(n^2-1)\sin\emptyset}}$
T.P.L.A.	$\sqrt{\dfrac{i}{1.6n(n+1)\sin\emptyset}}$
T.P.P.A.	$\sqrt{\dfrac{15i(n-i)}{8n(n^2-1)\sin\emptyset}}$
LO.L.A.	$\dfrac{i}{n^2}\sqrt{\dfrac{6(n-i)}{\sin\emptyset}}$
LO.L.D.	$\dfrac{i}{n^2}\sqrt{6(n-i)}$
LO.P.A.	$\dfrac{i}{n^2}\sqrt{\dfrac{3.75(n-i)}{\sin\emptyset}}$
LO.P.D.	$\dfrac{i}{n^2}\sqrt{3.75(n-i)}$

N.B. The abbreviations shown in this table stand for the assumptions adopted in deriving a particular expression as shown on Tables (3.3), (3.5).

The values of the coefficient A_i were computed and the results are shown on Figs (3.14) to (3.16). Obviously, particular patterns of tie tension distribution with wall height emerged with similarities. A reduction in the number of equations can be made by choosing two from each general approach. The following expressions have been selected:

(i)   T.L.L.D.)
)   Fig (3.14)
(ii) T.P.P.D.)

(iii) LO.L.A.   )
)   Fig (3.15)
(iv) LO.L.D.   )

(v)   T.L.L.A.)
)   Fig (3.16)
(vi) T.L.P.A.)

It will be seen in Chapter Five that the tie tension expression based on the local equilibrium energy approach has been recommended in designing for the internal stability of reinforced earth walls.

n=15

Parabolic tension & linear energy
assumptions.(T.P.L.D.)

linear tension & linear
energy assumptions.(T.L.L.D.)

Parabolic tension & parabolic
energy assumptions(T.P.P.D.)

Linear tension & parabolic
energy assumptions
(T.L.P.D.)
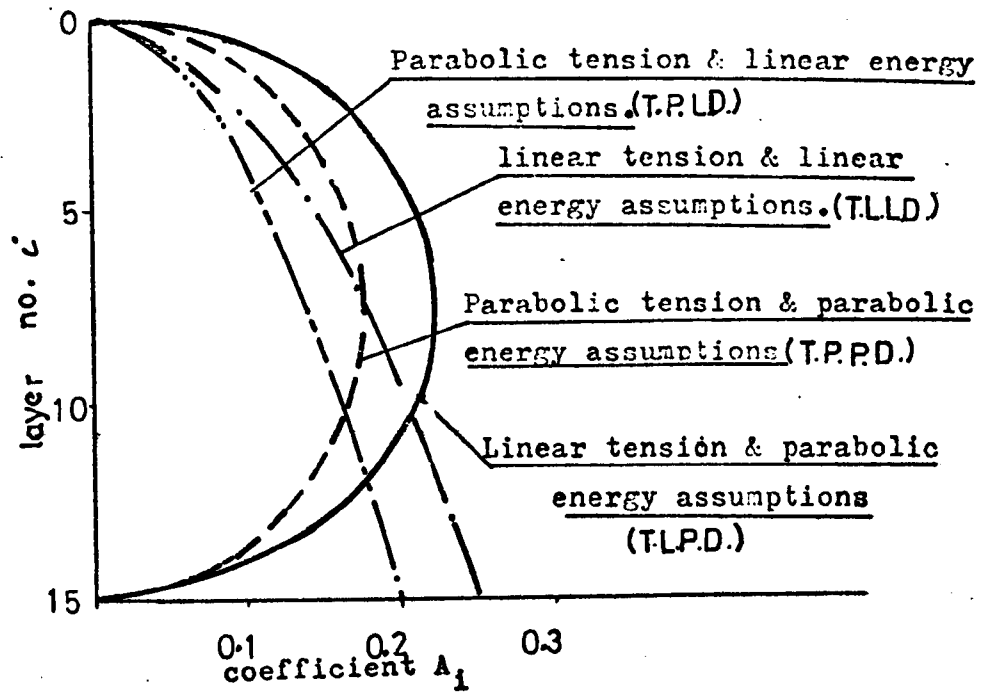
Fig(3.14) Comparison between tension expressions derived from
energy theory total equilibrium approach. (Pressure difference

n = 15

Linear tension & active earth pressure
assumptions.(L.O.L.A.)

Linear tension& pressure diff$\underline{^{nce}}$.
assumptions. also parabolic
tension & active earth press.
assumptions.(L.O.L.D. &
LO.P.A.)

Parabolic tension ,pressure
difference assumptions.
(L.O.P.D.)
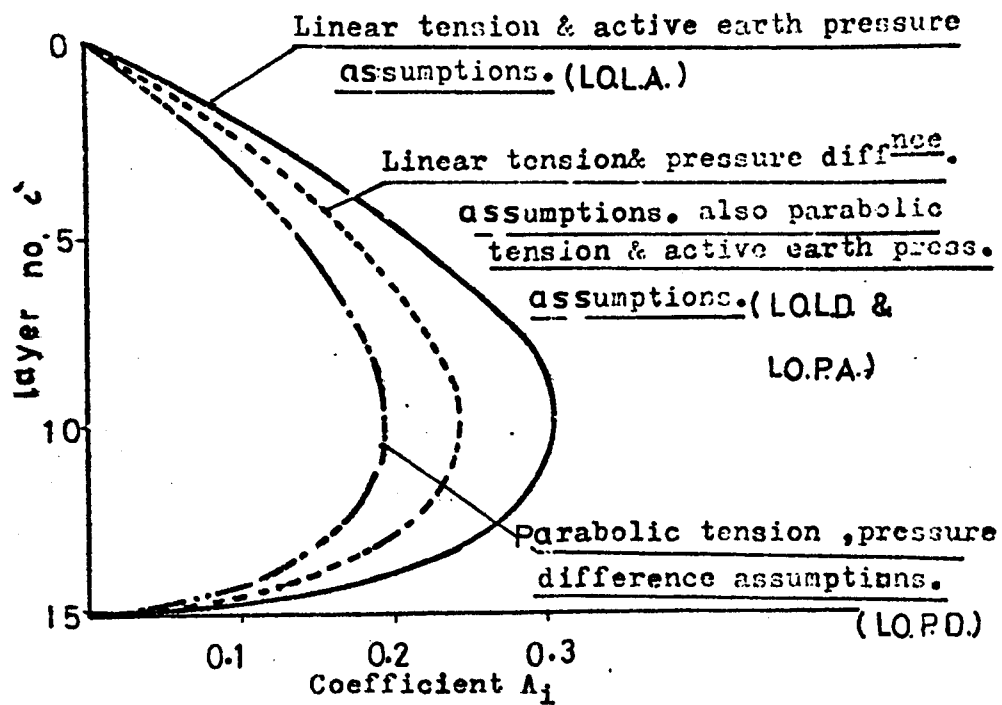
tension
Fig(3.15) Comparison between/ expressions derived from energy theory
local equilibrium approach.

$$n = 15$$

0

Linear tension & linear energy assumptions
(T·L·L·A·)

Parabolic tension & linear energy
assumptions.(T.P.L.A.)

Parabolic tension &parabolic energy
assumptions (T. P.P.A)

Linear tension &parabolic energy
assumptions. (T.L.P.A.)

layer no. i

5

10

15

0.1   0.2   0.3

coefficient A_i
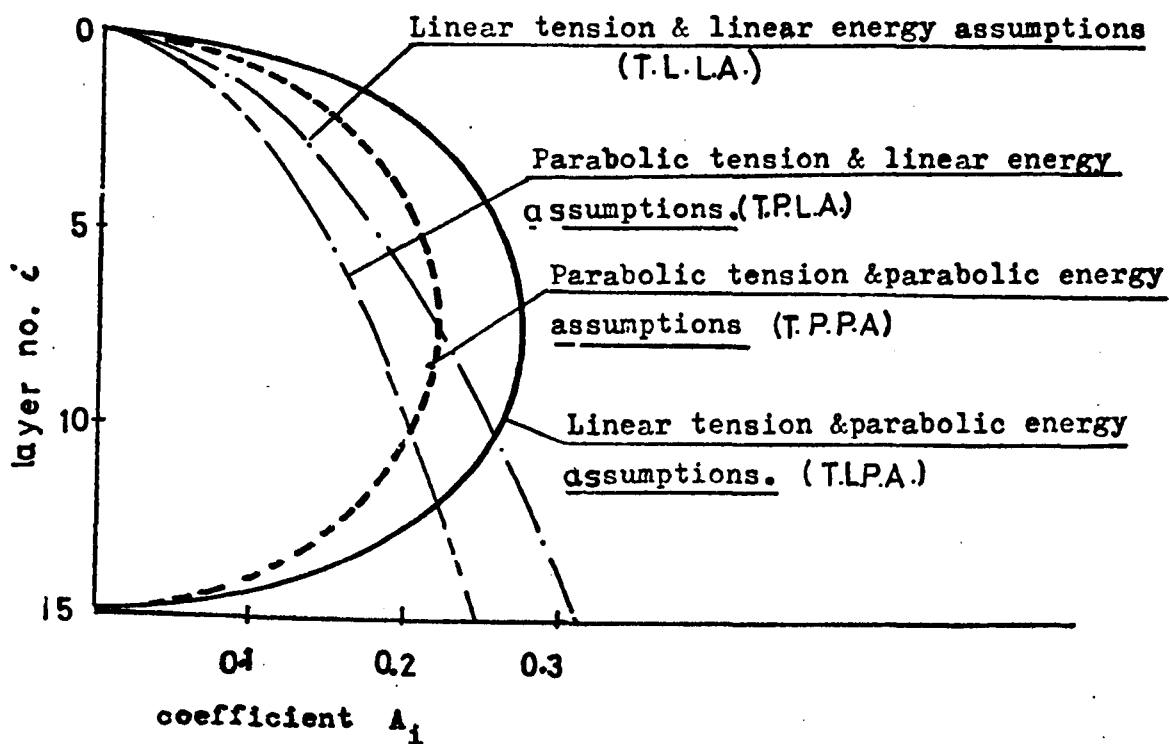
Fig(3.16) Comparison between tension expressions derived from energy
theory total equilibrium approach(Active earth pressure
assumptions)

3.8.5 Comparison between the energy theory and the existing theories

The analytical design expressions derived from the energy theory contain the same parameters, e.g. (K_a, L, h, ΔH, S, H), as the existing theories. However, the functional relationships between these parameters is different in the energy and the existing theories.

Because of these differences, it has been found difficult to compare generally between the energy and the existing theories. A detailed discussion and comparisons will be presented in future chapters in terms of test results.

3.9 Conclusions

The original methods of the reinforced earth wall design were based on the Rankine and Coulomb earth pressure theories, which assume that the backfill of a reinforced earth wall is homogeneous and isotropic. This assumption is unrealistic, since the presence of the ties in the soil mass modifies its properties. The Rankine theory neglects the shear stresses developed at the soil/tie interface.

For a wall with large numbers of layers, having a smooth back and assuming a linear tension variation over wall height in the Coulomb theory, the Rankine and Coulomb theories give identical tension expressions. The Coulomb theory can, however, be applied for walls with irregular geometry and a rough back.

Comparison between the Rankine, Coulomb, the Trapezoidal and Meyerhof's tie tension expressions showed that the latter two methods predict higher tie tensions than the Rankine and Coulomb theories. For practical purposes, i.e. when H/L ratio approaches unity and the values of $\emptyset$ are relatively high, the differences in predicted tie tensions, between the Rankine, Coulomb, the Trapezoidal and Meyerhof are relatively small (i.e. $\leq$ 25 per cent of Rankine values).

The Rankine theory has mainly been used in practice. This theory gives a linear tension distribution with wall height, implies a maximum tie tension near the wall face, and overestimates the tie tensions when applied to model reinforced earth walls.[7,17]

The methods of reinforced earth wall design based on an ultimate strength concept such as Banerjee's method, have been found [63] unsuitable for the reinforced wall design, mainly because these methods do not permit calculation of stresses in the ties at different wall levels.

A new energy theory is presented. This is based on the premise that the external work done by the earth pressure is stored as an elastic strain energy in the ties. By assuming an earth pressure distribution with wall height, a deflected shape of wall and a tie tension variation over the tie length, analytical expressions which can be used for the reinforced earth wall design were obtained.

Six energy expressions for tie tension have been chosen as representing the ranges of tension distribution with wall height and tie tension magnitudes,indicated by a simple comparative analysis carried out between the energy expressions.

It will be shown in Chapter Five that the local equilibrium energy approach assuming a linear tension variation over the tie length and an active earth pressure in the wall deflection equation (LO.L.A.), gives good agreement with the observed model wall behaviour.

CHAPTER FOUR

THE MODEL DESIGN, WALL BUILDING PROCEDURE AND INSTRUMENTATION

4.1. Introduction

The use of models in the solution of soil mechanics problems is an accepted practice.[37,53,56,71] Two types of models have mainly been used: Those which are intended to predict the detailed behaviour of the prototype and in which the principles of similitude are fully satisfied and the second types are those which serve as prototypes themselves and these require that the basic assumptions inherent in the analysis are satisfied, e.g. plane strain conditions.

In the present investigation the latter type of model was adopted. This was thought to be more appropriate in understanding the prototype wall behaviour on a qualitative basis, in testing the theories that may be used in designing full scale structures, in checking the theoretical assumptions on which the theoretical analysis was based and in examining different parameters related to the design of full scale walls.

This chapter will describe the test apparatus including the instrumentation for measuring stresses in the ties and the soil, and strains in the soil.

4.2. Details of Test Apparatus

4.2.1 The Model

Plane strain conditions were simulated by a rigid-sided open-fronted plywood box, Fig (4.1). The dimensions were chosen to give reasonable volume of sand which could be handled by one person. A maximum wall height of 500 mm was chosen to give measurable stresses and deformations in the wall. The width of the model was decided by adopting a width upon height ratio greater than 1·3, to minimize the effect of the side

ELEVATION

SIDE VIEW

PLAN
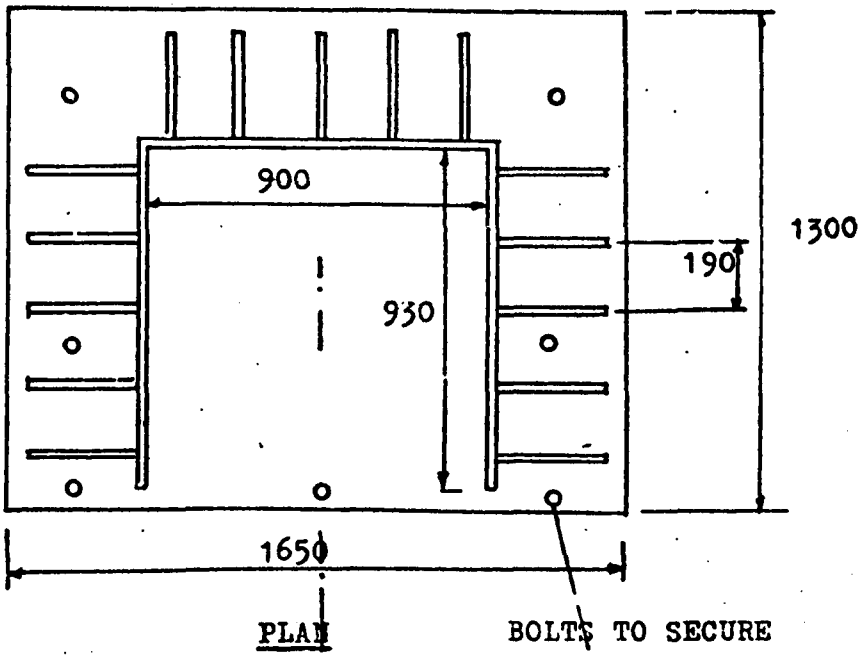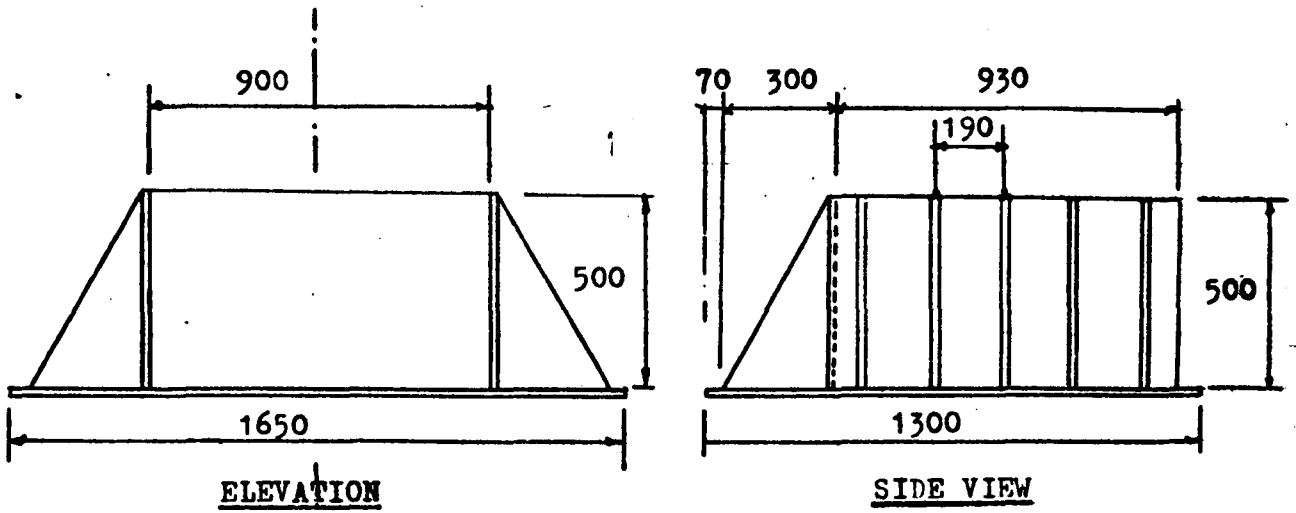
BOLTS TO SECURE
BASE OF BOX TO
THE FLOOR.

All dimensions are in mm

Fig. 4.1 Test Box.

wall shear stresses in reducing the earth pressure force on
the wall face.[43,58]   The length of the model was determined
by considering a length of the reinforced earth wall which
is approximately equal to the wall height and a distance
between the end of the wall and the rear side of the model
which reduces the effect of the model rear side on the internal
stresses.   Tests dealing with this effect will be described
later in the main test series.

4.2.2   Other features of the test apparatus

These includeda simple raining device consisting of a
perforated sand container which was adjustable to a constant
height above the layer being deposited to ensure a constant
density.   A false front was made for the box comprising five
perspex planks slotted into the sides of the box, Figs (4.2
and 4.3) to prevent excessive forward wall movement and
spillage of sand, to mount strain measuring devices at
different levels and to provide, through an aluminium bracer
(Fig 4.4 and 4.5) temporary support to the facing elements
while the wall was under construction.

4.2.3   Skin elements

Previous mention of rigid and flexible skin elements
in full scale walls has been made in Chapter One.   Since the
skin elements are assumed not to affect the internal stability
of the reinforced earth wall, the present study is restricted
to rigid skin elements only.

These were designed such that they could rotate freely
on each other to simulate the full scale panel behaviour.
The rigidity was ensured by adopting 6 mm thick perspex
panels.   More details about these panels will be given in
Chapter Five.

4.2.4   The soil

Dry sand was used in this investigation.   This sand had
a particle size distribution shown in Fig (4.6) and a specific
gravity of 2.65.   The maximum and minimum dry densities

Perspex spacer for mounting the strain coil

Elevation

100^{mm}

$8mm$ 900   mm $8mm$

25 mm
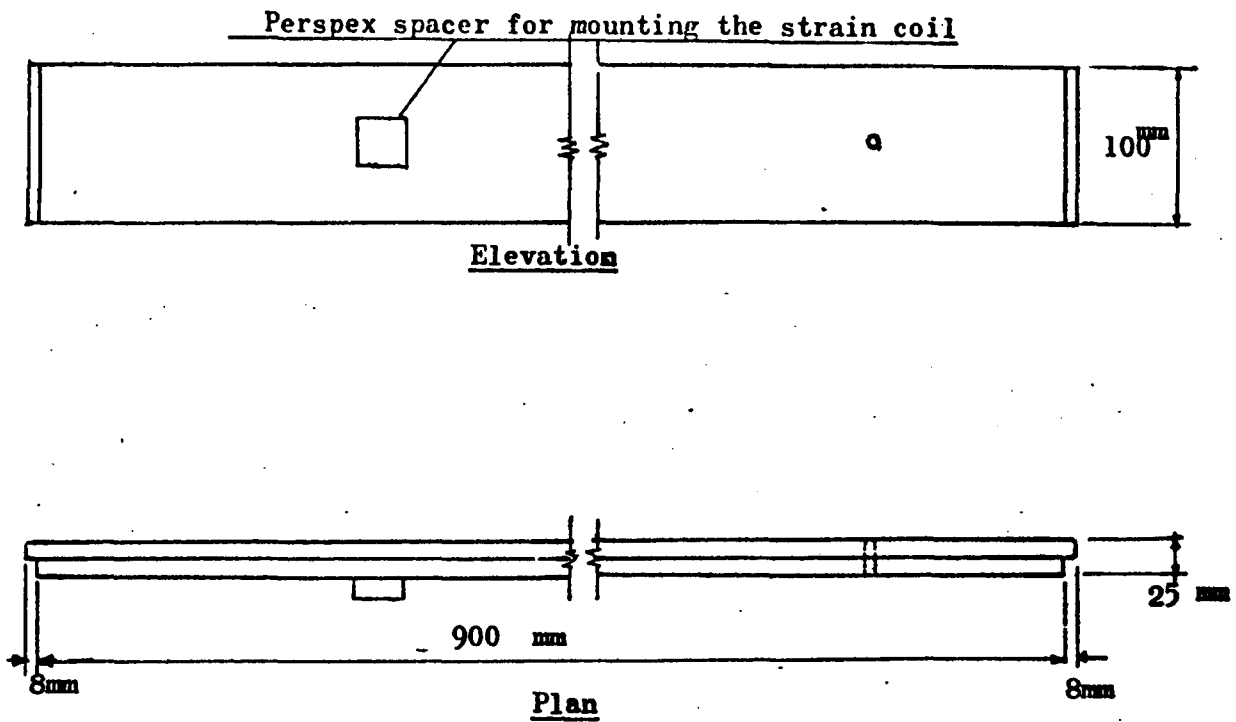
Plan

Fig 4.2   Details of a perspex plank

Aluminium clamps
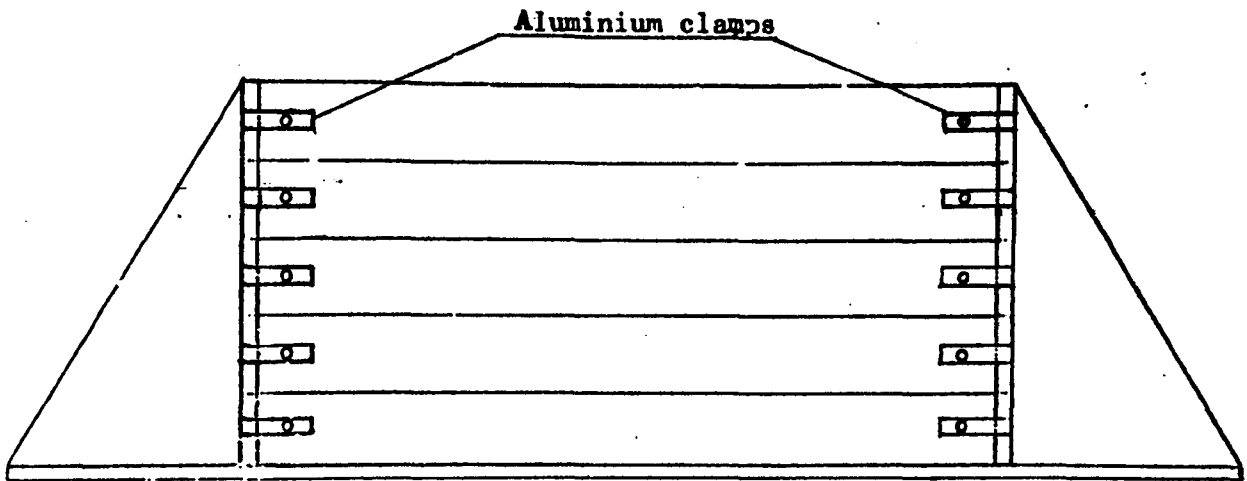
Fig. 4.3 Front view of the model with 5 perspex planks.
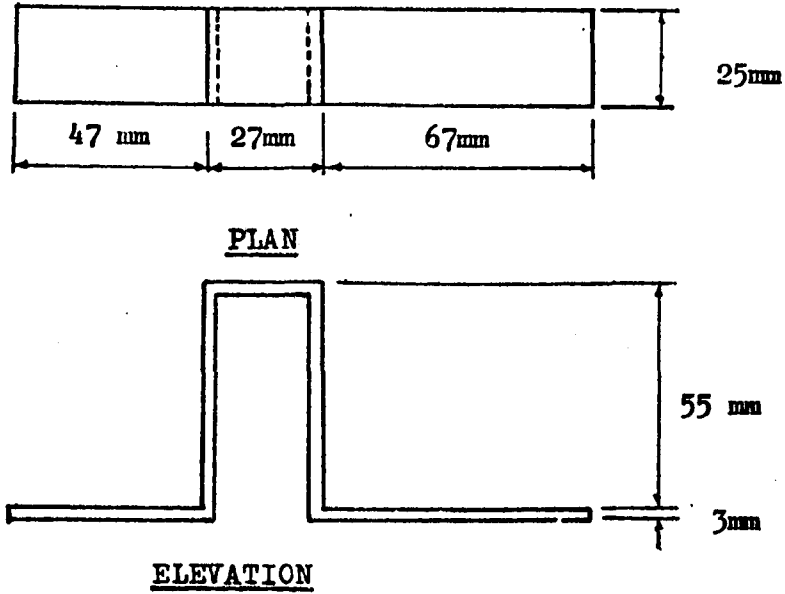
Fig.44 Aluminium bracer (used for wall construction.)
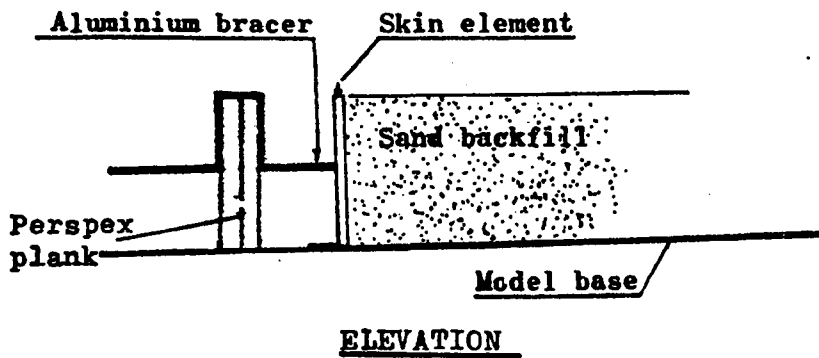
Fig.45 Skin element supported by an aluminium bracer
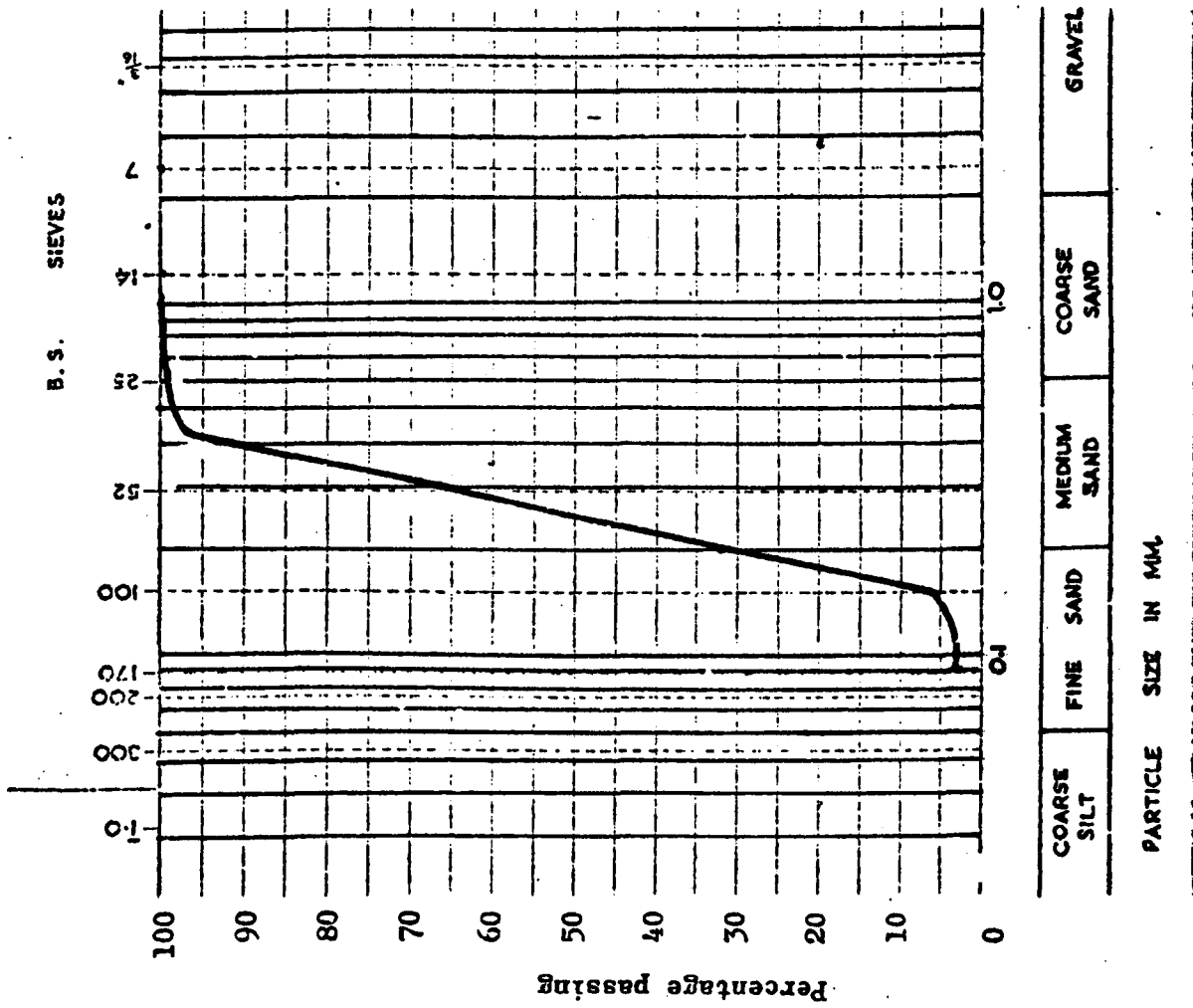
Fig. 4.6 Particle size distribution of the sand

determined according to reference (39), were 1.6954 and 1.3970 gm/cm^3 respectively.

The sand density has been shown previously to have little effect on the reinforced earth wall behaviour.[45] The present study was carried out at an average sand density of 1.6145 $\pm$ .0100 gm/cm^3.   This corresponds to a relative density of 76.5%.

The shear strength of the sand was measured using 100 mm diameter, and 200 mm high triaxial samples, tested in a dry and saturated condition.   These gave an angle of internal friction $\emptyset = 40.0^o \pm .50^o$ as shown in Figs (4.7) and (4.8).

4.2.5 The Ties

It has been noted that reinforced earth walls can fail by one of two mechanisms: (a) Breaking of the ties and (b) Slippage of the ties.   To study stability against breaking it was necessary to use a thin material for the ties such as aluminium foil, but to study slippage a more rigid tie such as perspex could be used.

Because of this, aluminium ties were cut in widths varying from 3 mm to 7 mm of thickness ranging between 20 and 45 μm.   The perspex ties were cut in 22 mm width from perspex sheets approximately 1.5 mm thick.

The ties were provided with extensions made of adhesive tape to allow for attachment to the perspex panels.

The coefficient of friction between the ties and the sand was determined using a controlled stress shear box, 134mm by 98.6 mm in plan, which was filled with compacted sand average density equal to 1.590 gm/cm^3.

Precautions were taken to ensure uniform distribution of the vertical stress and the effects from edges of the box were accounted for by conducting calibration tests while the box was empty, Figs (4.9a) and (4.9·b).

The coefficients of friction were found to be :
Aluminium foil/sand coefficient of friction
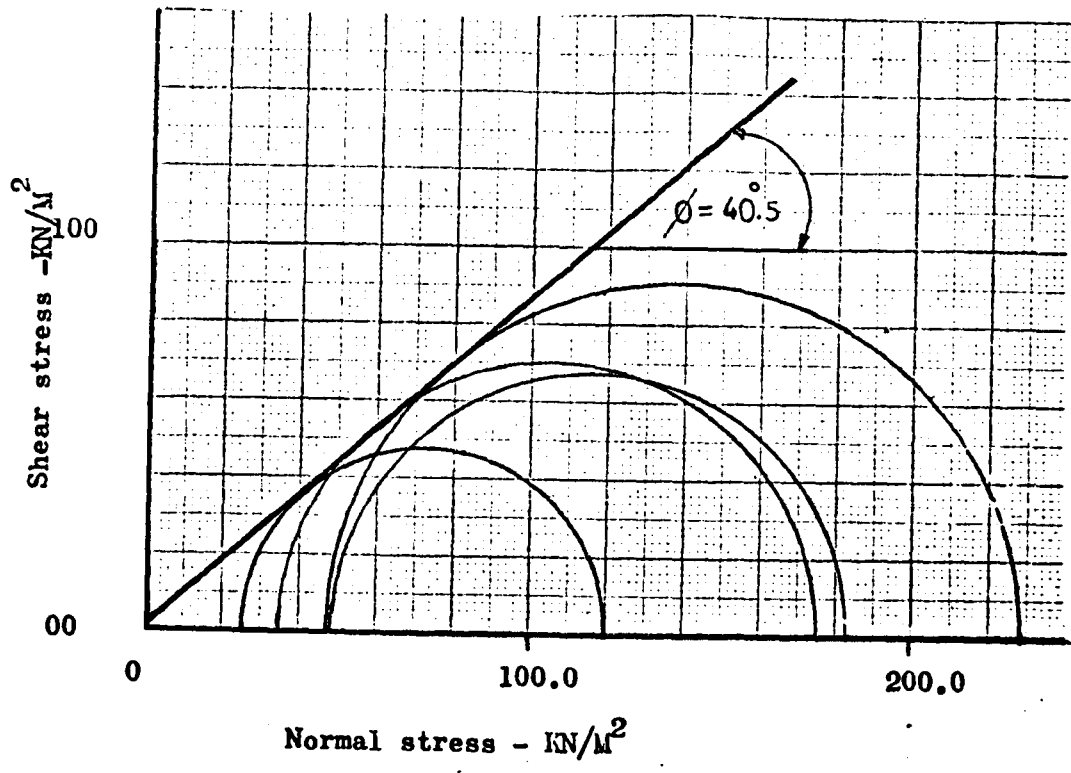
Fig. 4.7 Mohr envelopes for sand tested in a dry state (Triaxial test)
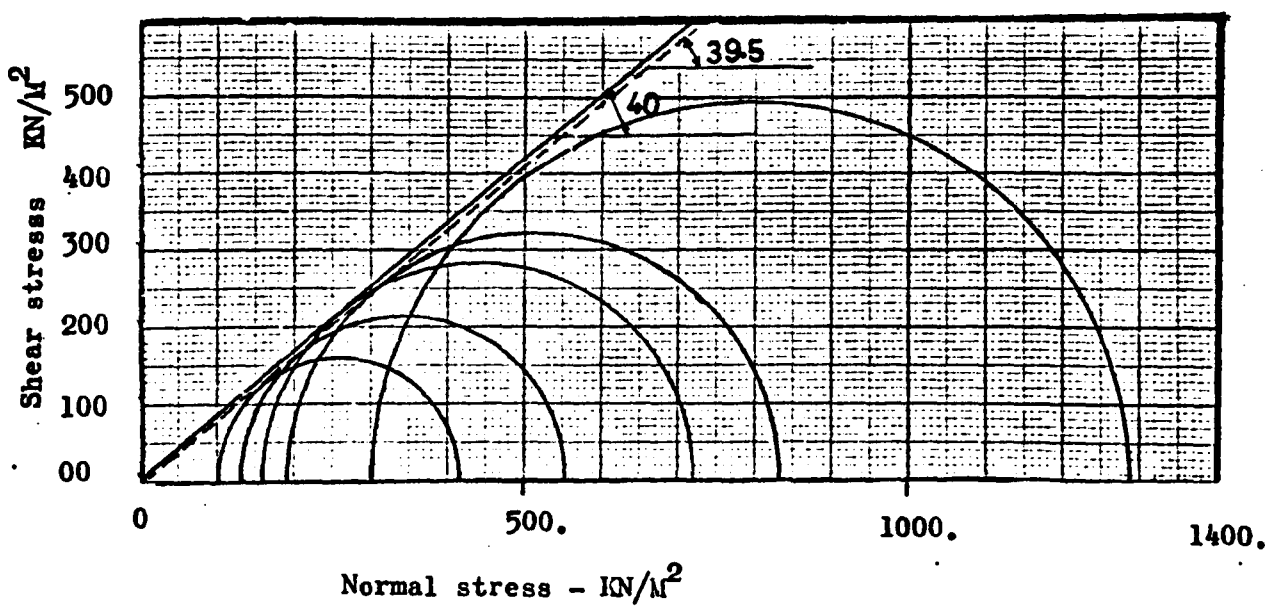
Fig. 4.8 Mohr envelopes for sand tested in a drained condition (Triaxial test)

f = 0.517, Fig (4.10a); perspex/sand coefficient of friction f = 0.398 (Fig 4.10b).

The aluminium foil/sand coefficieint of friction was also determined from a direct pull out test, Fig (4.11), which gave f = 0.503 as shown in Fig (4.12).

4.3   Wall Construction

The lowest section of the perspex false front was placed in position and clamped.   The lower panels were erected 50 to 70 mm behind it using spacers between the panels and the false front.   The panels were prevented from slipping forward by a small perspex upstand fixed in front of them.

To prevent the sand from spilling around the ends of the wall facing elements, cotton wool was packed between them and the sides of the box, Fig (4.13).

The sand was weighed and introduced behind the facing panels in 50 mm thick layers by pouring from the sand container held at a constant height of 500 mm above the layer being placed.   Each layer was levelled off horizontally and checked by a spirit level.

On reaching the level of the lowest series of ties, the ties were fixed to the panels, then laid on the soil surface. Construction proceeded in the same manner for subsequent layers.   The density of the sand backfill was determined from the known weight of the sand and the volume occupied.

4.4   Sand Density Control

One of the main problems in tests involving sand is in ensuring a uniform density throughout the volume of the container.

Preliminary tests were carried out on sand compacted by tamping, vibration and by a raining device, and the results indicated that deposition by raining gave a more consistent density than the other methods.

The density of the sand under the deposition procedure
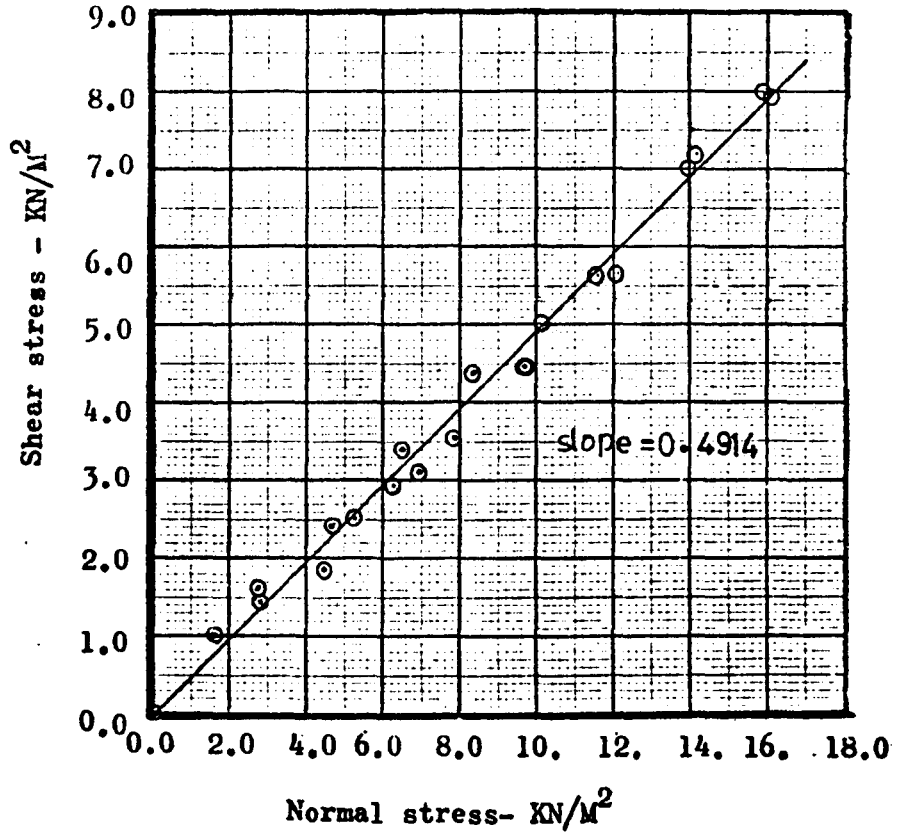
Fig.(4.9.a) Calibration for edge effect(Aluminium foil & sides of the shear box.)
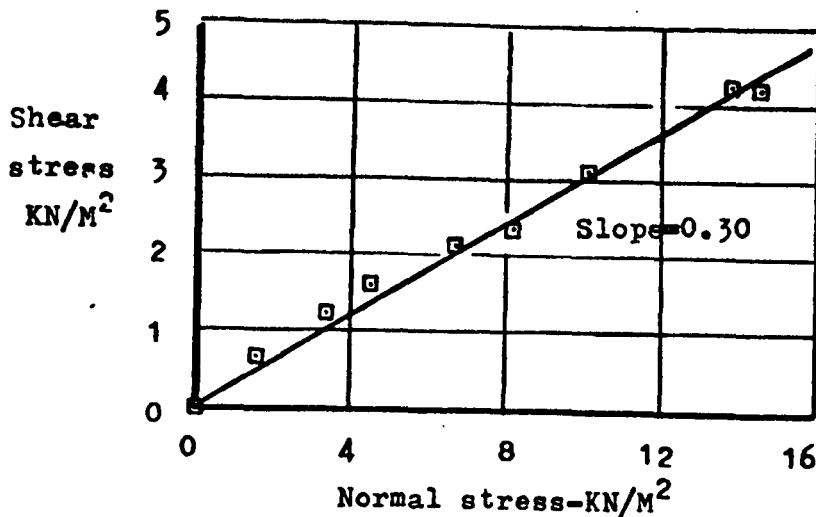
Fig.(4.9.b) Calibration for edge effect (Perspex & sides of shear box.)
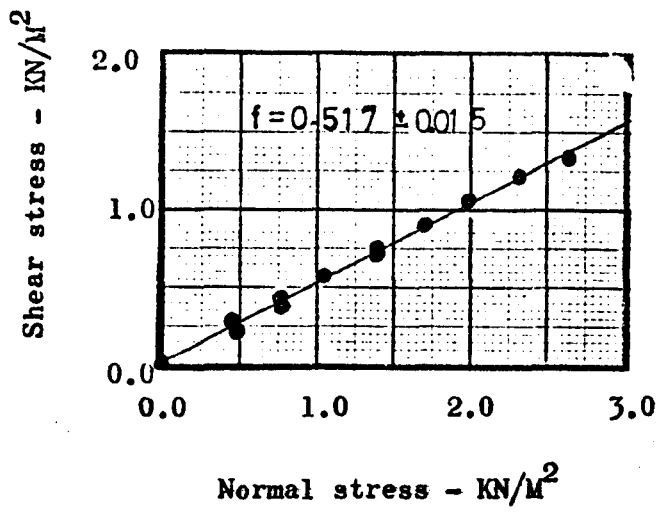
Fig.4.10.a Coefficient of friction between 45 μm aluminium foil & sand using controlled stress shear box.
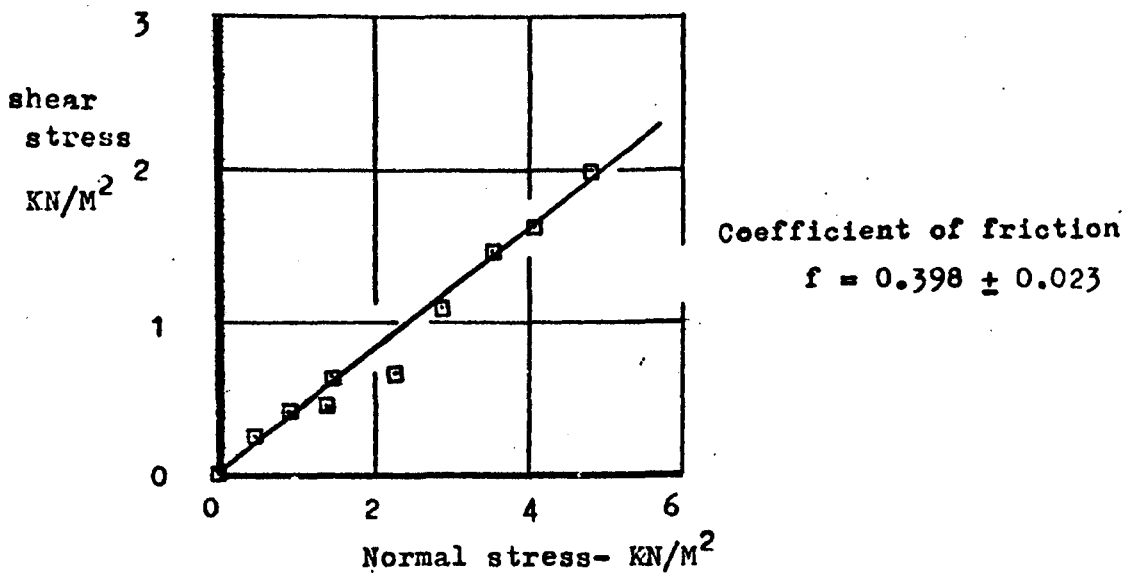
Fig. 4.10.b Coefficient of friction between perspex & sand using controlled stress shear box.

Graduated test box

500 x 500 x 500 mm

(internal dimensions)

Sand

Tie

Frame

Load
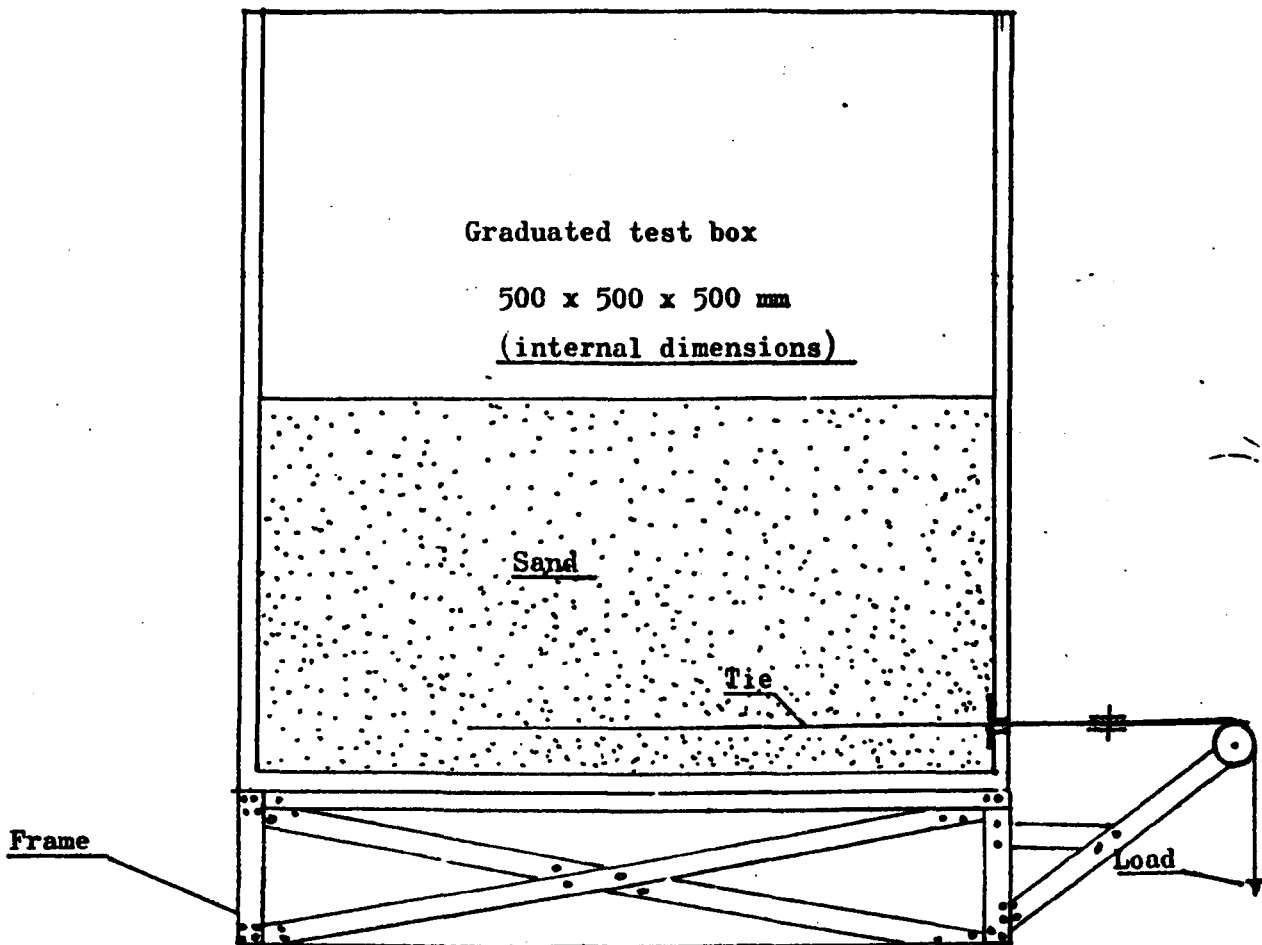
Fig. 4.11 Test box for determining the coefficient of friction by pull out

$f = 0.503 \pm 0.03$

Shear stress $-KN/M^2$

Normal stress $- KN/M^2$
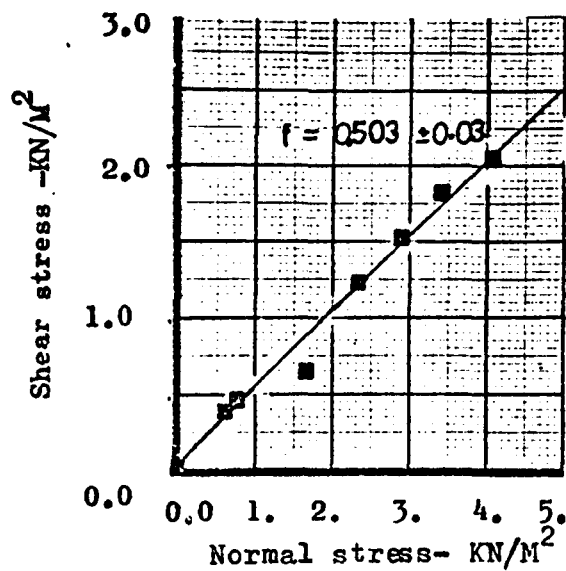
Fig. 4.12 Pull out test result (Coefficient of friction between 45 μm aluminium tie & the sand)
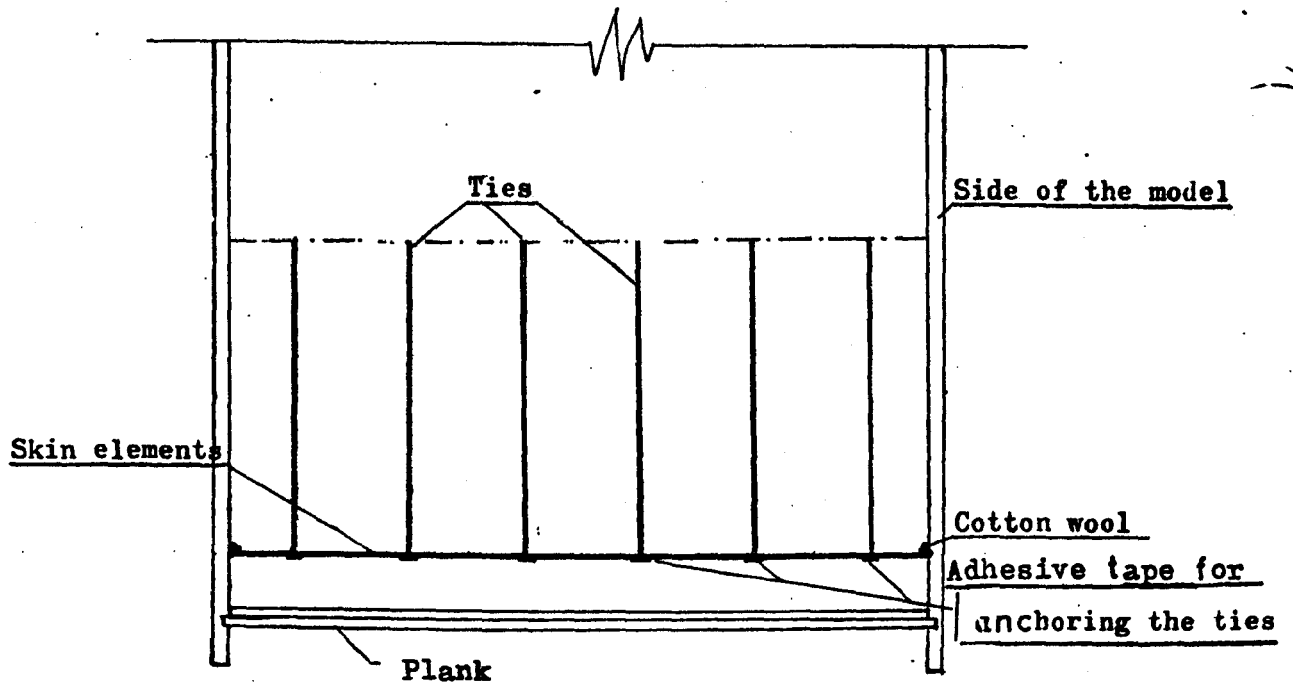
Fig. 4.13 Plan view of the model & the ties connected to the skin elements

was measured at various points within the sand mass in two
ways:

>   (1)   By using a miniature vane to obtain values for
>   torque and converting these to density by means of a
>   calibration curve, Fig (4.14) and Table (4.1).
>
>   (2)   By using perspex boxes (50 x 50 x 40 mm) at
>   various levels within the mass.   The results are
>   shown in Table (4.2).

The observations indicated that the perspex box system
gave more reliable results, a standard deviation of 0.44%
being obtained compared with 9% for the miniature vane method.
The difference in average density, 1.6159 gm/cm^3 compared with
1.556 gm/cm^3 was due to the height of deposition being
different in the two cases.

4.5   Stress Measurements on Ties

One of the objectives of the present investigation was
to monitor the stresses built up in reinforcing ties while
the wall was under construction.

In full scale walls, electrical resistance strain gauges
have been attached to the reinforcing ties, and the strains
measured have been converted to stresses by using the
appropriate value of Young's modulus for the tie material[14]
or by individual calibration of the ties.[29]

In model studies with aluminium foil ties 13 μm thick,
Lee et al[45]   used strain gauges mounted on brass strips
25 μm thick introduced in series with the aluminium foil.
In these tests the lead wires appeared to interfere with the
performance of the ties.

Preliminary tests by the author using commercially avail-
able strain gauges on aluminium ties 45 μm thick led to the
discovery that although the gauges worked well in tension,
distortion of the ties in situ caused the development of
bending strains in the gauges.
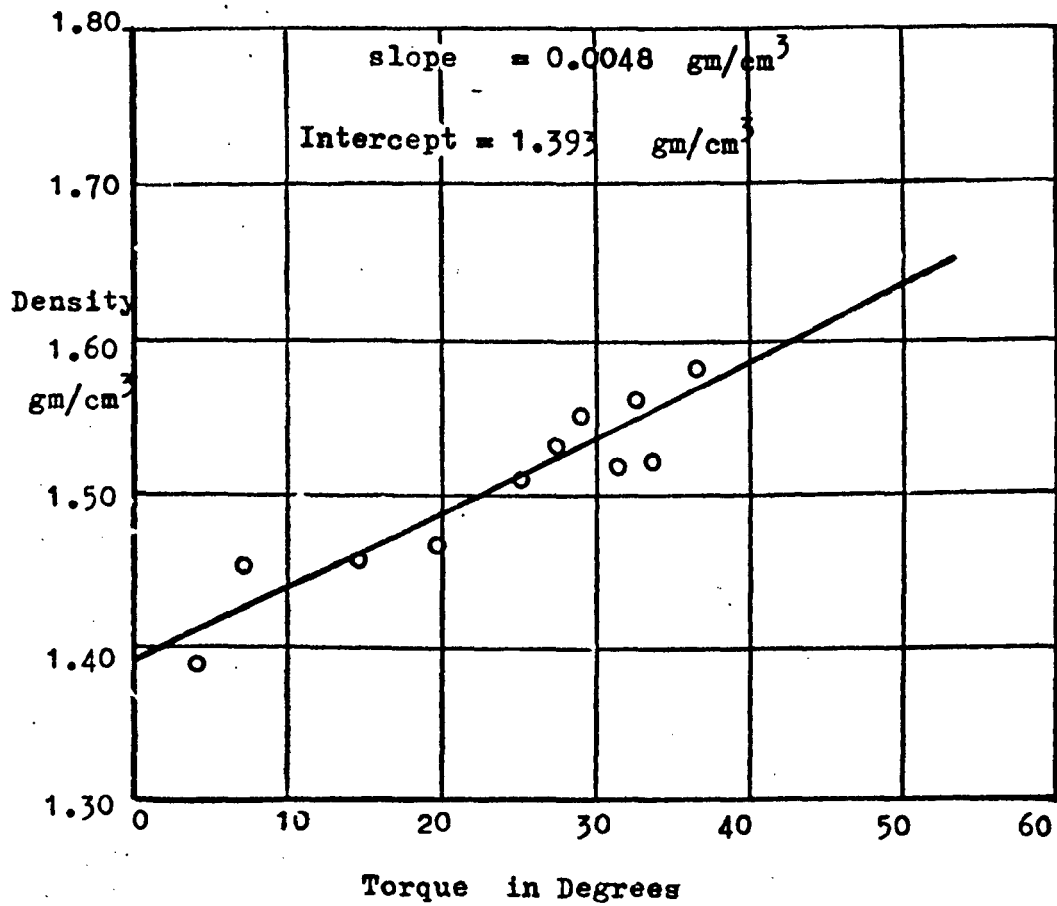
Fig.4.14 Calibration curve of the miniature vane shear test apparatus.

Position of vane shear
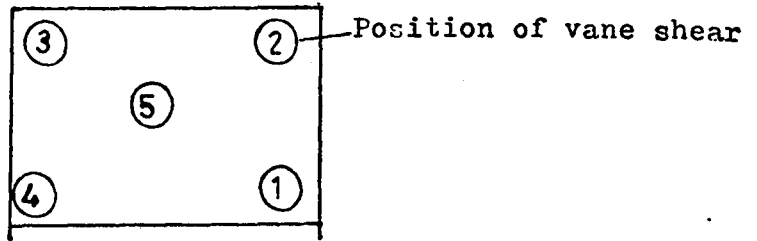
Layer height above base-mm	The miniature vane shear reading in degrees					
	1	2	3	4	5	Average
75	35	36.5	46	37	-	38.6
175	34	33	29	31	30	31.4
275	36	36	37	32	36	35.4
375	33	26	30	37	33	31.8
475	33	32	32	32	35	32.8

Average torque = 34± 9%

Table 4.1   Torque variation in degrees %,   "   density =1.556 ± 9%

perspex boxes
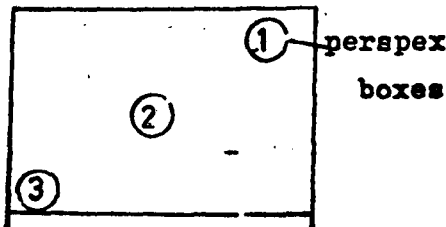
Layer height above base mm	γ_1	γ_2	γ_3	$\gamma_{av.}$
25	1.6212	1.6081	1.6103	1.6132
75	1.6190	1.6000	1.6290	1.6160
175	1.6178	1.6299	1.6103	1.6193
325	1.6221	1.6191	1.6180	1.6190
415	1.6150	1.6070	1.6128	1.6116

Average density

$\gamma_{av.}$ = 1.6159 ±.44%

Table 4.2 The density measurement at different layers of the wall

This bending effect was studied by means of a simple apparatus designed to produce measured tensile and bending stresses on a tie. Attempts were made to eliminate the effect of bending by using adhesive to make the gauges more rigid, and by measuring strain on both faces of the tie. The results of this investigation are summarised in Table (4.3). It was concluded that in order to minimize the bending effect the gauge must be rigid and the strains must be measured on both faces of the tie.

As a result of these tests it was decided to attach the gauges to small perspex strips glued in series with the aluminium tie, Fig (4.15). This configuration was used in the first series of model tests described in Chapter Five, and apart from some problems which arose in connection with the different properties of the perspex and the aluminium, gave reasonable results.

In order to study walls failing by pull out or under stable conditions, relatively rigid ties could be used. Because of this, and in order to eliminate problems arising from using two different materials, perspex ties were used. These were gauged on opposite faces, Fig (4.16) using strain gauges manufactured by Micro Measurements Company, Type EA-41-125BB-120. These gauges were mainly adopted for the stress measurement in the present investigation.

An attempt was also made to increase the bending stiffness of the tie at the strain gauges position to make them relatively insensitive to bending, Fig (4.17) shows the modified mounting for the strain gauges in the form of a gauged vertical perspex beam fixed to the ends of a slot in the perspex tie. This method of stress measurement was only used in a few tests because of the suspected modification of the frictional characteristics of the tie, since slots were made to accommodate the gauges.

All the strain gauges used in the model tests, whether mounted on aluminium foil or on perspex were calibrated using

Material Type	Range of tie thicknesses	No. of strain gauges mounted	Coating applied on gauges	Sensitivity to tensile stresses	Response to bending	Result of the test
Aluminium Foil	45 μm to 0.15 mm	One	Plastic coating	Sensitivity ranging between (100-26)μs/N	Bending strain is 8N axial load per each degree of rotation	Appreciable bending stresses
Aluminium Foil	"	Two gauges mounted back-to-back	Plastic Coating	Sensitivity (100-26)μs/N	"	Appreciable bending
Aluminium Foil	"	One	Plastic Coating plus Quick set adhesive	Sensitivity to axial stresses reduced by 46%	Bending strain 0.4N axial loading per degree of rotation	Improvement, i.e. less response to bending stresses
Aluminium Foil	"	Two gauges mounted back-to-back	Plastic Coating plus Quick set adhesive	"	Bending strain 0.1N axial load per degree of rotation	Bending resulted in nearly equal strains of opposite signs

TABLE (4.3)   Results of preliminary investigation into the stress gauges response to bending and axial stresses

TABLE (4.4)   Ranges of Calibration factors of the tension gauges

Gauge Type	Range of Calibration Factor
Strain gauges mounted on perspex beams and connected in series with aluminium tie (Fig 4.9)	(173-176) $\mu s/N$
Strain gauges mounted on perspex tie Fig (4.10)	(20-38) $\mu s/N$ For half and full bridge configurations respectively.
Strain gauges mounted on perspex beams and fixed in slots in perspex tie Fig (4.11)	(24-33) $\mu s/N$

FACING PANEL.

Perspex beam(6mm widex0.6 mm thick)

35 mm   35 mm

Quick set epoxy adhisive   Aluminium foil tie(4 mm wide,45 μm thick)
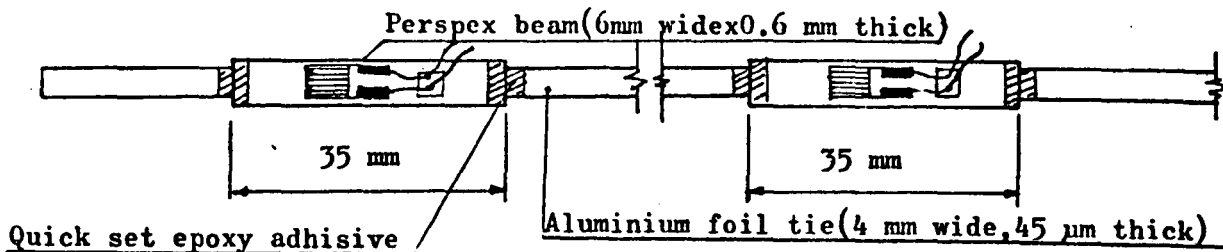
Fig.4.15 Preliminary tension gauge design connected in series with aluminium foil tie.

30 mm   50 mm   70 mm   100 mm

22 mm

400 mm

Plan

1.5-1.37 mm   Elevation
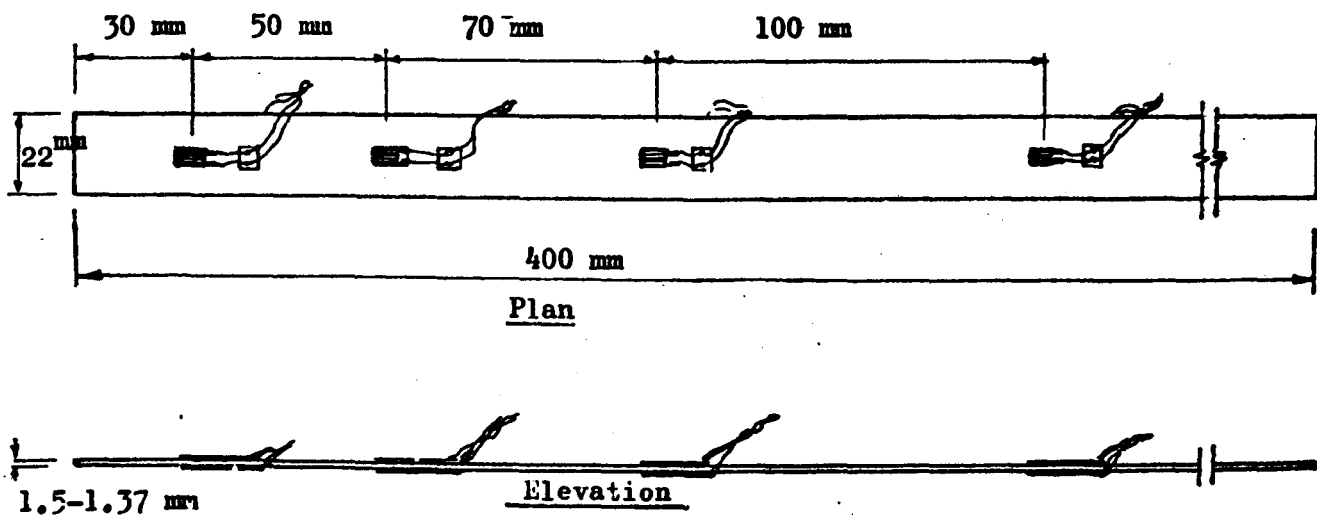
Fig.4.16 Perspex tie with 4 tension gauges

25 mm

22 mm

400 mm

Plan

40 mm   50 mm   50 mm

6 mm

Elevation
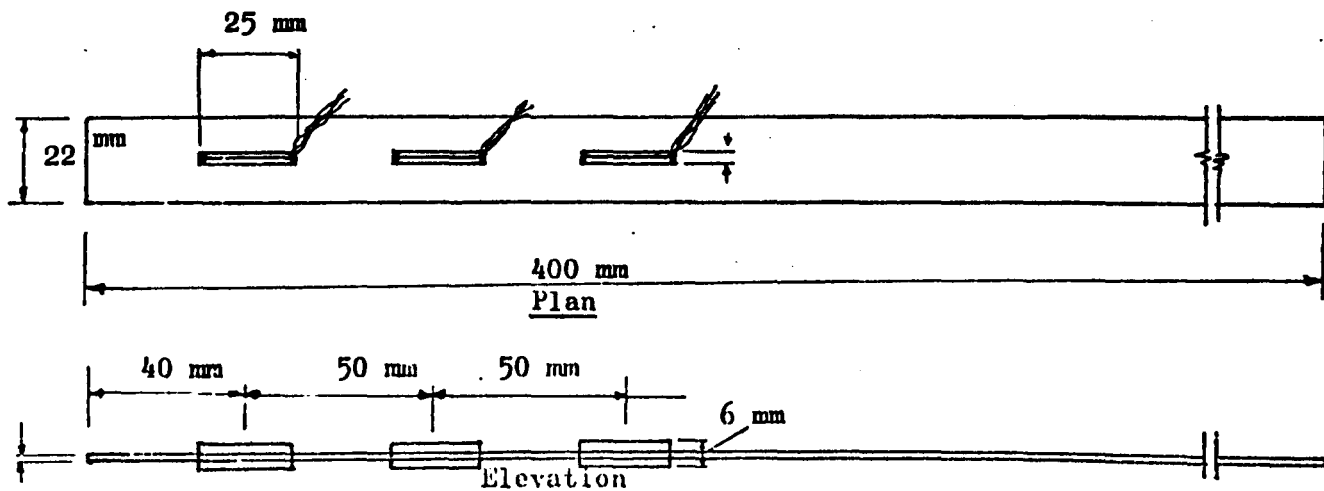
Fig.4.17 Perspex tie with 3 tension gauges(Low response to bending type)

Steel frame

Thermometer

Plastic tie
with 4 tension
gauges

Aluminium clamp

Weights
(1 lb.=4.45 N)

Dummy gauge

switch
box

strain
indicator

stand
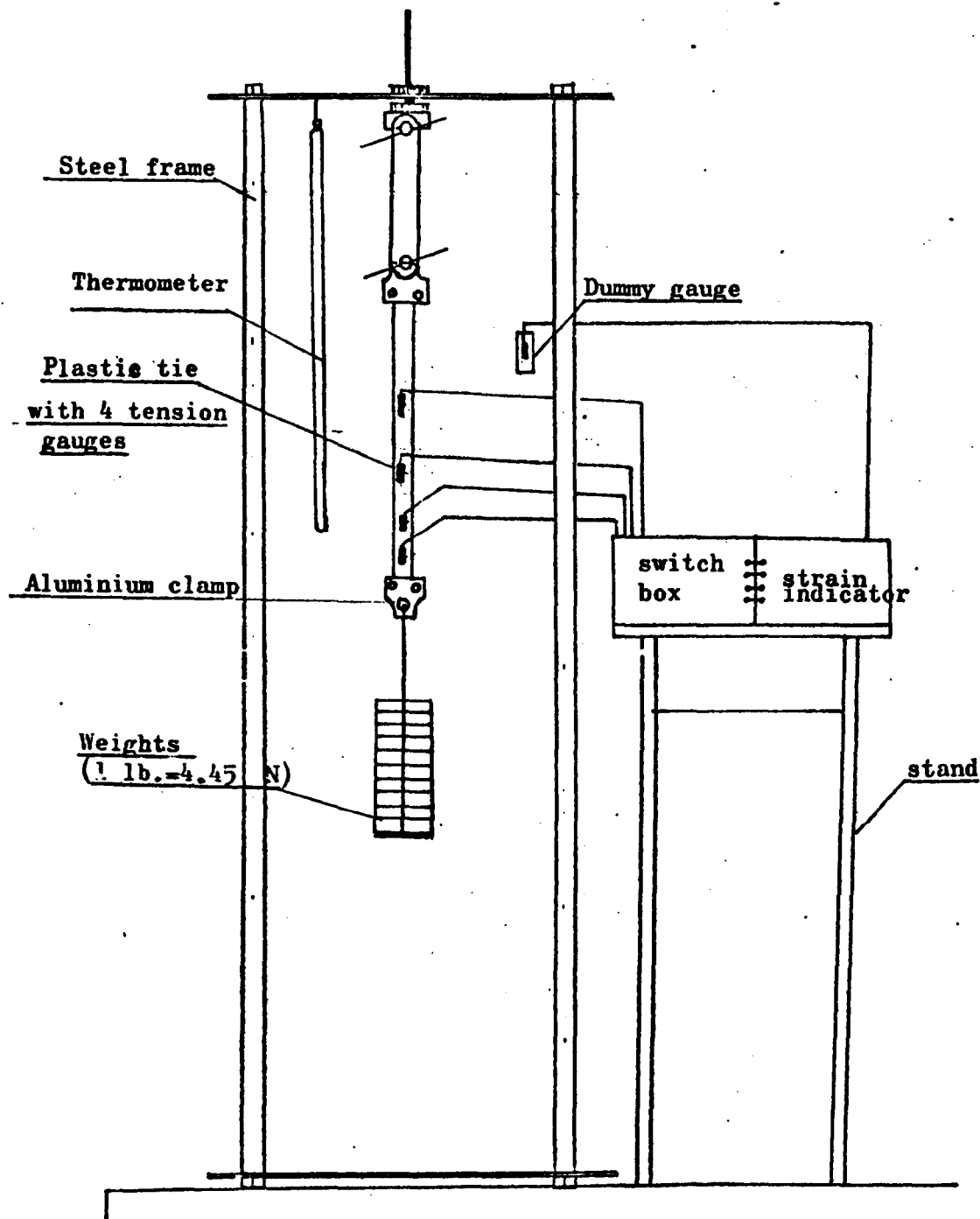
Fig. 4.18 Set up for the calibration of tension gauges
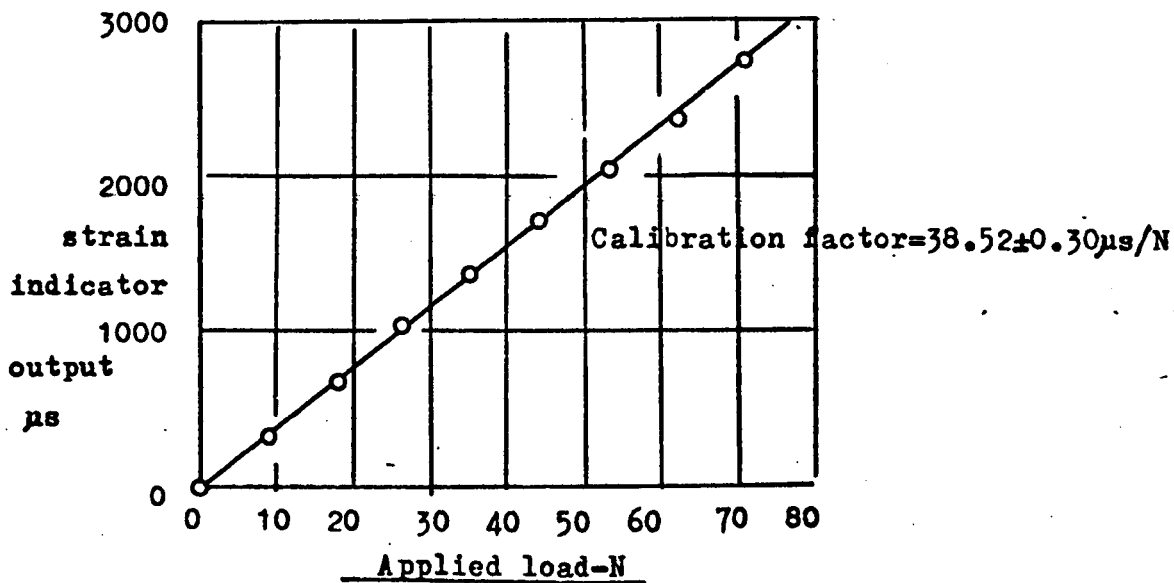
(a)
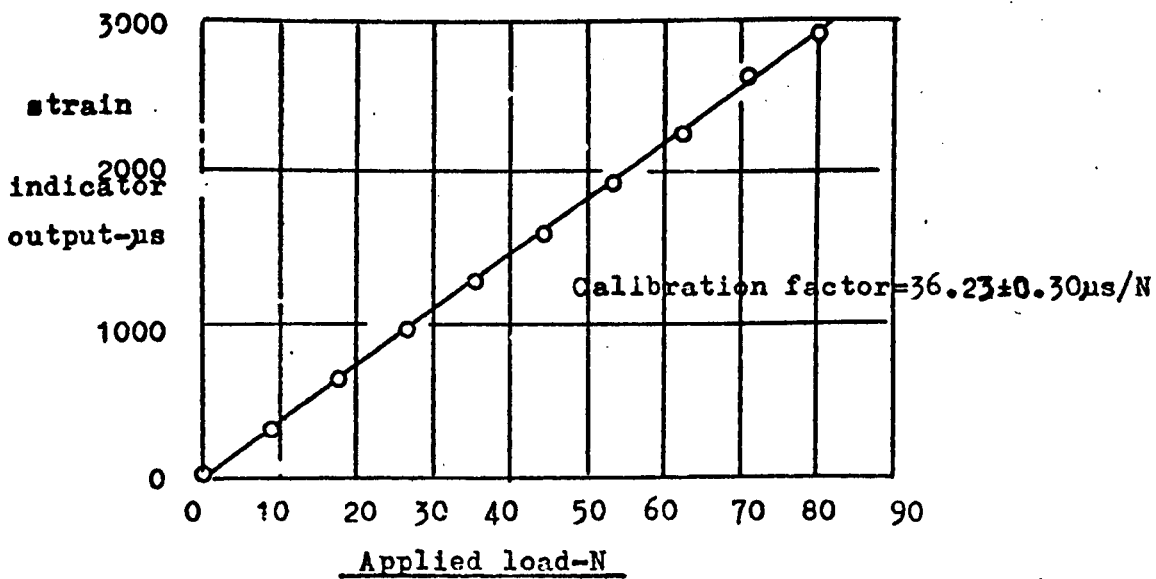
(b)

Fig.4.19 Typical calibration curves for strain gauges mounted on
perspex ties 22 mm wide, 1.5 mm thick

the loading frame shown in Fig (4.18), to provide a direct reading of stress <u>v</u>. electrical output. Precautions were taken regarding loading and unloading, repetition of loading cycles and the test temperature. Typical calibration curves are shown in Fig (4.19) and the range of the calibration factors obtained is shown in Table (4.4).

4.6 Strain Measurement in the Soil

4.6.1 Introduction

The importance of measuring the strain in models and full scale structure^s is well recognized by previous investigators.[27,55]

In the present study it is intended to observe the strains set up in the backfill of the model walls.

Selig[68] reported that the main requirements of a suitable strain gauge are that the gauge should freely follow the movement of the soil and the gauge/soil attachment should be satisfactory.

Most of the instruments used for strain measurements in soil are physically coupled. These consist of two discs connected by a sliding rod which provides a gauge length between the discs. Movement is measured by linear transducer incorporated in the sliding rod. These types of gauge have problems of placement and interference of soil due to presence of the rod in the gauge length.[68]

Other methods of strain measurement in soil use optical[12] or X-ray[57] techniques. The optical methods have the disadvantage that only the strains adjacent to the transparent side of a model can be observed. These are liable to be considerably affected by friction on the side of the model. The X-ray technique can only be used in thin models because of the limited power of penetration of the X-rays.

In the present investigation free field strain coils were developed from an original design by Truesdale and

Anderson,[74] and were used for strain measurement in the backfill of the reinforced earth model retaining walls and also in the wall deflection observations.

4.6.2 Theory of operation of the strain coils

The strain coils theory is based on the differential transformer principle. The driver and detector coils Fig (4.20), correspond to the primary and secondary transformer windings respectively. When a high frequency signal is applied to the driver coils, the magnetic field produced induces a voltage in the detector coils. The magnitude of the induced voltage is a function of the magnetic linkage and hence a function of the coils' separation. The output from the bridge is amplified so that a very small change in the spacing can be detected.

The coils are connected in opposing series so that when the separation of the embedded coils is identical to the reference coils the output voltage is zero. When the spacing of the embedded pair is altered the resulting voltage can be nulled by operating the micrometer attached to the reference pair. The change in distance required is identical to the change in spacing of the embedded pair.

4.6.3 Development of the strain measuring system

This consists of electrical equipment which plays an important role in the sensitivity and stability of the readings, and coils which act as sensing elements.

4.6.3.1 The electrical equipment

Truesdale and Anderson[74] originally used the electrical components indicated in Fig (4.21). Morgan and Gerrard[49] used a similar circuit, Fig (4.22) and added a filter tuned to the oscillator frequency to increase the stability of the output signal.

Reference coils

Adjustable Micrometer

Driver Coils Circuit

Tuned Amplifier and Detector Circuit

Output Device

Embedded coils
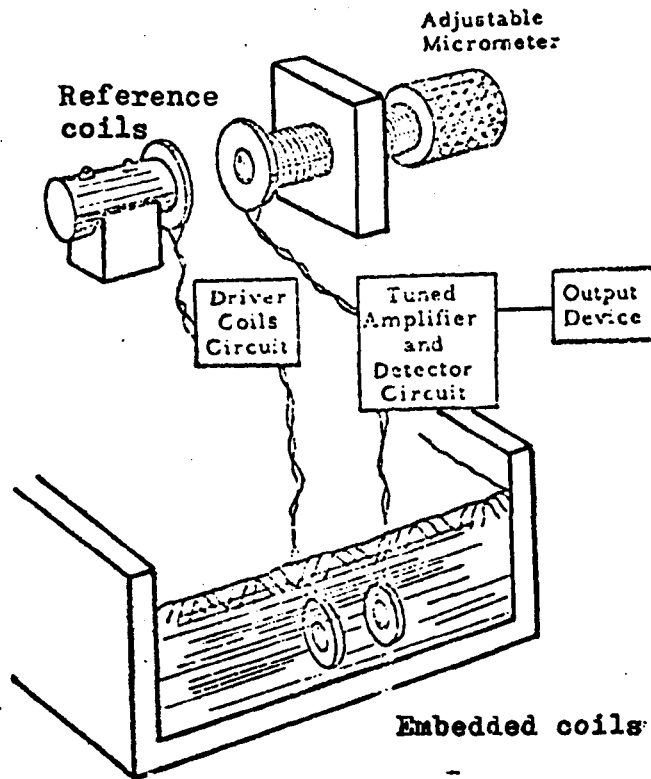
Fig.420 Principle of operation of soil strain coil.
(After Truesdale & Anderson(74))
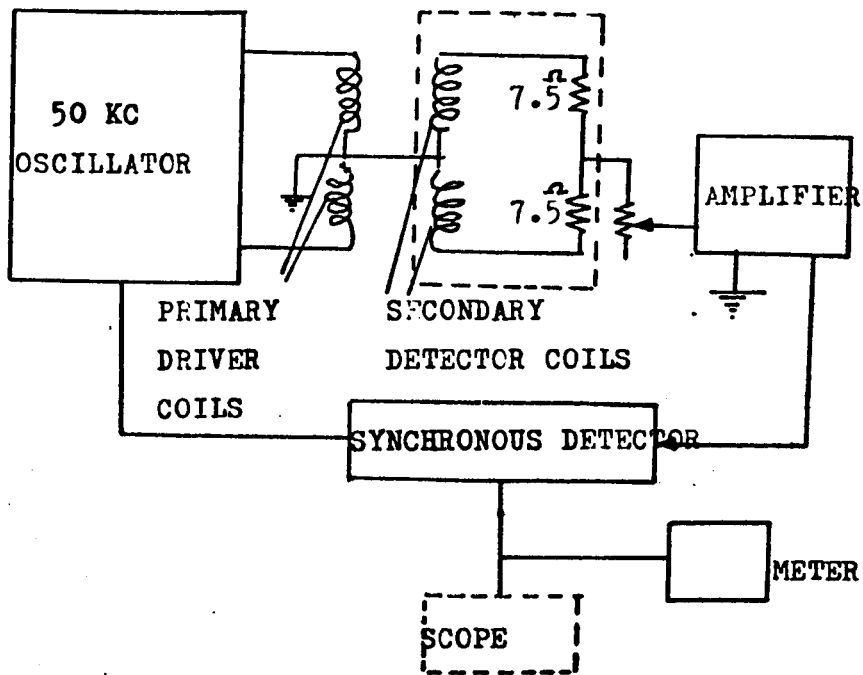
Fig. 4.21   Block diagram of soil strain gauge(After Truesdale et al[74]).
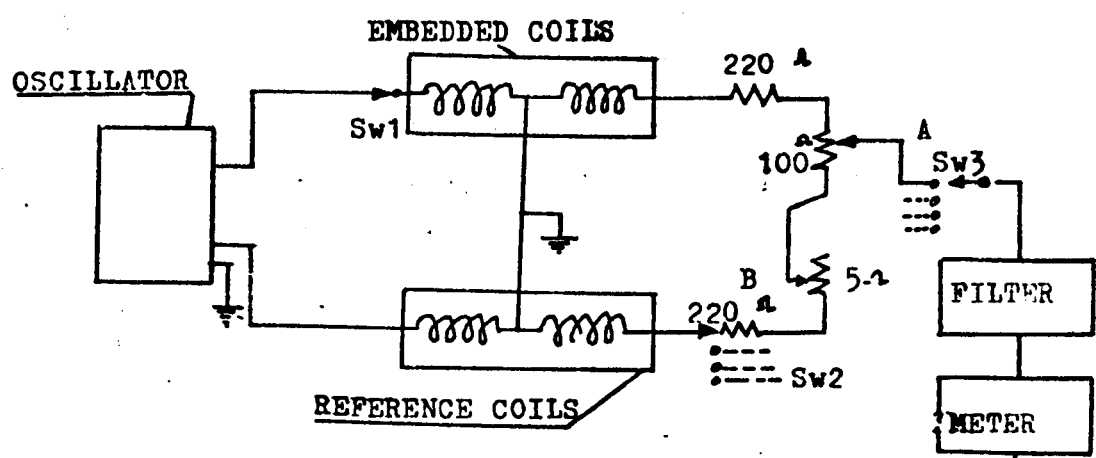
Fig 4.22   Block diagram of soil strain gauge (After Morgan et al [49]).
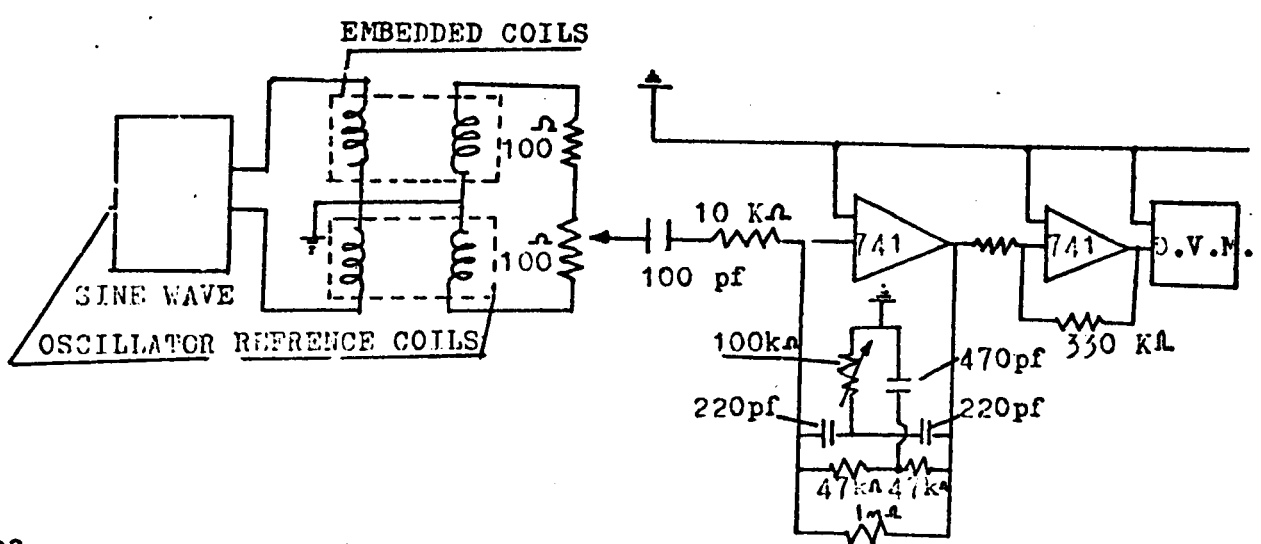
Fig 4.23   Block diagram of soil strain gauge used in   the present study

In the present study a measuring circuit consisting of an available oscillator, a voltmeter and locally constructed filter amplifier unit was assembled, Fig (4.23).   The circuit was designed so that it would pass and amplify only at a frequency equal to 15 KHZ which has been found[49] to give maximum sensitivity.

The new feature of the present circuit is the D.C. filter amplifier unit which increased the stability and sensitivity of the system.

4.6.3.2 The coils

In the original design by Truesdale and Anderson[74] no detailed information was given about coil construction.

Generally, the coil size is determined by the relative size of the coil with respect to the soil mass, the coils' separation and the sensitivity desired.   For laboratory use small coils are needed to decrease the coils' effect on the sand medium.

An empirical approach was undertaken to determine the coil sizes needed in this study.

Two sets of coils were manufactured.   The first sets of coils were produced with the specifications shown on Table (4.5) and were used in the sensitivity,linearity checks and in assessing the effect of the sand medium on the calibration factor of the coils.

TABLE (4.5)   Specifications of the first set of the strain coils

Coil outside diameter	49 mm
Coil inside diameter	14 mm
Wire diamter	0.12 mm (40 S.W.G.)
Number of turns	1,500
Coil electrical resistance	140 Ω
Coil inductance	33 m.H.

AY glue and HY 951 hardener were used to bind the coils.

The second set of coils was intended for measuring the strain in the wall backfill. The coils had to be as small as possible to minimize disturbance of the soil mass in which they were installed, and using fine lead wires to avoid any possible reinforcing effect of the soil and permit free movement of the coils. The separation of the coils had to be as large as possible to provide a long gauge length without reducing sensitivity. Taking these requirements into consideration the coils were designed with the specification shown in Table (4.6) and eighteen pairs were manufactured.

TABLE (4.6)   Specifications of the second set of the strain coils

Coil outside diameter	23 mm
Coil inside diameter	7 mm
Wire diameter	0.1 mm
Number of turns	1,800
Coil electrical resistance	290 Ω
Coil inductance	39 mH
Density after finishing and potting in araldite	1.8-2.1 gm/cm^3

4.6.3.2.1   The lead wires

If thin lead wires are used to connect the strain coils to the readout circuit, the wires will be magnetised and any agitation or presence of magnetic objects in their vicinity will cause considerable drift. Therefore thin flexible lead wires were used within the body of the sand up to the side of the model, where thick shielded wires were attached and then connected to the readout circuit.

The coils intended to measure the wall deflection were equipped with shielded wires.

4.6.4   Calibration of the strain coils

In an ideal situation the embedded coils and the reference coils movements are identical. Because of the small differences in manufacturing the coils, the movements of the

embedded and the reference coils are slightly different. Therefore a calibration procedure is needed to deduce the movement of the embedded pair of coils from the observed readings of the reference coils.

The calibration procedure is also meant to assess the influence of the sand medium on the calibration factors established in air, to check linearity, reproducibility, and the stability of the readings and to assess the effect of translation or rotation of one coil with respect to the other coil on the calibration factor.

4.6.4.1 Air calibration of the strain coils

The strain coils and the reference coils were mounted on similar jigs, Fig (4.24) and the sensitivity, linearity and reproducibility of the readings were checked.

A sensitivity as good as the bench micrometer resolution $(1 \times 10^{-3} \text{mm})$ was obtained with a driving voltage and frequency settings equal to 6V and 15 KHZ respectively for the large diameter coils. In the case of the small diameter coils this sensitivity was achieved by adopting a voltage and frequency settings of 12V and 15 KHZ respectively.

By changing the strain coils separation, bringing the circuit to null position using the micrometer attachment on the reference coils and observing the readings on both micrometers a calibration curve was drawn for each pair of strain coils, Figs (4.25) and (4.26). The strain coil readings were found to vary linearly with the reference coil readings in the ranges of coils spacings adopted. The average calibration factor of the strain coils intended for measuring the strains in the model was 1.1024 with a standard deviation equal to 0.0158, i.e. 1.4 per cent which showed that the variation in the winding of these coils was small.

22^{mm} 50^{mm} 22^{mm} 50^{mm} 22^{mm}

24 mm diam. Coils

Micrometer

Perspex base   Elevation

To measuring circuit.

Spring   12 mm dia. Tuflon rod. 100^{mm}

To measuring circuit.

400 mm
plan
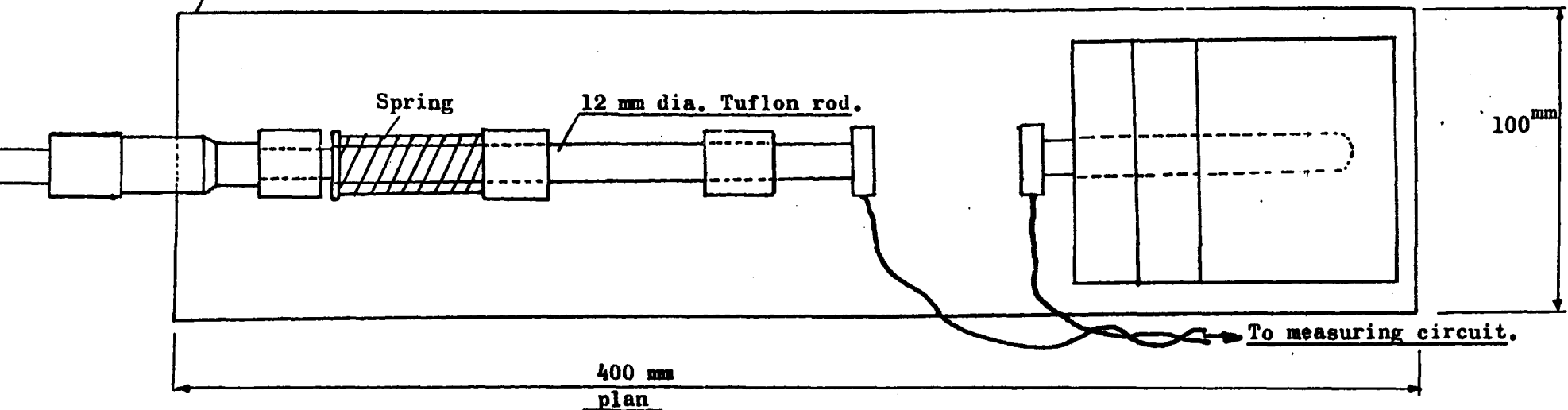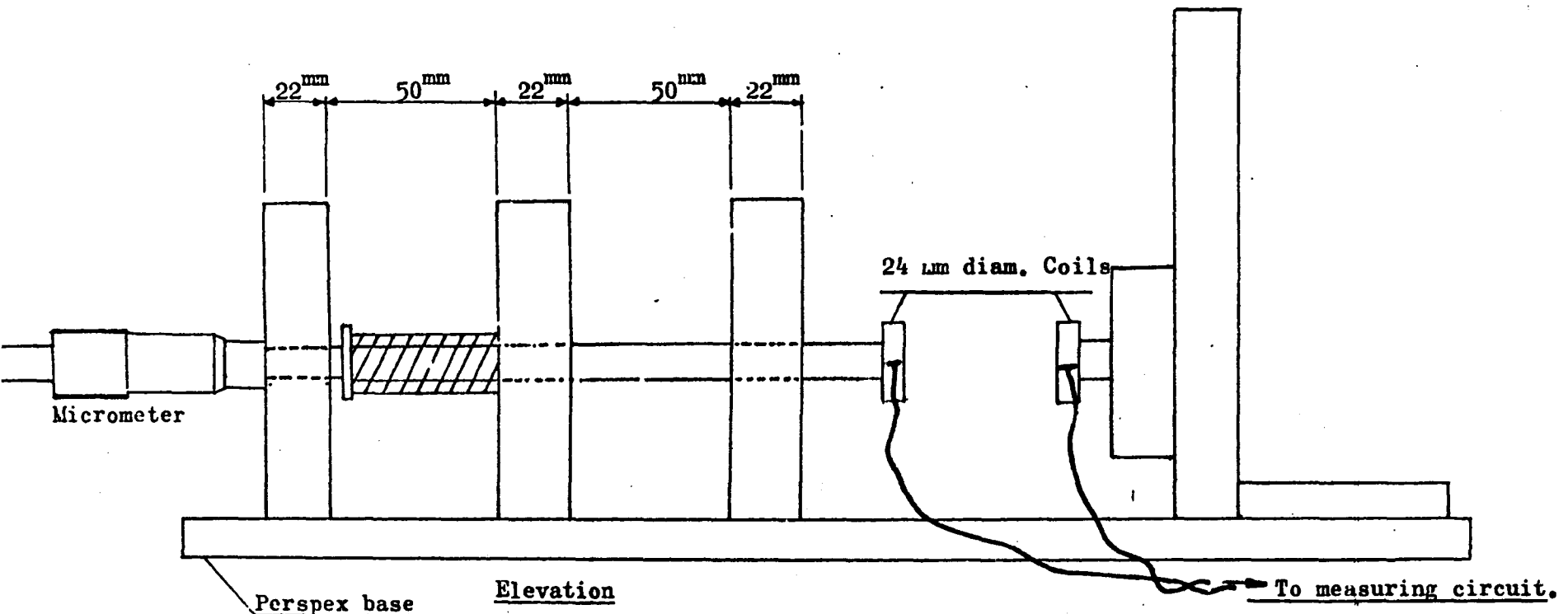
Fig.4.24 THE REFERENCE COILS MOUNT(Scale :   1:2)

Fig. 4.25 AIR CALIBRATION OF STRAIN COILS
FOR MEASUREMENT OF STRAIN IN THE WALL BACKFIL

FREQUENCY = 15 KHZ

VOLTAGE = 12 V

INITIAL COILS SPACING = 40 MM

PAIR NO.3
calibration factor=1.173

PAIR NO.4
calibration factor=1.106
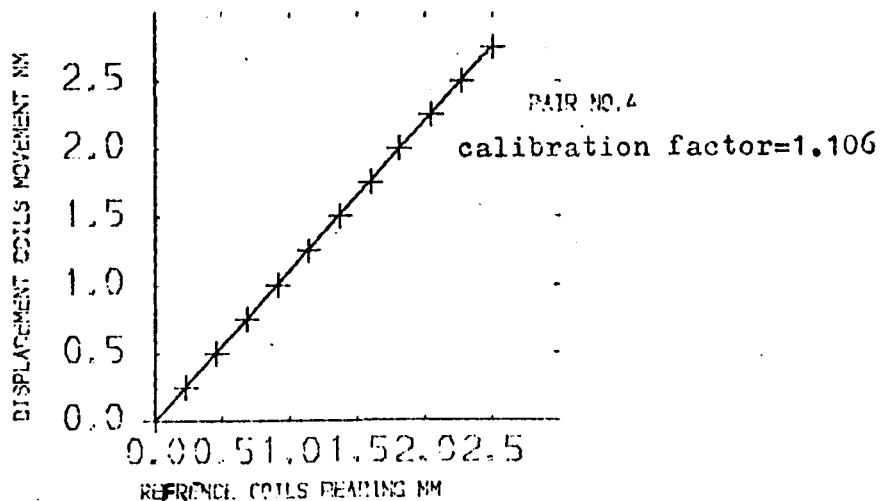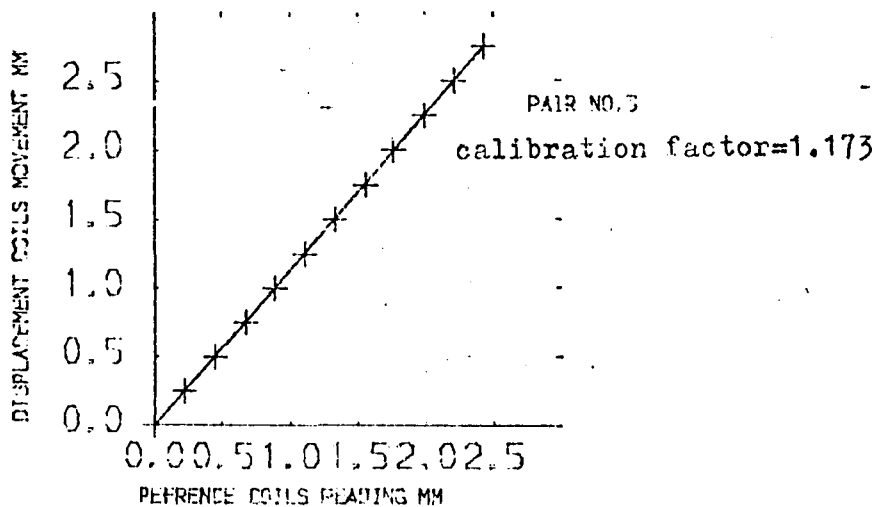
Fig.4·26 AIR CALIBRATION OF STRAIN COILS
FOR MEASUREMENT OF WALL MOVEMENT

FREQUENCY = 15 KHZ

VOLTAGE = 12 V

INITIAL COILS SPACING = 50 MM

PAIR L2

calibration factor=0.994

PAIR T3

calibration factor=1.032
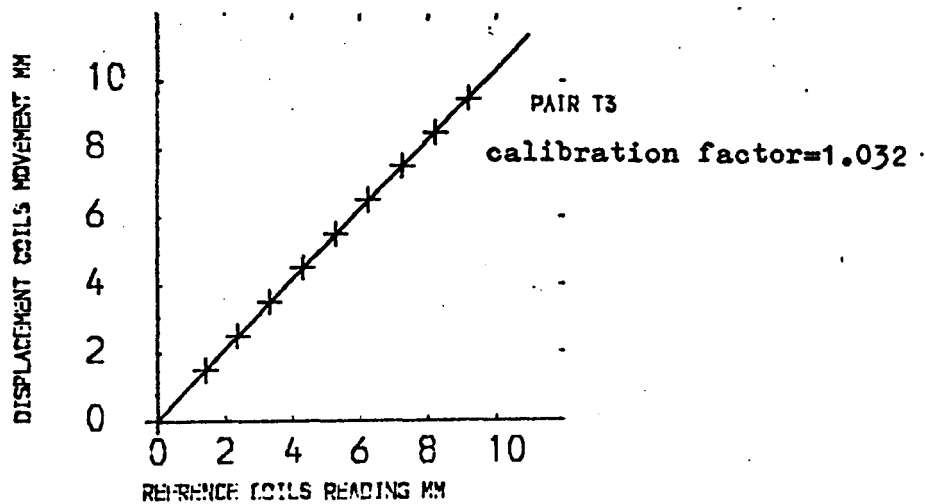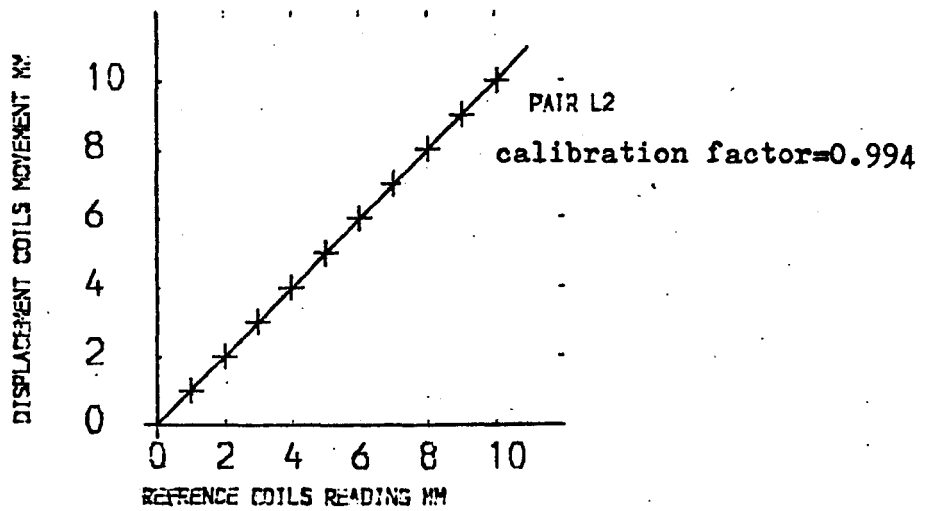
4.6.4.2   Effect of sand on the strain coils performance

This calibration test was intended to assess the effect of the sand medium on the sensitivity and linearity of the coil readings which had been established in air.

The large diameter coils were fixed on perspex discs and placed on top and bottom of a standard triaxial dry sand sample, Fig (4.27).   Wooden spacers were provided at the top and bottom of the perspex discs to keep the coils away from metal that would otherwise interfere with the coil performance.

The strains measured from the overall deflection of the sample were found to be in agreement with the strains measured using the strain coils, Fig (4.28).   For the range of the strains investigated the variation was linear.   Thus the sand can be considered to have no effect on the strain coils' performance.

4.6.4.3   Errors arising from the coils' misalignment

The embedded coils and the reference coils have to be initially placed coaxial and parallel.   Deviation from this will result in decreasing the calibration factor of the coils. Truesdale et al[74] found that the allowable relative rotational and lateral misalignment increased with increasing coils' spacing.   If the coils could be placed with not greater than 10°-15° relative rotation and/or lateral misalignment of 10 per cent of the coils' spacing, the errors could be neglected.

Morgan et al [49] studied the effect of misalignment on the calibration factors of strain coils 24 mm in diameter and initially placed 13.5 mm apart.   A decrease in the calibration factor of approximately 1 per cent was noted for 2.5 mm coils' lateral misalignment and 10° coils' relative rotation.

The coils developed in the present investigation were assumed to behave in a similar manner to the coils developed by previous investigators with regard to the rotational and lateral misalignment.
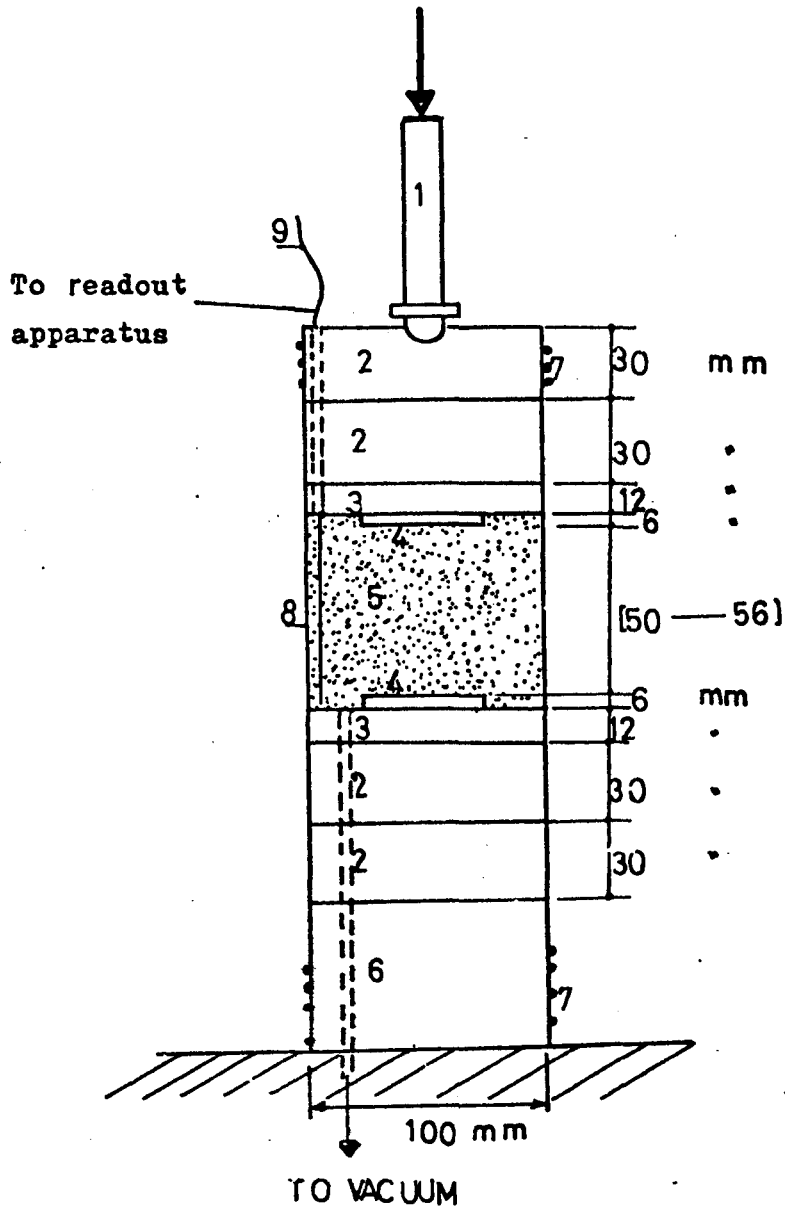
Fig.4.27 <u>Set up for testing the performance of the strain coils in</u>

<u>a sand medium.</u>

1- Ram
2- Wooden spacers
3- Perspex discs
4- Strain coils
5- Sand sample
6- Triaxial base
7- O-rings
8- Rubber membrane
9- Lead wires
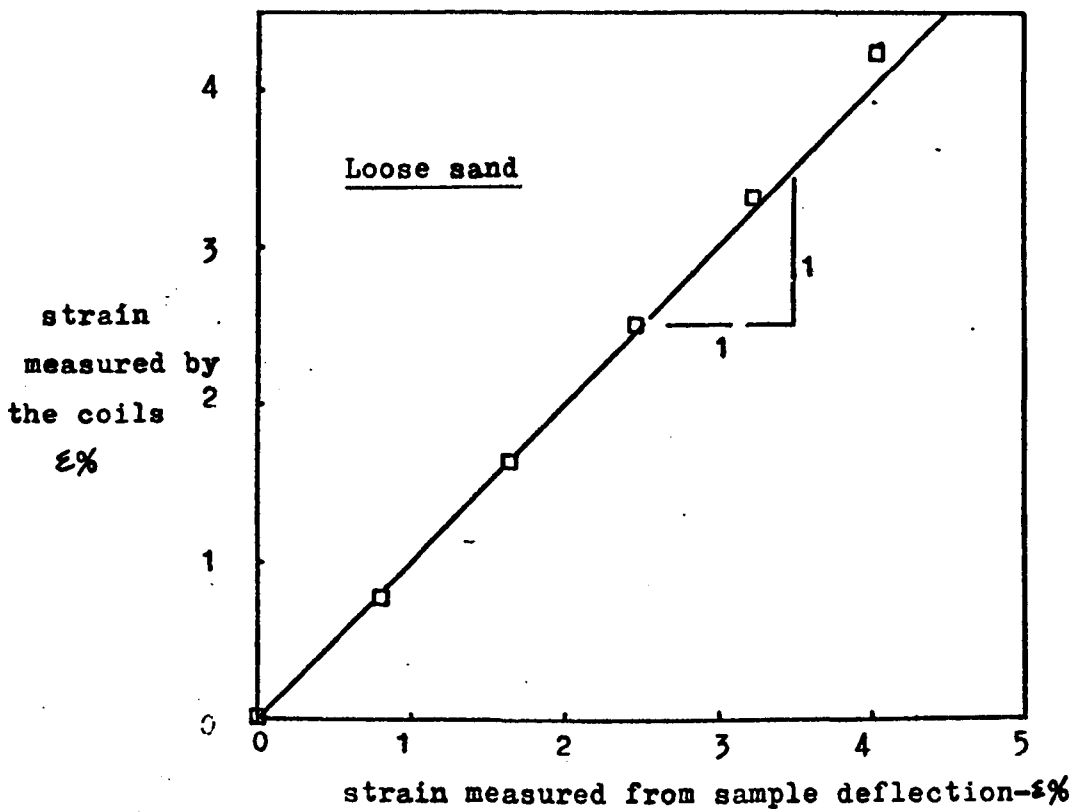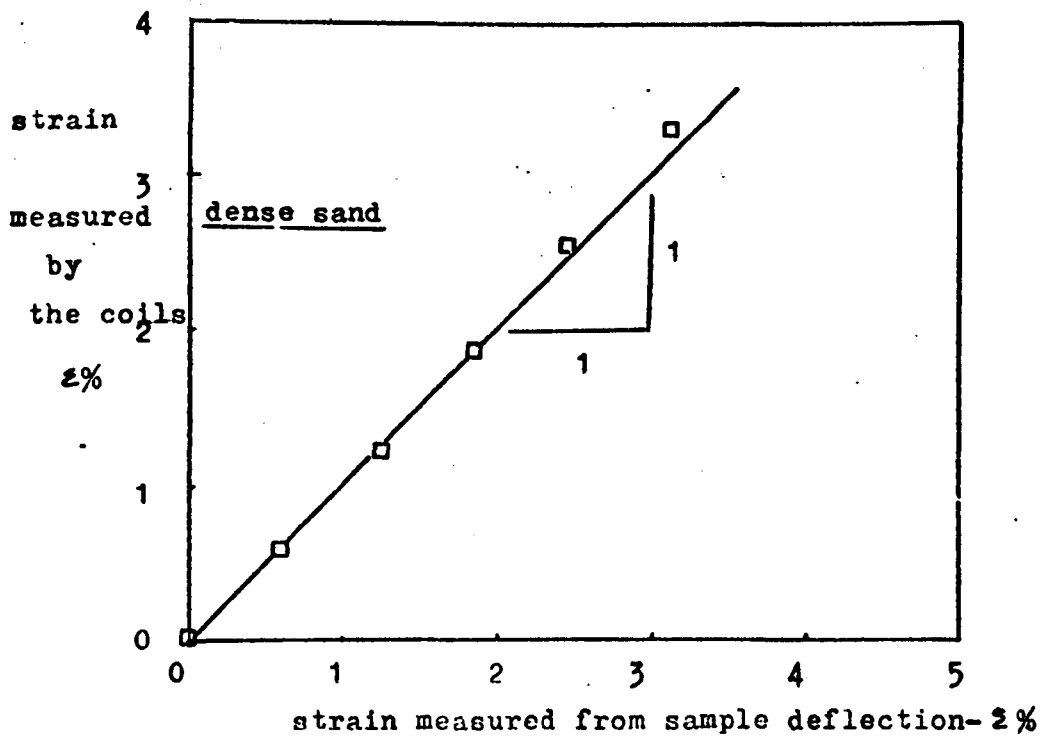
Fig.4.28 Effect of sand on the strain measured by the strain coils.

4.6.5 Coils'placement in the sand

4.6.5.1 Vertical placement for measuring horizontal strains

Coaxial and parallel alignment of the strain coils was achieved by means of a simple jig consisting of an aluminium plate with two parallel slots made to accommodate the coils and give small tolerances to prevent the sand jamming between the coils and the sides of the jig, Fig (4.29).

After the coils were placed and covered completely with sand a series of readings was taken, the average of which was adopted as the initial reading of the coils. The initial coils' separation was assumed equal to the reference coils' separation.

4.6.5.2 Horizontal placement for measuring vertical strains

A method similar to Truesdale et al[74] was adopted. An alignment rod 1 mm diameter was passed through the strain coil which was initially placed flat on the sand surface. The level of the second coil was marked off on the alignment rod and the sand was distributed up to that mark. The second coil was then placed and it was gently pressed down. The alignment rod was removed after the upper coil was completely covered with sand. The initial reading was taken from which the initial coils' separation was registered.

4.7 Stress Measurement in the Soil

Pressure cells were chosen to measure the pressure distribution in the backfill of model reinforced earth walls.

An attempt was made to construct a pressure cell to handle specific low stress levels in the model based on design by Morgan et al[49] and Scala[59] . Unfortunately, calibration under hydrostatic pressure revealed that the pressure cell was not very sensitive to small pressure changes (sensitivity obtained was $\doteq$ 1 $\mu s/KN/m^2$). This was thought
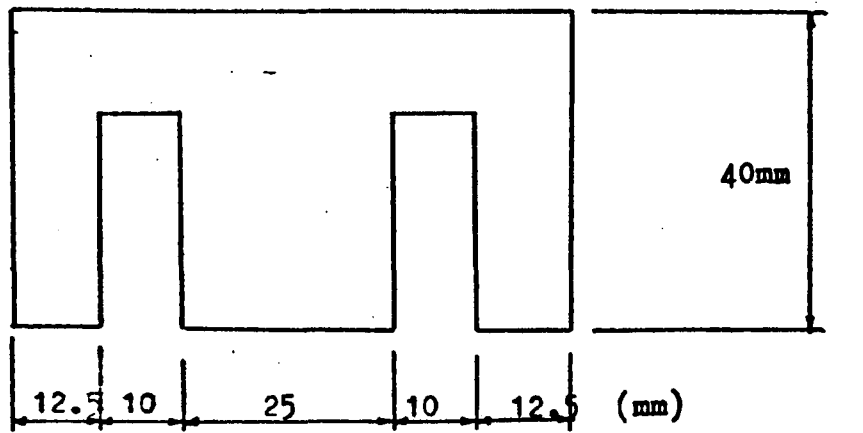
PLAN
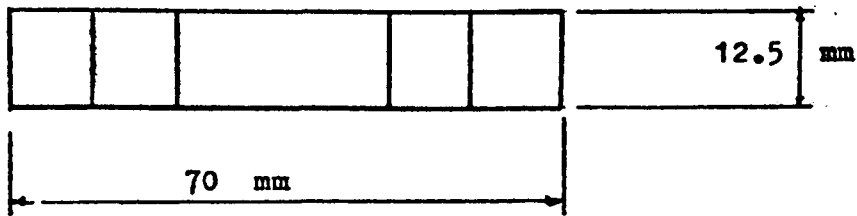
ELEVATION

Fig. 4.29 Jig for vertical placement of strain coils in model walls.

to be due to the small central deflection to diameter ratio
($1/5,000$) adopted in the design and the further stiffening of
the cell diaphragm by the insulating wax and araldite layers
Fig (4.30).

It was therefore decided to use available Redshaw type
pressure cells previously used by Neale[50]   Fig (4.31).

One of the basic difficulties in using pressure cells
is in obtaining a relationship between applied pressure and
output signal.   Other observers[49]   have shown that this
relationship varies depending on whether the cell is
calibrated hydrostatically, triaxially or in plane strain.
The following section describes calibration procedures and
results for Redshaw pressure cells under the three types of
applied pressure.

4.7.1 Calibration of Redshaw pressure cells

4.7.1.1 Calibration under hydrostatic pressure

This was intended to examine the pressure cell sensitivity
to applied pressure and can also be used to convert the cell
responses into pressure units when the cell was placed in the
triaxial sample or in the box for calibration.

Eight Redshaw pressure cells were calibrated hydrostati-
cally by placing them in turn in a triaxial cell and applying
hydrostatic pressure.   The water pressure was varied ten
times between 0 and 300 KN/m^2 to remove initial material
non-linearity and then readings from three loading and
unloading cycles of the pressure cell response and the
applied pressure were recorded to establish a calibration
factor for each presssure.   A typical test result is shown
in Fig (4.32).

4.7.1.2 Sand calibration

It has been reported[49]   that in order to interpret
the pressure cell readings care must be given to the

Sensing element

(strain gauges)

25.40 mm

18.42 mm

Rubber sealant
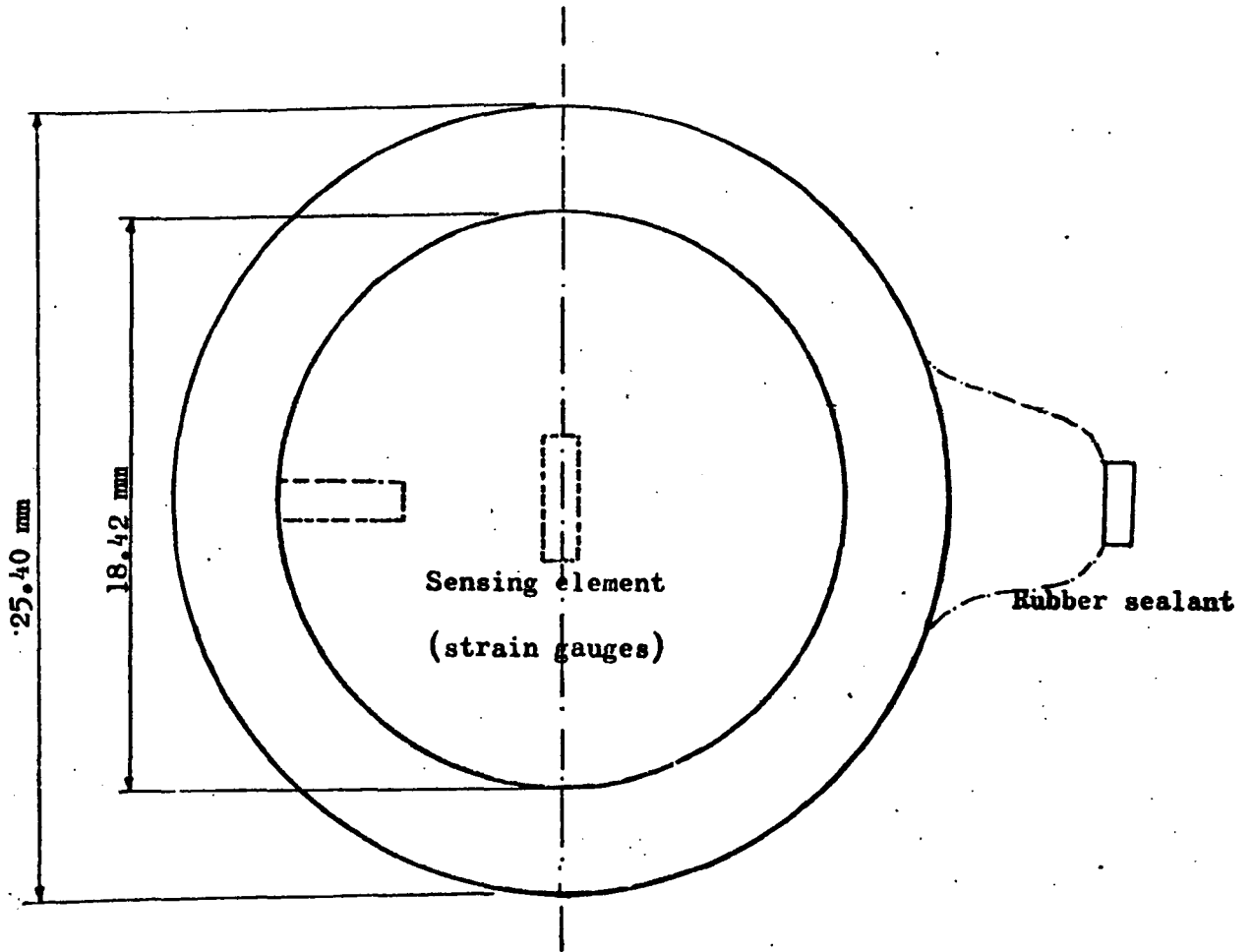
Section A-A of the miniature pressure cell

bakelite disc   backplate   insulating wax   araldite

Lead wires

1.0

1.5

1.5

1.4

A

A

2.49   1.0mm   18.42 mm   3.49 mm
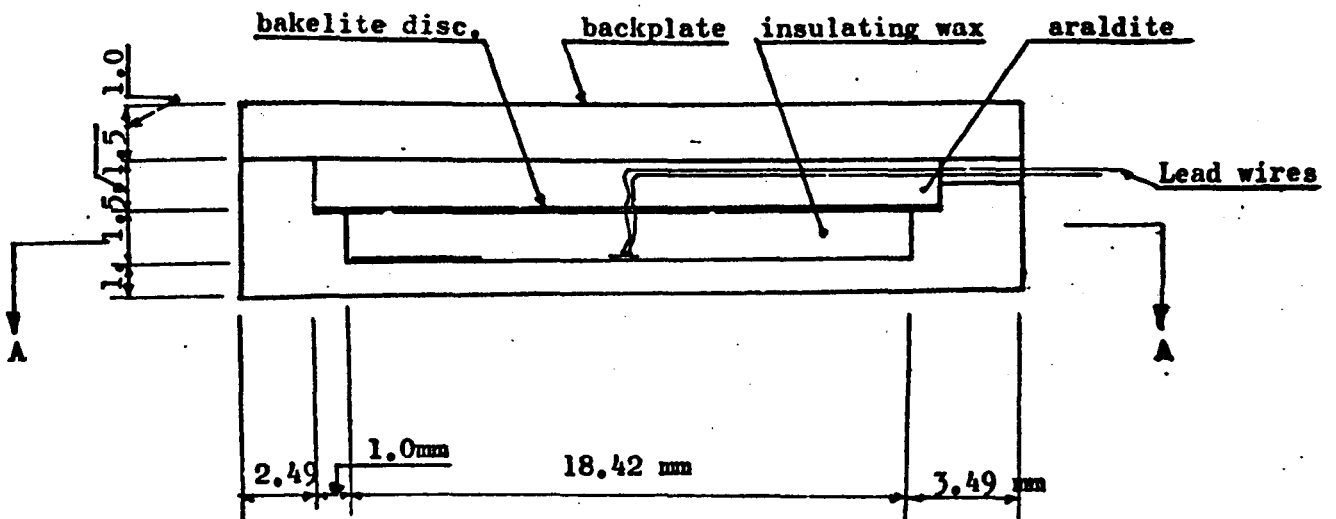
Fig.4.30 The miniature pressure cell X-section
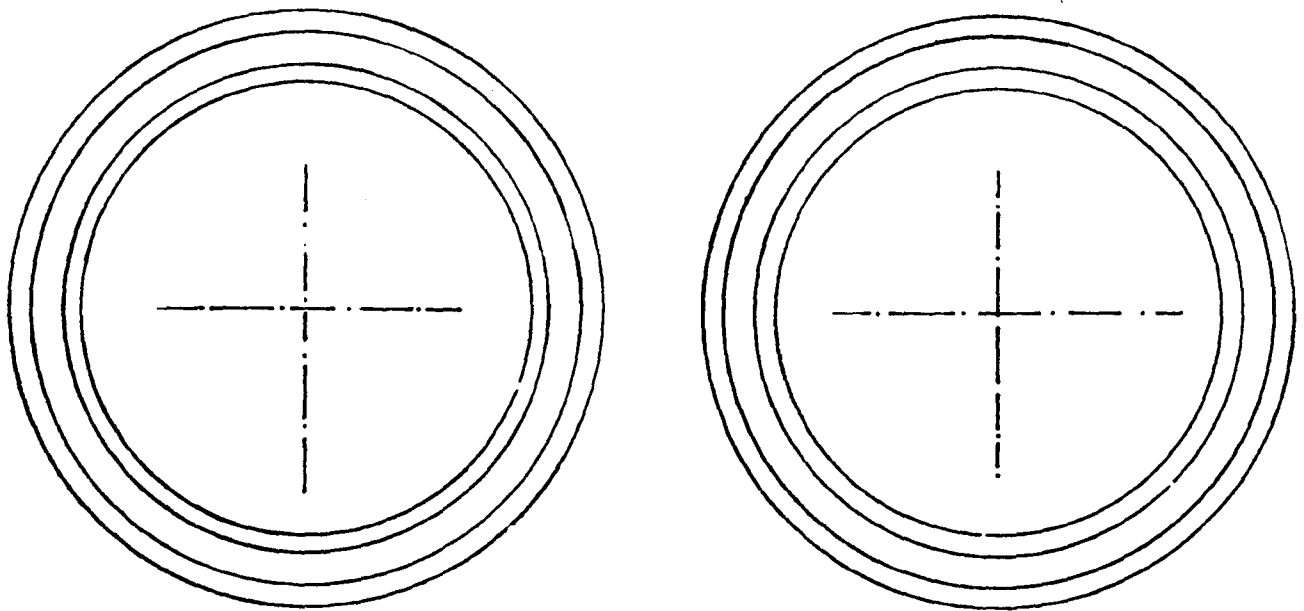
Plan
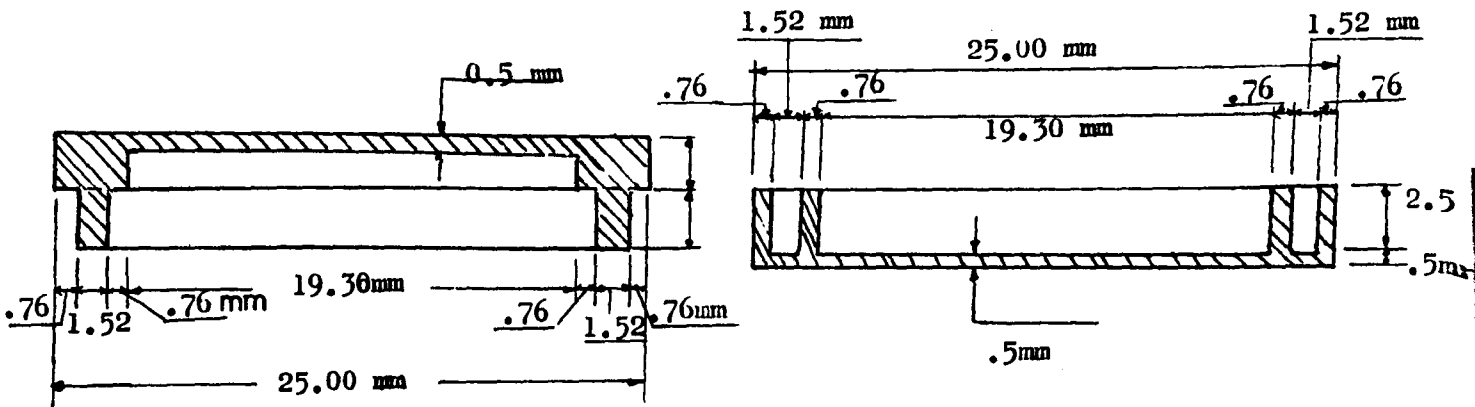
Elevation

Upper diaphragm   Lower diaphragm

Fig.431 Details of Redshaw pressure cell
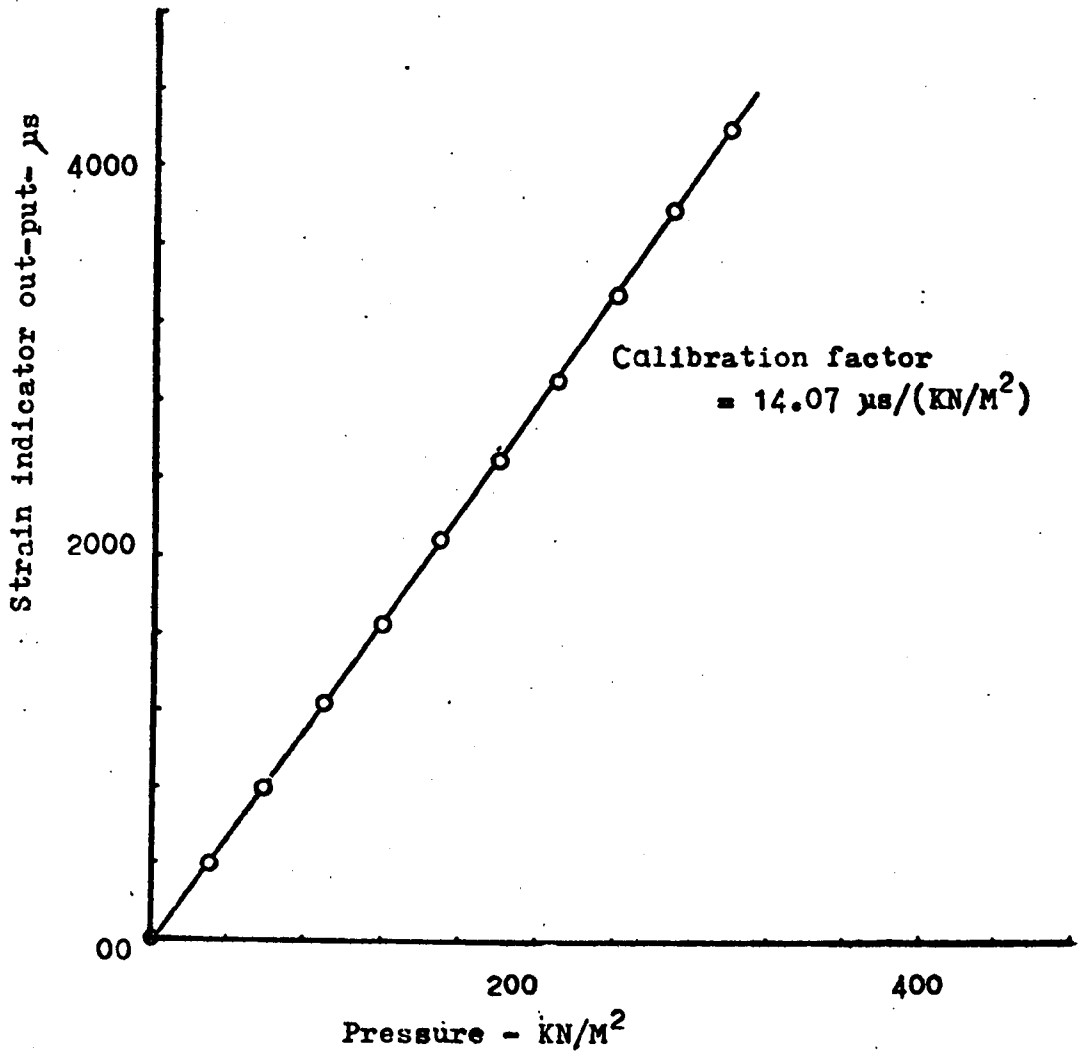
Fig.4.32 Calibration curve of pressure cell No. 5 under hydrostatic pressure.

reproducibility in the calibration procedure, of the pressure cell placement, the stress field and the density of the soil.

In this investigation the pressure cells were calibrated in triaxial sand samples to allow for the vertical and horizontal stresses calibration and in the test box to obtain the same stress field as the one to which the cells will be subjected when used in the model. The cell placements in the two calibration procedures was adopted as recommended by Hadala.[31]

4.7.1.2.1 Triaxial calibration

The pressure cells were placed in turn in horizontal and vertical orientations in the middle of a triaxial sand sample 200 mm high and 100 mm in diameter, prepared at an initial density which was approximately equal to the model sand density. Assembly and preparation of the samples proceeded as in the case of the conventional triaxial test.

Vertical stresses σ_1 were varied by applying static load on top of the ram and horizontal stresses σ_3 were applied through the cell pressure.

The strain indicator readings and the corresponding applied pressures were plotted and the relationship was approximated by a straight line to get a calibration factor for the vertical and horizontal stress measurements, e.g. Figs (4.33) and (4.34).

4.7.1.2.2 Plane strain calibration

The test box was closed at its front and the pressure cells were placed on top of a sand layer 50 mm thick and covered by a thin layer of sand, Fig (4.35). The initial readings were taken at this stage and layers of sand 50 mm thick were deposited using the raining device. The density of each layer was measured using small perspex boxes and the cell responses were recorded. This procedure was repeated for the subsequent layers, until the full height of the model
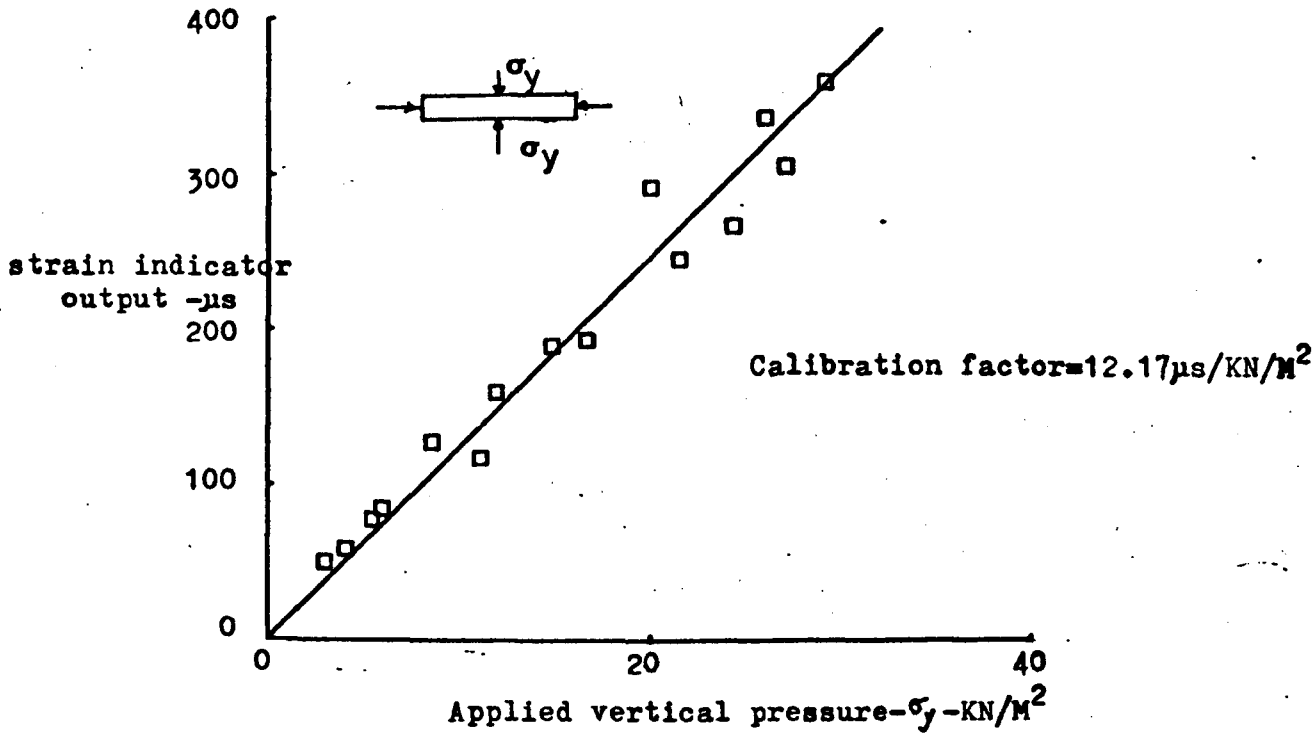
Fig.4·33 Triaxial calibration of pressure cell No. 5 for vertical stress measurement .
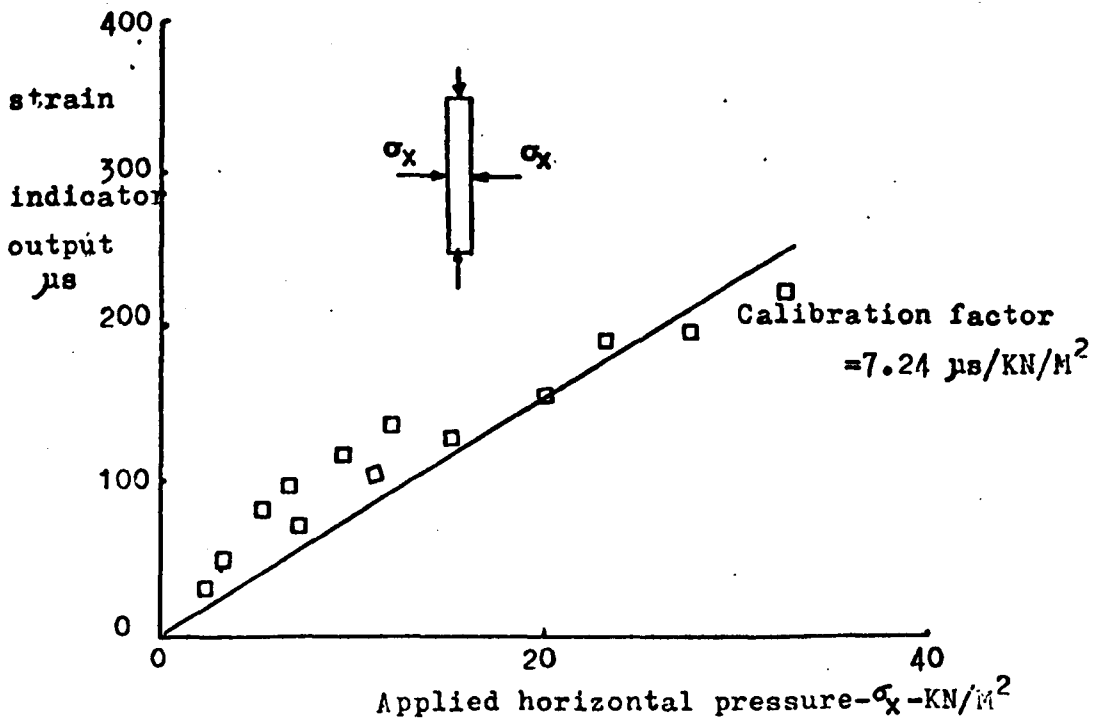
Fig.434 Triaxial calibration of pressure cell No. 5 for horizontal stress measurement.

Lead wires connected to the measuring circuit

PLAN
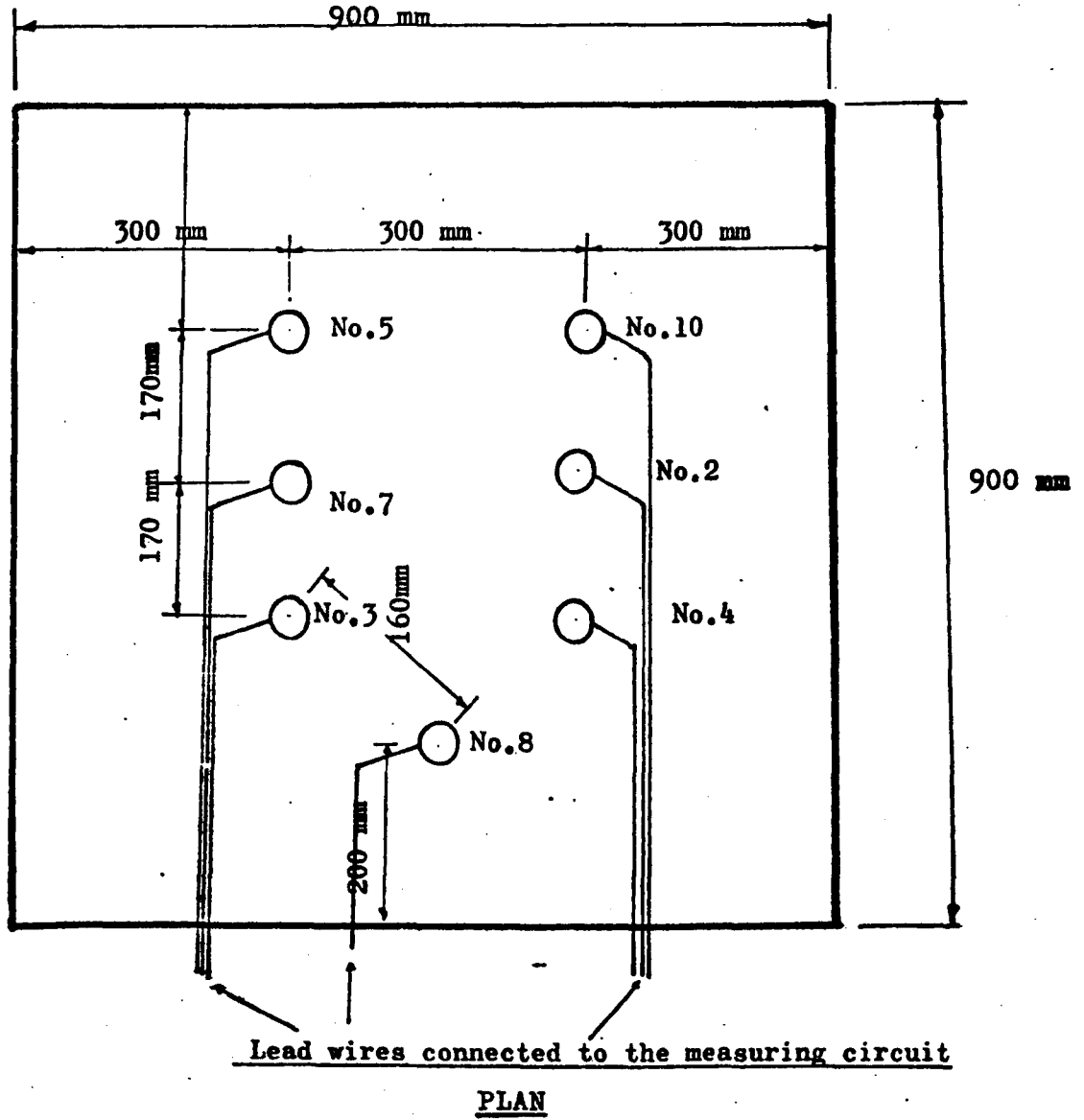
Fig.4.35 Placement of pressure cells during calibration test
(Cells placed 50 mm from the bottom of the model)
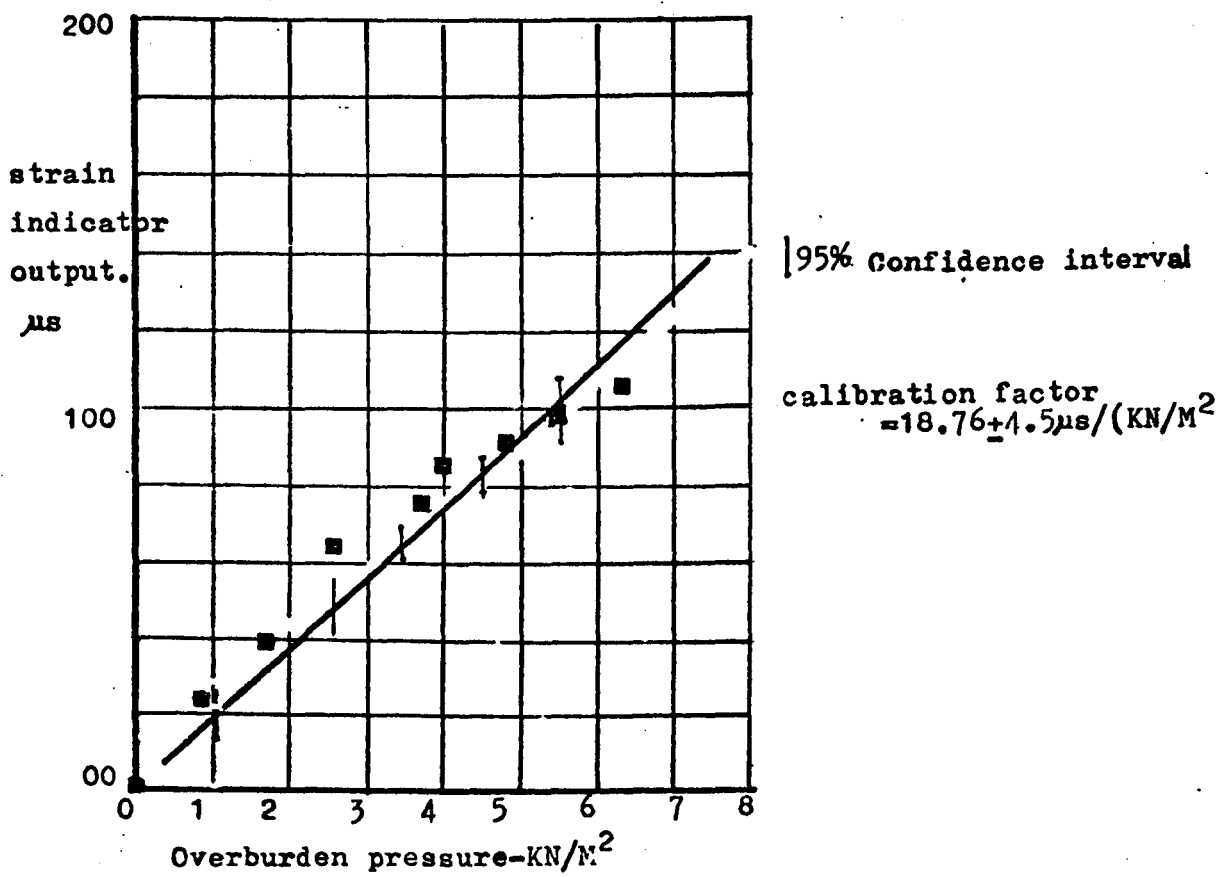
Fig. 4.36 Sand calibration curve for pressure cell No. 5 (from box).

was reached. The vertical stresses were computed from the layers' densities and their corresponding overburden heights. The pressure cell responses were plotted against the overburden pressures.   The relationship was assumed linear and a calibration factor was obtained using regression analysis, e.g. Fig (4.36).

4.7.2 Advantages and disadvantages of each method of calibration

4.7.2.1 Triaxial calibration

(i) Advantages

(a) The pressure cell can be subjected to different stress ratios and more thorough investigation into the cell behaviour can be made.

(b) The applied stresses can be accurately measured.

(ii) Disadvantages

(a) The pressure cells will be subjected to plane stress conditions when placed in the model, while these were calibrated in a triaxial stress situation.   This might lead to an error in the calibration factor.

(b) The method is time consuming since each cell has to be tested separately.

4.7.2.2 Plane strain calibration

(i) Advantages

(a) The pressure cells are subjected to the same stress field in which they will be placed.   .

(b) Less time is needed since eight of them could be calibrated in one test.

(ii) Disadvantages

(a) The pressure cells could only be subjected to one stress condition.

(b)   The vertical stresses could only be approximately determined as equal to the overburden pressure.   This would result in an inaccuracy of the calibration factors.

(c)   The calibration for the horizontal stresses is difficult to get.

The calibration factors obtained from the plane strain calibration procedure were adopted to interpret the pressure cell readings observed in the main test series, since these were found to give more consistent results than the calibration factors of the pressure cells established in the triaxial cell.

4.8   <u>Conclusions</u>

(1)   An apparatus has been designed and constructed, which can be used for building model walls.   Different accessories which can give relatively uniform beds of sand or support the model wall as it is built up, were provided.

(2)   Instrumentation consisting of:
    (i)   Tension gauges
    (ii) Free field strain coils
    (iii) Pressure cells
were developed and calibrated.   These can be used to monitor the model wall behaviour.

CHAPTER FIVE

MODEL TEST RESULTS

5.1 Introduction

5.1.1 Review of previous model tests

In this section a review of previous model tests, carried out to study the internal stability of reinforced earth walls, failing by tie breaking or tie pull out, will be presented. Most of these model reinforced earth walls tested failed by tie breaking and this failure mode will first be considered. Few model tests have been previously conducted to study the tie pull out mode of failure. A limited number of model walls were instrumented, and some model walls reported were tested under a surcharge load. The test results from these various studies will now be discussed.

5.1.1a Tie breaking mode of failure

Model reinforced earth walls designed to fail by tie breaking were mainly intended to test the validity of the theoretical approaches suggested for designing reinforced earth walls assuming this type of failure.

The factors influencing the critical height of walls failing by tie breaking and considered by previous investigators, included the tensile strength of the tie material, the tie length, the backfill density, the vertical tie spacing, the skin elements, and the foundation conditions. A review of the reported results on the influence of these factors on the critical wall height will be given in this section.

5.1.1.a.1 Tensile strength of tie material

The effect of the tensile strength of the tie on the critical height of rectangular model reinforced earth walls with uniform tie distribution was investigated, using steel pins as backfill, by Schlosser and Vidal[67] Schlosser et al [63], Long et al[47] and Bonfante et al[9] Bacot[3],

Binquet et al [7], Chapuis et al [17], Lareal et al [42], Lee et al [45] and Schlosser et al [63] used models with sand backfill. The critical wall heights observed in these tests were found to increase with increasing tensile strength of the tie which was varied by varying the tie width [3,7,17] or the horizontal tie spacing. [45,47,67]

The observed critical wall heights were compared mainly with the Rankine theory prediction [3,17,45] and in some studies the observed critical wall heights were compared with the theoretical critical wall heights predicted by Meyerhof and the Trapezoidal design methods. [7,9] The critical wall heights predicted by the three methods were seen to be appreciably lower than the observed critical heights with the exception of one study [45] in which the observed critical wall heights were found to be in fair agreement with the Rankine theory prediction when medium dense sand was used as backfill material.

The discrepancy between the predicted critical wall heights using the Rankine theory and the observed data was attributed by Schlosser et al [63] to the simplifying assumptions on which the Rankine theory was based. Long et al [47] attributed this discrepancy to the rigidity of the skin elements used in building the walls. Tests by Long et al [47] conducted to study the effect of the skin element rigidity on the critical wall height, revealed that the skin element rigidity only slightly increases the critical height of low model walls. For high walls the skin element rigidity was noted to have no effect on the critical wall height.

5.1.1.a.2 The tie length

The influence of the tie length on the critical height of model reinforced earth walls was studied by Schlosser and Vidal [67], Levadoux et al [46], Bacot [3], Schlosser et al [61,66], Long et al [47] and Chapuis et al. [17] The critical wall height was found to increase with increasing tie length. Bacot [3] indicated that the ratio between the critical

height of the wall and the tie length $\frac{H_c}{L}$, lay between
2.5 - 3.55. Schlosser and Vidal [67] and Long et al [47]
compared the observed critical wall heights with the
theoretical values predicted by the conventional design
methods. Fig (5.1) shows the relationship between the
experimental results and the theoretical results using the
Rankine, the Trapezoidal and Meyerhof methods and is taken
from a review paper by Symons. [72] The information on
which this figure is based is contained in the papers by
Schlosser and Vidal, [67] Long et al [47] and Schlosser. [61] The
Trapezoidal and Meyerhof methods predicted a similar pattern
to the experimental results but the magnitudes of the
theoretical critical heights were lower than the observed
results. The Rankine method predicted a critical wall
height which was independent of the tie length. Schlosser
et al [66] compared the experimental critical wall heights
with the theoretical values predicted by the Meyerhof method,
Fig (5.2). This method underestimated the observed critical
wall height but followed a similar pattern to the experimental
data. In this study Schlosser et al also showed that a
reinforced earth wall could be built to slightly greater
height on flexible foundations than on rigid foundations.

5.1.1.a.3 Soil density and vertical tie spacing

Tests conducted by Long et al [47] in which the back-
fill density was varied presented difficulty in keeping
other parameters nearly constant. The change in density
resulted in changing the angle of internal friction $\emptyset$, and
hence the earth pressure coefficient.

The critical wall height was found to vary directly with
$\frac{1}{\gamma}$ and the experimental results were nearly 23 per cent
greater than the theoretical results calculated from the
Rankine theory.

Observations on critical wall heights reported by
Lee et al, [44,45] using loose and medium dense sand, indicated that
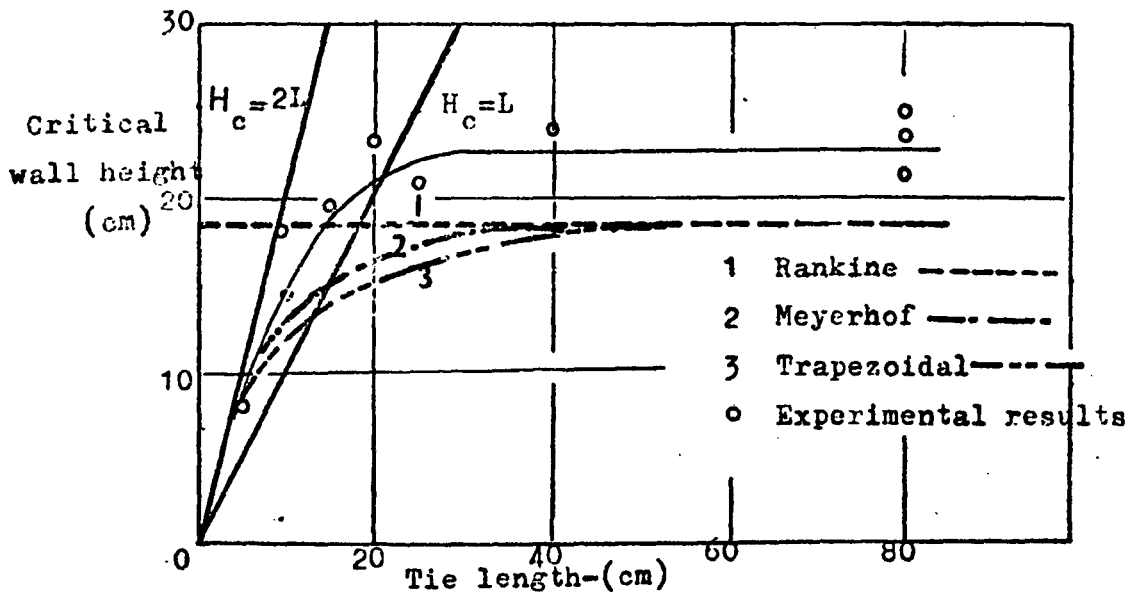
Fig. 5.1 Experimental & theoretical critical wall height V tie length(taken from a paper by Symons[72]).
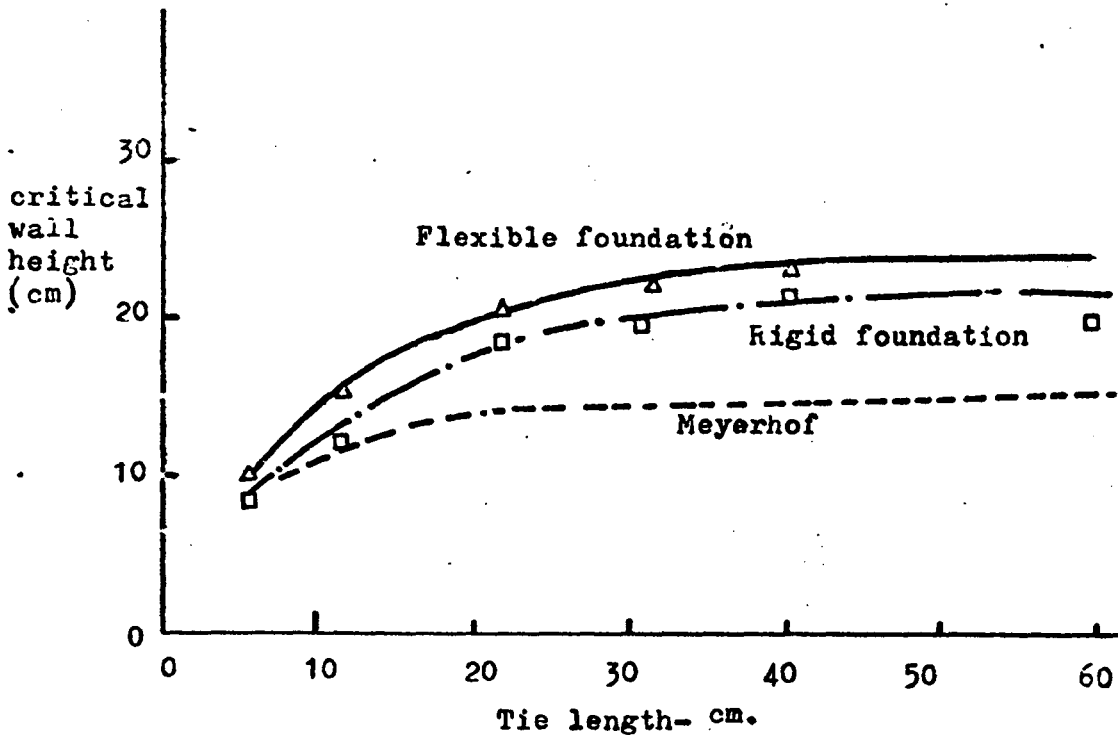
Fig. 5.2 Experimental & theoretical critical wall heights -V tie length. (After Schlosser et al [66])

there was no noticeable difference between the critical height of walls built using loose and medium dense sand.

Long et al[47] investigated the effect of varying the vertical tie spacing ΔH, on the critical height of model reinforced earth walls. The test results showed that the critical wall height H_c, varies almost linearly with $\frac{1}{\Delta H}$.

5.1.1.b Tie pull out mode of failure

As stated in the introduction the observations described in Section 5.1.1a referred to walls failing by tie breaking. Fewer tests have been conducted into the pull out failure mode. Schlosser and Vidal[67] first recognised this type of failure which was brought about by slipping of the ties from the reinforced earth mass. Their test results indicated that for rectangular walls the minimum ratio between the tie length to total wall height $\frac{L}{H}$ should be approximately equal to 0.8 to prevent this type of failure.

Some tie pull out tests were carried out by Bacot,[3] Lareal et al[42] and Levadoux et al[46] working in France and indicated an increasing critical wall height with increasing tie length.

Lee et al[45] studied walls failing by the tie pull out mode of failure, using loose and medium dense sand as backfill. The observed adherence length at failure was compared with the theoretical adherence length calculated by the Rankine and Coulomb adherence length expressions derived by Lee et al[45] The Coulomb methods were found to be in better agreement with the observed data than the Rankine theory, Fig (5.3).

5.1.1.c Instrumented reinforced earth model retaining walls

Some of the model tests previously described were instrumented to provide additional information regarding the
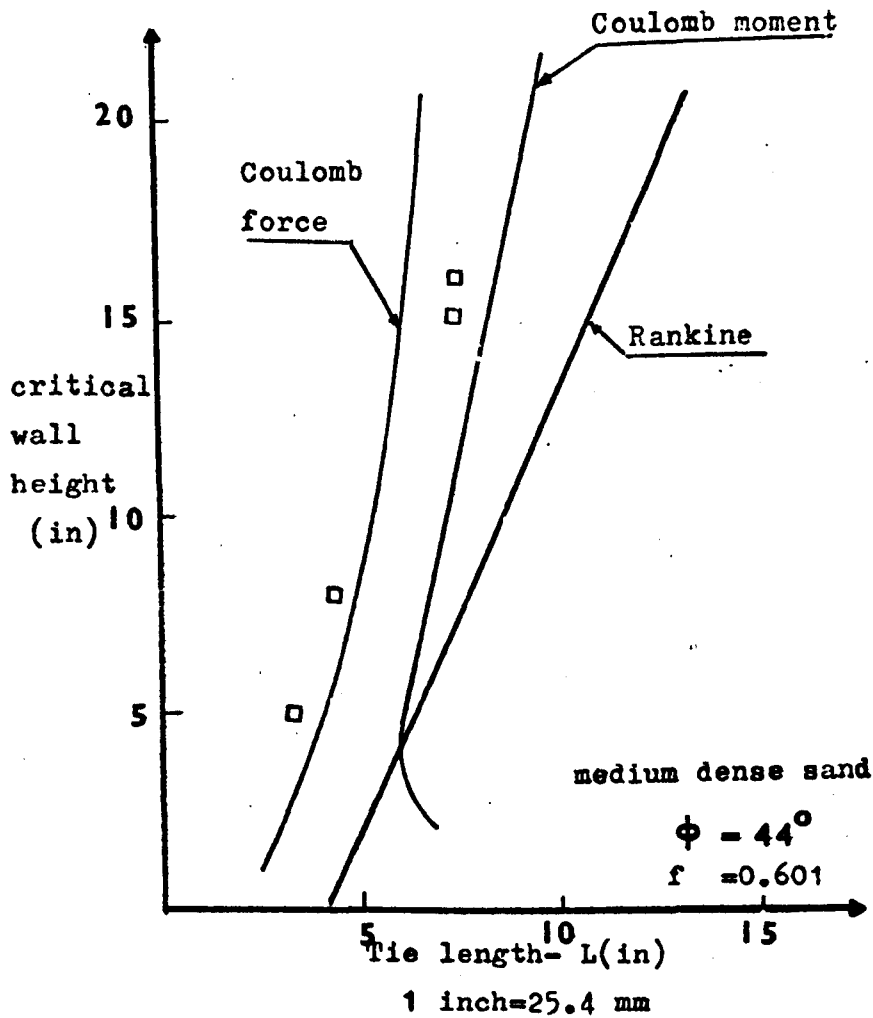
Fig. 5·3   Comparison between experimental & theoretical adherence
length(After Lee et al[45]   )

performance of the reinforced earth walls.

Schlosser and Vidal [67] and Long et al [47] used pressure recorders to measure the variation in vertical stresses at the base of model reinforced earth walls. The results were generally scattered but the average recorded stress compared well with the theoretical vertical stress computed from the backfill density γ and the fill height h.

Lee et al [45] attempted to instrument eight model reinforced earth walls to obtain stresses in the ties, vertical and horizontal stresses in the soil, and horizontal wall deflection. Strain gauges were used to measure stresses in the ties near the reinforced earth wall face and in a few cases the strain gauges were located along the tie. The lead wires seemed to present a problem by affecting the stress distribution around the tie and in most of the tests only tie stresses at the reinforced earth wall face were measured. In these model tests no great emphasis was placed on the vertical and horizontal stresses measured by the pressure cells because of calibration problems, and the horizontal wall deflection was measured relative to a deflected wall position.

5.1.1.d Model reinforced earth wall with surcharge

Schlosser et al [65] reported results of model tests carried out to study failure of reinforced earth walls under a surcharge point load. A method of designing for this type of load was proposed.

5.1.1.e Conclusions from previous model tests

(1) Most of the reinforced earth retaining walls tested were rectangular in cross-section with a uniform tie distribution. The majority of these model tests used elliptical metal skin elements, aluminium foil ties and sand or stainless steel pins as backfill.

(2) The majority of the model tests reported were

based on an ultimate strength concept and only
conditions at failure were observed. This approach
only gives an overall safety factor against failure
by tie breaking and leads to an uneconomic design.

(3) The study of tie pull out mode of failure in
model tests was limited to the observation of wall
heights as the tie length was increased. No attempt
was made to assess the stability of ties at different
wall levels or to check the assumptions on which the
theoretical design approaches assuming this type of
failure, were based.

(4) Few model tests were reported in which the stresses
in the ties, the vertical soil stresses and wall deflec-
tion were measured. No attempt was made to measure
the strain in the backfill of model reinforced earth
retaining walls, which helps in indicating the state
of stress in the reinforced earth backfill.

5.1.2 Objectives of this study

The present study was intended to serve as an extension
to the previous model studies.

Model reinforced earth walls using an ultimate strength
concept will first be considered, with the aim of assessing
the theoretical approaches based on this failure concept.
The advantages and disadvantages of the ultimate strength
approach for designing reinforced earth walls will be out-
lined.

An optimum design of a reinforced earth retaining wall
requires checking the safety factors against tie breaking
and tie pull out failure, at each tie level in the reinforced
earth wall. This can only be done by measuring the stress
distribution in the ties. Measurement of stresses and
strains in the soil, and wall deflection will contribute to
the understanding of the reinforced earth wall behaviour and
allow the various assumptions on which different theories
are based to be checked. This approach will also be followed
up in the present experimental programme.

5.1.3 Summary of the model test programme

The present model test programme consisted of five tests series designated A, B, C, D and E. A summary of these test series will be outlined in this section.

Properties of ties, skin elements and sand used in these tests are shown in Table (5.1). Previous mention of the skin elements and ties design has been made in Chapter Four sections (4.2.3) and (4.2.5) respectively.

Series A tests

Series A tests were intended to determine a minimum distance between the rear side of the model and the back of the reinforced earth wall at which the effect of the friction between the soil and the rear side of the model on the reinforced earth wall behaviour can be neglected.

In this series 33 reinforced earth walls were built up to an unstable height at which the ties pulled out of the sand mass. The critical height of these walls was observed as a function of the distance between the back of the wall and the rear side of the model, which was varied by constructing a movable wall inside the model.

Results of model reinforced earth walls tested in series A, in which the presence of the rear side of the model was known not to influence the critical wall height, were used as experimental data and the corresponding theoretical adherence lengths were computed and were compared with the observed adherence length.

Series B tests

The objective of series B tests was to examine the reinforced earth theories intended for the reinforced earth wall design assuming tie breaking failure. Eight model walls were built using 20 μm thick aluminium foil ties and the maximum height of the walls was observed as the tie width was varied. The experimental critical heights were

TABLE (5.1) - Properties of the ties, skin elements and sand used in the present model test programme

Components	Properties of the components			
	Series A & C	Series B	Series D	Series E
Ties	Aluminium foil ties Thickness = 45 μm Width = 4.4 mm f = .510 Tie Length Series A = 305-315mm Series C = 400 mm	Aluminium foil ties Thickness = 20 μm Width (Varied) Length = 400 mm R_t = 1.011 $\pm$ .033 N/mm	Perspex ties Thickness = 1.5 mm Width = 22.7 mm Length (Varied) f = 0.398	Perspex ties Thickness = 1.37 mm Width = 22.3 mm Length = 400 mm f = 0.398
Skin elements	Perspex panels Thickness = 6 mm Width = 150 mm Height = 100 mm Weight = 1N	Perspex panels Thickness = 6 mm Width = 150 mm Height = 100 mm Weight = 1N	Perspex panels Thickness = 6 mm Width = 300 mm Height = 250 mm Weight = 5.4N	Series E tests used the same skin elements as Series A and D to allow varying the tie spacing.
Backfill material	Sand γ_{min} = 1.397 gm/cm^3 γ_{max} = 1.6954 gm/cm^3 γ = 1.6145 gm/cm^3		Relative density D_r = 76.5% G = 2.65 ϕ = 40° K_a = 0.217	

compared with the theoretical predictions using the conventional and the energy theories and also with previous relevant model test results.

Series C tests

The series C model reinforced earth walls were intended to serve as preliminary walls to investigate the methods of tie tension and wall deflection measurements.

Three walls were built in this series to a maximum height of 500 mm. The forces in the ties and horizontal wall deflection were observed during the construction of the walls, using the preliminary tension gauge design shown in Fig (4.15) in Chapter Four, and the strain coils respectively. The tension gauges, apart from problems regarding the use of two different materials in the gauge construction, gave reasonable results. The strain coils satisfactorily measured the wall deflection.

Series D tests

The objective of this test series was to investigate the tie pull out mode of failure using an ultimate strength approach. In this test series it was also intended to observe variation in tie tension along a tie length and with increasing fill height above the tie level. The effect of the tie length on the maximum tension in the tie was assessed.

In investigating the influence of tie length on the maximum tie tension various parameters such as the tie level above the wall base can affect the maximum tie tension. To reduce the number of parameters involved and to get measurable stresses in the ties, large vertical tie spacing (250 - 125 mm) was adopted. Twenty-two model reinforced earth walls were built in this series, with varying tie lengths and horizontal tie spacing.

Series E tests

This test series was intended to study the internal stability

of reinforced earth walls on a non-ultimate strength basis.
The previous tie breaking failure tests provide a method of
designing reinforced earth walls failing by tie breaking,
based on the most stressed tie in the wall which has been
assumed to be at the bottom of the wall [67] . This approach
will lead to an overdesign for the ties in the middle and
top of the wall. The pull out failure tests provide no
information regarding the actual safety factors against tie
pull out failure at different reinforced layers and because
of the limited results from these tests, cannot be used to
check the assumptions on which various theories were based.
To overcome the limitations of the tie breaking and tie pull
out tests series E was designed.

This test series consisted of 35 walls built to a
maximum height of 500 mm using a constant tie length of 400
mm. The tie tension was measured at different locations
along a tie length and at various levels in the wall. The
horizontal and vertical tie spacings were varied and the
maximum tie tension over the wall height was determined and
compared with different theories. The non-dimensional
tension parameter X and the safety factors against tie pull
out at different tie levels, were computed and   compared
with the corresponding theoretical values.

In this test series the walls were also instrumented to
measure the horizontal and vertical strain in the soil, the
horizontal wall deflection and the vertical stresses in the
soil.

5.2   Series A Tests
Model rear wall effect on maximum height of reinforced earth wall

5.2.1   Introduction

It has been mentioned in Chapter Four, Section 4.2.1
that side effects on reinforced earth wall behaviour could
arise from width upon height ratio of the model [43] and also
from rigidity of the sides of the model [2] These effects
have been taken care of in the design of the model by

adopting a width upon height ratio of 1.8 and stiffening the sides of the box to ensure its rigidity.   A third possibility which might be of lesser importance, could arise from the limited extent of the model in the direction of the ties. If the distance between the rear side of the model and the back of a reinforced earth wall is not large, the friction of the rear side of the model would result in lowering the earth pressure on the back of the reinforced earth wall and this, in turn, could lead to a change in the vertical stress distribution in the reinforced earth fill.

To investigate this problem, reinforced earth walls were designed to fail by tie pull out mode of failure, since this is more dependent on the vertical stress distribution than the tie breaking mode of failure.   Two sets of walls were built using tie lengths equal to 315 and 305 mm. These tie lengths were chosen to give critical wall heights which would cover the range of wall heights intended to be built in the model.   In each set of walls the distance between the back of the wall and the rear side of the model was varied by constructing a movable barrier fitted inside the model and the maximum height of the walls was observed.

The apparatus used in building the walls, the material properties and the method of wall construction will be outlined in the following section.

5.2.2 Apparatus and wall construction

Box dimensions and skin elements used for building walls in series A tests are shown in Figs(5.4) and (5.5) respectively. The ties used consisted of 45 μm thick aluminium foil, of average width 4.4 mm.   The soil/tie coefficient of friction used was 0.51 and the average density of the sand backfill was 1.6143 gm/cm^3.   The horizontal and vertical tie spacings were kept constant at 150 mm and 100 mm respectively.   Tie lengths adopted in this series were 315 and 305 mm.   The wall construction proceeded as was described in Section (4.3) in Chapter Four.

930 mm

500 mm

|← 150 mm →|

100 mm

907 mm

100 mm

100 mm

6mm

100 mm

10 mm

Side View

150 mm

128 T

Elevation

6 mm

Plan
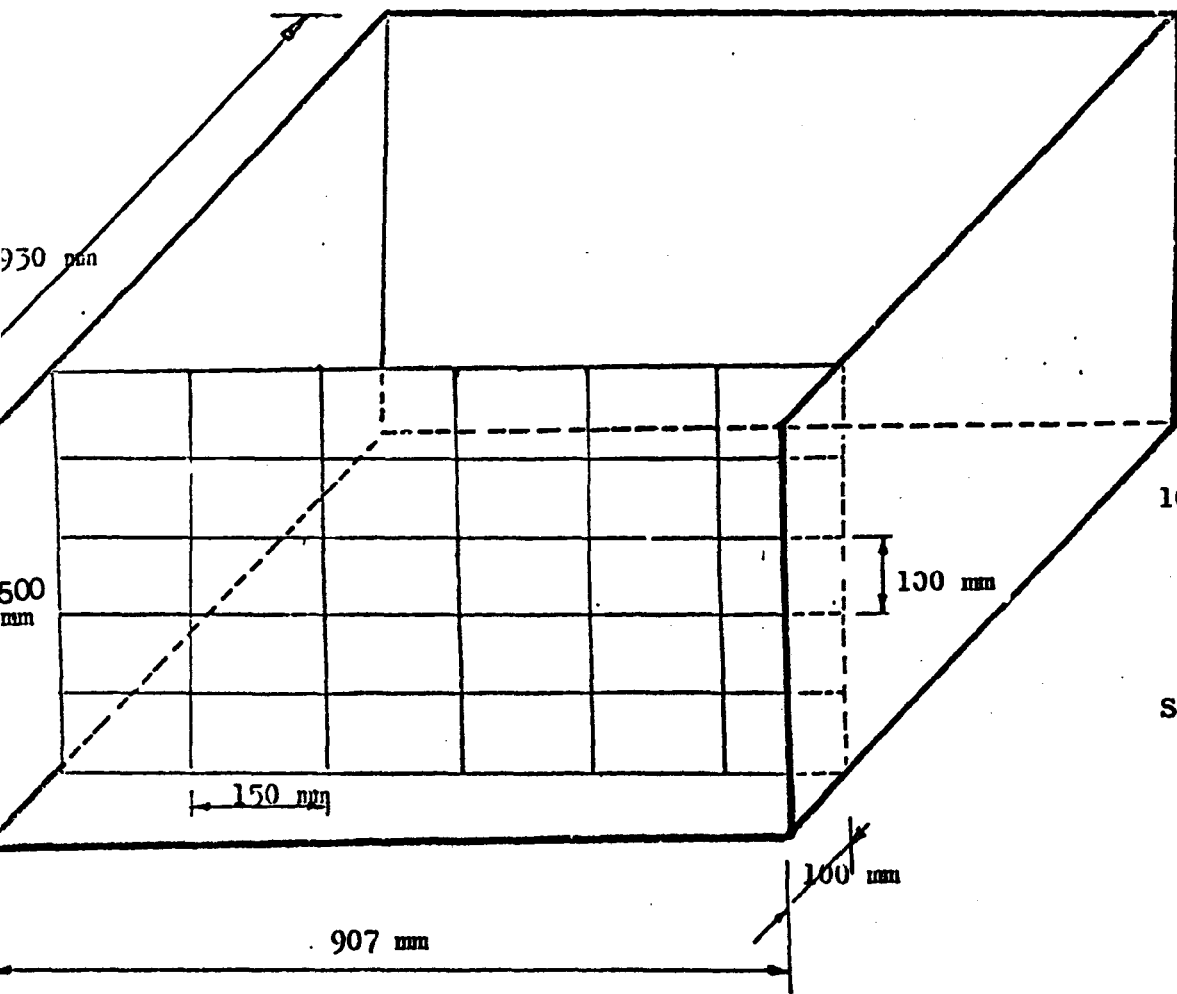
Fig.5.4 Test model & perspex panels (Series A,B,C   )

(No. of panels = 30, No. of ties per panel = 1)
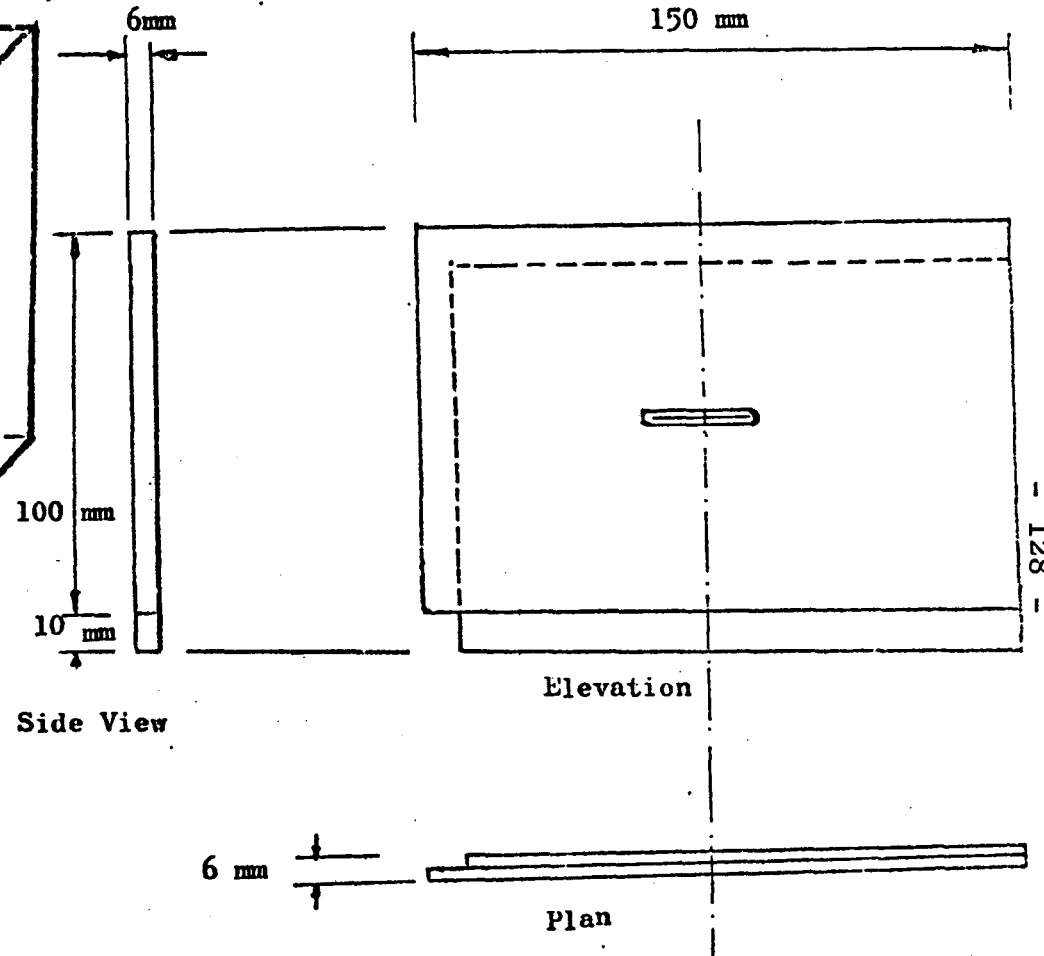
Fig.5.5 Perspex panel dimensions

Initially the walls failed at lower heights than was expected. This was mainly because of the aluminium clamps used to anchor the ties after they were passed through the skin elements Fig (5.6a). The edges of the clamps tore the aluminium foil ties before the walls reached their maximum height. This resulted in an early tie breaking failure instead of a pull out failure. Adhesive tape was later used to fix the ties to the skin elements Fig (5.6b), and this proved to be a more satisfactory method than the aluminium clamps.

All the walls built using the adhesive tape to attach the ties to the skin elements, failed by tie pull out. Some of these walls were used as data for comparison between experimental and theoretical adherence lengths. These were termed series A(1), and they will be presented later when discussing the results of the series D tests.

5.2.3 Series A test results

The results of series A tests regarding the relation between the parameters H_c and LB shown in Fig (5.7), and the subsidiary observations made during the wall construction and after failure of the walls will be summarized in this section.

(i) The observed critical wall heights H_c and the corresponding distance LB between the back of the wall and the movable barrier, are shown in Table (5.2) and Fig (5.8). The graph showed that when LB is greater than about 250 mm an almost constant failure height was given. Some scatter in the data was noted for the 315 mm tie length, when LB was small. This is possibly because this length was just critical for tie pull out failure as indicated by the energy theory. By examining the ties after failure of the walls built using 315 mm tie length, some of the ties at the wall bottom were found broken.
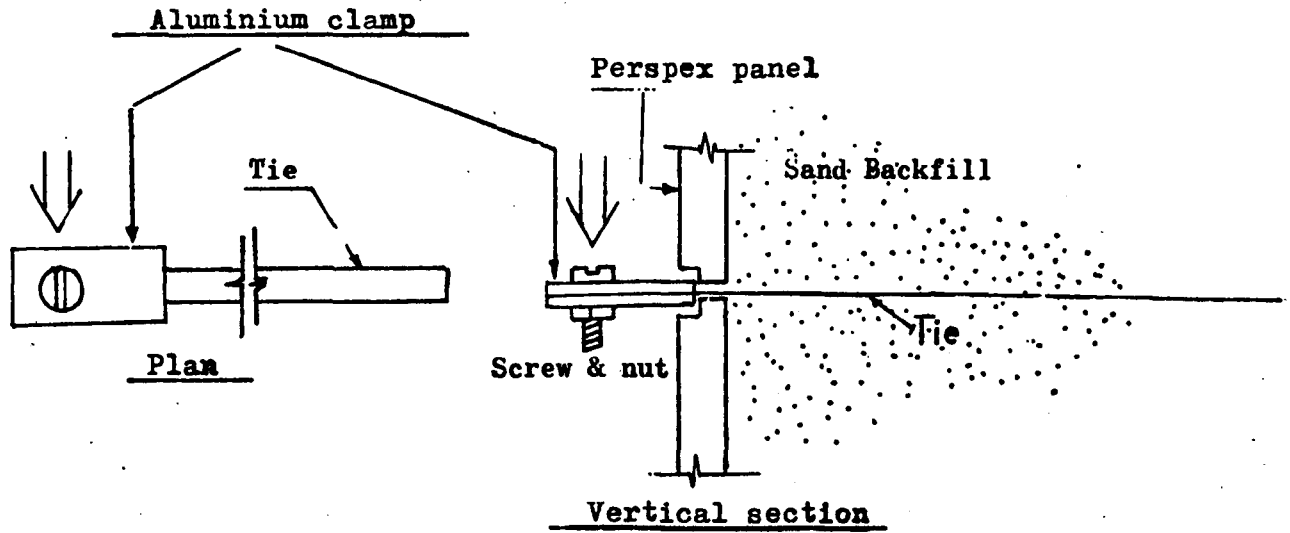
Fig.56.a Aluminium clamp for tie-panel connection
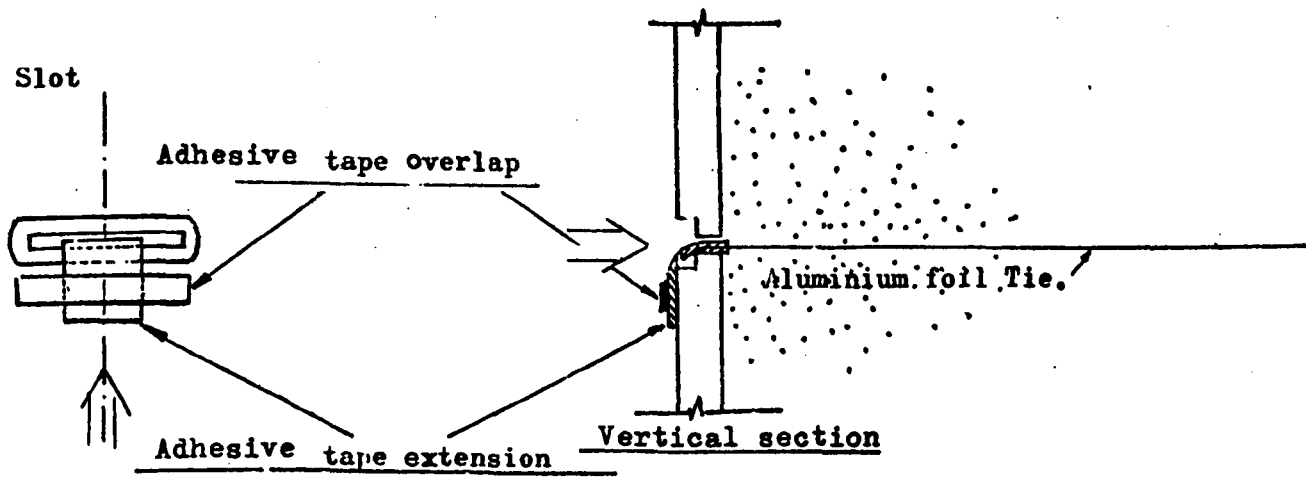
Fig 56.b Adhesive tape attachment for tie-panel connection

Fig. 56 The first & 2nd. tie-panel connection
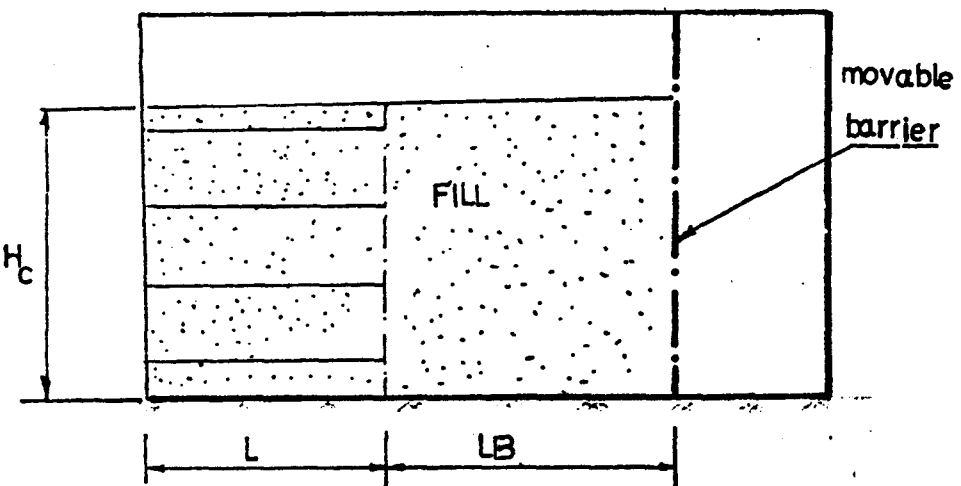
Fig.5.7 Series A tests parameters
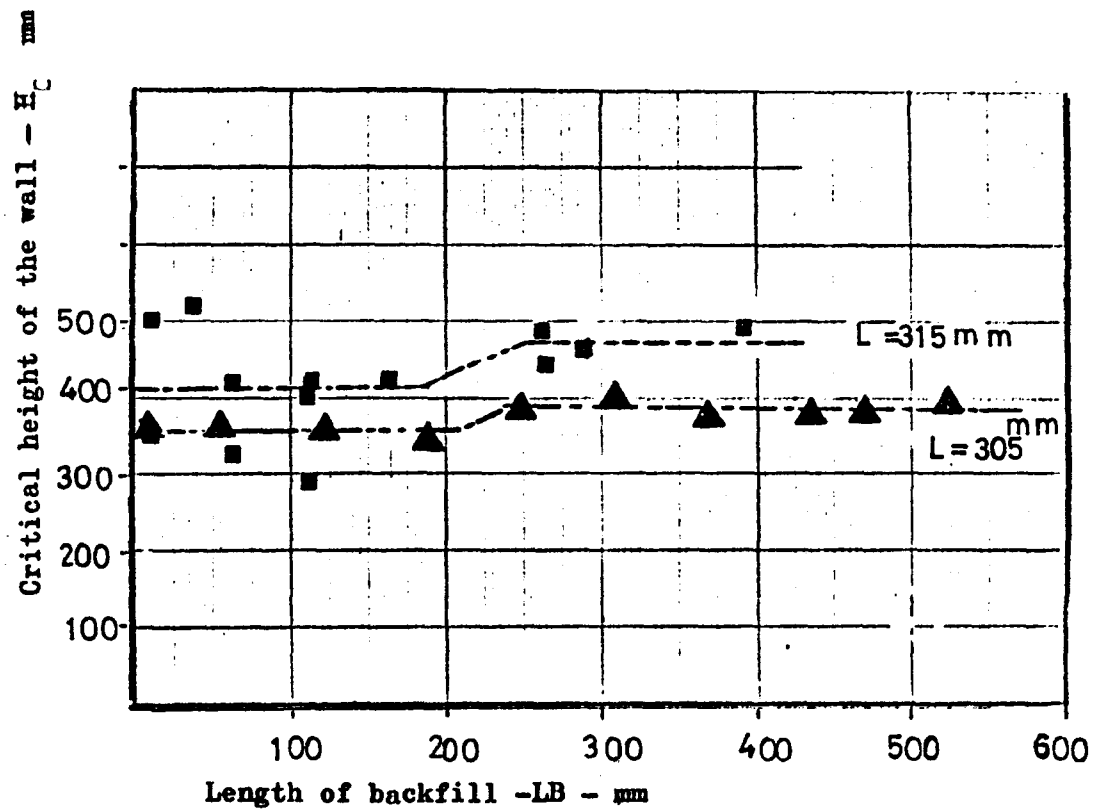
Fig. 5.8   Backfill length V Critical height

TABLE (5.2) - Series A Test Results

	L = 315 mm				L = 305 mm		
Test No	LB mm	H_c mm	γ gm/cm^3	Test No	LB mm	H_c mm	γ gm/cm^3
7A	115	290	1.545	18A	125	355	1.592
8A	115	400	1.626	22A	5	350	1.609
9A	115	420	1.626	23A	55	355	1.649
10A	65	325	1.632	24A	250	385	1.609
11A	65	420	1.614	25A	190	340	1.613
12A	15	350	1.637	26A	310	400	1.624
13A	15	495	1.614	27A	370	376	1.627
14A	15	500	1.613	28A	435	380	
15A	40	520	1.610	29A	470	380	1.591
16A	165	420	1.610	33A	525	395	
17A	265	490	1.591	Wall design parameters			
19A	290	460	1.605	b = 4.39 mm		ΔH = 100 mm	
20A	265	447	1.582	f = 0.51		S = 150 mm	
21A	395	490	1.626	t = 45 μm		$\emptyset$ = 40°	
						K_a = 0.217	

(ii) Failure of the walls by tie pull out was observed to be catastrophic and abrupt. The measured deformations were small before failure.

(iii) The inclination of the failure surface with the horizontal plane was determined approximately by measuring the position of the failure plane, at the wall surface, after failure of the walls. The average value of all tests was 67.8°. This is slightly greater than the theoretical value given by the Coulomb failure plane which is equal to 65° based on a triaxial angle of friction $\emptyset = 40^{\circ}$ measured at an average density equal to 1.605 gm/cm^3.

(iv) The wall deflection at 150 mm above the base of the model was also observed, during the construction of the wall and just prior to the collapse of the wall. This was expressed as a ratio of the total wall height prior to failure. An average value of this was 0.675%.

5.2.4 Conclusions

(i) The tests conducted in this series aimed at determining a distance, LB, between the back of the reinforced earth wall and the rear wall of the model, which when adopted, would produce a minimum effect by the rear wall on the stresses in the reinforced earth fill. The walls built with varying LB, failed at low heights when the distance LB was small, possibly due to the reduction in the vertical stresses by the friction of the rear wall of the model. An increase of the critical height of about 10% to 11.5% was noted when LB was greater than 250 mm. The critical height of the walls remained almost constant for the 305 mm tie length. With the 315 mm tie length some scatter in the data was noticed for small LB, but the general

trend of the observations remained the same as the results obtained for the walls built using the 305 mm tie length.   In the tests carried out in future series this distance was kept over 300 mm.

(ii)   Some of the walls tested in this series were used as data for comparison between the observed and predicted adherence length and will be presented later when discussing the series D tests.

(iii)   From subsidiary observations on the wall it was noted that the angle of inclination of the failure plane was approximately equal to the inclination of the theoretical Coulomb failure plane.

(iv)   The average ratio of the horizontal wall deflection and the total wall height was 0.675%. Probably this indicated that the soil backfill near the wall face was in an active state of earth pressure.[73]

5.3   Series B tests
Tie Breaking Mode of Failure

5.3.1   Introduction

In the previous test series the reinforced earth walls were designed to fail by tie pull out.   The tests were mainly intended to study the effect of friction of the rear side of the model on the critical height of the wall.

In the present test series eight walls were built and were designed to fail by tie breaking.   These tests were intended to compare the actual tensile stresses developed in the ties with the predicted values.   The main observation made in this series was of the maximum stable height to which the walls could be constructed.   Some subsidiary observations on the positions of breakage of the ties and the distance of the failure plane from the inside of the skin elements were also made.

Comparisons were made between the critical heights of

walls tested in this series and the Rankine, the Trapezoidal, Meyerhof, Banerjee and the Energy theories and are discussed in the results and the conclusions of the present test series.

5.3.2 Apparatus and wall construction

The model and properties of the materials used in series B tests will be described in this section.

The present test series used the test model and skin elements previously adopted in series A tests and schematically shown in Fig (5.4) and (5.5). The ties were cut from aluminium foil rolls 20 μm average thickness in 400 mm lengths . This length was adopted to exclude a tie pull out failure. The tensile strength R_t of the tie material was determined using the loading frame shown in Fig (5.9). Tests to rupture on 15 samples of varying widths of tie from 4.4 mm to 17.1 mm, gave a value of R_t = 1.011 $\pm$ 0.33 N/mm. The horizontal and vertical tie spacings adopted in this series were 150 and 100 mm respectively. The method of wall construction followed the sequence of wall building procedure previously described in Chapter Four, Section (4.3).

5.3.3 Series B test results

The main observations made on walls built in this test series, were of the critical height. Subsidiary observations were also made on the position of the failure plane. These test results will be presented and compared with theoretical predictions in this section.

A summary of series B test results is shown on Table (5.3). Fig (5.10) shows the observed critical wall heights and the corresponding tie width B, which is proportional to the tensile strength of the tie. The theoretical results were compared with the observed critical heights and all of the Energy theories gave closer agreement than the existing theories. The Conventional design methods using the

Steel frame

Test piece

Aluminium clamps

Weights
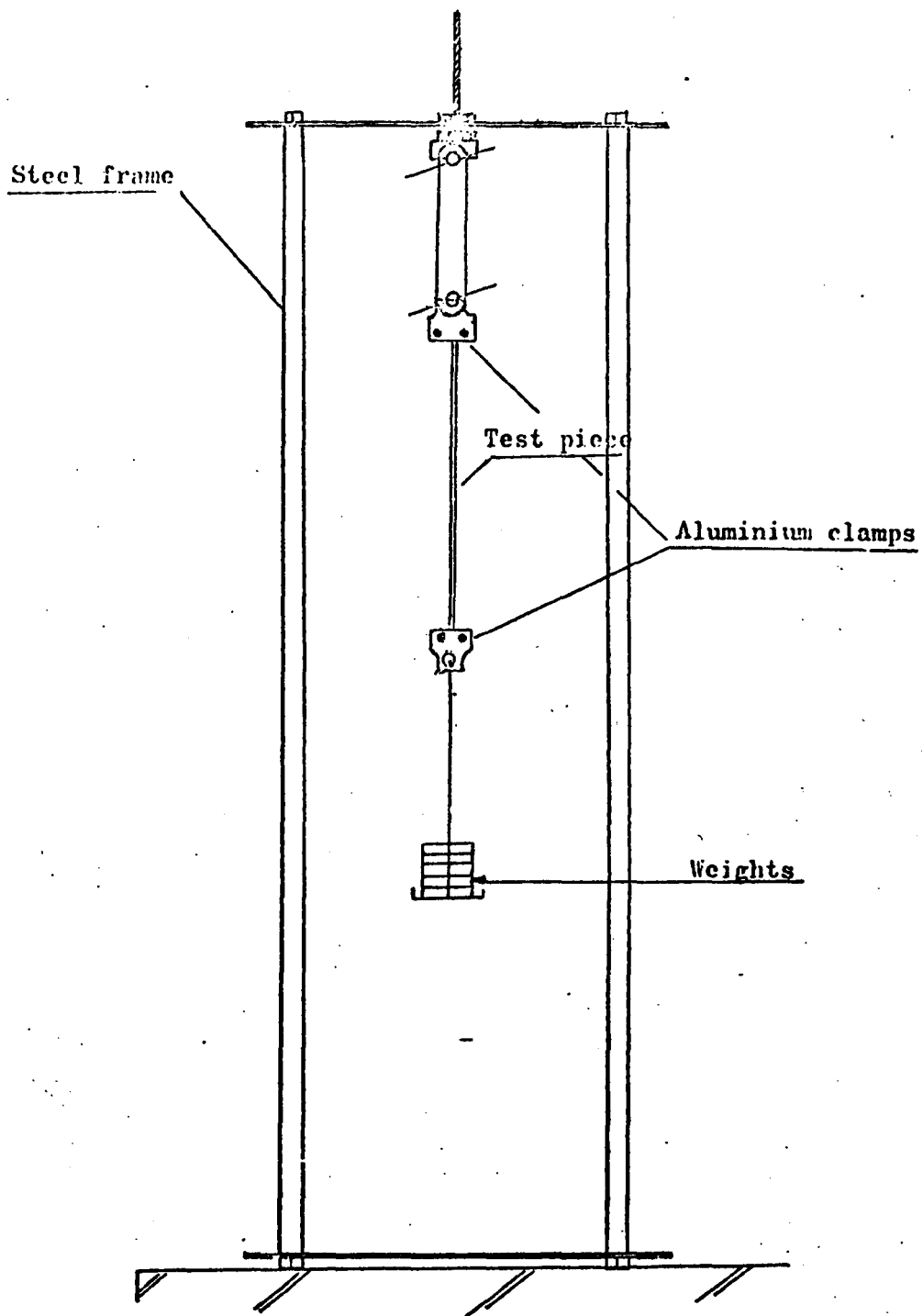
Fig. 5.9 Determination of the tensile strength of aluminium ties

by static loading of specimen

Fig. 5.10 Comparison between experimental & theoretical critical wall heights.
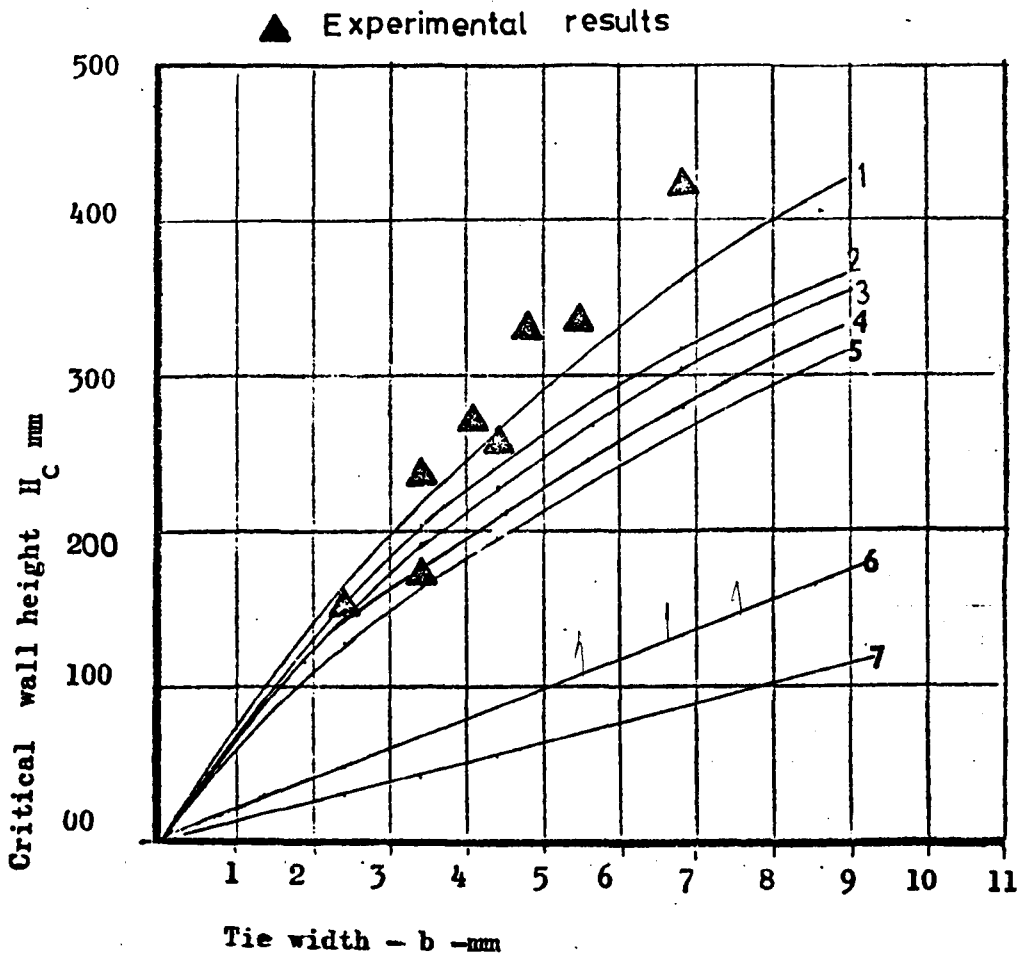
1- Energy theory(T.P.P.D.)
2-   "   "   (T.L.L.D.)
3-   "   "   (LO.L.D.)
4-   "   "   (T.L.L.A.)
5-   "   "   (LO.L.A.)
6- Rankine, Trapezoidal & Meyerhof methods.
7- Banerjee(first tie break)

Rankine, the Trapezoidal and Meyerhof methods predicted practically the same critical wall height and substantially underestimated the observed critical wall height. Banerjee's expression based on the assumption of breaking of the first tie at the bottom of the wall, gave appreciably lower values than the observed data.

Two observations were made in order to determine the approximate position of the failure plane.

(a)   After each test the positions at which the ties broke were noted.   The average value of the tie breaking position at each tie level was determined and was plotted against the wall height as shown in Fig. (5.11).   The observed average tie breaking positions are generally contained within the Coulomb failure wedge.   Most of the ties at the top of the walls did not break and failed by pulling out.

(b)   The position of the failure at the surface of the wall was noted in each test.   The average inclination of the failure plane with the horizontal was 63.8° which was nearly equal to the theoretical inclination of the failure plane for an unreinforced wall, given by $\Theta = 45^{\circ} + \frac{\emptyset}{2}$.   For $\emptyset = 40^{\circ}$, the appropriate value for the backfill as placed, $\Theta = 65^{\circ}$.

5.3.4   Comparison between series B test results and previous test results

In the foregoing section the series B test results were presented and were compared with the values predicted by various theoretical approaches.   In this section comparison will also be made between the critical wall heights observed in series B tests and the similar   model test results conducted in France by the Laboratoire Central des Ponts et Chaussées[7]   and in the U.S.A. by Lee et al[45]   .

TABLE(5.3) – Summary of Series B Test Results

(Tie breaking mode of failure)

Wall design parameters	Test No.	Tie Width b – mm	Critical height H_c – mm	Θ	γ gm/cm^3
$\gamma = 1.614$ gm/cm^3 $D_r = 76.5\%$ $\emptyset = 40^{\circ}$ $K_a = 0.217$ $L = 400$ mm $\Delta H = 100$ mm $S = 150$ mm $t = 20$ μm $R_t = 1.011$ N/mm	1B	2.39	150	62.1	1.615
	2B	3.41	235	64.19	1.616
	3B	4.42	255	66.8	1.603
	4B	5.64	335	57.7	1.584
	5B	6.81	420	–	1.629
	6B	3.40	170	64.3	—
	7B	4.12	270	64.3	1.614
	8B	4.78	330	67.45	1.6405

Θ = inclination of the failure plane measured at
the surface of the wall.
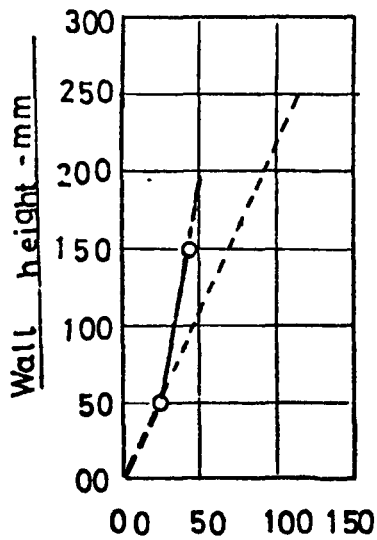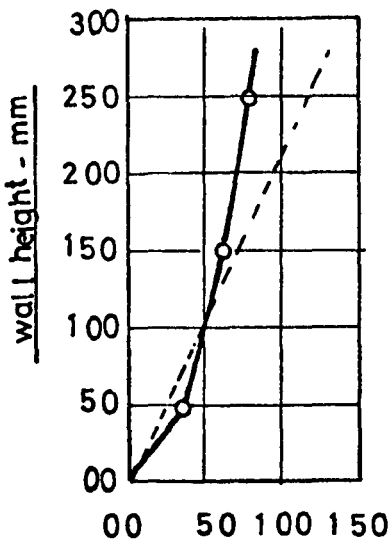
O Observed average tie breaking position

------ Coulomb failure plane
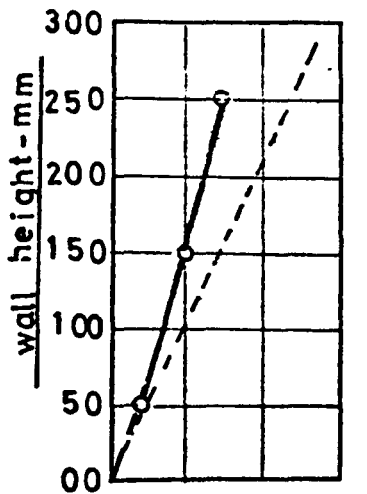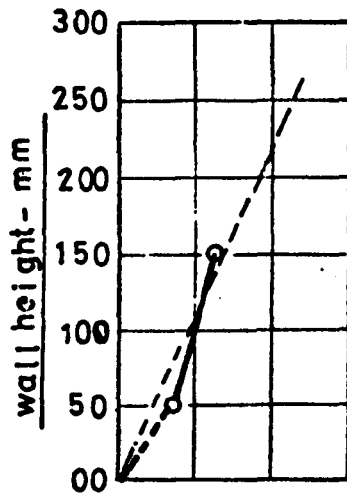
Fig.5.11 Average tie breaking position from wall face V wall height. (series B tests).

The French results were obtained using 9 μm aluminium foil having a tensile strength equal to 0.525 N/mm width, with ties length equal to 600mm. The tie width was varied from 3 to 10 mm. The sand was medium dense with an average density equal to 1.5350 gm/cm^3 and $\emptyset = 35^o$. Lee's model tests used sand at two densities, a medium dense sand with $\emptyset = 44^o$ and a density of 1.496 gm/cm^3 and loose sand with $\emptyset = 31^o$ and a density of 1.3575 gm/cm^3. The ties used were cut from aluminium foil 13 μm thick with an average tensile strength of 1.267 N/mm width. The average tie length and width were 400 and 3.9 mm respectively. Both the French and Lee's model tests used elliptical skin elements 30 mm and 25 mm in height respectively. In the French tests, as with the present laboratory model tests, the tie width was varied while the horizontal and vertical tie spacing was kept constant. In Lee's tests the horizontal tie spacing was varied and the tie width and the vertical tie spacing were kept constant.

Fig (5.12) shows the experimental results from the Glasgow, the French, and Lee's model test results, plotted against the non-dimensional parameter $\dfrac{S. \Delta H}{A_r}$ i.e. the soil area bounding a tie divided by the tie cross-sectional area A_r. These test results followed the same pattern and gave the same order of critical heights. The differences in density seemed not to affect the experimental values. The Glasgow laboratory test results were slightly higher than the French, and Lee's results, possibly due to different skin elements being used.

5.3.5 Conclusions

(i) The observed critical wall heights increased with increasing tensile strength of the tie and were found to be in closer agreement with the Energy theories than the existing theories. The Rankine, the Trapezoidal and Meyerhof methods predicted practically similar critical heights

△   Glasgow test results

♦   French test results

○   Lee's test results (medium dense sand)

▣   Lee's test results (Loose sand)
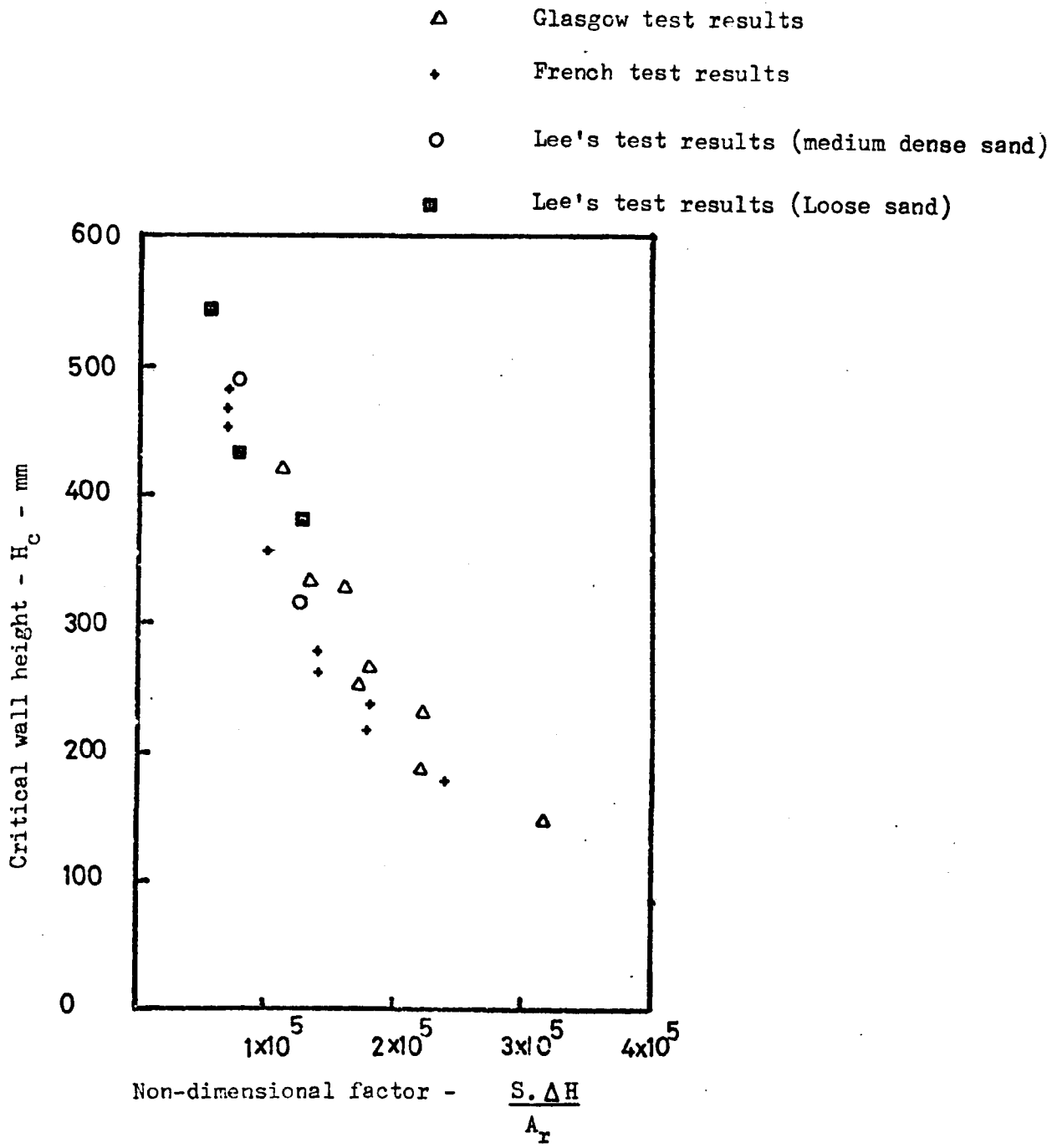
Fig. 5.12 Comparison between the Glasgow, the French and
Lee's tie breaking failure test results.

which were appreciably lower than the observed results.
The discrepancy between the critical heights predicted
by these latter methods and the observed values, ranged
between 61% - 72% of the observed critical heights.
The Banerjee equation based on the breaking of the
first tie at the bottom of a wall assumption, also
appreciably underestimated the observed critical heights.

(ii)   The critical wall heights observed in this test
series were shown to be consistent with previous model
test results carried out in France and in the U.S.A.
The differences in density and skin elements used
seemed to have no significant effect on the experimental
results.

(iii)   The average inclination of the experimental
failure plane measured at the wall surface and by
observing the distances from the wall face at which tie
breaks were found to be in reasonable agreement with
the theoretical Coulomb value for an unreinforced wall
given by $\theta^{\bullet} = 45^{\circ} + \emptyset/2$.

5.4   Series C Tests
Preliminary walls

5.4.1   Introduction

The series A and B tests were designed to fail by tie
pull out or by tie breaking and no observation on the actual
stresses in the ties and the soil were made.   In the D and E test
series the intention is to monitor the wall behaviour to study
the prefailure conditions in the wall.   The present test
series consisted of three walls designed to act as preliminary
walls for checking the performance of the instrumentation
used for tie tension and wall deflection measurements.

The various stages in developing a reliable method for
measuring stresses in the ties were presented in Chapter Four.
It has also been mentioned that a preliminary tension gauge
design consisting of 0.60 mm thick 6 mm wide x 35 mm long

perspex strip on which strain gauges were mounted on both
faces was constructed.   This was connected in series with
the aluminium tie in the manner shown in Fig (4.15) in
Chapter Four, and was used for tie tension measurement in
the present test series.

The horizontal deflection of the model wall face was
initially measured using dial gauges.   This system required
additional accessories to provide a fixed datum for mounting
the dial gauges, which was found to occupy appreciable space
in front of the model and obstructed the wall construction.
To avoid this difficulty, a set of strain coils previously
described in Chapter Four was used in this test series for
measuring the horizontal deflection of the front face of the
wall.

The result from this test series indicated that the
methods of stress measurement in the ties adopted in this
series, apart from inconsistencies in the coefficients of
friction introduced by using two different materials for
the tie and mounting the gauges, gave reasonable results.
The strain coils satisfactorily measured the deflection of
the front face of the wall.

5.4.2 Apparatus and wall construction

. The series C tests used a similar arrangement of box and
skin elements previously used in Series A and Γ tests and
schematically represented in Figs (5.4) and (5.5). The
ties used in this series were 400 mm in length cut in 4 mm
widths from a 45 μm thick aluminium foil roll.   The
horizontal and vertical tie spacings adopted were 150 mm
and 100 mm respectively.   The tie dimensions were chosen
such that the wall would not fail within the height of the
model, thus allowing investigation of the performance of
the instruments used for monitoring the tie tension and the
horizontal deflection of the wall face for the maximum range
of height available in the model.   The walls were constructed
in a similar manner to Series A and B tests, adopting the
wall building procedure previously described in Chapter Four,
Section (4.3).

5.4.3   Series C test results

The test results obtained from Series C tests included the observations made on the tie tension and the horizontal deflection of the reinforced earth wall face.   These will be presented in this section.

5.4.3.a   The tie tension

The tie tension was measured in two model walls, using the preliminary tension gauge design previously described in the introduction of this test series.

In the first test the tie tension variation along a tie length and with increasing overburden height was observed using tension gauges fixed in series at three locations along the aluminium foil tie Fig (5.13a).   Two gauged ties were placed at two different wall levels and the tension developed in the ties was observed as the fill height was increased.   The test results are shown in Table (5.4) and Fig (5.14) and indicated a maximum tie tension near the wall face which decreased towards the free end of the tie.

In the second test the tie tension near the wall face Fig (5.13b) was observed.   The results from this test are shown in Table (5.5) and Fig (5.15) and indicated an increasing tie tension with wall depth.

5.4.3.b   The wall deflection measurements

As shown in Fig (5.16), the outward deflection of the front face of the wall was measured using five pairs of strain coils which had been previously calibrated against a pair of reference coils.   The strain coils were fixed in pairs at each tie level one on the wall facing and the other on a fixed datum provided by 25 mm thick perspex planks situated in front of the model.   Wall deflection measurements were taken after the placing of each 50 mm thick sand layer.

The measured horizontal wall deflection in the various

Fig (5.13a) Tie tension measurement along a tie length
(Series C tests)
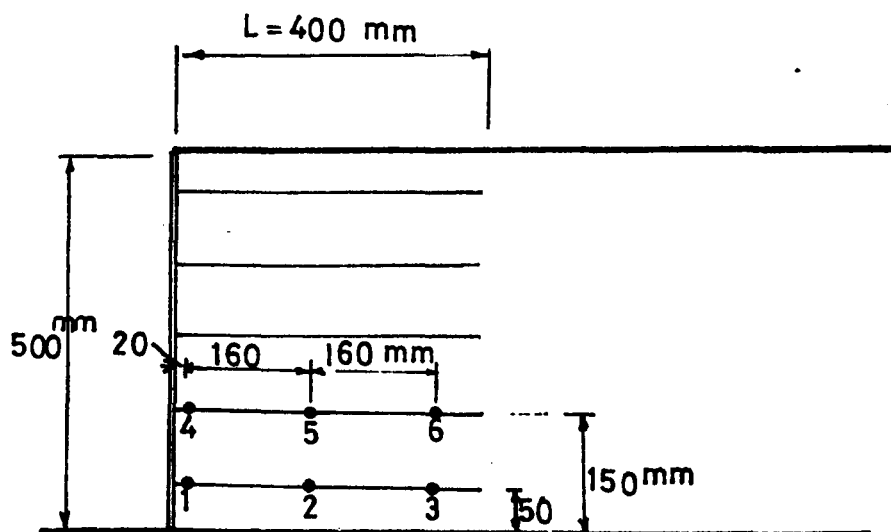
TABLE (5.4) - Measured tie tension along the tie length
(Series C tests)

Total Wall height mm	Measured tie tension along tie length - N (Fig 5.13.a)					
	1	2	3	4	5	6
100	0.67	0.55	0.42			
200	4.8	6.3	3.7	0.74	0.60	0.42
300	13.25	8.2	4.9	7.9	5.3	3
400	15.2	9.6	6.2	9.3	6.6	3.7
500	16.7	10.6	7.5	10.6	7.2	4.9

Fig (5.13b) Tie tension measurement at 20 mm from the wall face (Series C tests)

Locations of tension gauges(20 mm from wall face)
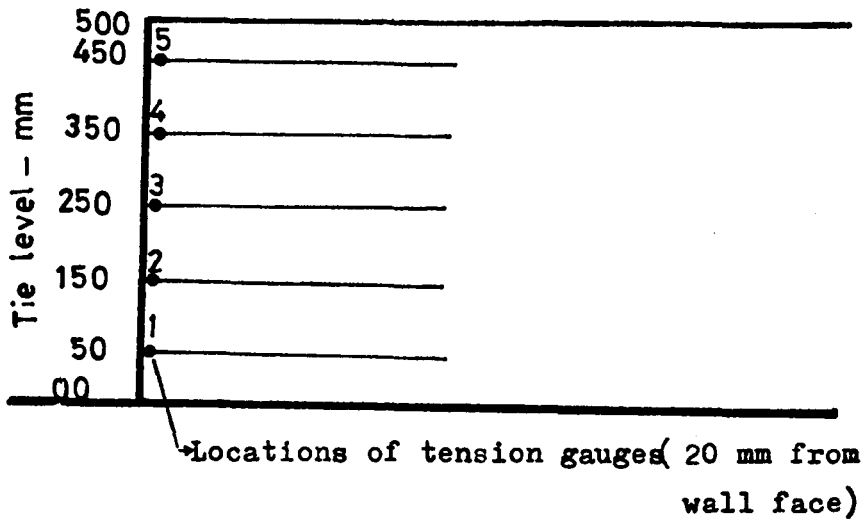
TABLE (5.5) - Measured tie tension near the wall face (Series C tests)

Total Wall height mm	Measured tie tension - N @ locations 1 - 5, Fig (5.13.b)				
	1	2	3	4	5
200	2.7	-	-	-	-
300	9.8	2.41	0.40	-	-
400	9.9	4.66	4.3	2.8	-
500	13.5	6.2	2.0	10.0	3.5
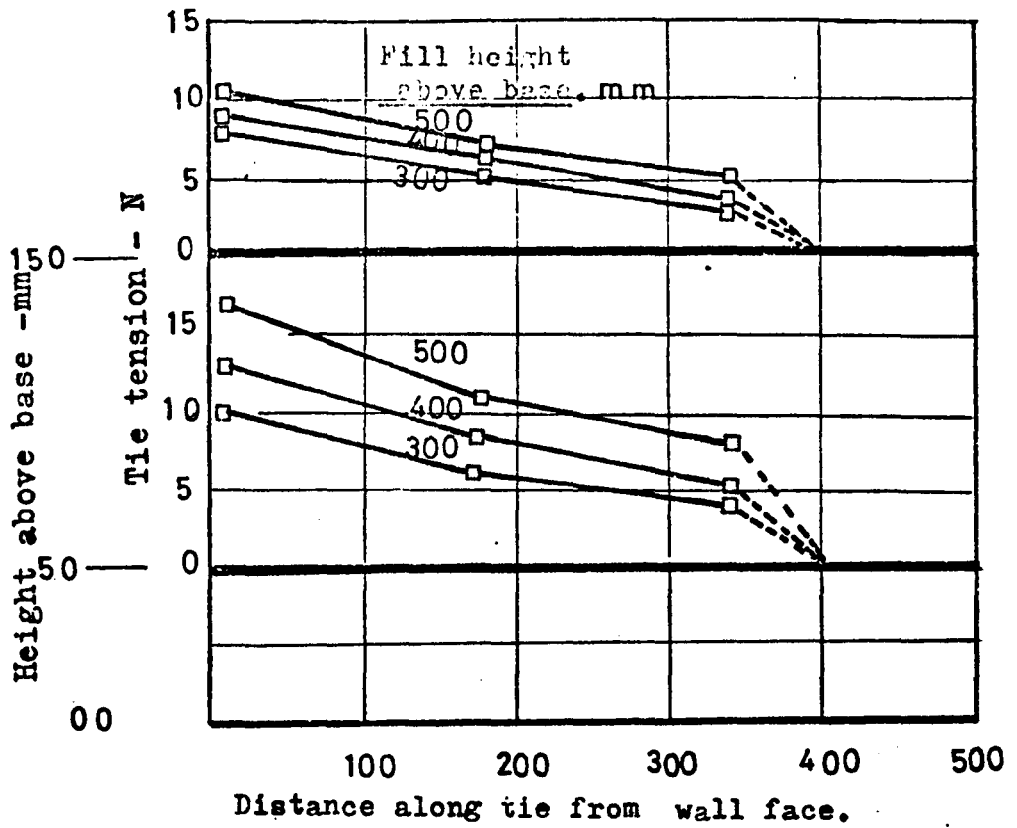
Fig. 5.14 Variation in tension along ties observed in series C - tests using preliminary tension gauge design
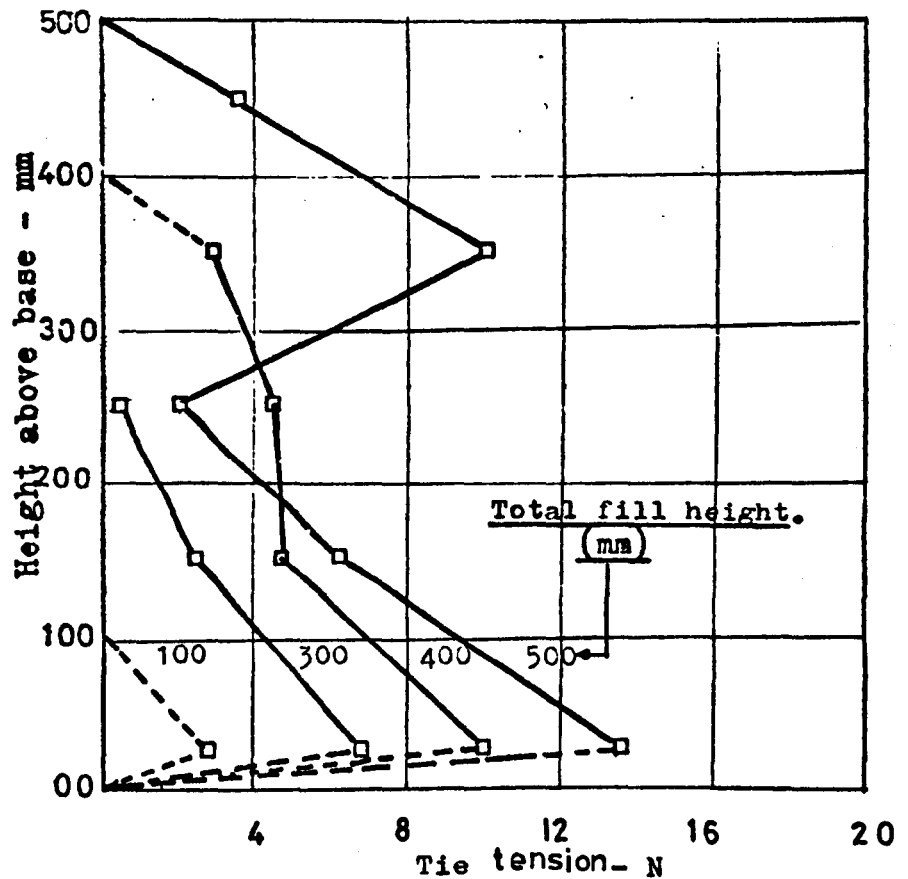
Fig. 5.15 Variation in tie tension with wall depth observed in series C - tests using preliminary tension gauge design.

False front

(5 perspex
Planks , 25 mm
thick)

Strain coil transducers(35-40 mm C.C.)

Lead
wires to
read-out
box

.100 mm

REINFORCED

EARTH

WALL

Perspex spacers

Skin element

base
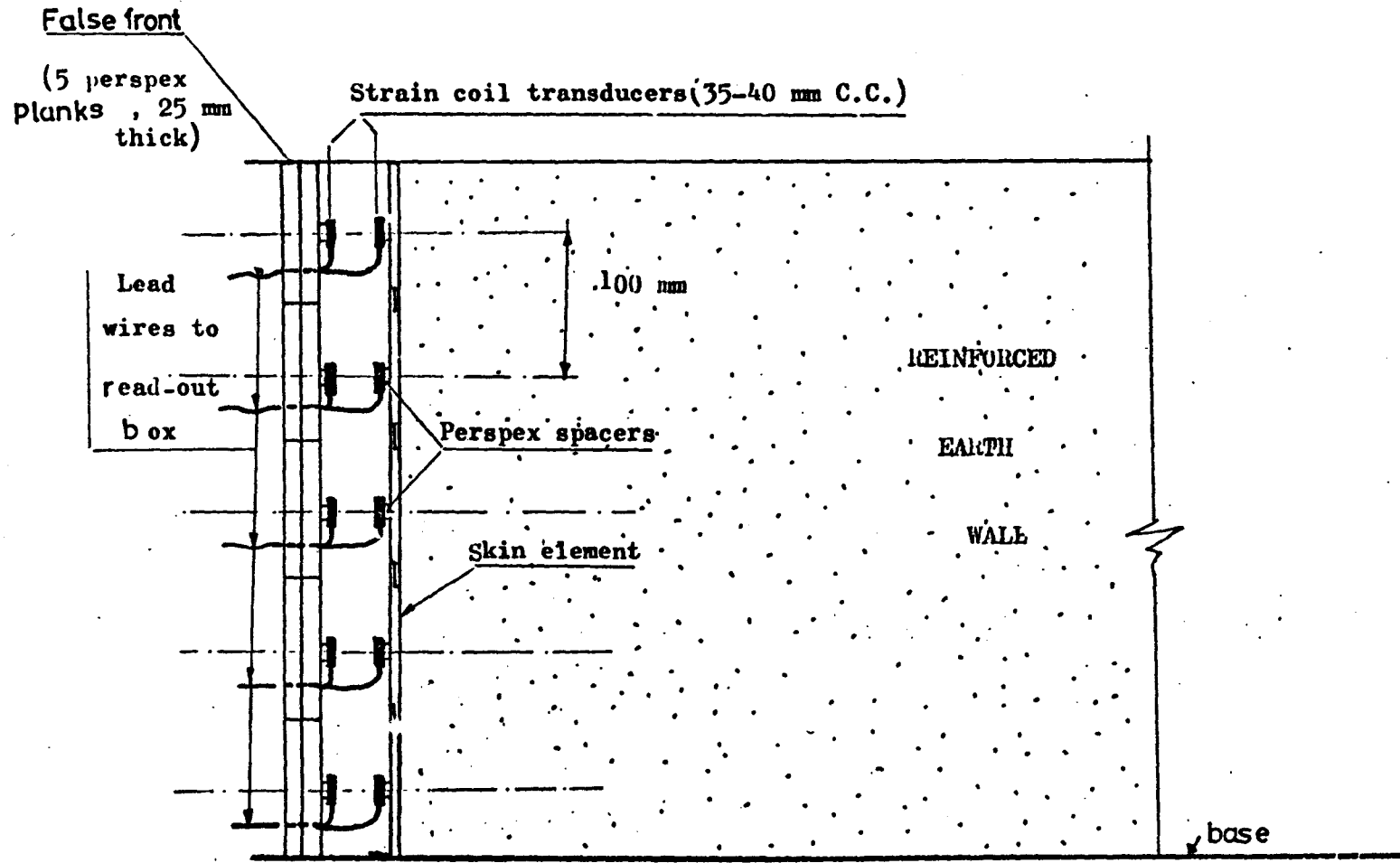
Fig 5.16 Arrangement of strain coils for the measurement of wall movement

stages of the wall construction was plotted against the wall depth, Fig (5.17) and showed a maximum wall deflection approximately at midheight of the wall.

5.4.4 Discussion of Series C test results

The results of the tie tension measurement using strain gauges mounted on perspex strip and fixed in series with the aluminium tie, gave reasonable tie forces regarding their magnitude and pattern. However, the present method of tie tension measurement was noted to have the limitation of using different materials for the tie and for mounting the strain gauges. The perspex and the aluminium have different coefficients of friction with the sand. Possibly this would result in modifying the shear stresses developing at the soil/tie interface and this in turn would probably affect the tie tension distribution along the tie length.

In the D and E test series the strain gauges will be mounted directly on the perspex ties in the manner described in Chapter Four, Section (4.5)

Measurement of the horizontal wall deflection using the strain coils was satisfactory and possessed certain advantages over the dial gauge system, which was initially tried. The coils being uncoupled did not obstruct the movement of the wall and the coils could easily be installed in the test apparatus. The readings are accurate enough ($\doteq \frac{1}{1,000}$ mm), provided that the distance between the coils is kept in the range of coils' separation used in the calibration. This can easily be achieved by providing suitable spacers to locate the coils at a predetermined initial separation Fig (5.16).

5.4.5 Conclusions

(1) The tie tension measurement using strain gauges mounted on perspex and connected in series with the aluminium tie gave reasonable results. An improvement in the tie tension measurement can be made by adopting
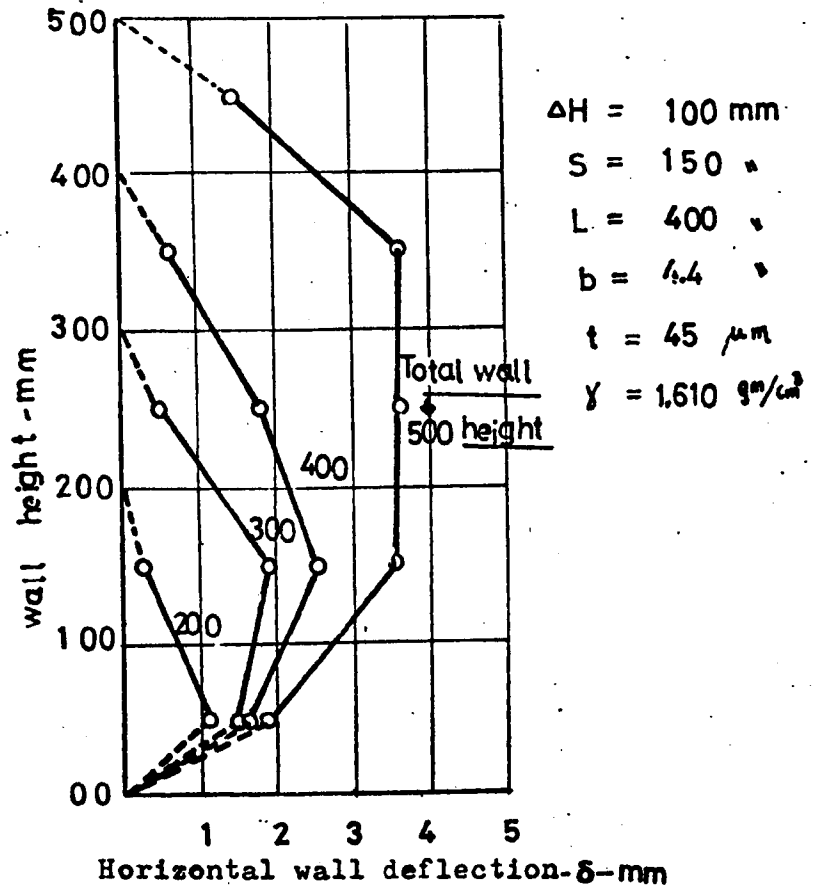
Fig. (5.17) Observed horizontal wall deflection V wall height above base. (Series C tests , wall no. C2)

a perspex tie on which the strain gauges can be mounted. This overcomes the disadvantages of using two different materials.

(2) The wall deflection measurement using the strain coils was satisfactory. This method has the advantage that the strain coils being uncoupled did not obstruct the movement of the wall. The coils could easily be installed and monitored.

5.5 Series D Tests
Tie pull out failure

5.5.1 Introduction

Series D tests consisted of 22 model reinforced earth retaining walls, intended to investigate a tie pull out mode of failure. In this test series it was also intended to observe the tie tension variation along a tie length and with increasing fill height above the tie level. The influence of the tie length on the maximum tie tension was also assessed in this test series.

In order to study the effect of the tie length on the maximum tie tension, the wall design parameters such as the horizontal and vertical tie spacings and the soil density have to be considered. To decrease the number of parameters involved, the maximum tie tension was assumed to vary linearly with the horizontal tie spacing as noted in previous model tests.[45] A large vertical tie spacing was adopted (250 - 125 mm) and the wall built consisted of one or two reinforced layers. The soil density was kept constant.

The tie length as well as the horizontal tie spacing was varied in this test series. The main observations were of tie tension variation along a tie length and with increasing fill height above the tie level and the maximum wall height at failure. From these observations the

curves showing the tie tension distribution along a tie length were drawn. The curves of the maximum tie tension versus height of fill above the tie level were constructed and compared with the theoretical values. The maximum shear resistance of the tie at failure, was computed from the observed maximum tension values and was plotted against mean vertical stress γh to obtain a measure of the tie/soil angle of friction from failing reinforced earth model walls. The influence of the tie length on the maximum tie tension was assessed and was compared with the theoretical predictions. Comparison was also made between the adherence lengths observed in the present and the series A tests and the adherence lengths calculated by various theoretical approaches.

The test apparatus and method of wall construction adopted in the Series D tests will be outlined in the following section.

5.5.2 Apparatus and wall construction

This test series used the box and skin elements shown in Figs (5.18) and (5.19) respectively. The skin elements consisted of 6 mm thick perspex panels 300 mm wide and 250 mm high, which were designed to allow more than one tie to be fixed on each facing element. Using these skin elements it was possible to vary the horizontal and vertical tie spacings to suit the requirement of each test. Perspex ties of 1.5 and 22.7 mm average thickness and width respectively with lengths ranging between 170 - 500 mm, were used in this series. The soil/tie coefficient of friction determined from a controlled stress shear box was 0.398. A vertical tie spacing of 250 mm was adopted in most of the tests although in a few cases walls were built using a vertical tie spacing of 125 mm. Three horizontal tie spacings of 100, 150 and 300 mm were used to construct the walls in the present test series. A summary of tie lengths, the observed critical heights and tie spacing are shown in Table (5.6). The walls tested in this series were
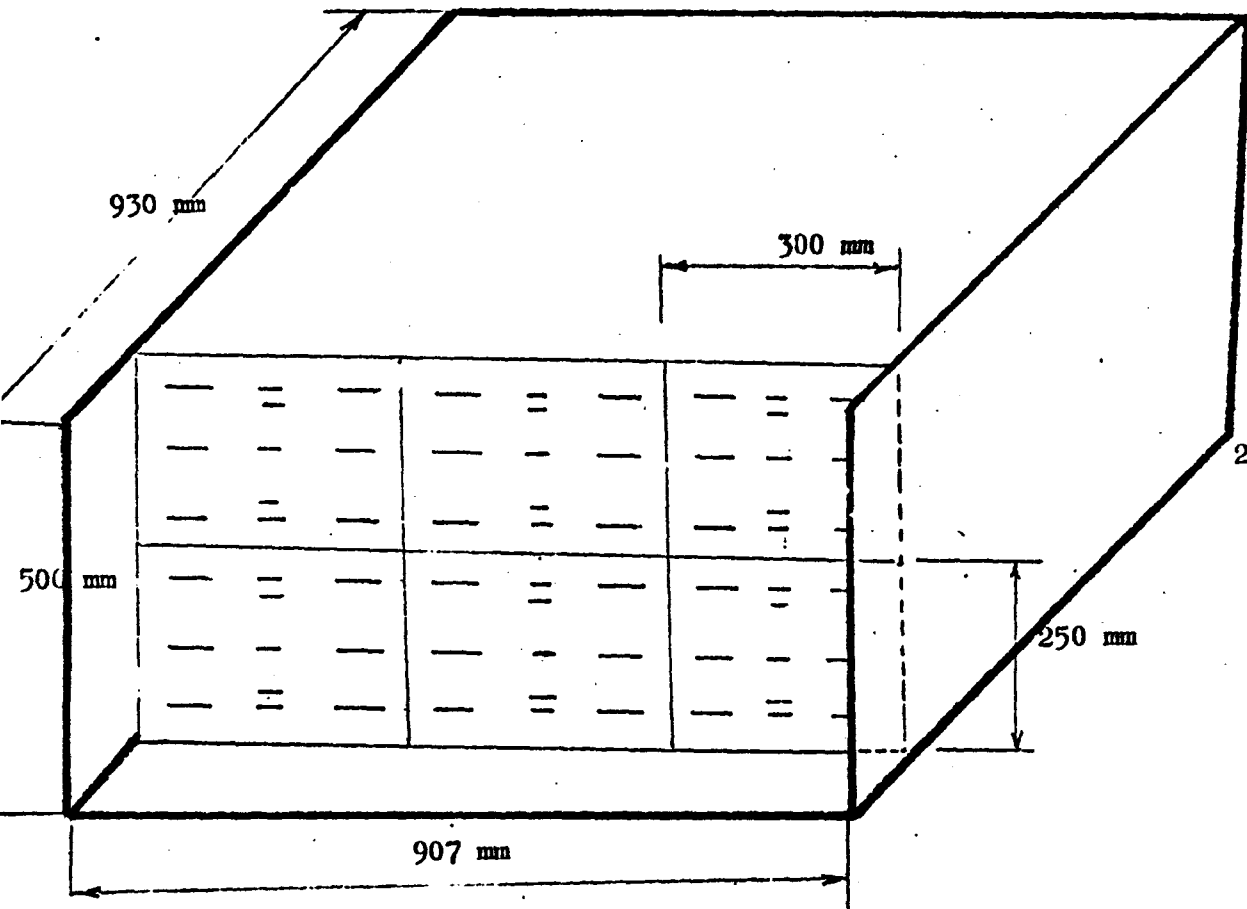
Fig.5.18 Test model & perspex panels (Series D, E   )

(No. of panels = 6, Maximum No. of ties   per panel = 9)
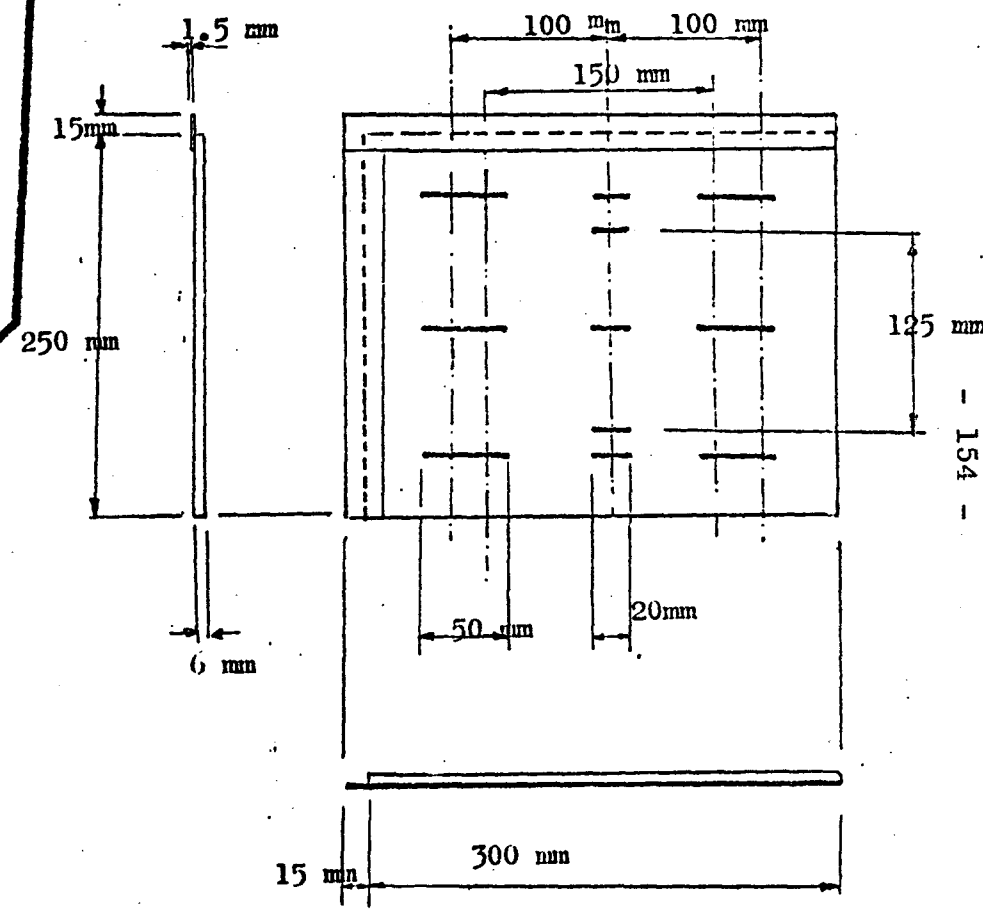
Fig5.19 Perspex panel dimensions

TABLE (5.6) - Summary of Tie Lengths, Spacings and
Critical Wall Heights of Series D Tests (ΔH = 250 mm)

Test No.	L mm	H_c mm	S mm	H_c/L
1(D)	500	440	300	0.88
2(D)	480	375	300	0.78
3(D)	480	315	300	0.66
4(D)	480	365	300	0.76
5(D)	460	330	300	0.72
6(D)	490	410	300	0.84
7(D)	470	340	300	0.72
8(D)	460	350	300	0.76
9(D)	500	360	300	0.72
10(D)	500	465	300	0.93
11(D)	450	310	300	0.69
12(D)	440	320	300	0.73
13(D)	440	278	300	0.63
14(D)	250	330	150	1.32
15(D)	250	358	150	1.43
16(D)	250	350	150	1.40
17(D)	240	305	150	1.27
18(D)	170	310	100	1.82
20(D)	250	265	300	1.06 ΔH= 125
21(D)	170	350	100	2.06
22(D)	167	340	100	2.04

constructed as outlined in Chapter Four, Section (4.3).
The tie tension was observed using strain gauges mounted
on both faces of the perspex tie as shown in Fig (4.16)
in Chapter Four.   This method of tie tension measurement
gave more satisfactory results than the method previously
adopted for measuring tie tension, in Series C tests. On a
few occasions the tension gauge shown in Fig (4.17) in
Chapter Four was used to check the tie tension magnitude
observed in this test series.   It was found that the tie
tension measured using the latter tension gauge was similar
to the tie tension measured using strain gauges directly
mounted on the perspex tie.

5.5.3   Theoretical background for Series D tests based on
the Energy Theory (Total equilibrium approach)
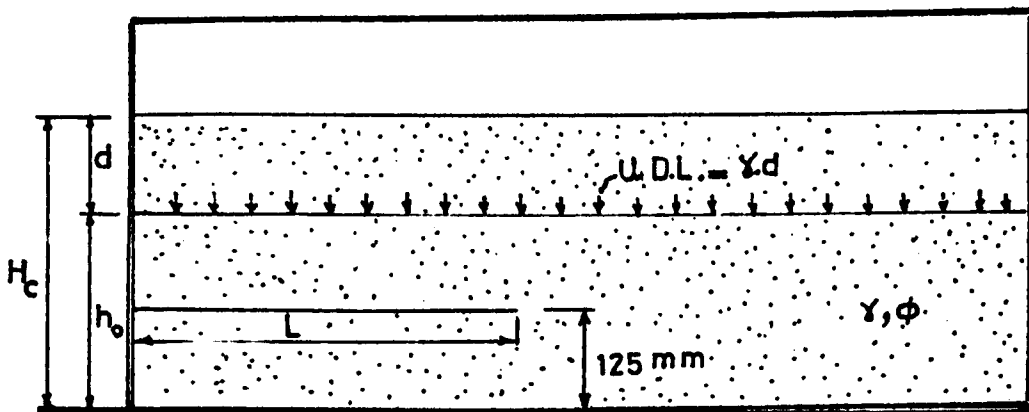
Fig (5.20)   Theoretical analysis of Series D tests

Using the total equilibrium approach, the tie tension
expressions were derived in Chapter Three for a case of a
reinforced earth wall comprising n layers.   A distribution
factor was assumed to obtain the external work done at each
tie level.   In the present test series walls were built
with one or two reinforced layers and the tie tension
expressions can be derived using the total equilibrium energy
approach by directly equating the external work and the
internal strain energy stored in a tie.

As shown in Fig (5.20), a reinforced earth wall of height

h_o acted on by a surcharge equal to γd is considered.
The height of the wall h_o in this series corresponds to the
height of the lower facing element and d is the height of
sand lying above the lower skin element. For the assumed
linear and parabolic tie tension distributions over the tie
length and a pressure difference in the wall deflection
equation, the total equilibrium energy approach gives the
following tie tension expressions:

(i) Assuming linear tie tension distribution

$$T = \left(\frac{\sin\phi\; K_a^{2.5} \cdot \Delta H}{2L}\right)^{\frac{1}{2}} \cdot \gamma \cdot Sh_o ((h_o + 2d)^2 + 2d^2)^{\frac{1}{2}} \quad \dots \text{(T.L.D.)}$$

$$\dots\dots\dots (5.1)$$

(ii) Assuming parabolic tie tension distribution

$$T = \left(\frac{\sin\phi\; K_a^{2.5} \cdot \Delta H}{3.2L}\right)^{\frac{1}{2}} \cdot \gamma \cdot Sh_o ((h_o + 2d)^2 + 2d^2)^{\frac{1}{2}} \quad \dots \text{(T.P.D.)}$$

$$\dots\dots\dots (5.2)$$

The form of the tie tension expression derived in
Chapter Three, using the local equilibrium approach, can be
used directly in the analysis of Series D tests.

5.5.4   Series D test results

The Series D test results consisted of the tie tension
measurements and the observed adherence lengths at failure
of the walls. A summary of the tie tension observations is
shown in Appendix (IV) and typical test results of these
observations as well as the observed adherence lengths will
be presented and compared with the corresponding theoretical
values in this section.

5.5.4.a   Observations on tie tension

As shown in Fig (5.20) the tie tensions were observed
in a reinforced layer lying at 125 mm above the base of the
model. The effect of increasing fill height on tie tension
was observed at two, three and four locations along the tie,
depending on the tie length.

5.5.4.a.1 The variation in tie tension along a tie

Fig (5.21) shows the observed tie tension variation over the tie length. This indicated a maximum tie tension close to the wall face which decreased to zero at the free end of the tie. The observed mode of tie tension variation along a tie remained almost the same for different tie lengths and overburden heights used in the tests. As tie tension measurements were made at only one wall level in this test series, the ties at the upper wall levels may have different mode of tie tension variation. This problem will be dealt with in Series E tests.

5.5.4.a.2 Variation in tie tension with fill height above tie level

The curves of the experimental and the theoretical maximum tie tension versus fill height above the tie level are shown in Fig (5.22). The observed tie tension increased with increasing fill height and the results indicated a tie length effect on the maximum tie tension. For long ties, the Rankine tie tension expression which is independent of the tie length predicted higher tie tension than the experimental results. As the tie length was decreased the discrepancy between the Rankine theory and the observed data decreased. The Energy theory based on the total equilibrium energy approach (T.L.D.) was found to give a general agreement with the observed results. The local equilibrium approach (LO.L.A.) predicted relatively higher tie tension than the experimental results.

5.5.4.b The tie pull out resistance

At the moment of failure the maximum tie tension was assumed equal to the tie resitance F_r against failure by pull out. This is also a common assumption used by most of the theoretical adherence length expressions. Table (5.7) gives the values of the force F_r and the corresponding over-burden pressure, which was calculated from the measured

density γ , during the test and the overburden height h.
The shear stress was then calculated and plotted against
the overburden pressure γh. This gave an angle of friction
between the tie and the soil equal to 22° Fig (5.23), which
compared quite well with the tie/soil angle of friction of
21.5° measured using a controlled stress shear box test.
This result probably indicates that the total length of a
tie lying near the bottom of a reinforced earth wall is
effective against tie pull out failure.

5.5.4.c <u>Effect of tie length on the tie tension magnitude</u>

For three wall heights of 250, 300 and 350 mm the values
of the maximum tie tension were interpolated from the
maximum tie tension versus fill height above the tie level
curves. The maximum tietension per unit wall width T_m/S
was plotted against the tie length. A typical result is
shown in Fig (5.24). The experimental values showed a
decrease in the maximum tie tension with increasing tie
length.

The experimental results were compared with the
theoretical values predicted by the Rankine, the Trapezoidal,
Meyerhof and the Energy theories, Fig (5.24). The Rankine
the Trapezoidal and Meyerhof methods predicted a tie tension
which is of different pattern from the experimental results
and also of higher magnitude. The Energy theories (T.P.D.)
and (T.L.D.) predicted nearly similar pattern and magnitude
to the experimental results. The Energy theory local
equilibrium approach (LO.L.A.), predicted tie tension values
which were of a similar pattern to the experimental results but
of higher magnitudes.

5.5.4.d $\dfrac{T_m}{\gamma H^2}\sqrt{\dfrac{L}{\Delta H}}$ Versus   horizontal tie spacing curve

According to the energy theory the quantity $\dfrac{T_m}{\gamma H^2}\sqrt{\dfrac{L}{\Delta H}}$

varies linearly with the horizontal tie spacing S,
irrespective of the variation in the tie length L. The
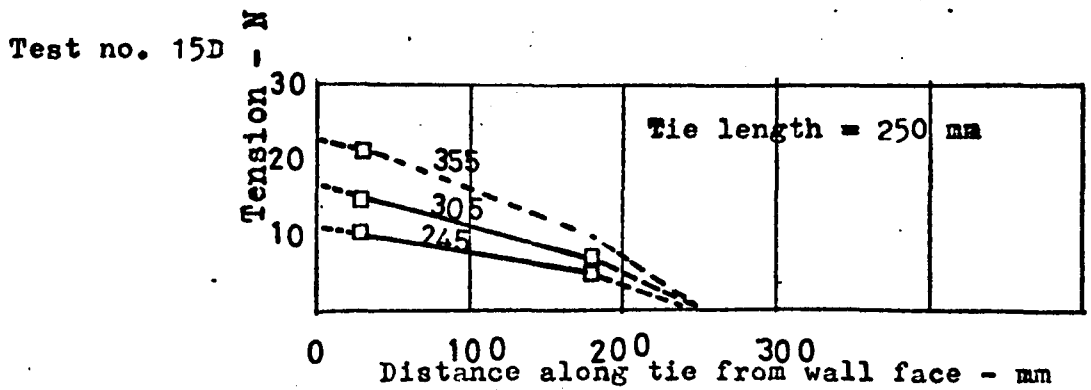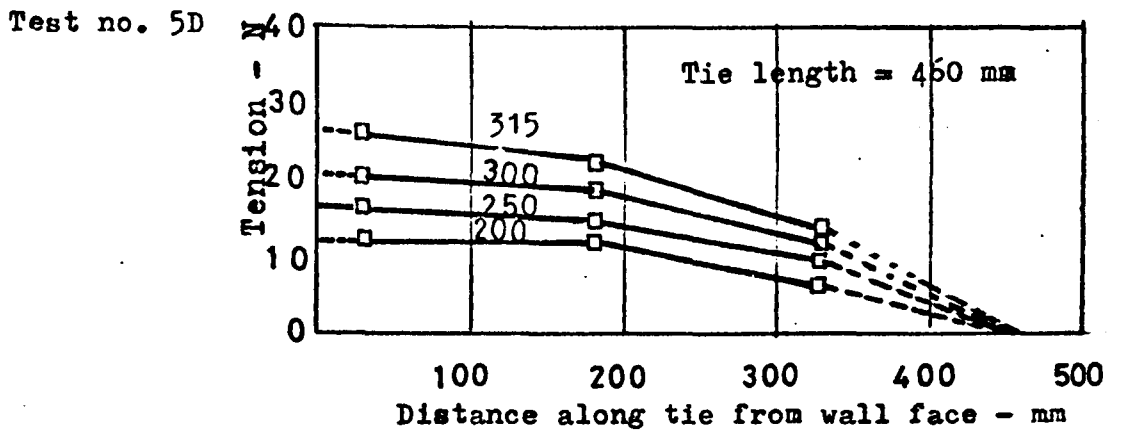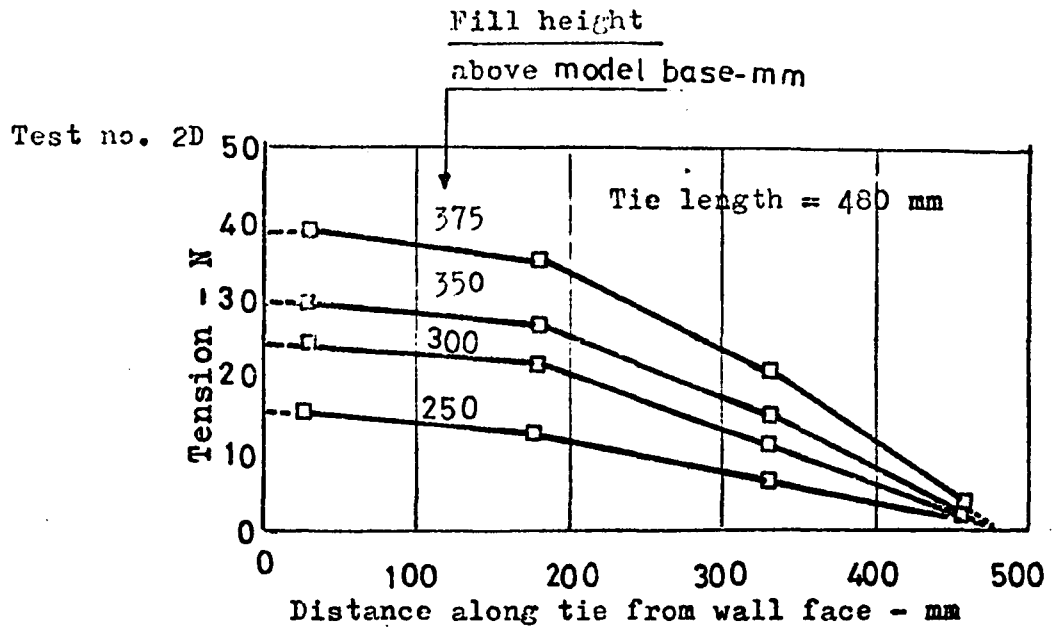
Fig.(5·21) Variation in tie tension along tie (Series D tests).
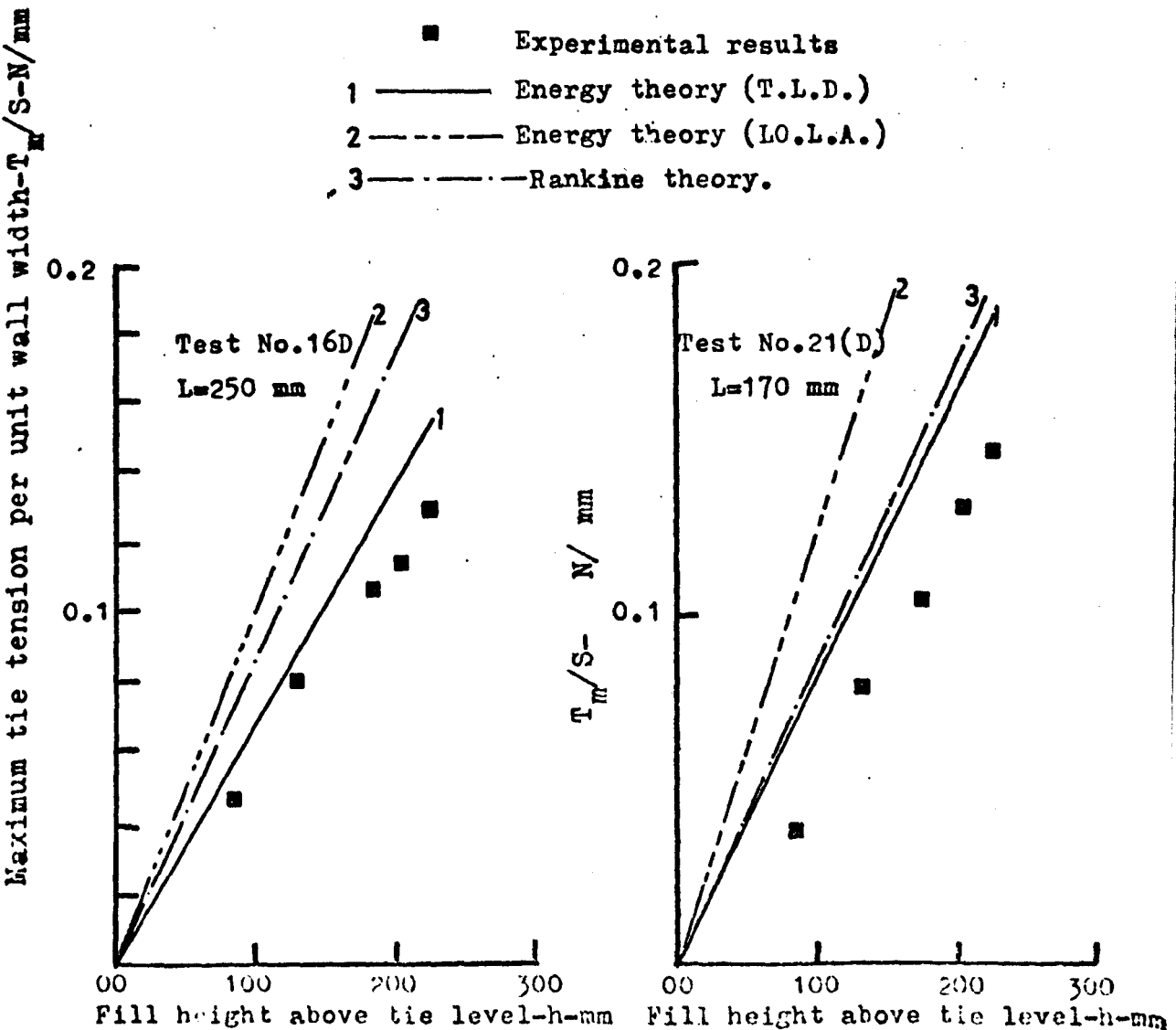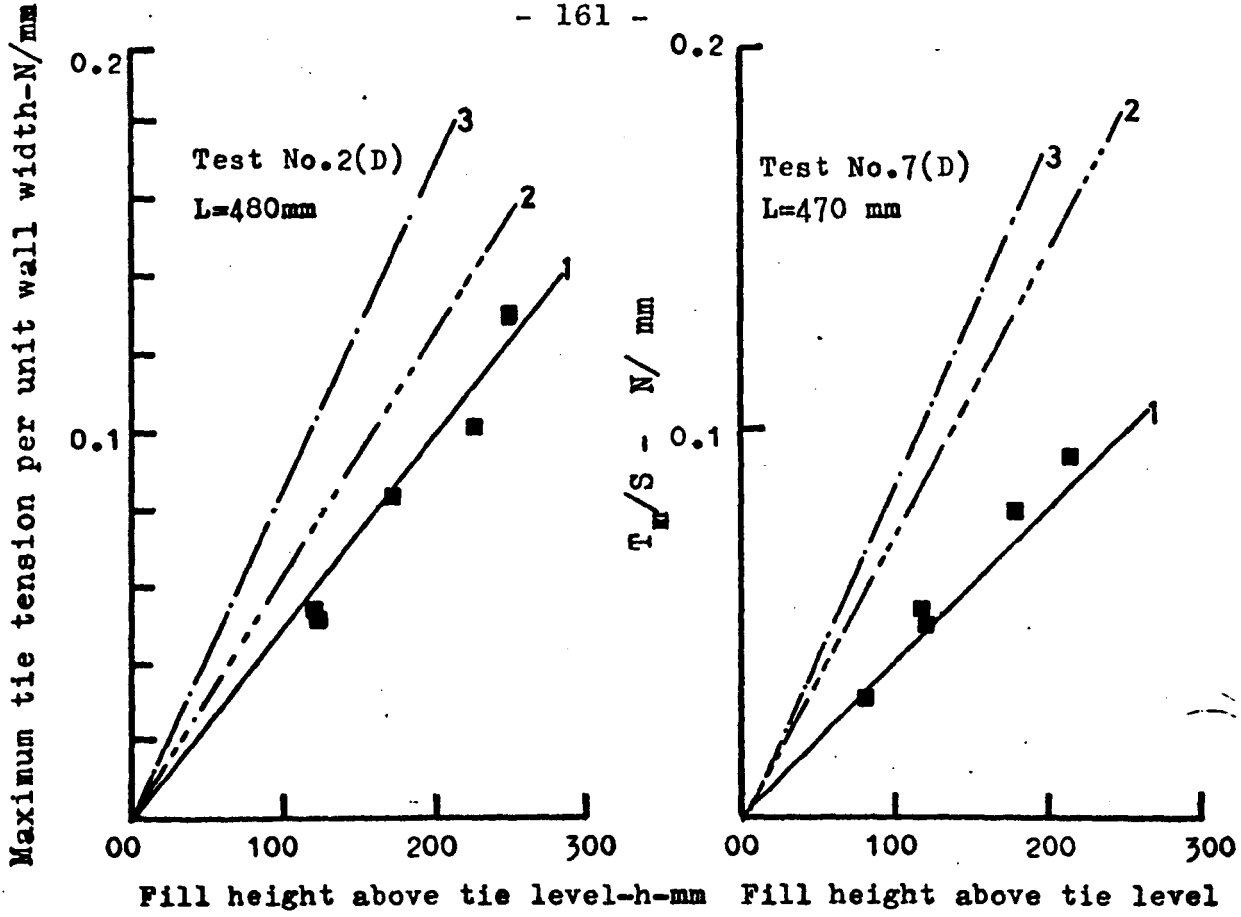
Fig. 5-22 Experimental & theoretical tensions V fill height above tie

TABLE (5.7) - The Maximum Tie Resistance against Pull Out
F_r and the corresponding Overburden Pressure (Series D
Test Results)

Test No.	L mm	γ gm/cm^3	γh kN/m^2	F_r - N	$\tau = \dfrac{F}{2 b L}$ kN/m^2
1(D)	500	1.610	4.97	52.49	2.31
2(D)	480	1.610	3.94	33.81	1.55
4(D)	480	1.610	3.79	31.10	1.43
5(D)	460	1.610	3.23	26.01	1.245
6(D)	490	1.610	4.50	36.79	1.65
7(D)	470	1.610	3.39	28.11	1.32
8(D)	460	1.618	3.55	32.07	1.535
9(D)	500	1.622	3.74	31.89	1.405
10(D)	500	1.6146	5.38	47.37	2.08
11(Γ)	450	1.6146	2.93	22.28	1.09
12(D)	440	1.610	3.08	27.22	1.363
13(D)	440	1.6033	2.41	21.13	1.057
14(D)	250	1.6010	3.21	16.59	1.462
15(D)	250	1.6220	3.70	21.00	1.852
16(D)	250	1.589	3.51	19.30	1.705
17(D)	240	1.5960	2.81	15.84	1.450
18(D)	170	1.6146	2.93	10.19	1.323
20(D)	250	1.610	3.19	20.06	1.768
21(D)	170	1.6167	3.57	11.90	1.421
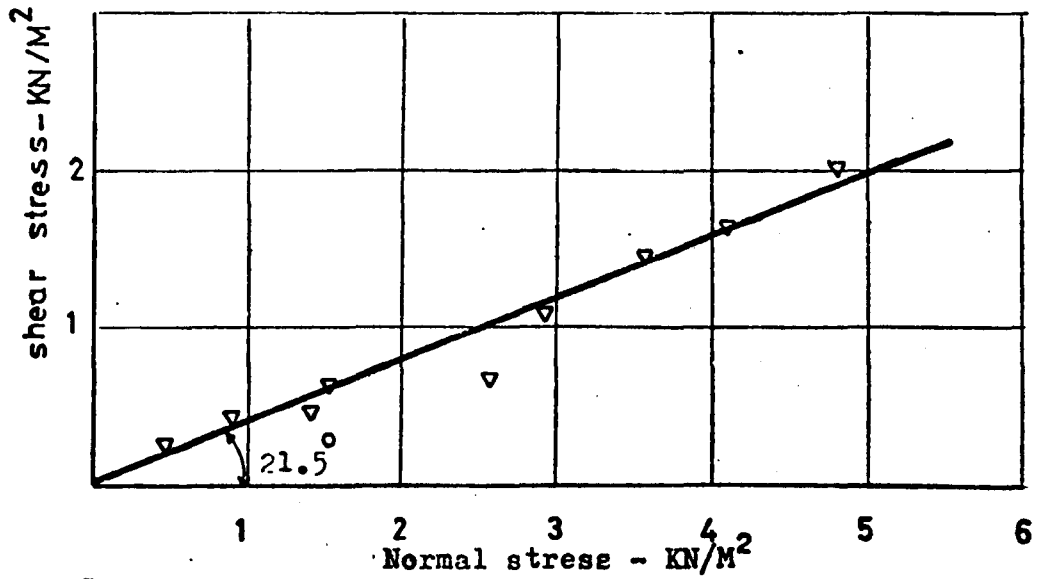
Fig.5.23 Perspex/soil angle of friction obtained by a shear box test.
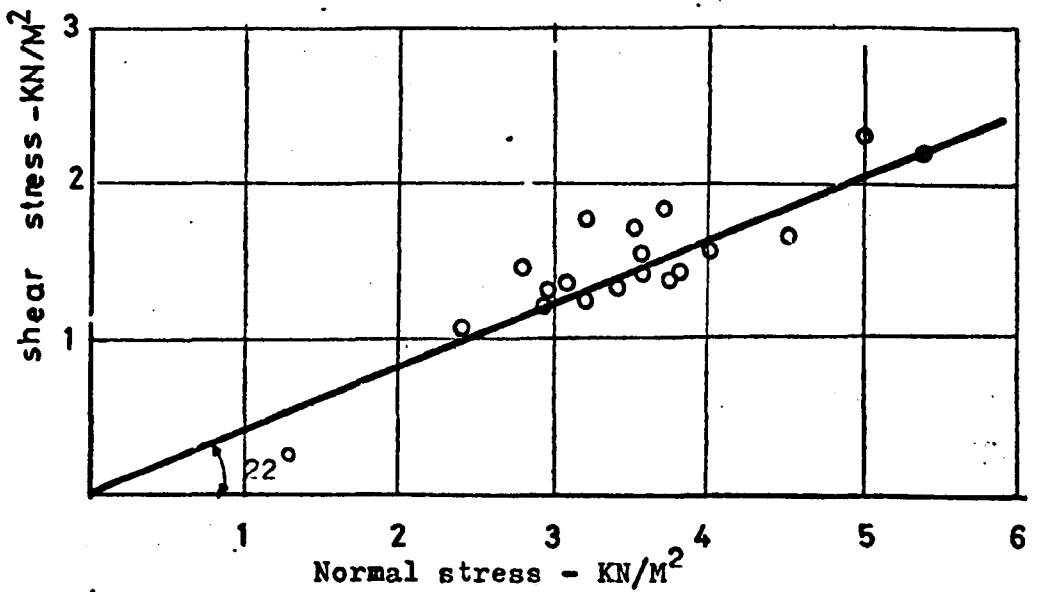
Fig.5.23 Perspex tie /soil angle of friction calculated from pullout failure tests results
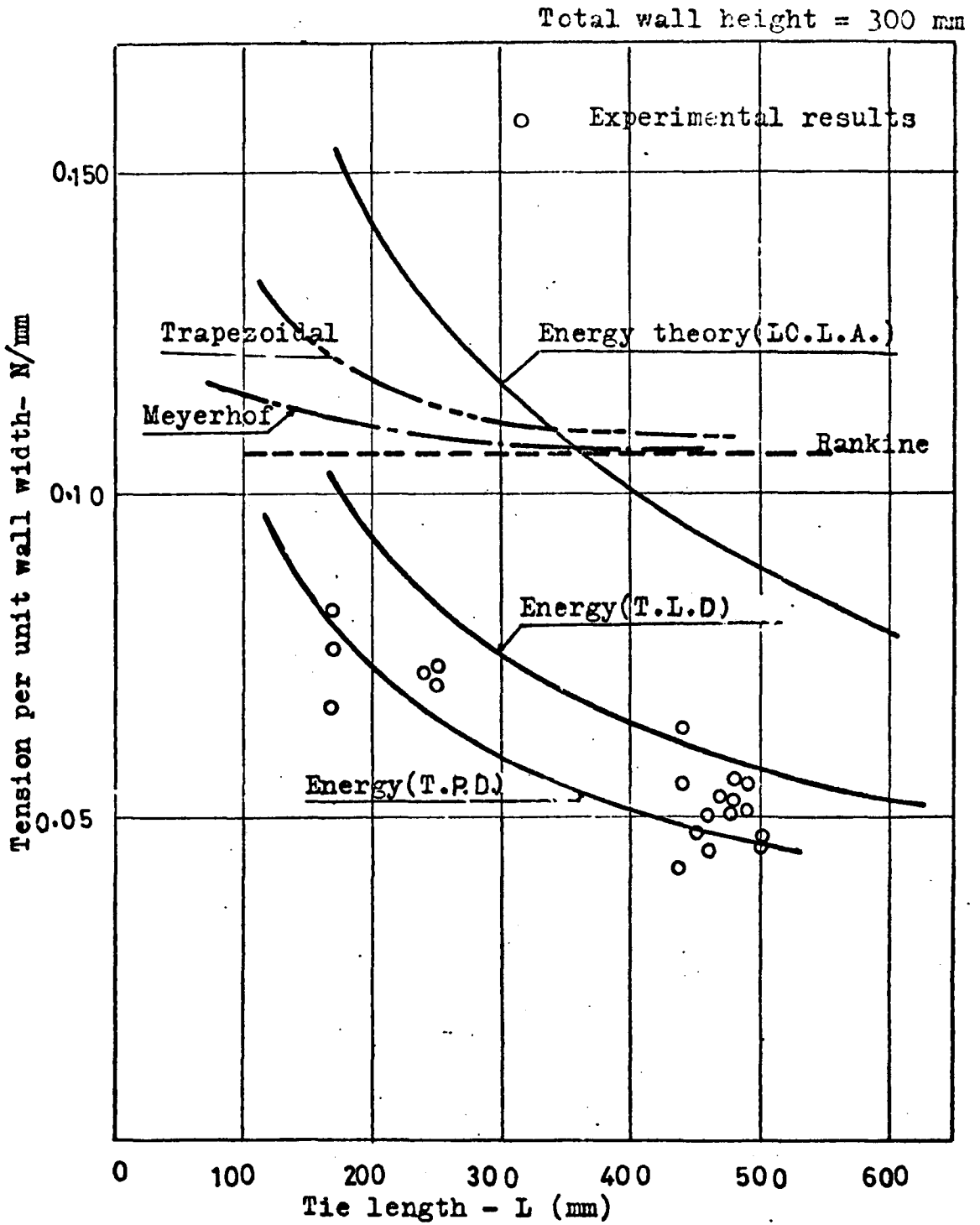
Fig. 5.24 Theoretical & experimental variation in tension with tie length.

experimental values of this quantity were calculated for wall heights of 300 and 350 mm and were plotted against the horizontal tie spacing S, Fig (5.25). The experimental values of $\dfrac{T_m}{\gamma H^2} \sqrt{\dfrac{L}{\Delta H}}$ varied almost linearly with the horizontal tie spacing in agreement with the energy theory prediction. The Rankine theory, which does not take the tie length effect into account, gave a non-linear variation of $\dfrac{T_m}{\gamma H^2} \sqrt{\dfrac{L}{\Delta H}}$ with respect to the horizontal tie spacing S.

5.5.4.e Comparison between experimental and theoretical adherence length

Two sets of experimental adherence lengths were made available for comparison with different theories. The first set of data was obtained from Series A tests, as has been mentioned previously. The walls were built with horizontal and vertical tie spacings of 150 and 100 mm respectively. The ties were cut in 4.4 mm width from aluminium foil which has a coefficient of friction of 0.51 with the sand. The second set of data consisted of the failure heights and the corresponding tie lengths noted in the present test series Table (5.6). Both experimental results were compared with the theoretical predictions as shown in Figs (5.26a) and (5.26b).

Generally all the different theories predicted longer ties than the experimental results with the exception of the energy theory, total equilibrium approach (T.L.L.D.) which slightly underestimated the adherence length, when compared with the Series D test results. The adherence lengths predicted by the energy theory local equilibrium approach (LO.L.A.), were generally closer to the observed data than the adherence lengths predicted by the existing design approaches.
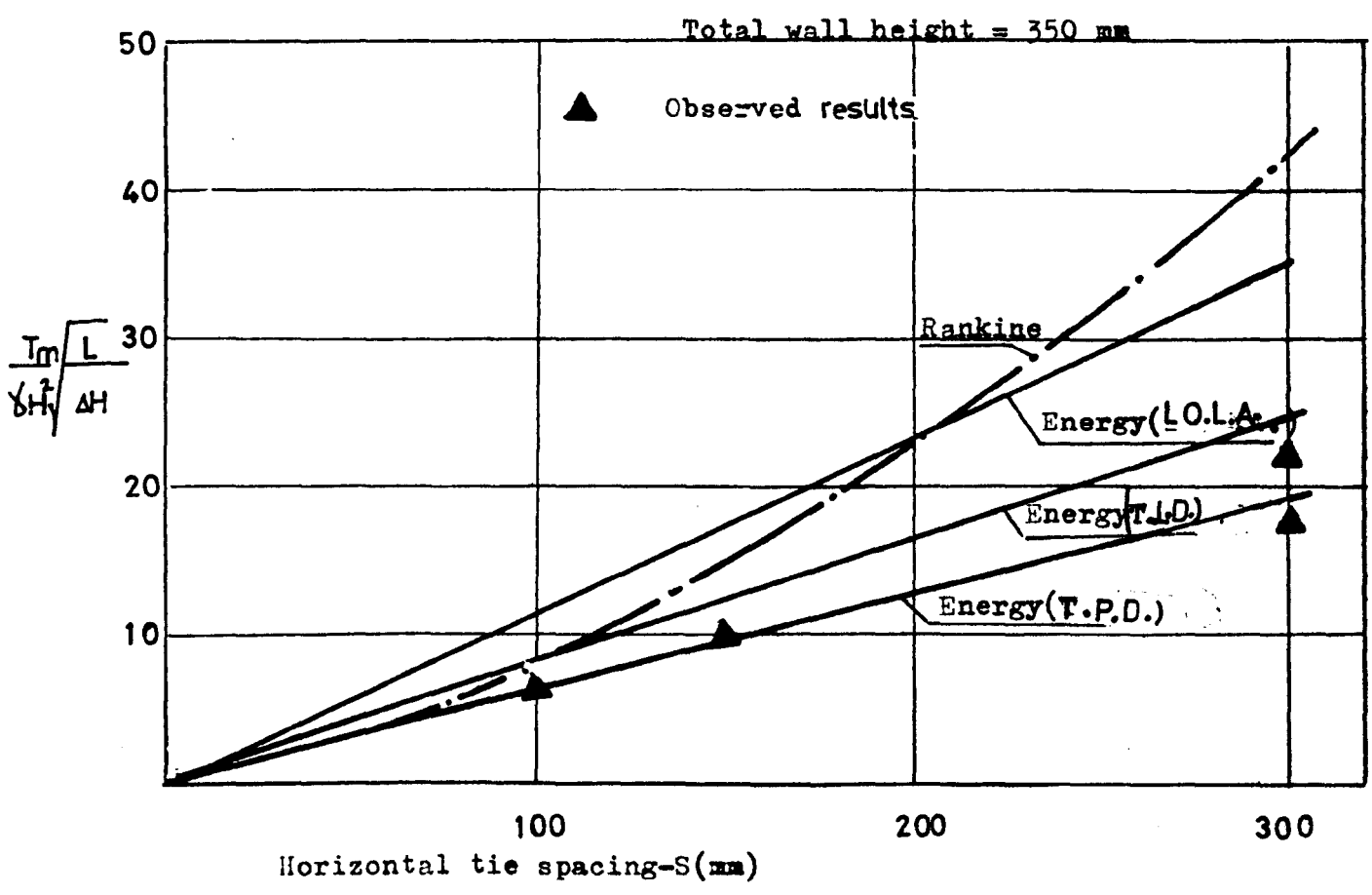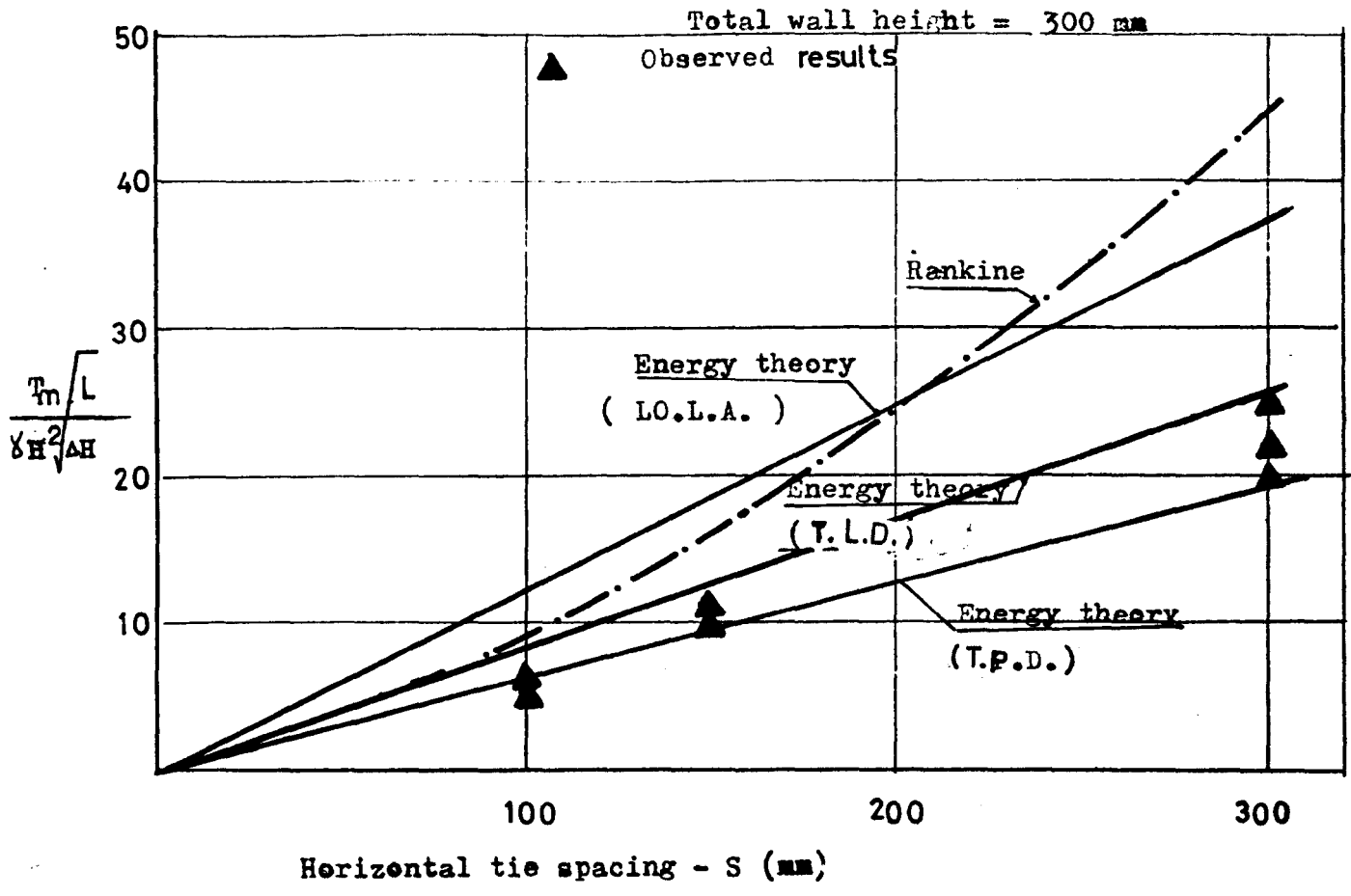
Fig.5.25 Experimental & theoretical values of $\dfrac{T_m}{\gamma H^2}\sqrt{\dfrac{L}{\Delta H}}$ v horizontal tie spacing.

□ Observations

1-1 Energy theory(T.L.P.D.)

2-2 " " (T.L.L.D.)

3-3 " " (LO.L.A.)

4-4 Coulomb Moment

5-5 Coulomb Force

6-6 Rankine(Only tie length beyond Coulomb plane effective)

7-7 Banerjee

8-8 Rankine(All tie length assumed effective)

9-9 Meyerhof

Design parameters.

$S = 150$ mm, $\Delta H = 100$ mm , $\gamma = 1.615$ gm/cm^3

$\phi = 40^o$, $f = 0.510$, $b = 4.39$ mm
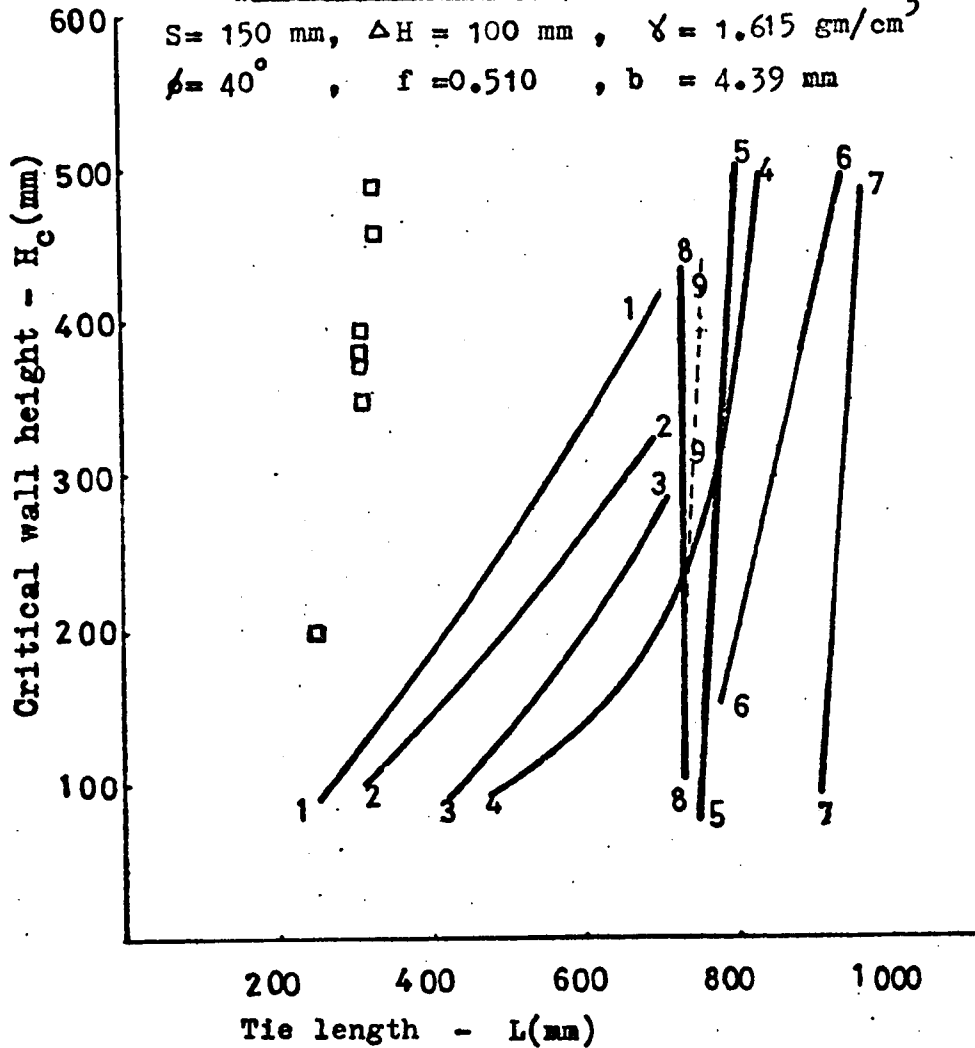
Fig(5.26.a) Comparison between experimental & theoretical adherence length(series A(1) test results·).

□   Observations

1-1   Energy theory(LO.L.A.)

2-2   Banerjee

3-3   Coulomb Force

4-4   Coulomb moment

5-5   Rankine theory

6-6   Energy theory(T.L.L.D.)

7-7   Rankine(Only tie length beyond Coulomb plane effective)

8-8   Meyerhof

Design parameters

$S = 300$ mm

$\Delta H = 250$ mm

$\gamma = 1,620$ gm/cm^3

$\phi = 40^\circ$

$f = 0.398$

$b = 22.7$ mm
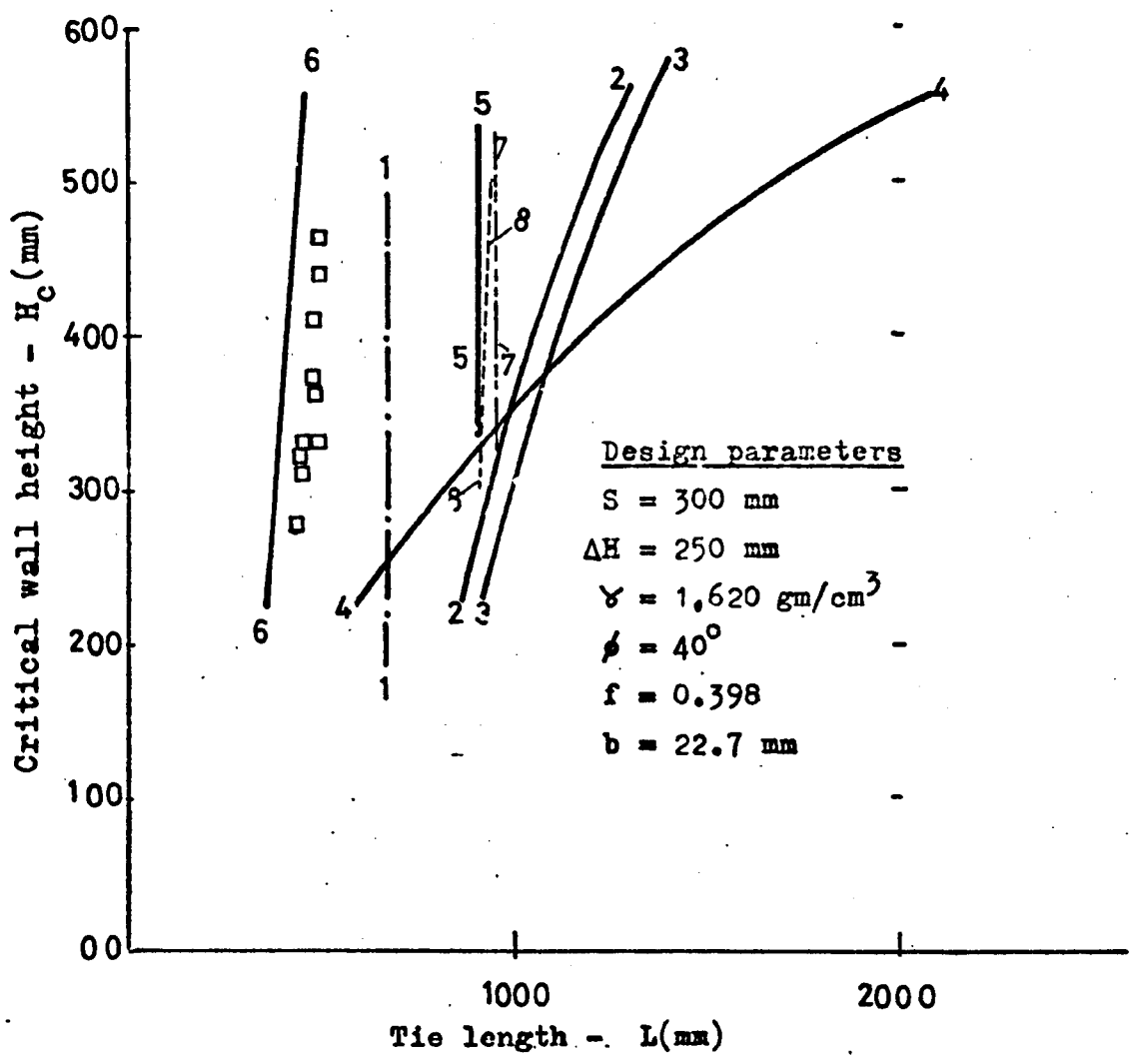
Fig(5.26.b) Comparison between experimental & theoretical adherence
length(series D tests results).

5.5.5 Conclusions

(i) From tie tension measurements in a reinforced layer lying 125 mm above the base of the model, a maximum tie tension was observed near the wall face, and was found to decrease to zero at the free end of the tie. This mode of tie tension variation remained almost the same for different tie lengths and over-burden heights used in the tests.

(ii) The observed maximum tie tension was noted to increase with increasing fill height above the tie level. The Energy theory (T.L.D.) predicted a maximum tie tension which was in general agreement with the observed values, for all tie lengths adopted in the tests. The local equilibrium energy approach(LOLA) predicted comparatively higher tie tension than the observed results. The Rankine theory predicted higher tie tension than the experimental values and the discrepancy between the Rankine values and the experimental results, decreased with decreasing tie length.

(iii) The angle of friction between the perspex ties and the sand, estimated from the measured force in the tie prior to the wall failure and the corresponding overburden pressure, agreed well with the perspex/sand angle of friction measured using a controlled stress shear box test. This probably indicates that for a reinforced layer lying near the base of a wall, all the tie length is effective against tie pull out failure.

(iv) The maximum tie tension was noted to decrease with increasing tie length. The Rankine, the Trapezoidal and Meyerhof methods gave theoretical values of maximum tie tension which were of different pattern from the experimental results and appreciably higher in magnitude than the observed values. The Energy theory expressions took into account the tie length effect on the maximum tie tension, and gave nearly the same mode of variation as the experimental results.

The Energy theory (T.L.D.) and (T.P.D.) predicted nearly
similar pattern and magnitude to the experimental results,
although the local equilibrium energy approach (LO.L.A.)
predicted relatively higher values than the experimental
results.

(v) In agreement with the energy theory prediction, the
experimental values of $\dfrac{T_m}{\gamma H^2} \sqrt{\dfrac{L}{\Delta H}}$ were found to vary

almost linearly with the horizontal tie spacing.

(vi) Comparison between the theoretical and the
experimental adherence lengths, showed that generally
all the theories predicted longer ties than required for
stability.   The Energy theory (LO.L.A.) predicted
adherence lengths which were closer to the observed
results than the existing design methods.

5.6. Series E Tests

Instrumented not carried to failure tests

5.6.1 Introduction

The present test series was intended to study the
internal stability of model reinforced earth walls by
observing the stresses and strains in the ties and in the
soil during and after the wall construction.

In the previous Series B and D tests the internal
stability of the model reinforced earth walls was studied
on an ultimate strength basis and the main observations were
concerned with conditions at failure.   Although the tie
breaking failure test results allowed a comparison to be
made between the theoretical and the observed maximum tie
tension, it gave no indication of the state of stress in
the ties at the middle and top of the wall.   The tie pull
out test results gave an overall adherence length, but the
actual safety factors against tie pull out failure were not
revealed from the test results.   The observations made on
walls failing by tie breaking or tie pull out were limited

and cannot be used to investigate fully the assumption on which the theoretical analyses were based.

The Series E tests were designed to overcome the limitations noted in the previous test series. Walls in this test series were built with the five horizontal tie spacings shown in Table (5.8). Using each of the five tie spacings an average of seven walls were built to obtain a record of the tie tension distribution along a tie length and in different levels of the walls, the horizontal and vertical strains in the soil, the vertical stresses in the soil and the horizontal wall deflection. A number of walls were built at each tie spacing, because for each wall built, not more than two ties were instrumented, in order to avoid the reinforcing action of the lead wires on the walls.

From the results of the tie tension observations the curves of the tie tension variation along a tie length at different levels were constructed. The curves of the maximum tie tension over the wall height, and the maximum tie tension versus fill height above a tie level were drawn and compared with the Rankine and the Energy theories predictions. The Rankine theory was chosen since it is mainly used for the design of full scale walls and also since the Coulomb, the Trapezoidal and Meyerhof methods give similar results to the Rankine theory as shown in Chapter Three, especially for $\frac{H}{L}$ ratio and $\emptyset$ values used in the present test series. The potential failure surfaces formed by joining the positions of the maximum tie tension in each tie level were constructed. Curves showing the variation in the horizontal and vertical strains in the soil, the variation in the vertical stresses in the soil and the horizontal deflection of the face of the walls were also drawn.

Using the results of the tie tension measurements, the non-dimensional tension parameter and the safety factors against tie pull out were evaluated from the results of the Series E tests and compared with the corresponding theoretical values.

TABLE (5.8) - Design Parameters of Series E Tests

Design parameters		
ΔH mm	S mm	Skin elements
250	100	Width = 300 mm Height = 250 mm Thickness = 6 mm
83.3	100	Width = 300 mm Height = 250 mm Thickness = 6 mm
83.3	150	
83.3	300	
100	150	Width = 150 mm Thickness = 6 mm Height = 100 mm

Tie length = 400 mm   Soil density = 1.610 gm/cm^3

Tie width = 22.3 mm $\emptyset = 40^o$

Tie thickness = 1.37 mm

The test apparatus, the wall design and properties of the test materials will be outlined in the following section.

5.6.2 Test apparatus, and wall design

The test model and accessories used for building the walls in the present test programme were described in Chapter Four, Section (4.2).

In designing the present series of model walls the main design parameters of a reinforced earth wall were first considered. These were the vertical and horizontal tie spacings, the skin elements, the size of the tie, the properties of the soil backfill (γ and $\emptyset$), the soil/tie coefficient of friction and the total wall height.

In practice the vertical tie spacing is chosen to give an optimum height of compacted layer[41], a reasonable skin element size and weight and an easy method of wall building procedure to avoid bracing the wall during construction. The horizontal tie spacing is restricted only by the size of the skin element if concrete panel skin elements are used, and by the flexural rigidity of the skin element, if elliptical metal skin elements are used. Lesser restrictions are imposed on the vertical and horizontal tie spacings in the model. In the present test series tie spacings were varied to provide a wider scope for comparison between the experimental data and the theoretical predictions. Table (5.8) shows the vertical and horizontal tie spacings and skin elements used in each set of tests. The skin elements were assumed to have no effect on the internal stability of the wall and were chosen to allow the tie spacing to be varied.

This test series used perspex ties to facilitate the measurement of the tie tension. The tie width was kept nearly the same as in the Series D tests at 22.3mm. A tie length of 400 mm was found necessary to exclude tie pull out mode of failure for walls built up to a maximum height of 500 mm

using the tie spacings shown in Table (5.8).   The soil
density, the angle of internal friction of the soil and the
tie/soil coefficient of friction were the same as in the
Series D tests at 1.610 gm/cm^3, 40° and 0.398 respectively.

The walls were constructed in the manner described in
Chapter Four, Section (4.3).   The instrumentation used
consisted of strain gauges mounted on the perspex ties for
measuring the tension in the ties, strain coils for measuring
the strain in the reinforced earth backfill and also for
measuring the horizontal deflection of the face of the walls.
Pressure cells were used to measure the vertical stress
distribution in the backfill of the walls.   The development
and calibration of these instruments was described in Chapter
Four.

A summary of the Series E test results is shown in
Appendix (V)   . Typical test results of this test series
will now be presented.

5.6.3.a   Tie tension variation along the ties

Figs (5.27) and (5.28) show typical test results of
the tie tension distribution along the tie length observed
in the present test series.   The maximum tie tension was
found to occur in the front half of the tie and decreased
to zero at the free end of the tie.   This pattern remained
almost unchanged for different vertical and horizontal tie
spacings adopted in the construction of the walls in this
test series.   The tension distribution on ties at the
bottom of the Series E walls, gave a similar pattern to that
observed in the Series D tests.

The present tie tension observations will be used to
evaluate the experimental safety factors against pull out
later in this study.

5.6.3.b   Maximum tie tension variation over the wall height

The maximum observed tie tension at each tie level in
the five walls studied in this test series was found to have
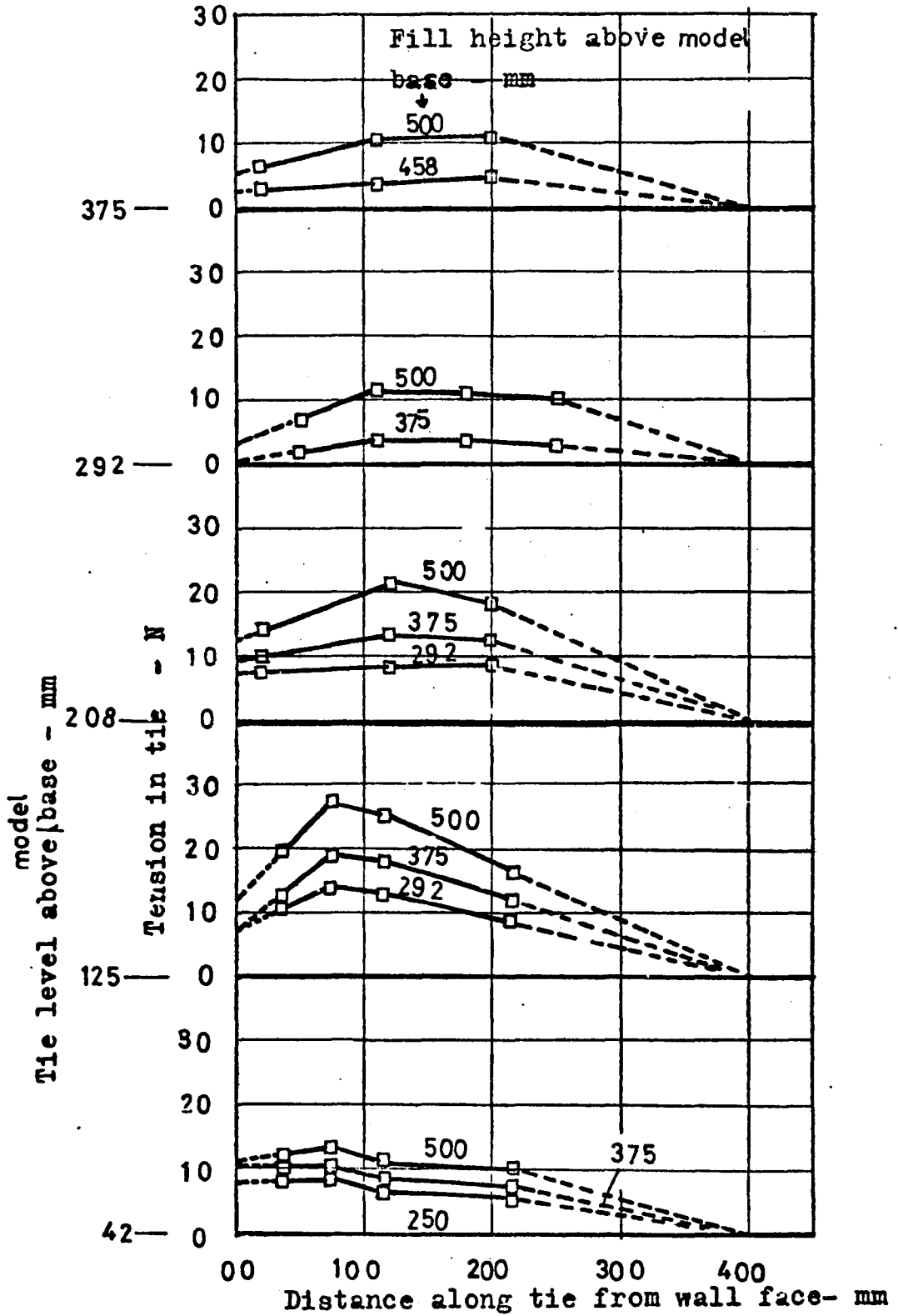
Fig.(5.27) Variation in tie tension along ties located at different levels in the wall (Model wall series E ΔH = 83.3 mm , S = 300 mm)
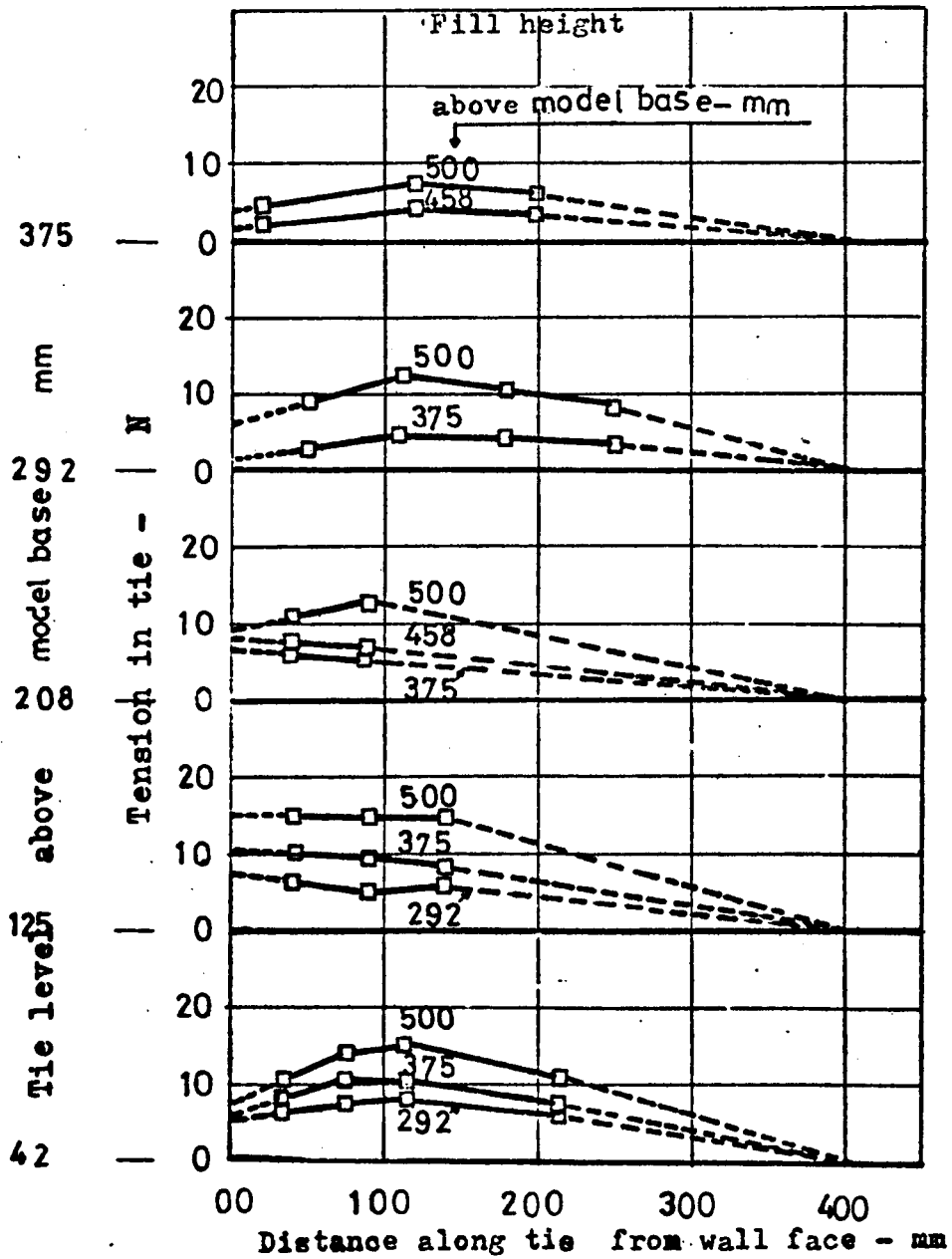
Fig(5.28) Variation in tie tension along ties located at different levels in the wall. (Model walls series E , ΔH = 83.3 mm, S = 150 mm)

a similar pattern of distribution with wall depth. Typical
test results from the walls studied are shown in Figs (5.29)
and (5.30). The experimental maximum tie tension generally
increased with increasing wall depth and a decrease in the
value of the observed tie tension was noted at the tie
level just above the base of the wall Fig (5.29). This is
possibly due to the fixity of the toe of the wall.

Figs (5.29) and (5.30) also show a comparison between
the observed and the theoretical maximum tie tension
envelopes, calculated using the Energy theory (LO.L.A.) and
(T.L.L.D.) and the Rankine theory (using K_a and K_o earth
pressure coefficients).

In Fig (5.29), the Energy Theory (LO.L.A.) generally
followed the pattern of the points of observed maximum tie
tension, but predicted higher magnitudes. The discrepancy
between the Energy theory (LO.L.A.) and the observed results
decreased for the case of the smaller tie spacing shown in
Fig (5.30). In this figure also the Energy theory (T.L.L.D.)
slightly underestimated the observed maximum tie tension,
although in Fig (5.29) this method predicted a maximum tie
tension envelope which fell approximately within the observed
results.

At the top of the wall, as shown in Fig (5.29), the
observed maximum tie tension approached the Rankine values
using K_a, and in Fig (5.30) the observed maximum tie tension
was greater than the Rankine theory prediction using an
active earth pressure coefficient K_a, but less than the
Rankine values based on an at rest earth pressure coefficient,
K_o.

At the bottom of the walls, the Rankine theory predicted
higher tie tension than the observed results.

5.6.3.c <u>Maximum tie tension versus fill height above the tie
level</u>

Fig (5.31) shows that the observed maximum tie tension
increases with increasing fill height. The corresponding
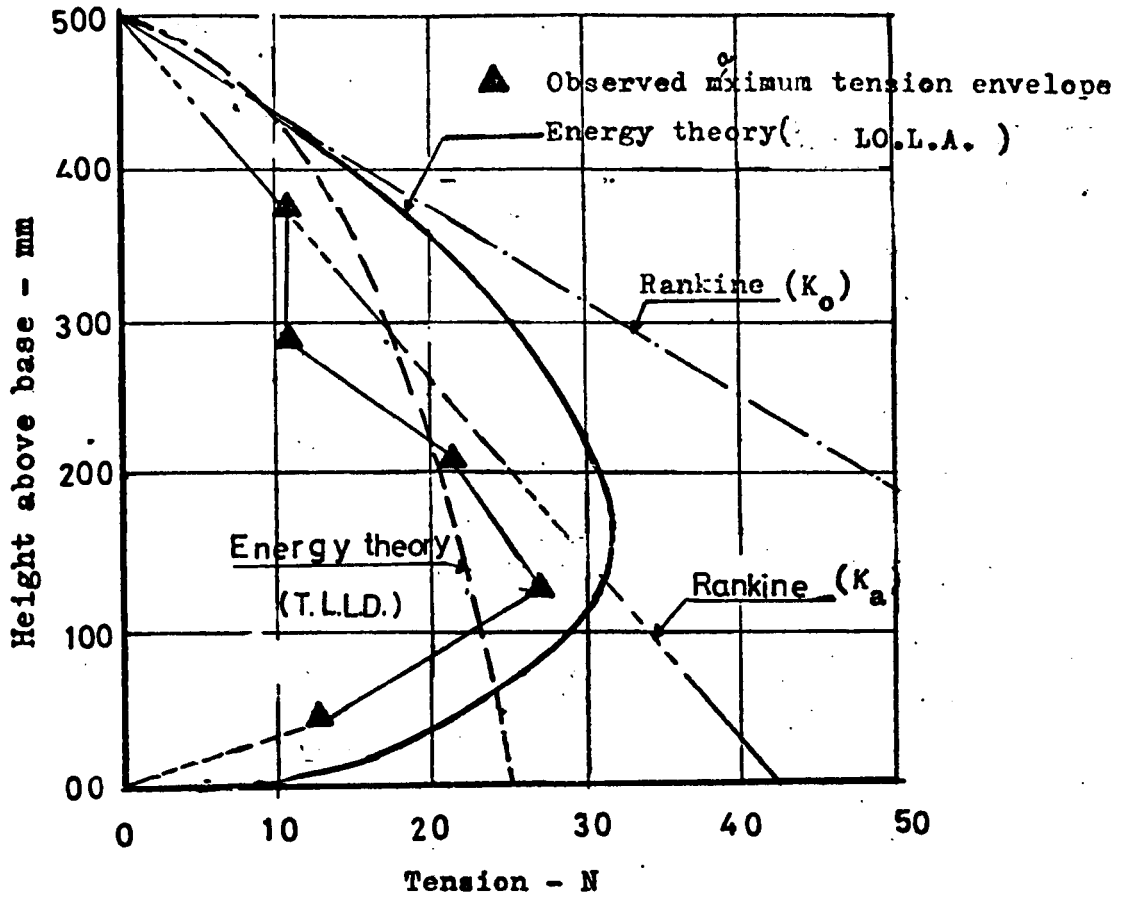
Fig.5·29 Experimental & theoretical maximum tension envelopes
(Model walls series E , ΔH = 83.3 mm, S = 300 mm)
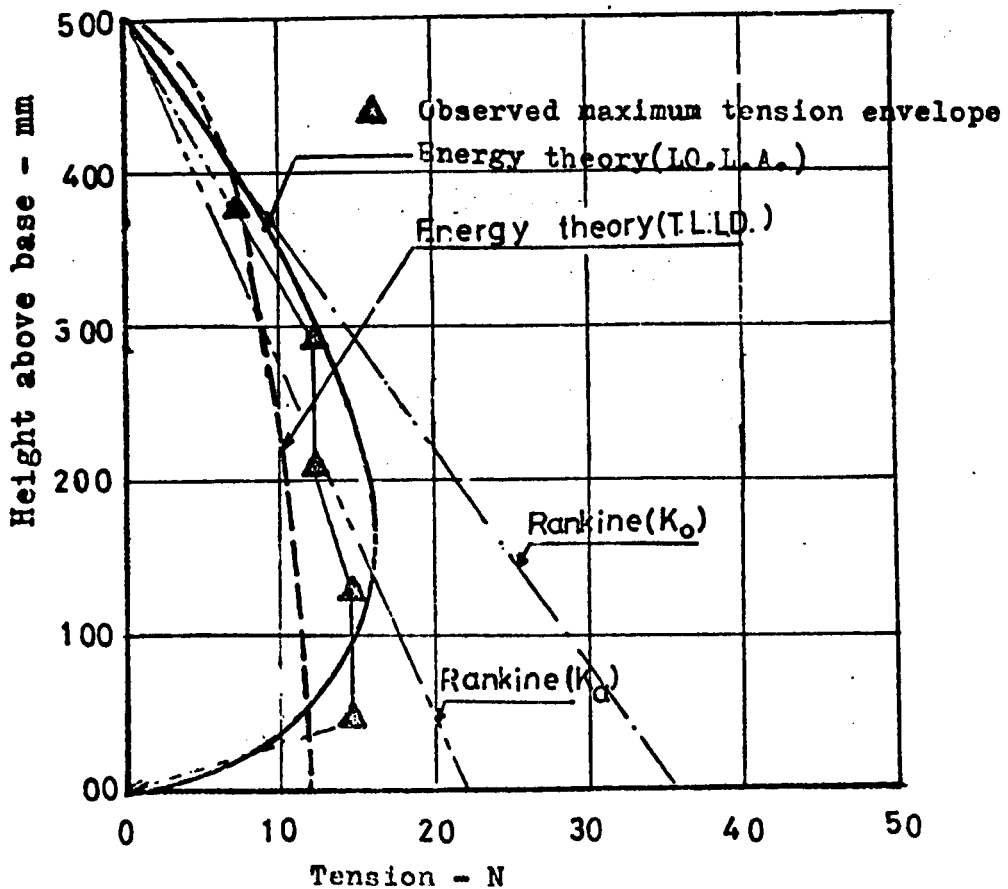
Fig.5·30 Experimental & theoretical maximum tension envelopes
(Model walls series E , ΔH = 83.3 mm , S = 150 mm)
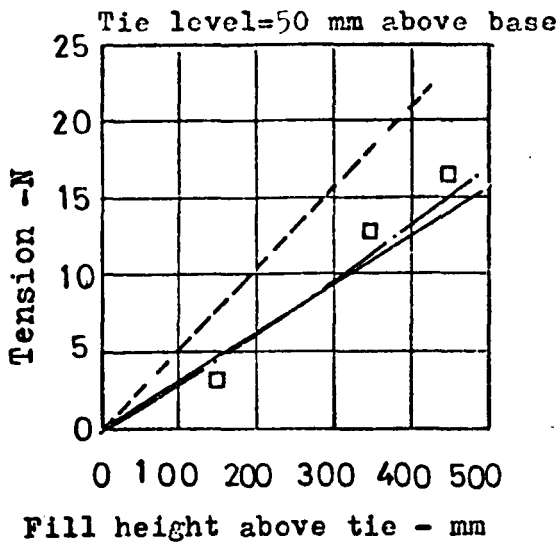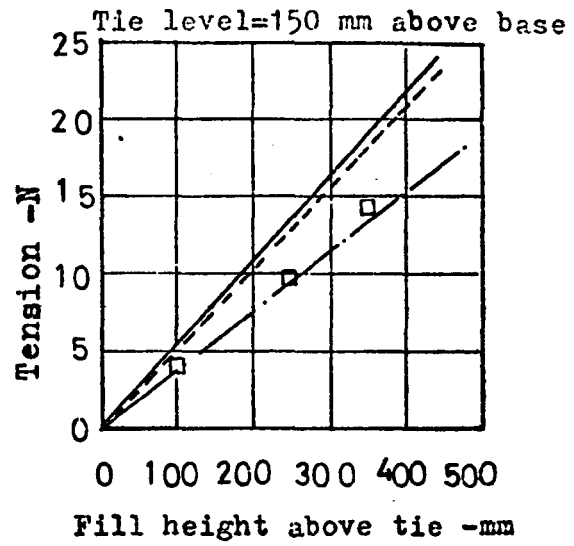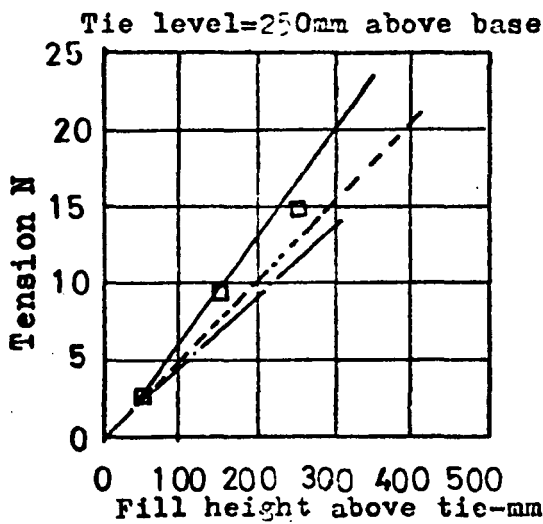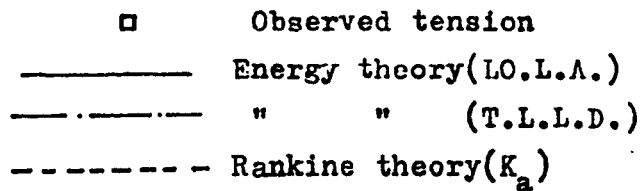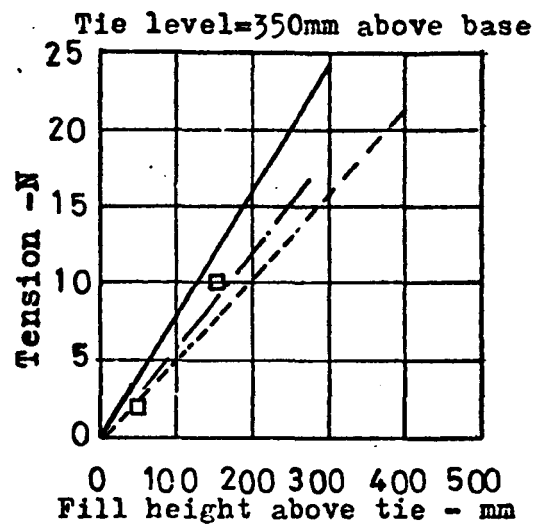
Fig 5.31 Experimental & theoretical maximum tension V fill height above tie level (Model walls series E ,ΔH=100, S=150 mm).

theoretical curves calculated from the Energy theory (LO.L.A.) and (T.L.L.D.) and the Rankine theory gave a linear variation of tie tension with increasing fill height. The Rankine theory was found to predict higher tie tension for the ties near the bottom of the wall, Fig (5.31) a and b, and slightly smaller values for the ties near the top of the wall, Fig (5.31) c and d.

5.6.3.d The maximum tension curve

Fig (5.32) shows the curves formed by joining the observed positions of the maximum tension in the ties at different wall levels. The observed maximum tension curve, in Series E tests, was nearly coincident with the Coulomb failure plane, near the bottom of the wall. Near the top of the wall, the observed maximum tension curve, for the case of relatively small tie spacings, Fig (5.32) a and c, tended to shift away from the Coulomb failure plane towards the face of the wall.

Symons,[72]   Price[52]   and Schlosser et al[63] accounted for reinforced earth wall behaviour on the basis of the maximum tension curve. This was reported as dividing the reinforced earth wall into two zones. In the first zone, located near the face of the wall, the soil is in an active failure state and tends to pull out the ties. In the second zone, located behind the maximum tension curve, the shear stresses exerted by the soil on the ties, are directed towards the back of the wall, and the soil is anchoring the ties.

Symons,[72]   Price[52]   and Schlosser et al[63] also reported that the maximum tension curves vary with various factors, not investigated here, such as the foundation condition, the soil tie coefficient of friction and the geometry of the wall.

5.6.3.e Horizontal strain in the soil

The horizontal strain in the backfill of some of the reinforced earth walls built in the present Series E tests,
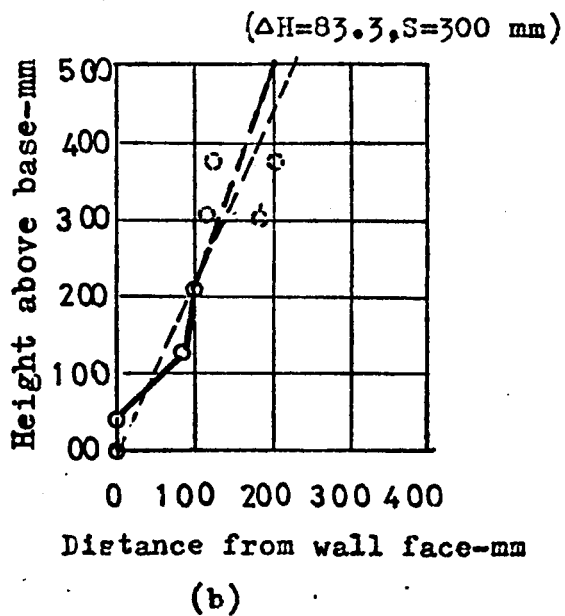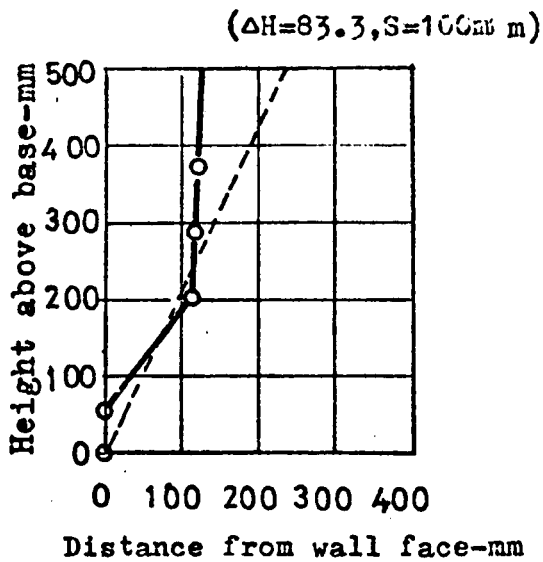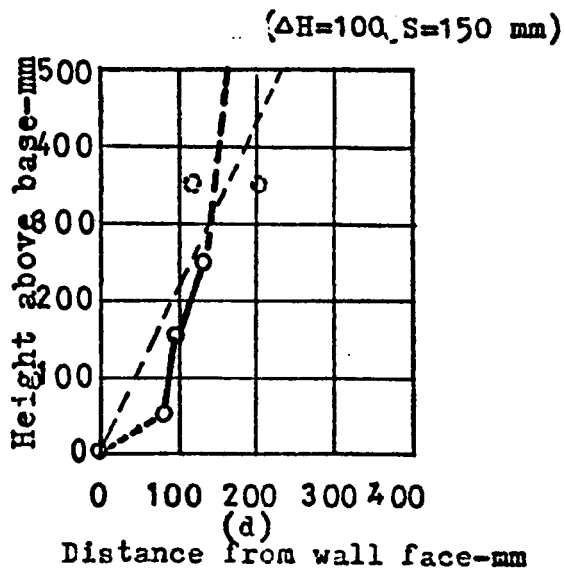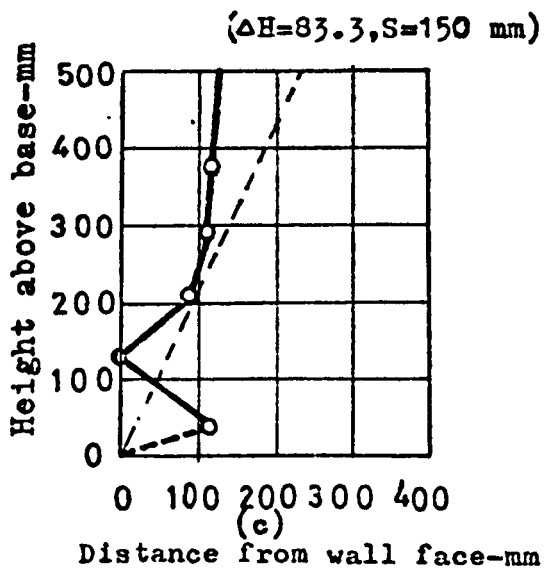
Fig. 5.32 The maximum tension curve (Model walls series E tests).

was measured at three different wall levels using the strain
coil transducers described in Chapter Four, Section (4.6).

As shown in Fig (5.33) and (5.34) the horizontal strain
in the sand is a maximum near the wall face and decreases
towards the back of the reinforced earth wall. The
variation of the horizontal strain in the sand with wall
height is shown in Figs(5.35) and (5.36).   The horizontal
strain increased with wall height to a maximum near the
middle of the wall, then decreased towards the   top of
the wall.   The horizontal strain in vertical sections close
to the wall face and near the middle of the reinforced earth
wall, Fig (5.35) were found to be +ve, indicating expansion
and probably the soil was tending towards an active state
of stress.   In a section lying furthest from the face of the
wall -ve strains were observed, indicating compression, and
probably the soil was tending towards a passive state of
stress.

The magnitude of the horizontal strain was found to
increase with increasing vertical tie spacings, Figs (5.35),
(5.36).

5.6.3.f   Vertical strain in the soil

Fig (5.37) shows the observed variation of the vertical
strain in the soil with the distance from the face of the
wall, measured at three levels in the reinforced earth wall.
The vertical strains in the soil were generally compressive
having a maximum value near the wall face.   This is
probably due to the effect of the horizontal thrust acting
at the back of the wall.

5.6.3.g   Vertical stress in the soil

The variation in the vertical stress at the bottom of
Series E model reinforced earth walls was measured using
the Redshaw pressure cells, previously described in Chapter
Four, Section (4.7).   In some cases the pressure cell
readings were found to lie near the overburden pressure,
Fig (5.38).   In other cases, the pressure cell readings
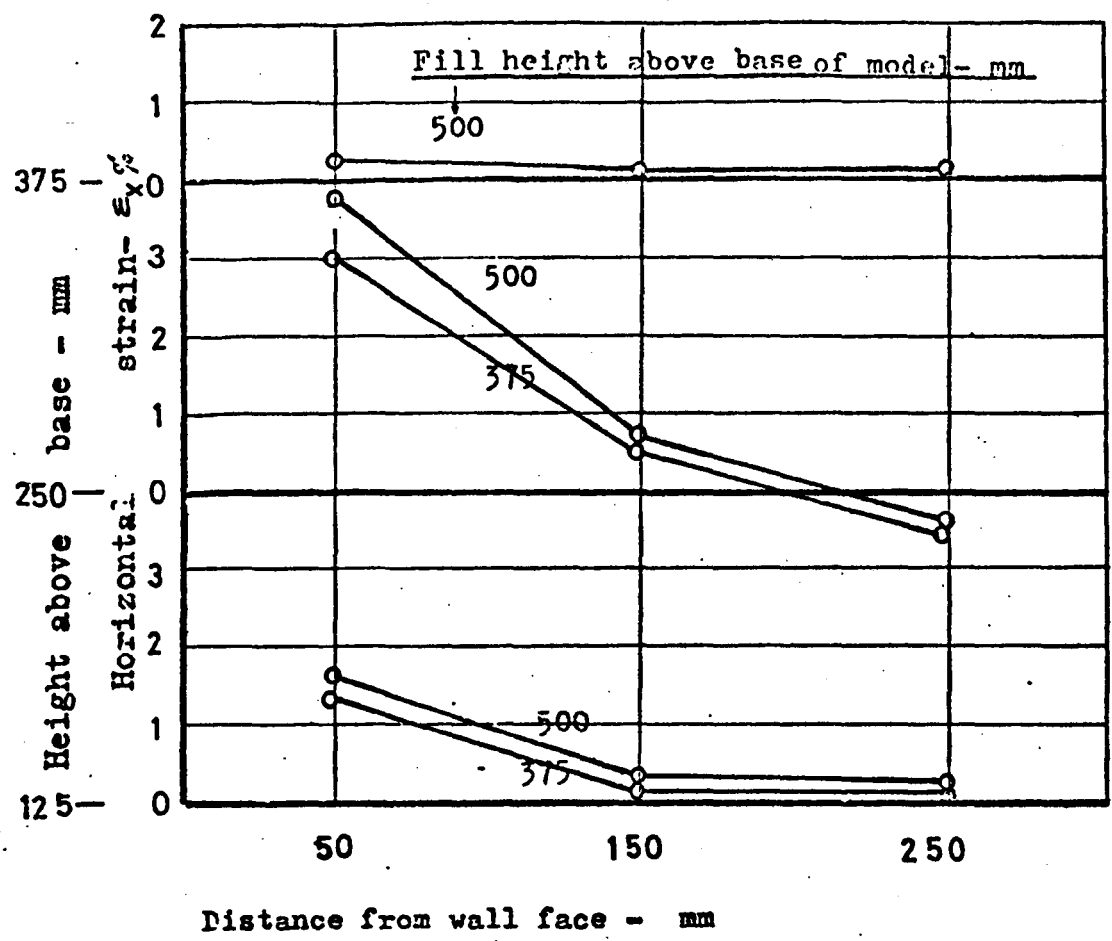
Fig. (5.33) Variation in horizontal soil strain with distance from wall face
(Series E walls ,   ΔH=250, S=100 mm)
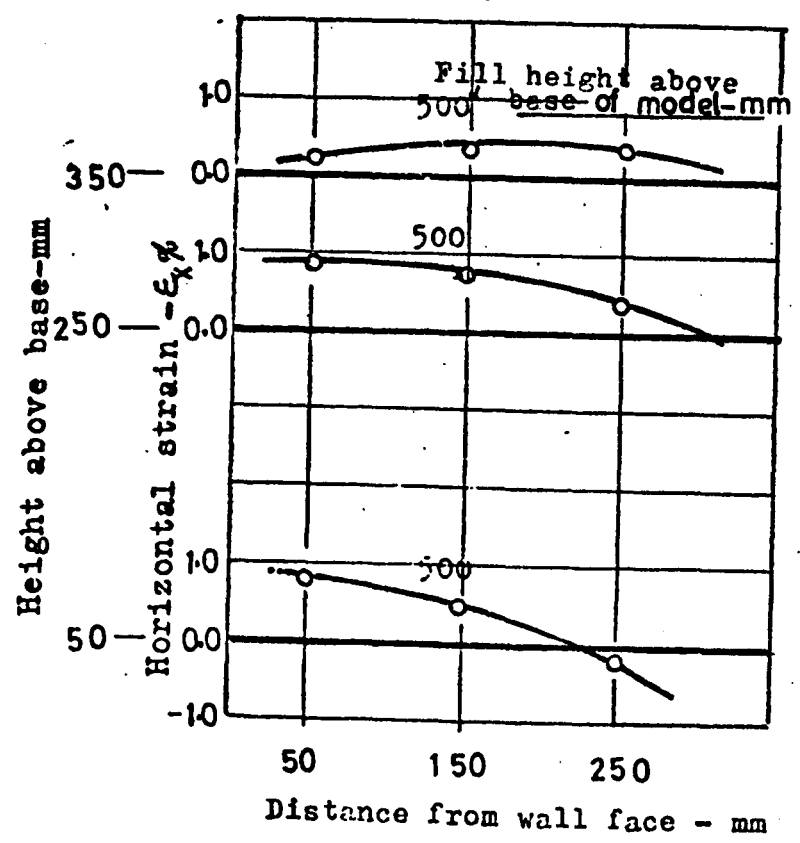
Fig.(534) Variation in horizontal soil strain with distance from
wall face   (Series E walls, ΔH=100   , S= 150 mm)
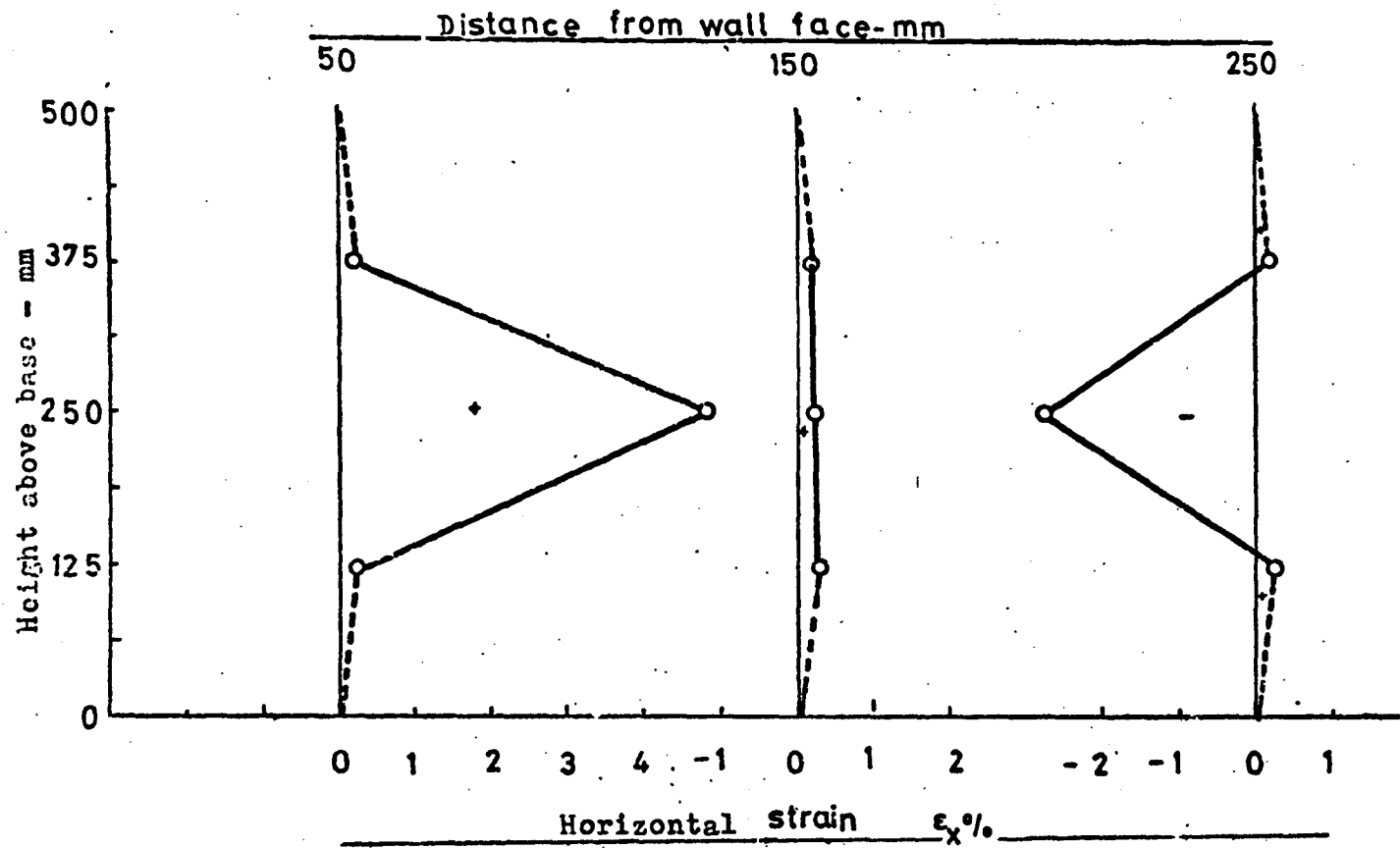
Fig. (5.35) Variation in horizontal/soil strain with wall height at three vertical sections from the wall face (Series E walls, ΔH=250, S=100 mm)
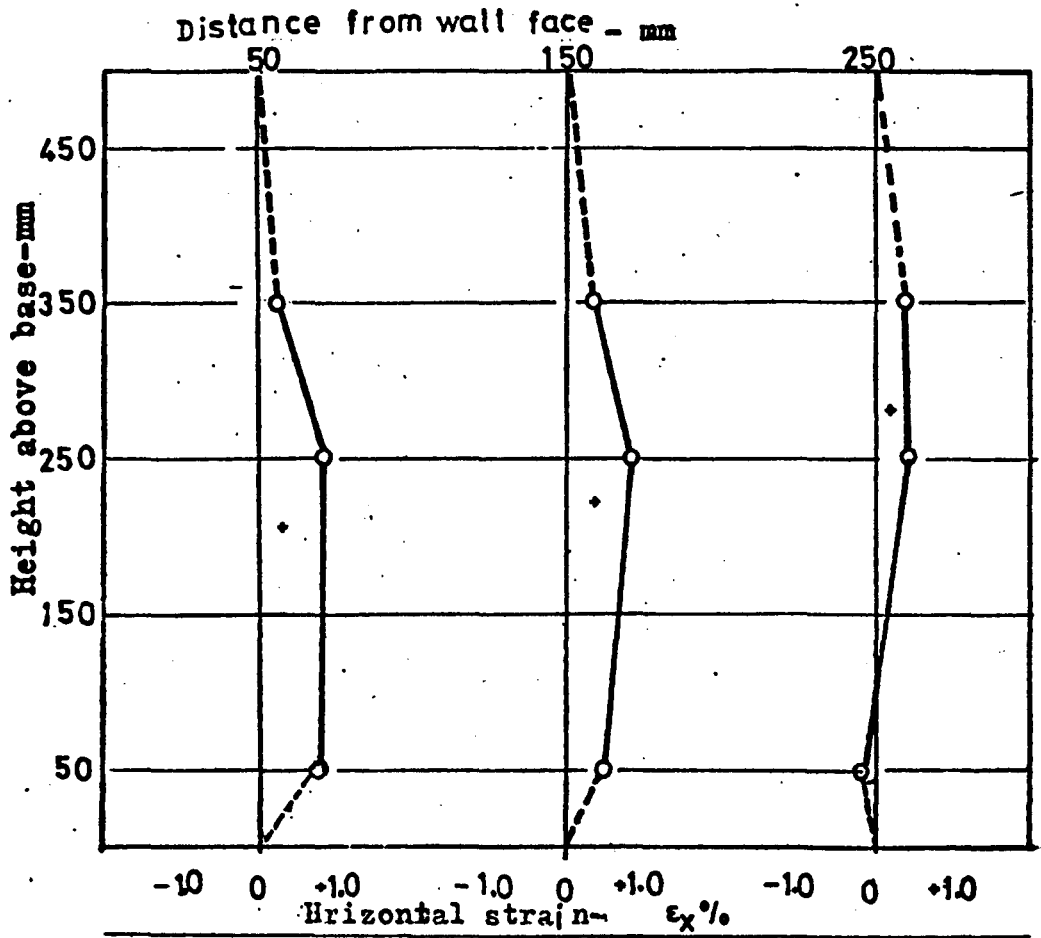
Fig. 536 Variation in horizontal soil strain with wall height at three vertical sections from wall face.(Series E walls∆H=100, S=150mm)
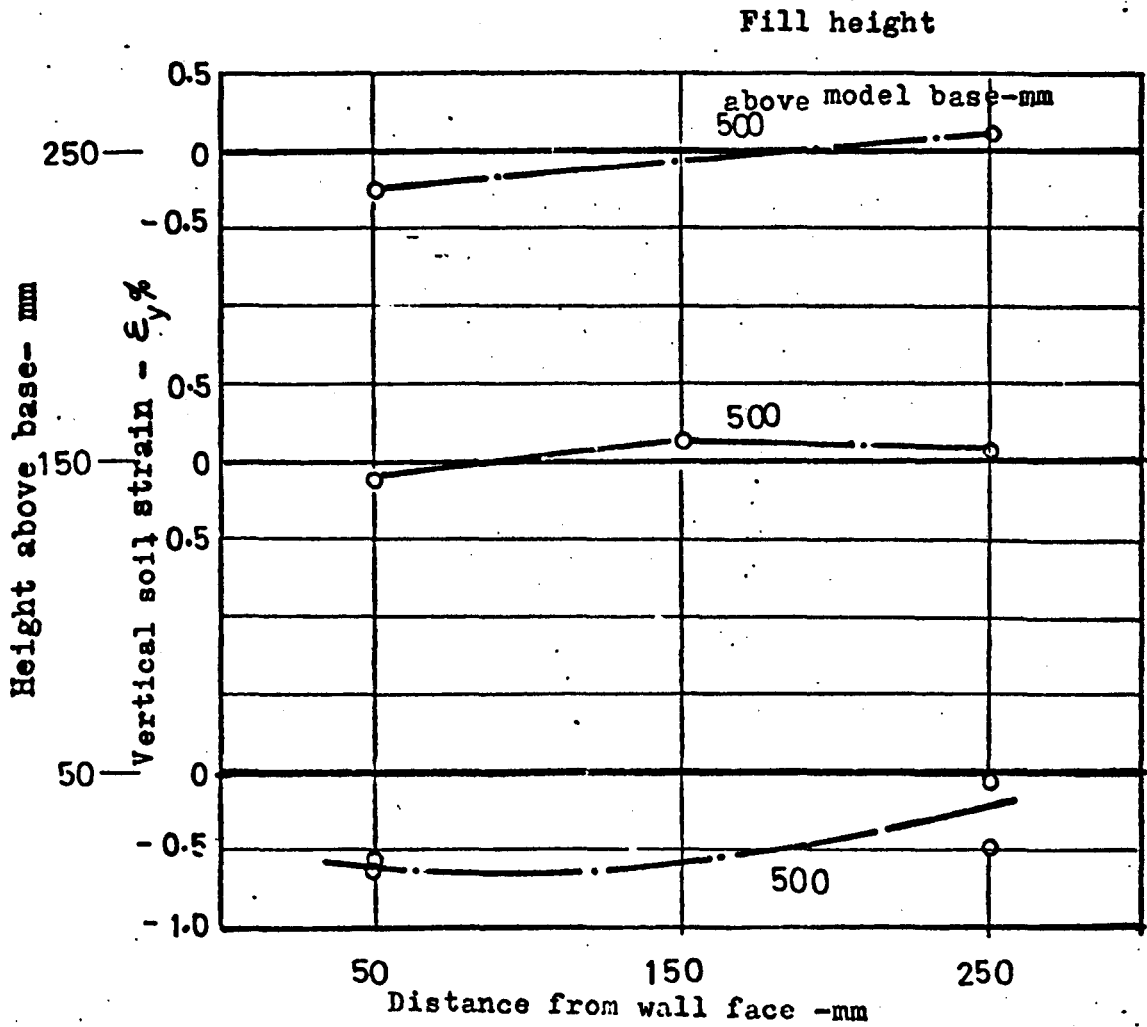
Fig.537 Variation in vertical soil strain with distance from wall face at three levels in the wall(Series E , ΔH=100, S=150 mm).
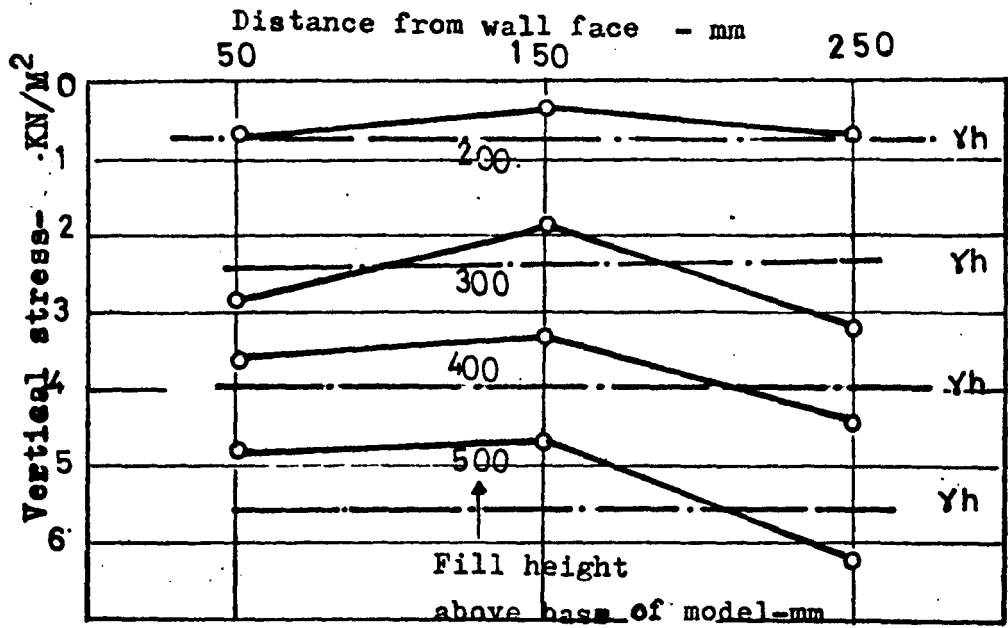
Fig.5.38 Variation in the vertical soil stress at a section 150 mm above base of the wall (Series E , ΔH=100 , S=150 mm)
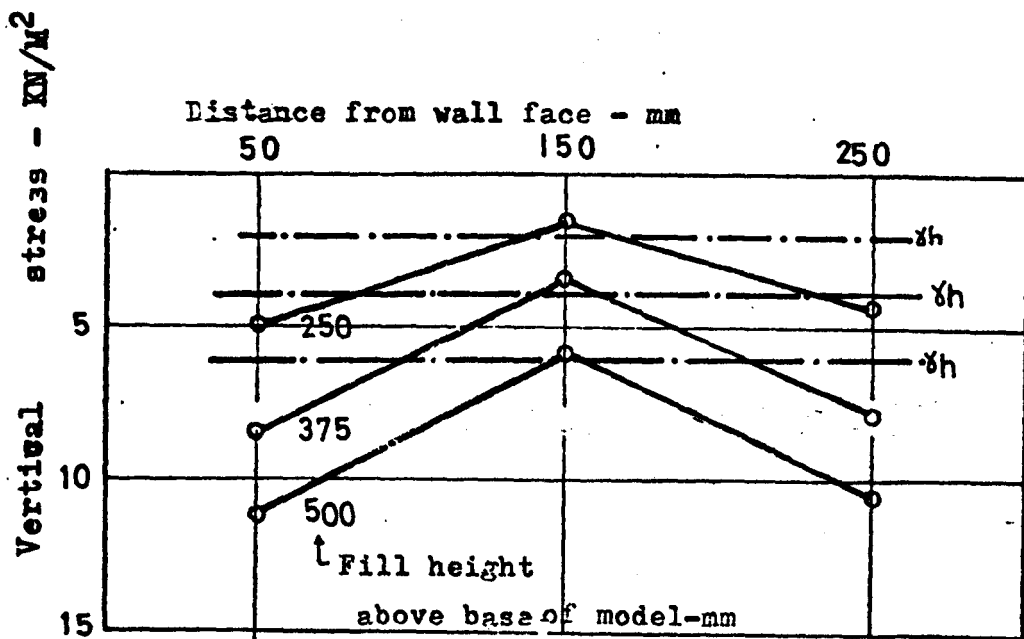
Fig.5.39 Variation in the vertical soil stress at section 125 mm above wall base (Series E , ΔH=250, S=100mm)

were nearly twice the overburden pressure, Fig (5.39)
indicating an instrumental error.

The vertical soil strain patterns shown in Fig (5.37)
and the corresponding soil stress pattern, shown in Fig
(5.38), do not appear to be compatible. Although the soil
strain patterns Fig (5.37) appear to indicate the effect of
the horizontal thrust acting at the back of the wall, the
soil stress pattern showed an opposite effect to what was
expected. Doubts must be cast on the earth pressure measure-
ments, with particular regard to the behaviour of the
pressure cells. Previous investigators [28,44,50] using
pressure cells for the soil stress measurement, have had
similar problems.

5.6.3.h The horizontal wall deflection

Figs (5.40) and (5.41) show a summary of the horizontal
deflections of two model reinforced earth walls, measured
using the strain coils previously described in Chapter Four
Section (4.6). The observations were noted during and
after the wall construction. The maximum wall deflections
occurred near the midheight of the walls.

The calculated horizontal wall deflections from the
measured horizontal strains in the soil are also shown in
Figs (5.40)and (5.41) and these seem to compare reasonably
with the wall deflections measured directly by the strain
coils, with one exception at the top of the wall in Fig
(5.40) where the calculated deflection was smaller than
the observed value. This indicates compatibility between
the horizontal soil strain measurements and the observed
wall deflections.

5.6.4 Comments on Series E tests

In the Series E tests,the walls ,which were not carried to fail-
ure,were built with different vertical and horizontal tie
spacings, to a maximum height of 500 mm. In these tests
the tie tension, the horizontal and vertical strains in the
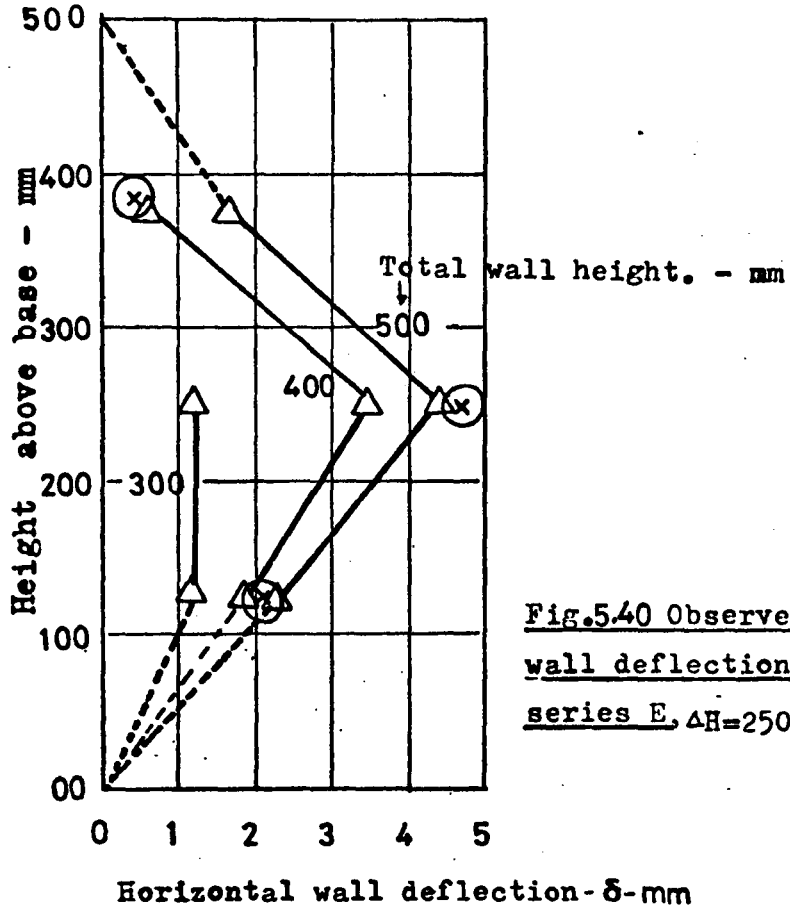
Fig.5.40 Observed horizontal wall deflection(Model wall series E, ΔH=250 mm, S=100)
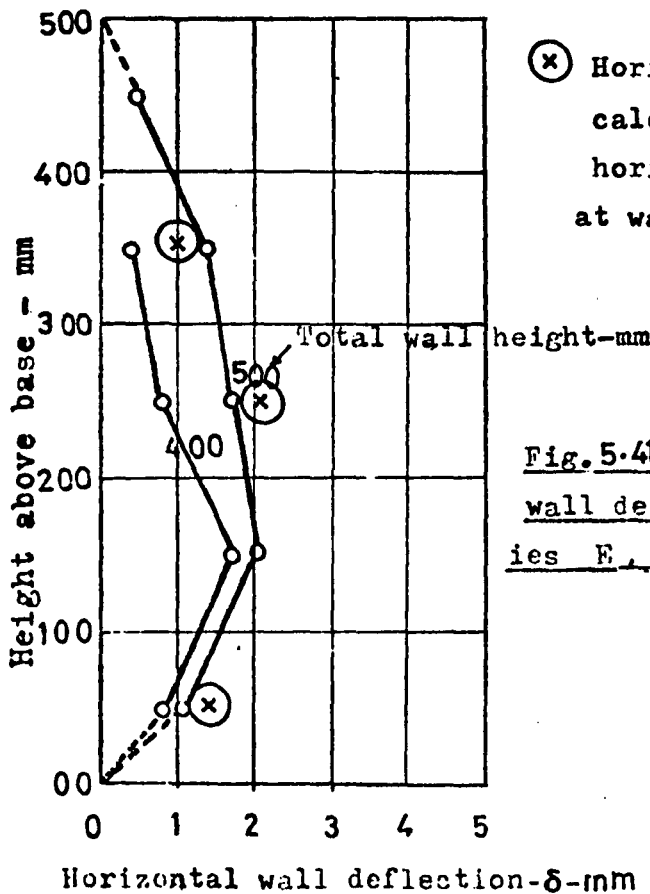
ⓧ Horizontal wall deflections calculated from the observed horizontal soil strain at wall height of 500 mm

Fig.5.41 Observed horizontal wall deflection(Model wall series E, ΔH =100 ,S=150 mm)

Horizontal wall deflection-δ-mm

soil, the vertical stresses in the soil and the horizontal
deflections of the wall face were observed and the results
were presented in the previous section. The observed
maximum tie tension variation with wall height and with
fill height above the tie level, was compared with the
corresponding theoretical values computed from the Energy and
Rankine theories.

The intention in Sections 5.6.5 and 5.6.6 is to use the
tie tension measurements in the Series E tests, to evaluate
the non-dimensional tension parameter $\mathcal{X}$ and the safety
factor against internal failure of the wall. The observed
$\mathcal{X}$ and safety factor values can be used to test the various
theories for reinforced earth wall design.

5.6.5 The non-dimensional tension parameter $\mathcal{X} = \dfrac{T_m}{\gamma h \, \Delta HS}$

The non-dimensional factor $\mathcal{X}$ was first advanced by
Schlosser and Vidal[67] in a study on a full scale wall.
If the wall behaves in accordance with the Rankine theory the
non-dimensional tension $\mathcal{X}$ will have a constant value at
different wall levels, which will correspond to the co-
efficient of active earth pressure K_a. Banerjee[5]
evaluated the non-dimensional tension, using the finite
element method, for walls in service conditions and reported
a value of 0.35 for the non-dimensional tension factor.

In the present study the non-dimensional tension $\mathcal{X}$ was
computed from the observed maximum tie tension at different
levels of Series E walls, built to a maximum height of 500 mm.
The experimental values were plotted against the fill height
above a tie level Fig (5.42). The experimental $\mathcal{X}$ values
were at a maximum near the top of the wall (i.e. small fill
heights above the tie level h) and decreased towards the
bottom of the wall. The theoretical non-dimensional tension
calculated from the local equilibrium energy approach (LO.L.A.)
gave a reasonable agreement with the observed non-dimensional
tension variation. The conventional and Banerjee methods,
predicted nondimensional tension values, which were of
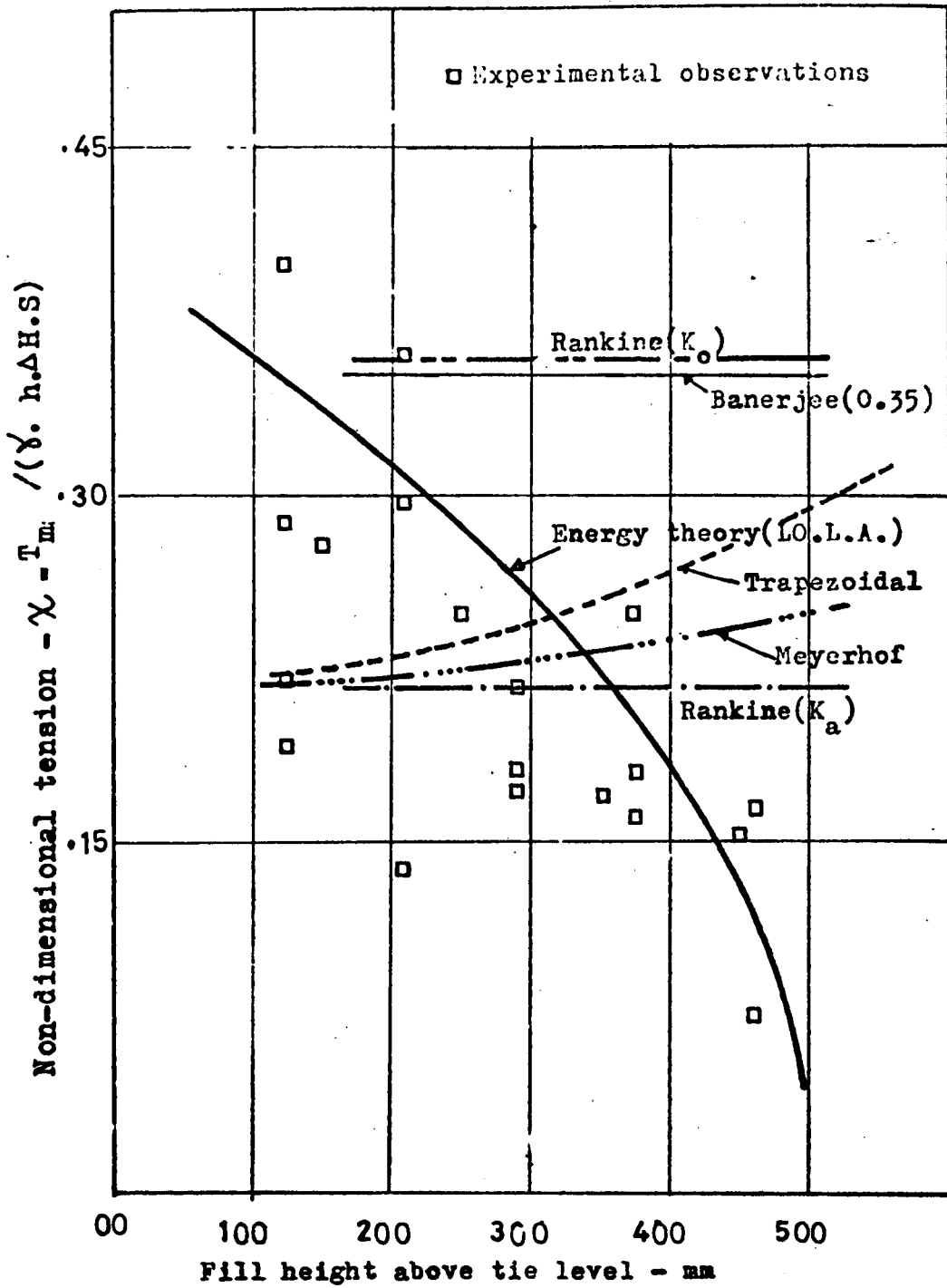
Fig.5.42 Experimental & theoretical non-dimensional tension χ V fill height above tie level(Model reinforced earth retaining walls H = 500 mm)

different pattern and magnitude from the experimental results. Hence the adoption of the conventional and Banerjee methods in the design of reinforced earth walls, assuming tie breaking failure, will result in an over or under estimate of the actual tension in the ties.

5.6.6 The internal stability of Series E model walls

5.6.6.a Introduction

An internal failure of a reinforced earth wall occurs normally by a tie breaking or tie pull out mode of failure. In practice, the safety factors against tie breaking failure are greater than needed for the design of a full scale wall since :——

(a) In order to account for corrosion which may occur during the lifetime of the structure, larger tie cross-sectional areas are adopted.

(b) The safety factors against tie breaking are estimated in practice using the yield stress of the tie material as a failure criteria instead of the ultimate stress which is greater than the yield stress. This leads to a hidden safety factor against tie breaking failure.

(c) The conventional theories usually over estimate the actual stresses in the ties. This results in a lower value of the theoretical safety factors compared with the actual safety factors against tie breaking.

Therefore a full scale wall is more likely to fail by tie pull out than by tie breaking. In the present study the safety factor against tie pull out of Series E walls will be studied in more detail than the safety factor against tie breaking.

5.6.6.b The safety factors against tie breaking of Series E walls

The safety factors against tie breaking, SF, can directly be estimated from the equation:

$$SF = \frac{A_r \cdot \sigma}{T_m} \quad \dots\dots\dots\dots\dots\dots \quad (5.3)$$

where: A_r is the tie cross sectional area

σ is the ultimate or yield stress of the tie material

T_m is the maximum tie tension

For constant A_r and σ values as in the case of the Series E tests, the safety factor depends on the tie tension. The actual safety factor against tie breaking of the Series E walls can be calculated from Equation (5.3) using the observed maximum tie tension envelope, for each tie spacing adopted in the construction of Series E walls, e.g. for the cases of the experimental and the theoretical maximum tie tension envelopes shown in Figs (5.29) and (5.30) the corresponding safety factors against tie break, were evaluated from Equation (5.3) and are illustrated in Fig (5.43).

The experimental safety factors against tie break were a maximum near the top of the wall and decreased towards the bottom of the wall. In Fig (5.43a) the experimental safety factor increased again at the bottom tie level.

In Fig (5.43a) the Energy theory (T.L.L.D.) and the Rankine theory predictions fell near to the minimum experimental results, although these methods, as shown in Fig (5.43b) tended to give an over or an under estimate of the experimental safety factor against tie break, depending on the wall level considered. The Energy theory (LO.L.A.) seemed to predict smaller safety factors against tie break at the top and the middle of the walls than the Rankine and the Energy (T.L.L.D.) theories. At the bottom of the walls, the Energy theory (LO.L.A.) gave larger safety factors against tie break than the Rankine and the Energy (T.L.L.D.) theories.

△–Experimental results

(a)

Safety factor against tie break(SF x σ)

(b)

Safety factor against tie break(SF x σ)

(σ = ultimate or yield stress of tie material
N/mm²)
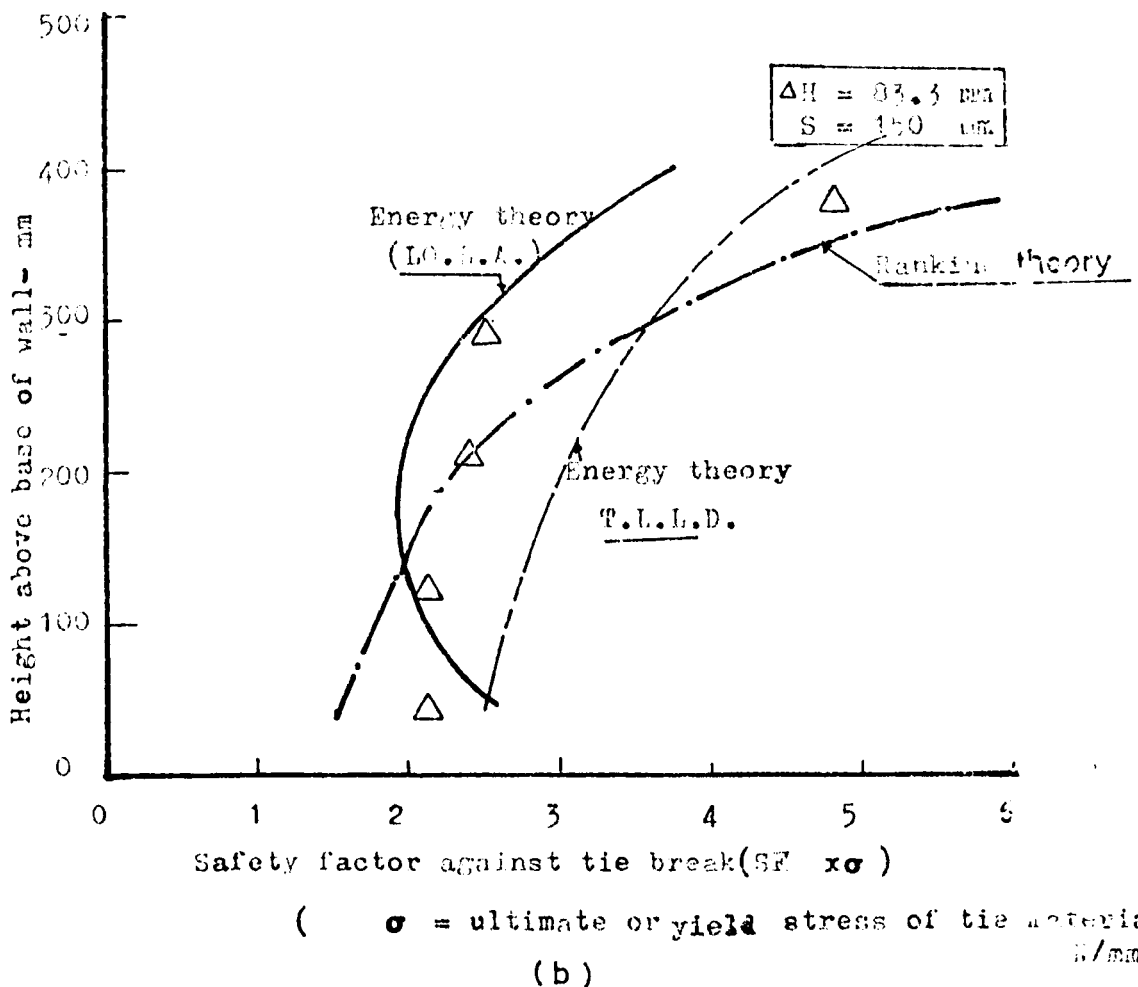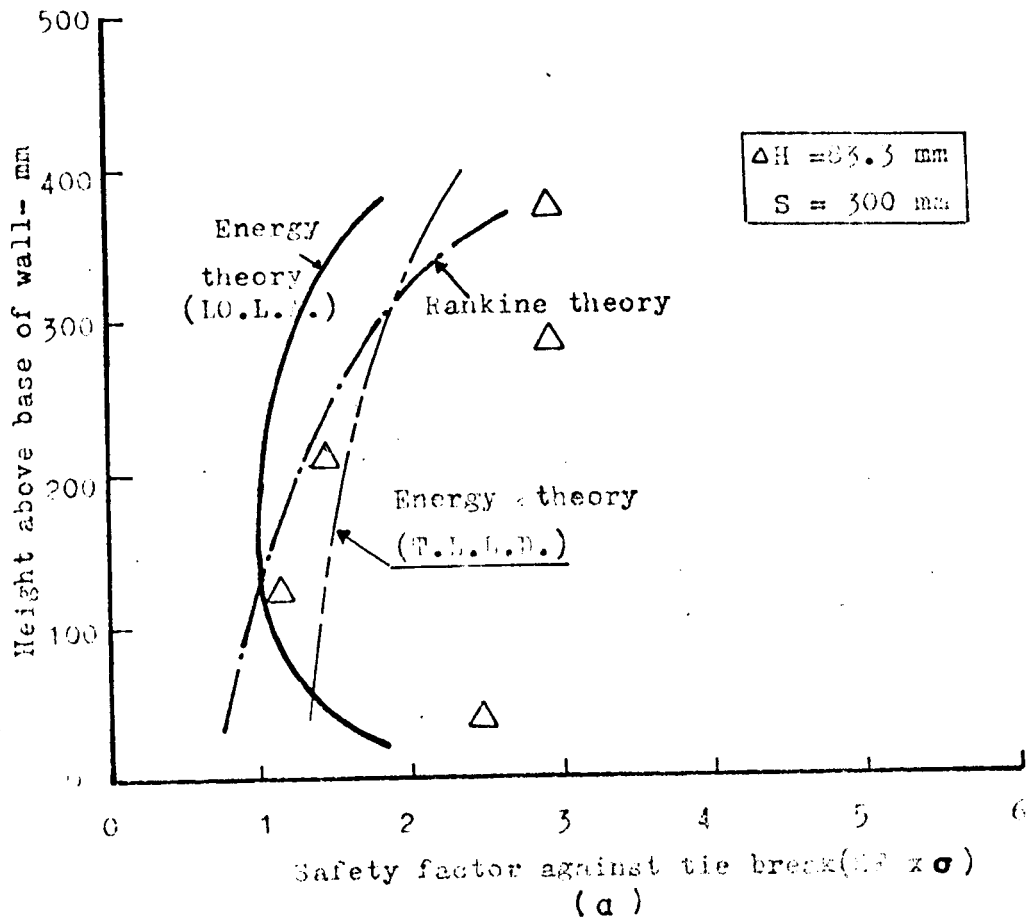
Fig. 5·43 Comparison between experimental & theoretical safety factor against tie breaking (Model walls, series B tests.)

5.6.6.c Safety factors against tie pull out failure of Series E Walls

For an optimum design of a reinforced earth wall, failing by tie pull out, a theoretical procedure for evaluating the safety factor against tie pull out at each tie level is needed.

The intention of the present study is to check the effect of the assumption of the tie length, which is effective in providing pull out resistance and also the effect of the tie tension (Maximum or average) on the experimental safety factor.   The experimental and the theoretical safety factors against tie pull out will also be compared.   This was done by evaluating the safety factors against tie pull out from the equation, $SF = \dfrac{2bL\gamma hf}{T}$ ....(5.4) and using:

(1)   The experimental maximum tie tension T_m and assuming all the tie length effective against tie pull out failure.

(2)   The experimental maximum tie tension T_m and assuming only the tie length extending beyond the maximum tension position on the tie, as effective against tie pull out failure.

(3)   The experimental average tie tension T_{av} and assuming all the tie length effective against tie pull out failure.

(4)   The experimental safety factor against tie pull out was also evaluated from the slope of the observed tie tension distribution along the tie length curves, using the following relationship, originally advanced by Schlosser and Vidal.[67]

$$SF = \frac{2b\gamma hf}{(\Delta T/\Delta L)} \quad \ldots\ldots\ldots\ldots\ldots\ldots\ldots (5.5)$$

Calculations of the safety factor against tie pull out based on equation (5.5) was facilitated by the computer programme shown in Appendix (V I)   .   The experimental safety factors calculated on the basis of the four preceding assumptions will be compared.   Comparison will also be made between the experimental and the theoretical safety factors against tie pull out of the Series E walls.

The results obtained from this analysis will now be presented.

5.6.6.d Experimental safety factors against tie pull out

Figs(5.44) to (5.47)show the experimental safety factors against tie pull out calculated on the basis of assumptions 1 to 4 mentioned in Section 5.6.6.c.   Methods 1, 2 and 3 gave reasonably smooth curves and indicated that for a rectangular reinforced earth wall with uniform tie distribution, the safety factors against tie pull out were a minimum at the top of the wall and increased to a maximum at the bottom of the wall.

The method number 4 based on the slope of the tie tension distribution along the tie length curves, is probably the most realistic approach for calculating the experimental safety factor against tie pull out, but the derivation of the safety factor based on this approach, depends to a great extent on the number of the observations of tie tension along the tie length.   For relatively few observations of tie tensions along a tie, as was the case of the Series E model tests, large scatter was noted in the experimental safety factor calculated from the slope of the tie tension distribution curves.   Because of this, it was decided to use the experimental safety factors calculated from the maximum tie tension and assuming that only the tie length extending beyond the maximum tension position as effective against tie pull out failure, for the comparison between the experimental and the theoretical factor of safety against tie pull out, since this method offered a minimum value of the experimental safety factor against tie pull out.

5.6.6.e Comparison between experimental and theoretical
safety factors against tie pull out

The experimental safety factors against tie pull out for the series E tests, calculated from the maximum tie tension and assuming all or part tie length effective and the corresponding theoretical predictions, computed from the

Assumptions used in calculating the experimental safety factor (S.F.)

1-1 All tie length effective.

2-2 Only tie length beyond maximum tension position effective

3-3 Average tension

4-4 Slope of the tension curve.
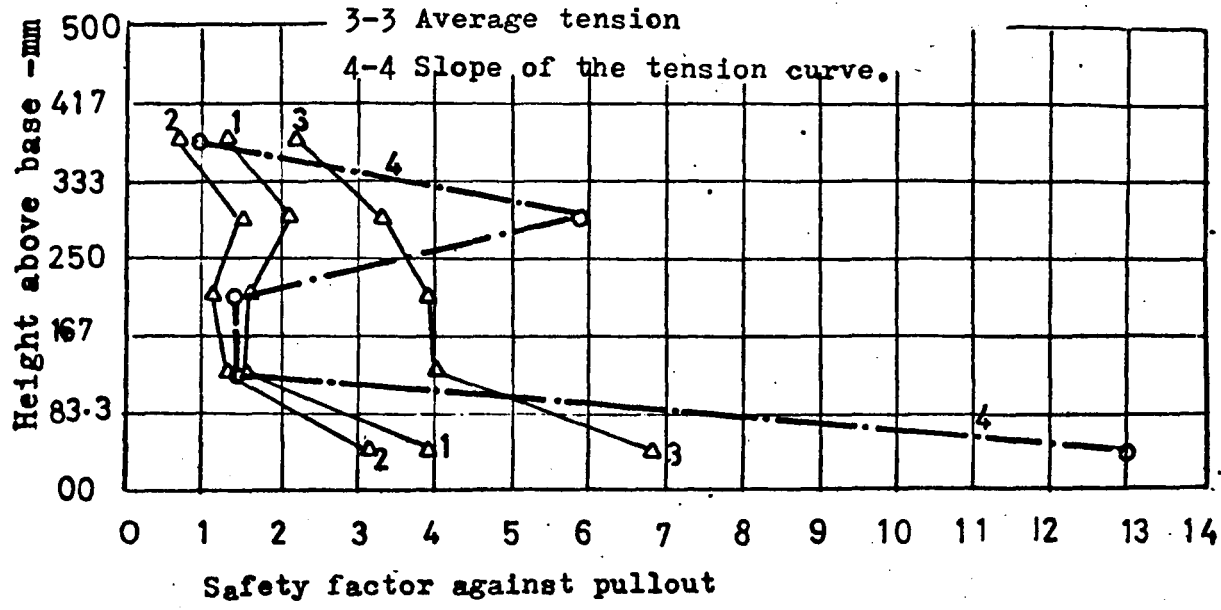
Fig. 5.44 Variation in experimental $\dfrac{\text{safety factor}}{}$ against tie pullout with wall height (Model walls series E , ΔH =83.3 , S = 300 mm)

Assumptions used in calculating the experimental safety factors (S.F.)

1-1 All tie length effective

2-2 Only tie length beyond maximum tension position effective.

3-3 Average tension.

4-4 Slope of the tension curve.
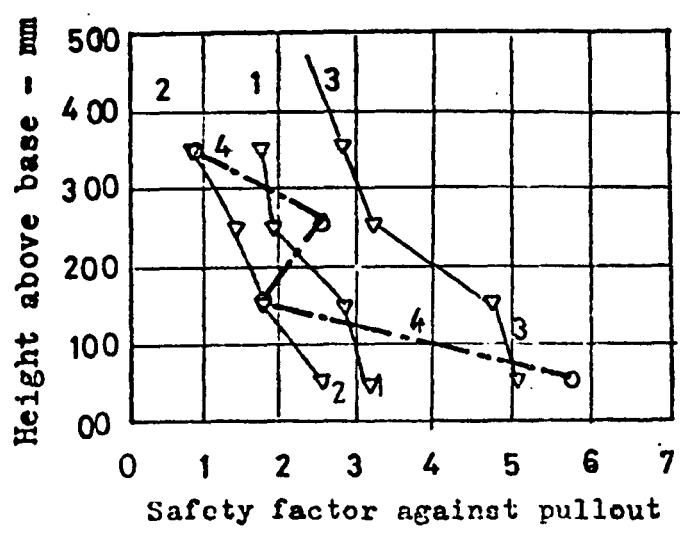
Fig(5.45) Variation in experimental $\dfrac{\text{safety factor}}{}$ against pullout with wall height (Model walls series E , ΔH=100 , S = 150 mm)

Assumptions used in calculating the
experimental safety factor (S.F.)

1-1 All tie length effective
2-2 Only tie length beyond maximum tension
position effective.
3-3 Average tension
4-4 Slope of the tension curve.
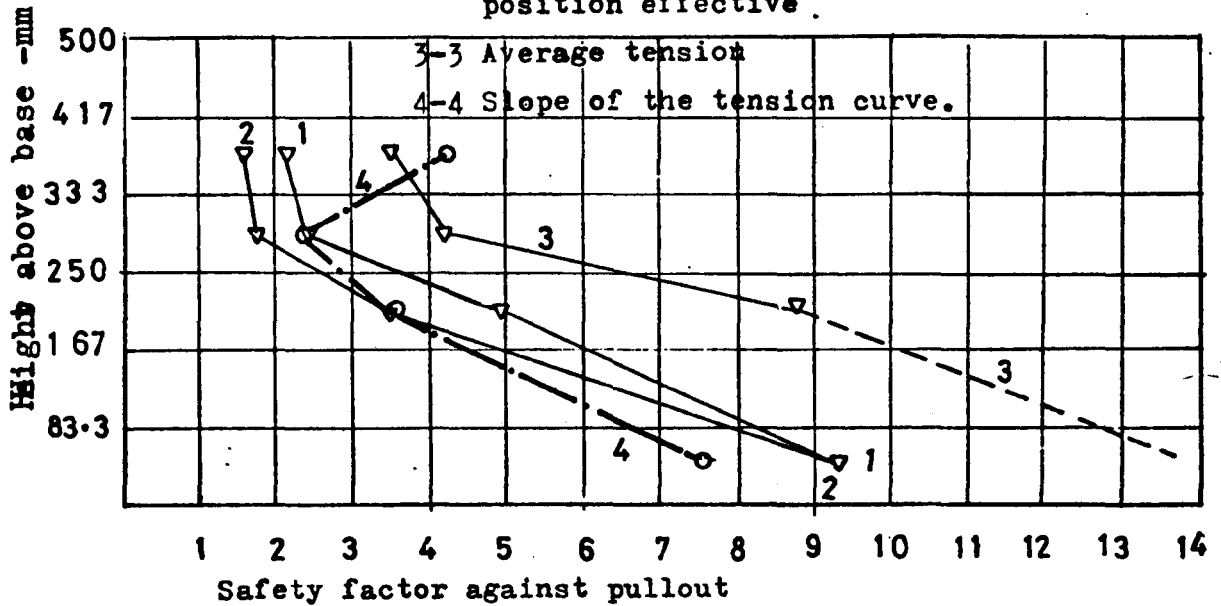
Fig.5.46 Variation in experimental safety factor against tie pullout with wall height (Model walls series E , ΔH =83.3 , S = 100 mm)

Assumptions used in calculating the experimental safety factor

1-1 All tie length effective
2-2 Only tie length beyond maximum tension position effective.
3-3 Average tension
4-4 Slope of the tension curve
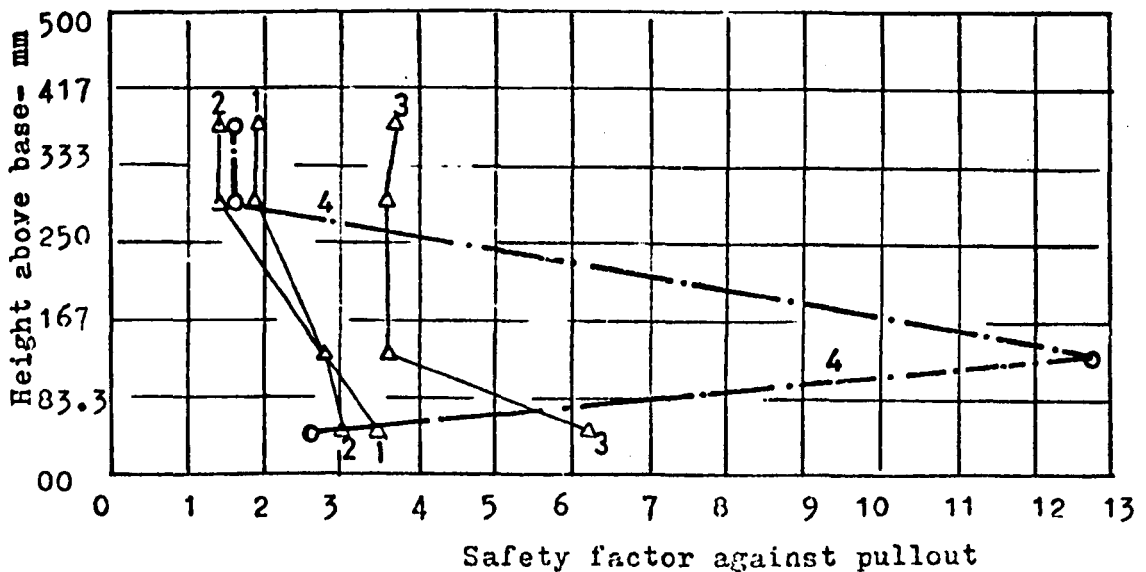
Fig(5.47) Variation in experimental safety factor against tie pull-out with wall height (Model walls series E, ΔH=83.3, S=150mm)

Rankine (all or part tie length effective), the Coulomb
force, the Coulomb moment, Banerjee and the Energy (LO.L.A.)
and (T.L.L.D.) methods, are all shown in Figs (5.48) to
(5.51).

The Rankine (all tie length effective), the Coulomb
force, the Coulomb moment and Banerjee methods predicted
constant safety factors with wall height, which seemed to be
generally greater than the experimental safety factors against
tie pull out at the top of the wall and to be smaller than
it at the bottom of the wall.

The Rankine (part length effective) predicted a linearly
varying safety factor against tie pull out with wall depth
which was generally smaller than the experimental values at
the bottom of the wall although at the top of the wall seemed
to lie near to the experimental results.

The Energy theory (LO.L.A.) predicted a non-linearly
varying safety factor against tie pull out, which appeared
to agree with the general trend of the experimental points,
although it did not correspond completely in magnitude with
the experimental safety factors against tie pull out.   The
Energy theory (T.L.L.D.) predicted safety factors against
tie pull out which were greater than the experimental values.

5.6.7   Conclusions from Series E tests

(i)   The tie tension distribution along the tie length
curves, for ties lying in different levels of the model
reinforced earth walls, had a maximum value of tie
tension in the first half of the tie which decreased
to zero at the free end of the tie.

(ii)   The plots of maximum tie tension versus wall height
and maximum tie tension versus fill height above the tie
level, indicated that the Rankine theory generally
underestimated the observed maximum tie tension at the
top of the wall, and overestimated it at the bottom of
the wall.   The Energy theory (LO.L.A.) was found to
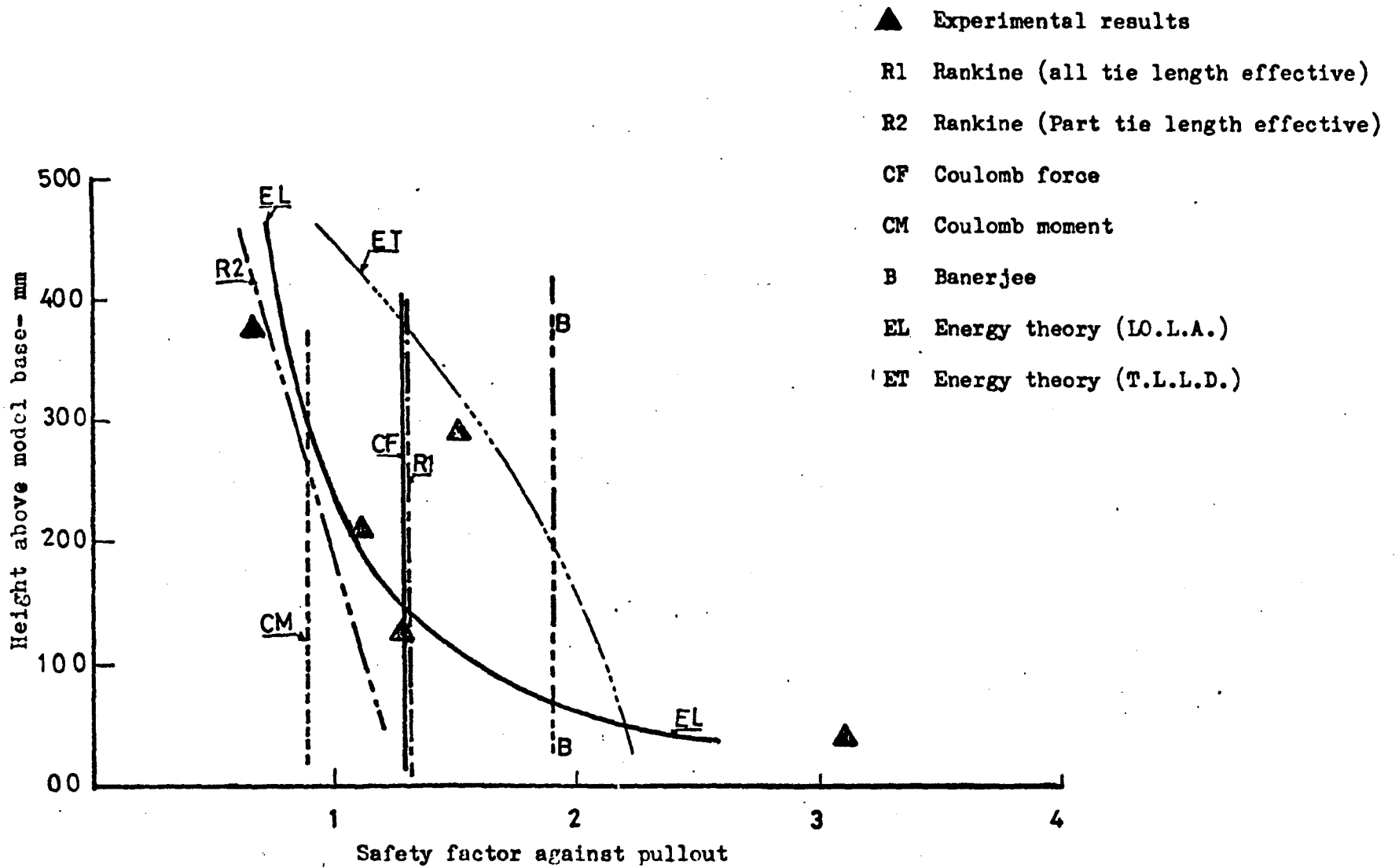
Fig (5-48)   Experimental and theorётical safety factors against tie pull out
(Series E tests, △ H ▪ 83.3, S ▪ 300 mm)

Legend:
▲   Experimental results
R1   Rankine (all tie length effective)
R2   Rankine (Part tie length effective)
CF   Coulomb force
CM   Coulomb moment
B   Banerjee
EL   Energy theory (LO.L.A.)
ET   Energy theory (T.L.L.D.)
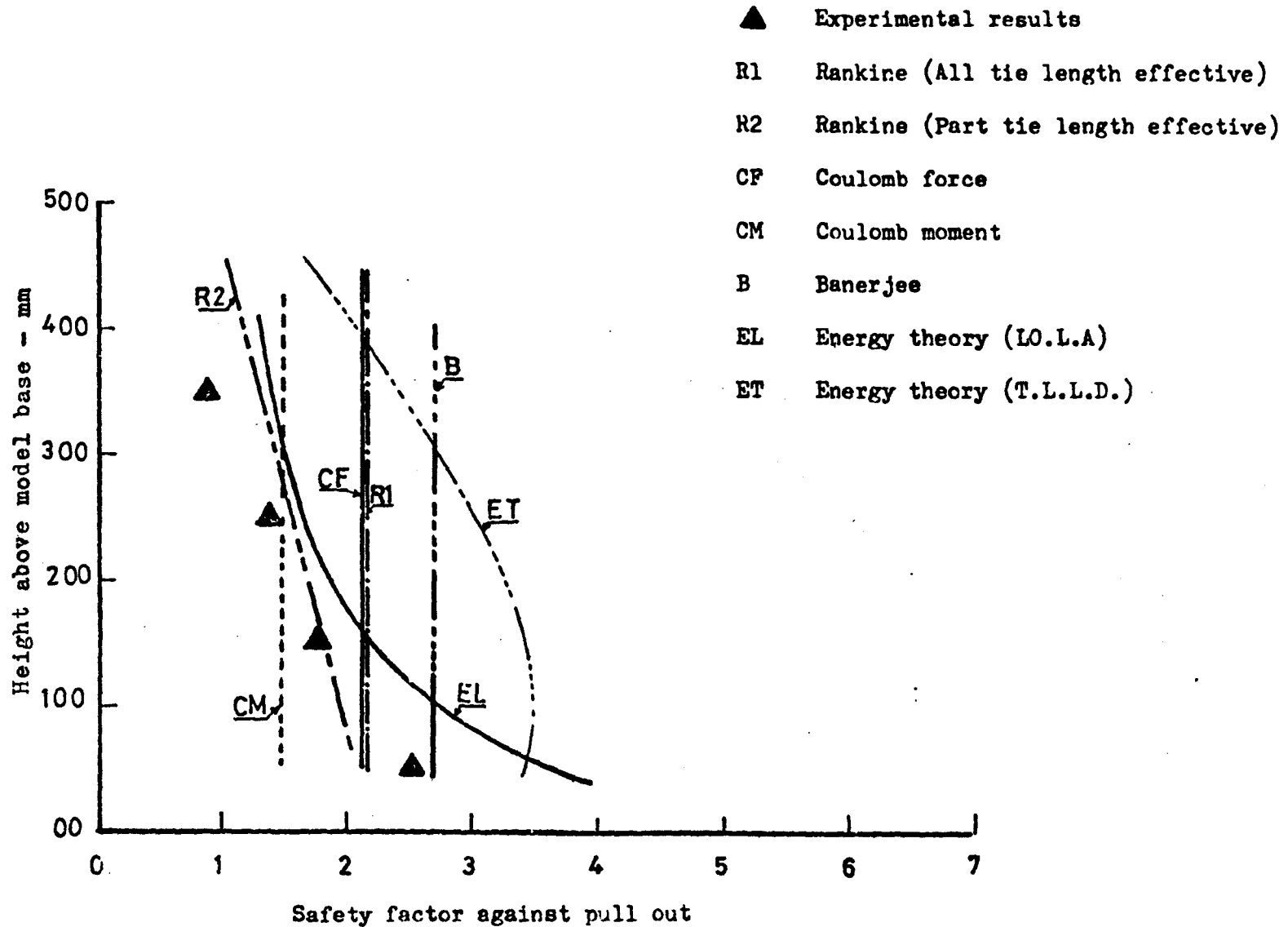
Fig. (5-49) Experimental and theoretical safety factor against tie pull out
(Series E tests, $\Delta H = 100$, $S = 150$)
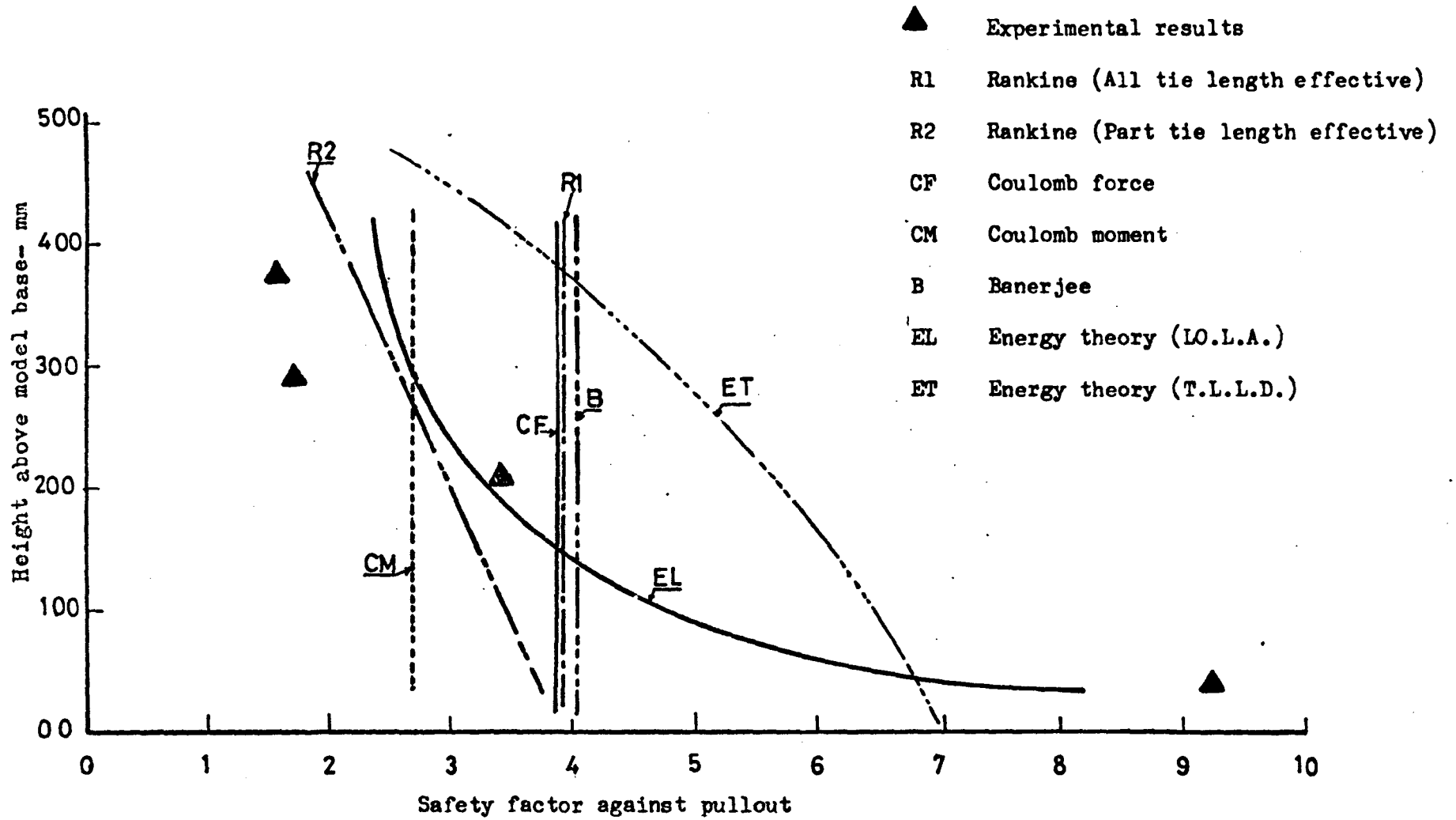
Fig (5-50)   Experimental and theoretical safety factors against tie pull out

(Series E tests, ΔH = 83.3,   S = 100 mm)

Legend:
- ▲ Experimental results
- R1 Rankine (All tie length effective)
- R2 Rankine (Part tie length effective)
- CF Coulomb force
- CM Coulomb moment
- B Banerjee
- EL Energy theory (LO.L.A.)
- ET Energy theory (T.L.L.D.)

Y-axis: Height above model base— mm
X-axis: Safety factor against pullout
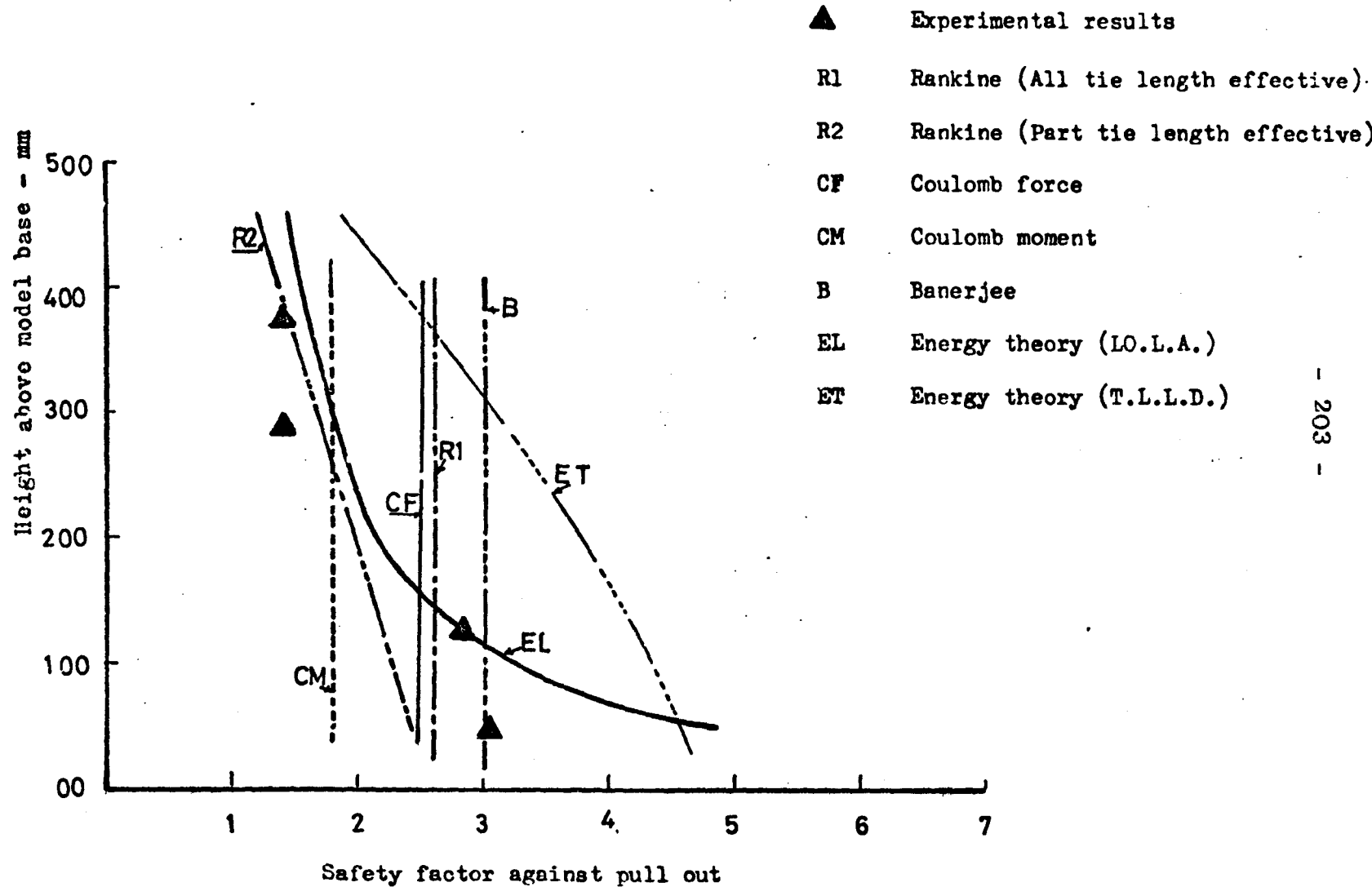
Fig(5-51) Experimental and theoretical safety factor against tie pull out

(Series E tests, $\Delta H = 83.3$,   S = 150 mm)

predict a similar pattern to the observed maximum tie
tension distribution with wall height, but with larger
magnitudes.   This discrepancy was noted to decrease
with decreasing tie spacing.   The Energy theory
(T.L.L.D.), predicted maximum tie tensions which lie
near to the observed values, although this method was
noted to underestimate the maximum tie tension for
walls built with relatively small tie spacing.

(iii) At the bottom of the wall, the curves formed by
joining the maximum tension positions in the ties, at
different wall levels, were found to be nearly
coincident with the Coulomb failure plane, for an
unreinforced earth wall.   At the top of the wall, these
curves were noted to shift away from the Coulomb plane
towards the wall face, when relatively small tie spacing
was adopted.

(iv)   From measurements of the horizontal strains in
the backfill of the wall, maximum positive strains were
observed near the wall face, indicating expansion and
probably the soil was tending towards an active state of
stress.   In a section lying furthest from the wall face,
negative strains were observed, indicating compression
and probably the soil was tending towards a passive
state of stress.

(v)   The maximum horizontal deflection of the wall face
was found to occur near the middle of the wall.   The
calculated wall deflections from the observed horizontal
soil strains, were found to lie close to the wall
deflections measured directly by the strain coils.
Hence the horizontal strain measurements were considered
to be compatible with the observed wall deflections.

(vi)   The vertical soil strain was a maximum and
compressive near the wall face and decreased towards
the back of the wall.   This was attributed to the
effect of the horizontal thrust acting at the back of
the reinforced earth wall.

(vii)   The Redshaw pressure cells used for the vertical
soil stress measurement, in some cases gave an
inconsistent indication of the vertical soil stress, and
in some other cases the measured vertical stress, by these
presure cells, was found to lie near the overburden
pressure γh.   The vertical soil strain pattern and
the corresponding soil stress pattern did not appear to
be compatible.   This was attributed mainly to the
errors associated with the pressure cells.

(viii)   The non-dimensional tension factor α, computed
from the observed maximum tie tension, was a maximum at
the top of the wall and decreased towards the bottom of
the wall.   This behaviour was reasonably predicted by
the Energy theory (LO.L.A.).   Banerjee's non-dimensional
tension factor was found to be different in magnitude
and pattern from the observed results.

(ix)   For a rectangular model reinforced earth wall with
uniform tie distribution, the safety factor against tie
breaking was a maximum near the top of the wall and
decreased with wall depth.   The Energy theory (LO.L.A.)
seemed to give a lower limit for the observed safety
factor. The Rankine and the Energy (T.L.L.D) theories predicted
higher safety factors than the observed values in some cases.

(x)   For the Series E model walls the experimental safety
factors against tie pull out were found to be a minimum
near the top of the wall and increased with wall depth.

(xi)   None of the theories agreed completely with the
observed safety factors against tie pull out, although
the Energy theory (LO.L.A.) seemed to predict the general
trend of the observed points.

5.7.   Conclusions from Chapter Five

Detailed conclusions were given at the end of each test
series carried out in the laboratory test programme.   A
summary of these conclusions will be outlined in this section.

Preliminary model walls were built to study the effect of the friction of the back of the model on the critical height of the reinforced earth walls and also to check the performance of the instrumentation designed to monitor the tie forces and wall deflections. A minimum distance of 250 mm was found necessary between the back of the model and the back of the reinforced earth wall. The strain coils initially developed to measure the strain in the soil were found to be applicable also in the measurement of the horizontal wall deflections. The stresses in the ties were satisfactorily measured by mounting strain gauges on perspex.

From the observed critical wall heights of walls failing by tie breaking and comparison with the theoretical predictions it was found that the Rankine, Meyerhof and the Trapezoidal methods predict practically identical critical wall heights which were about 28%-39% of the observed critical wall heights. The theoretical critical heights predicted by the Energy theory, (T.P.P.D.), (T.L.L.D.), (T.L.L.A.), (LO.L.A.) and (LO.L.D.) approaches, were noted to lie nearer to the observed values than the existing theories.

The Glasgow tie breaking failure test results were found to be consistent with the previous tie breaking failure tests conducted in France[7] and in the U.S.A.[45]

The adherence lengths obtained from walls failing by tie pull out were noted to be shorter than the theoretical adherence lengths predicted by the Rankine (all or part length effective), the Coulomb force, the Coulomb moment, Banerjee and the Energy theory (LO.L.A.).

In the Series D tests, the effect of the tie length on the maximum tie tension was assessed and the maximum tie tension was observed to decrease with increasing tie length. The Energy theory (LO.L.A.), (T. L.D.) and (T. P.D.) gave similar pattern to the observed data. The Energy theory (T. L.D.) and (T. P.D.) also reasonably agreed in magnitude with the observed tie tensions. The Rankine, Meyerhof and the Trapezoidal methods were found to give different pattern

and magnitudes from the observed results.

From tie tension measurements, on walls not tested to failure, a maximum tie tension was seen in the front half of the tie which decreased to zero at the free end of the tie.

From the plots of the observed and the theoretical maximum tie tension variation with wall height, the Energy theory (LO.L.A.) was found to predict similar patterns to the observed results but with larger magnitudes and the discrepancy was found to decrease with decreasing tie spacing. The Energy theory (T.L.L.D.) predicted a maximum tie tension which lay within the observed maximum tension points. For walls built with relatively small tie spacings this method predicted tie tensions which were about 25% lower than the observed values. At the top and middle of the wall the Rankine theory generally underestimated the observed maximum tie tension (by $\doteq 28\%$ of the observed value). At the bottom of the wall the Rankine theory overestimated the maximum tie tension by $\doteq 37\%$ of the observed value.

The observed non-dimensional tension factor $\mathcal{X} = \dfrac{T_m}{\gamma h . \Delta HS}$ was found to be a maximum at the top of the wall and decreased to a minimum value at the bottom of the wall. The Energy theory (LO.L.A.) reasonably followed the pattern of the experimental results. Banerjee and the Rankine methods gave constant values of the non-dimensional tension factor $\mathcal{X}$, which were different in magnitude and pattern from the observed results.

For rectangular reinforced earth walls with uniform tie distribution, a maximum safety factor against tie break was noted at the top of the wall, decreasing towards the bottom of the wall. For these walls also a minimum factor of safety against tie pull out was seen at the top of the wall and increased towards the bottom of the walls.

Comparison between the experimental safety factors against tie pull out and the corresponding theoretical values

computed from the existing , the Energy (LO.L.A.) and
(T.L.L.D.) theories, indicated that there was no general
agreement between the experimental safety factors against
tie pull out and the values predicted by the existing theories.
The Energy theory (LO.L.A.), predicted similar trends to the
experiment results, but it did not correspond completely in
magnitude with the experimental safety factors against tie
pull out. The Energy theory (T.L.L.D.) predicted higher
values of safety factors against tie pull out than the
experimental results.

From the horizontal soil strain measurements a maximum
+ve strain, indicating expansion, was observed near the wall
face and a -ve strain, indicating compression, was observed
at a section lying furthest from the wall face.

The deflections of the front face of the wall, calculated
from the horizontal soil strain measurements were found to lie
close to the measured wall deflections. Hence, compatibility
between the horizontal soil strain measurements and the
horizontal wall deflections appeared to exist.

The vertical soil strain was observed to be a maximum and
-ve indicating compression near the wall face and decreased
towards the back of the wall. This pattern was attributed
to the effect of the horizontal thrust acting at the back of
the wall.

The measurements of the vertical soil stress were found
to be inconsistent and the pattern of the vertical soil stress
distribution was incompatible with the observed vertical soil
strain measurements. This was attributed probably to the
difficulties associated with the pressure cells for the
soil stress measurements.

CHAPTER SIX

FULL SCALE REINFORCED EARTH RETAINING
WALLS

6.1 Introduction

6.1.1 Objectives of the present chapter

Reinforced earth retaining wall theories have been presented
in Chapter Three.   In Chapter Five, the behaviour of reinforced
earth retaining walls was studied on a laboratory scale model
and the reinforced earth theories were tested on the basis
of these model test results.

In the present chapter, reference will be made to full
scale walls reported in the literature and a brief review will
be given of the test results reported on these walls.   The
observations reported on Granton field wall[29] will be
considered in order to investigate the similarities and
differences between model wall and field wall behaviour,
to compare the reinforced earth theories with the field wall
behaviour, and to investigate the effect of compaction on the
stresses and deformations measured in the Granton wall.

6.1.2 Literature review

In Chapter Two reference has been made to full scale
reinforced earth retaining walls reported in the literature.
The main walls which were instrumented and reported were:

(a)   The Incarville experimental wall
(b)   Dunkirk harbour wall
(c)   Los Angeles County wall, and
(d)   The Granton reinforced earth wall

A brief review of these walls will now be given.

6.1.2.a   The Incarville experimental wall

This was reported by Schlosser & Vidal[67] and Schlosser[62].
The wall was 10 m x 10 m in cross-section and 165 m long.

The backfill material consisted of gravelly sand, with angle of internal friction $\emptyset$ and an average backfill density of 40° and 20 kN/m^3 respectively. A number of ties were equipped with strain gauges at 1.7m intervals. The vertical and horizontal pressures were measured using Glotzl pressure cells. Aluminium ties were used, with Young's modulus equal to 6.86 x 10^4 MN/m^2 and tensile strength equal $\top_{\scriptstyle C}$ χ 324 MN/m^2.

At the bottom third of the wall two ties were coupled together and spaced at 1m centre to centre. In the middle third single ties were placed at 1m intervals and at the top third of the wall, single ties were placed at two metre intervals. The skin elements were elliptical in cross-section 0.25m high giving a vertical tie spacing of 0.25m.

6.1.2.a.1 The Incarville wall test results
(i) Tie tension

The tie tension distribution along a tie length showed a substantial variation. Generally a maximum tie tension was observed near the wall face and decreased towards the free end of the tie. The shape of the tie tension distribution curves was influenced by wall construction procedures such as compaction.

The observed maximum tie tension was drawn versus the wall height and compared with the Rankine and the Trapezoidal methods. At the top of the wall, the maximum tie tension was found to lie near the Rankine theory prediction using an at rest earth pressure coefficient K_o. Near the bottom of the wall, the observed maximum tie tension was nearly equal to the theoretical tie tension predicted by the Trapezoidal method.

(ii) Vertical stresses in the soil

The vertical stress distribution along horizontal sections in the Incarville wall was non-linear, being at a maximum near the wall face and decreasing towards the back of the wall. The ratio of the horizontal soil stress to the

vertical soil stress $\frac{\sigma_x}{\sigma_y}$, was found to vary between 0.5-0.6
at the top of the wall to 0.35 at the base of the wall. The
measured stress ratio at the top of the wall was found to be
greater than the coefficient of earth pressure at rest K_o and
this has been attributed to compaction stresses.

6.1.2.b Dunkirk wall[41]

This was built as part of a storage yard in Dunkirk
harbour in France. The wall was double-faced, 15m high by
15m wide, was approximately 1,000m long and carried a 1,200
tonne travelling crane. The wall was founded on a rather
soft ground, and because of this the reinforced earth method
was the only feasible solution, Barclay.[6]

Three test sections in the wall were equipped with
strain gauges for measuring tie tension. Long et al [47]
and Schlosser[61] presented some of these results which
indicated a maximum tie tension near the wall faces and
decreased to a minimum value at the line of symmetry of the
wall.

The forces developed in the ties as a result of the
passage of the crane have been compared[63] with the theoretical
values calculated from an assumed vertical stress distribution
suggested by Schlosser et al.[63] At the top of the wall,
the predicted tie forces were appreciably higher than the
observed tie forces. At the bottom of the wall the theoretical
and the observed values appeared to approach similar values.

6.1.2.c The Los Angeles County wall

This was reported by Chang[14], Chang et al[15] and
Chang et al[16] The wall was built on Highway 39 near Los
Angeles. The reinforced earth fill had a maximum height of
16.8m, built on an embankment composed of random fill.

The Rankine method was adopted for the design of
reinforcements against both tie breaking and slippage failures.

The backfill material had an angle of internal friction

equal to 40°. The angle of friction between tie-soil was 31°.
The reinforcements consisted of galvanized steel strips 3 mm
in thickness, 60 mm width with a total length ranging between
7 and 14 metres. The elastic modulus of the strip material
was 1.97×10^8 kN/m^2 and Poisson's ratio was 0.28.

Wall instrumentation comprised:

(i)   slope indicators to measure internal deformations
of the embankment;

(ii)   settlement platforms for vertical settlement
observations;

(iii)   extensometers to measure soil strains;

(iv)   soil pressure cells;

(v)   strain gauges for measuring the strains in the
ties and the skin elements;

(vi)   gauge points for measuring the wall and skin
deformations.

These were monitored during the wall construction and one
year after the wall had been completed.

6.1.2.c.1   Test results

(i)   Tie tension

The observed tie tensions in the Los Angeles County wall
showed an appreciable variation with time. The maximum tie
tension was found to develop in the middle portion of the tie.
In some ties the tie tension increased with time and approached
the Rankine values based on an at rest earth pressure coefficient
K_o. In some other ties, the observed maximum tie tension was
found to vary with time and approached the Rankine values
based on an active coefficient of earth pressure K_a. The
variation in the tie tension with time was attributed to the
settlement and horizontal movements of the foundation.

Compressive tie forces were observed in some ties located
near the bottom of the wall. This was attributed to the
effect of the berm, constructed at the toe of the wall.

(ii) **The soil stresses**

The coefficient obtained by dividing the horizontal soil stress by the vertical soil stress $K = \dfrac{\sigma_x}{\sigma_y}$, was found to vary irregularly during the construction of the wall. This was attributed to compaction effects. As construction proceeded, the effect of compaction on the soil stress at a particular level appeared to become less. After the completion of the wall K values varied between 0.11-0.41 at one test section, compared with the active and an at rest coefficients of earth pressure of 0.22-0.36 respectively. At another test section K values varied in a wider range of 0.20-0.50.

(iii) **Strain in the ties and the soil**

The observed strain in the ties and in the soil were found to be compatible, except in one of the test sections in which near the top of the wall the strain in the ties was found to be higher than the strain in the soil. This was attributed probably to slippage between the soil and the ties.

(iv) **Field pulling tests**

Dummy ties of lengths varying between 1.5 m to 14 m were installed in the reinforced earth fill, under overburden heights ranging from 2.3 m to 11 6 m and were pulled out artificially.

The results indicated that the soil/tie angle of friction decreased with increasing overburden height over the ties level. The investigators reported that this anomaly cannot be explained on any theoretical basis. The safety factor against tie pull out was evaluated from the observed peak tie resistance against pull out. For a constant tie length the safety factor against tie pull out was seen to decrease with increasing overburden height. The observed peak tie resistance against pull out, was found to be greater than the theoretical skin friction force, when the tie length was over three metres.

6.1.2.d **The Granton wall**

The Granton wall was the first example of the use of the reinforced earth method in the U.K. Finlay and Sutherland[29]

reported on the wall geometry, structural components, method of construction and the results of the stresses and deformations observed on the wall during and after completion of the wall construction.

The Granton wall is 105.84 m in length, with some sections curved in plan. The height of the wall varies between 1.79 to 7.165 m measured from top of foundation slab to top of wall coping.

The wall was founded on a burnt oil shale (blaes) which was used to replace a soft clay layer, originally present on the site.

6.1.2.d.1 Material properties

The skin elements used in the Granton wall consisted of concrete panels, approximately 1.5 m x 1.5 m and 180 mm thick. The ties were of stainless steel 80 mm wide, 1.5 mm thick and 6.5 m in length. The average horizontal and vertical tie spacings were 0.75 m. The backfill material consisted of a burnt oil shale (blaes). This had an angle of internal friction of 46° and a cohesion $c = 41.4$ kN/m^2, measured at a field density of 16.65 kN/m^3, using an undrained triaxial test. The tie/soil coefficient of friction was 0.32.

6.1.2.d.2 Wall instrumentation

Electrical resistance, strain gauges were installed on ties to measure the tie tension at different locations along the tie length and also to measure the earth pressure on the panels.

The vertical and horizontal movements of the facing panels were measured by observing steel pins inserted in the panels.

6.1.2.d.3 Test results

(i) The tie stresses

The tie stresses in the Granton wall were found to increase from the face of the wall to a maximum in the front

half of the tie and decreased to zero at the free end of the
tie.   Comparison with the Rankine theory indicated that the
average measured tension on the tie was 72% of the theoretical
Rankine value using a design value of K_a = 0.30. For K_a = 0.163,
the appropriate value for the fill as placed, the measured
average tie tension was 30% greater than the Rankine prediction.
The compaction procedure was noted to affect the tie tension
distribution as well as its magnitude.

(ii)   The wall movement

The total downward vertical wall movement over a wall
height of 6.30 m was 35 mm.   The first horizontal wall move-
ments were taken after part of the fill had been placed. The
average translation movement between panel joints was 4.7 mm
and the rotational movement due to outward tilt of the panel
was very much larger than the translation movement.   This was
of the order of nearly 50 mm and was mainly attributed to
compaction procedure.

(iii)   Pressure on the panels

Pressures on the panels observed at the Granton wall were
found to be affected by the compaction equipment and pressures
greater than those corresponding to the active earth pressure
were observed.

6.1.3   Conclusions from reports on field walls

(1)   In the Incarville wall, the tie tension distribution along
the tie length, showed a substantial variation.   This was
attributed to the effect of the wall construction procedure.
At the top of the wall, the observed maximum tie tension was
nearly equal to the Rankine values based on the at rest
coefficient of earth pressure K_o.   At the bottom of the
wall, the maximum tie tension appeared to be coincident with
the theoretical values calculated from a Trapezoidal vertical
stress distribution.

(2)   In the Dunkirk harbour double-faced wall, a maximum tie
tension was observed near the wall face decreasing to a minimum

value at the line of symmetry of the wall.

(3)   In the Los Angeles County wall, a maximum tie tension was found to occur in the middle portion of the tie and it showed an appreciable variation with time. ` The variation of the tie tension with time was attributed probably to the settlement and horizontal movement of the foundation.

(4)   In the Granton wall, the tie tension increased from the back of the wall to a maximum in the front half of the tie and decreased to zero at the free end of the tie.   The magnitude of the tie tension was found to be affected by the compaction operation.

(5)   In the Incarville wall, the ratio of the horizontal to vertical soil stresses was found to be greater, at the top of the wall, than the at rest coefficient of earth pressure K_o.   This was attributed to the effect of compaction.   At the bottom of the wall, the stress ratio was greater than the coefficient of active earth pressure K_a, but less than K_o.

In the Los Angeles County wall the effect of compaction on the stress ratio was noted to diminish with increasing fill height above the instrumentation level.

6.2   Detailed Study of Tie Tension in a Full Scale Wall

In the foregoing section, a literature review of the test results obtained from walls at Incarville, Dunkirk, Los Angeles and Granton was presented.

Unlike a model wall, a full scale wall is affected by the construction procedure.   In an attempt to analyse the tie tension in a full scale wall, the observations made on the Granton field wall will be considered, since details of the Granton wall data are more accessible to the author than any other field wall.

The aim of the present section is, therefore, for the Granton wall:-

(1) To study the effect of compaction on the observed maximum tie tension, by means of a simplified theoretical analysis.

(2) To compare the observed maximum tie tension with the Energy and the Rankine theories.

(3) To compare the observed and predicted non-dimensional tension X .

(4) To evaluate the experimental safety factors against tie break and tie pull out and to compare the minimum observed results with the theoretical values.

(5) To outline the similarities and differences between the observations from a model wall and the behaviour of the full scale wall at Granton.

The results of these analyses will now be discussed.

6.2.1   Effect of compaction on tie tension

6.2.1.a   Introduction

The use of compaction equipment was reported by Casagrande[13] as causing an increase in the lateral earth pressure in conventional retaining walls.   After the passage of the compaction equipment, part of the lateral pressure developed by soil compaction is relieved.   The remaining part of the lateral pressure developed by soil compaction was referred to by Sowers et al[69] as the residual compaction pressure.   Sowers et al[69] also reported that the residual compaction pressures are considerably larger than the at rest earth pressures.   D'Appolonia et al[22] found experimentally that the lateral pressures in the soil build up with increasing number of roller passes.   Aggour and Brown[1] attempted to predict theoretically the lateral pressure developed during compaction behind conventional retaining walls.

In the case of full scale reinforced earth walls the process of compaction was reported to have an effect on the

tie tension in the Incarville[67] and the Granton[29] walls.
The ratios of the horizontal to vertical soil stresses, which
were greater than the at rest coefficient of earth pressure
K_o, observed in the Incarville wall, were attributed to
compaction.[67]   In the Los Angeles County wall, the effect
of compaction on the stress ratio in the soil was found to
diminish with increasing fill height above the instrumentation
level.[14]

In the present section it is intended to show the effect
of compaction on the maximum tie tension observed at the
Granton wall.   This was done by considering for each tie,
the curves of the observed maximum tie tension versus fill
height, e.g. Fig (6.1).   The corresponding theoretical curves
shown were straight lines.   To simplify discussions, the term
$\frac{\Delta T}{\Delta h}$ shown in Fig (6.1) was evaluated from the observed and
the theoretical curves and plotted against fill height above
the tie level.   For the case illustrated by Fig (6.1), the $\frac{\Delta T}{\Delta h}$
values calculated from the Energy (LO.L.A.) and the Rankine
theories were constant and equal to 0.99 and 1.52 respectively.

6.2.1.b Results of the analysis

As shown in Figs (6.2) and (6.3), the increase in the
observed tie tension per unit increase in fil_1 height $\frac{\Delta T}{\Delta h}$,
above the tie level was computed for the cases of six ties
in the Granton wall and drawn versus the fill height above the
tie level.   The corresponding theoretical $\frac{\Delta T}{\Delta h}$ values
calculated from the Energy (LO.L.A.) and the Rankine theories
were constant.

The general trend of the observed $\frac{\Delta T}{\Delta h}$ with increase in
fill height, was for a high value at low fill heights,
followed by a reduction in the value of $\frac{\Delta T}{\Delta h}$ as the fill height
increased, until $\frac{\Delta T}{\Delta h}$ tended towards the theoretical constant
value as the wall approached its maximum height.

The variation of the observed $\frac{\Delta T}{\Delta h}$ values with fill height,
appears to be due to compaction stresses, since the compaction
operation has been found[29]   as affecting the tie tension in

☐   Observed points.
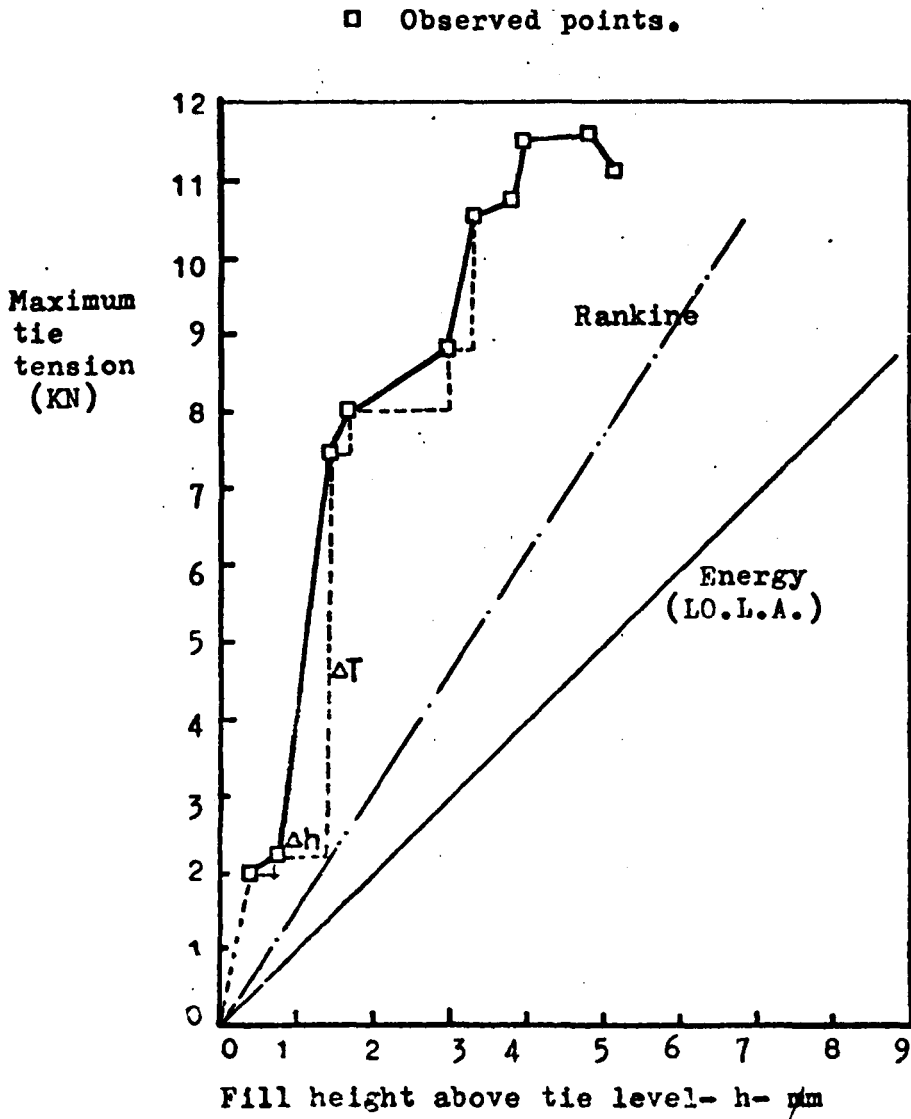
Fig.(6.1)   Observed & theoretical maximum tie tension v
            fill height above tie level(Tie D2 , level 1.125 m
            above wall base- Granton wall).
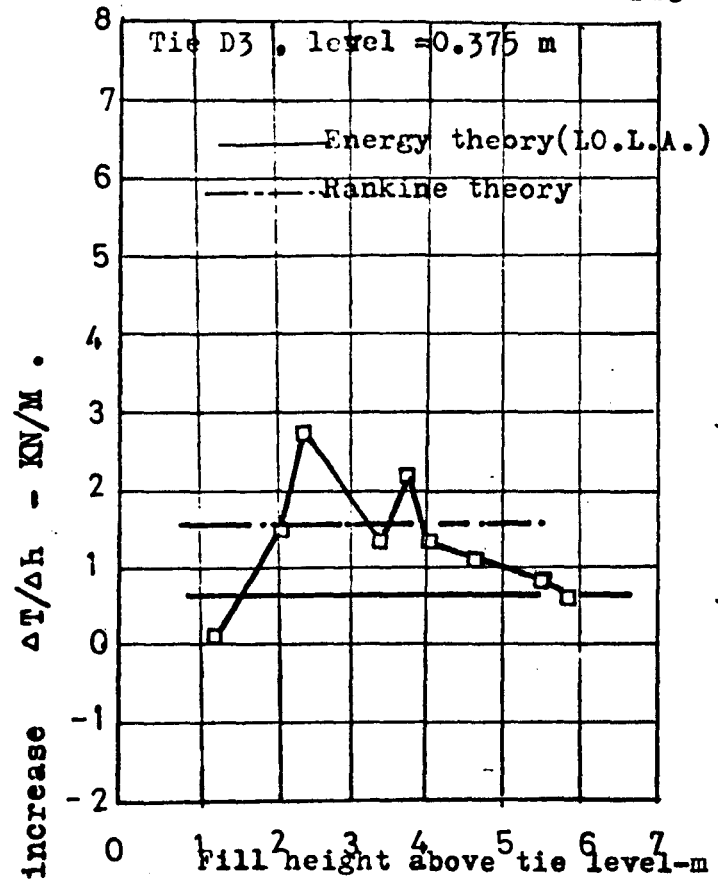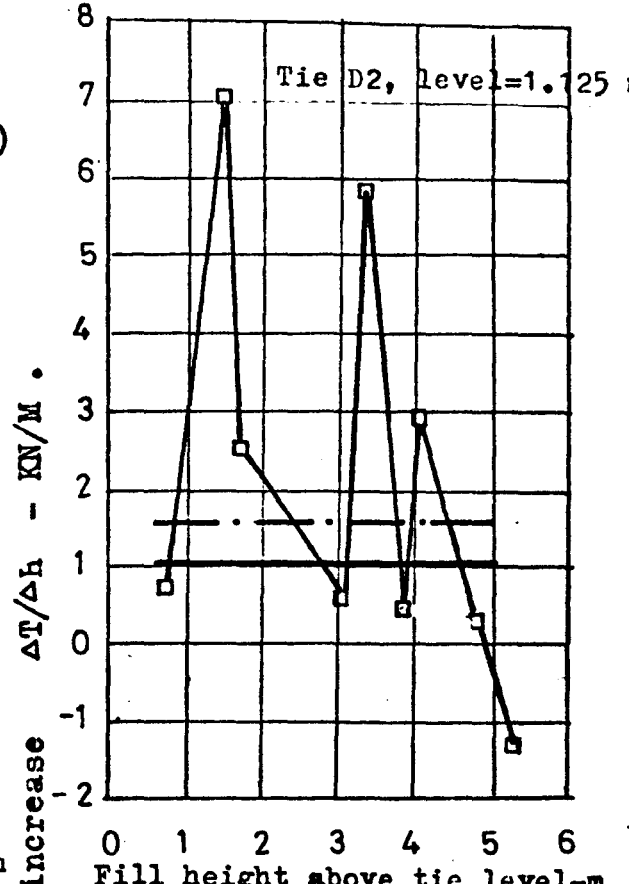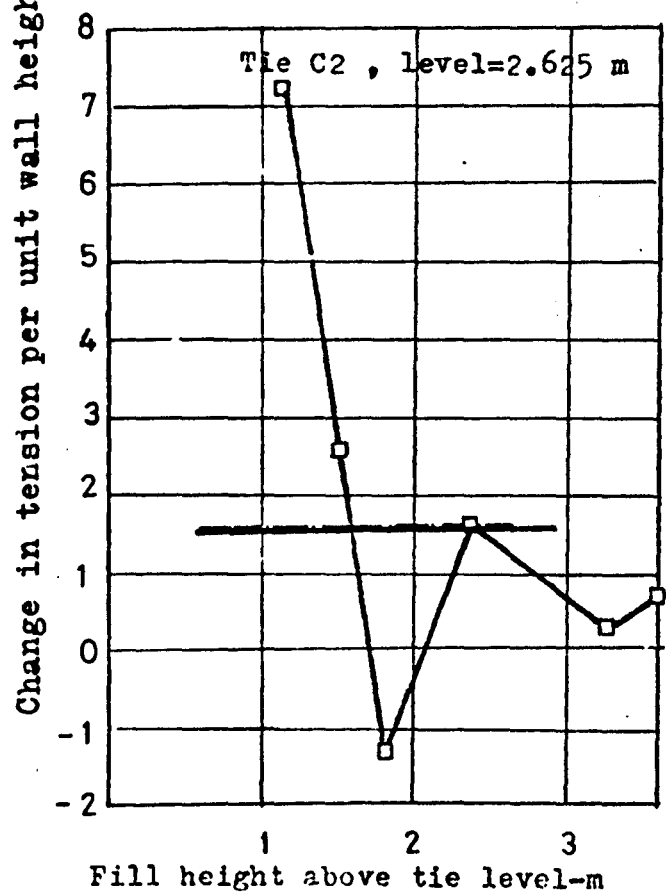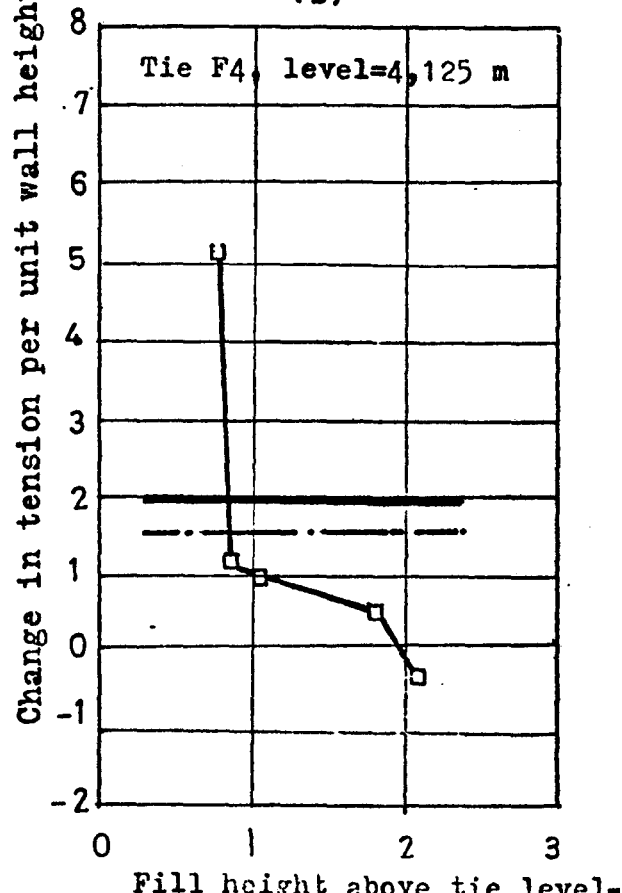
Fig.6.2 Experimental & theoretical $\Delta T/\Delta h$ V fill height above tie level (Granton reinforced earth wall).

Tie H4

level =1.125 m

Fill height above tie level -m
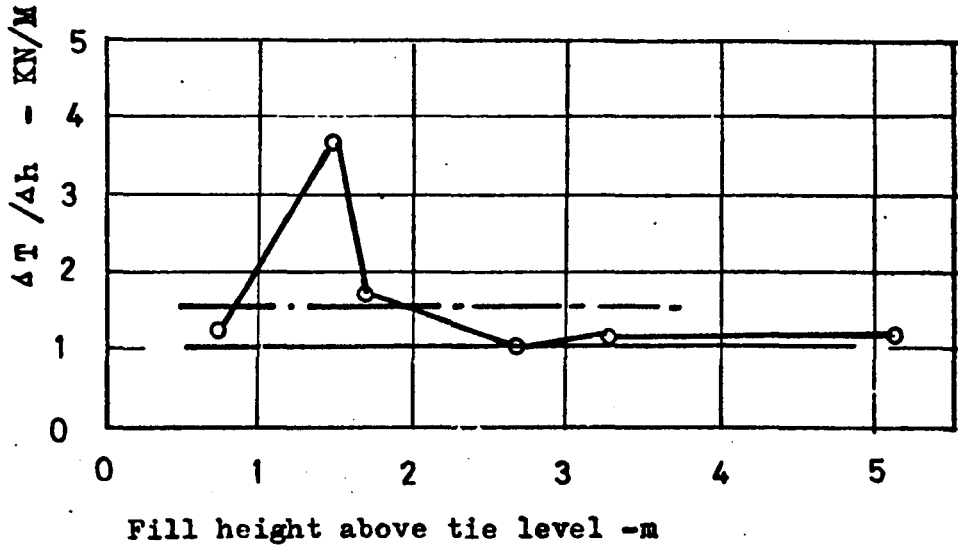
(a)

———— Energy theory(LO.L.A.)

—·—— Rankine theory.

Tie G4

level = 2.625 m

Fill height above tie level - m
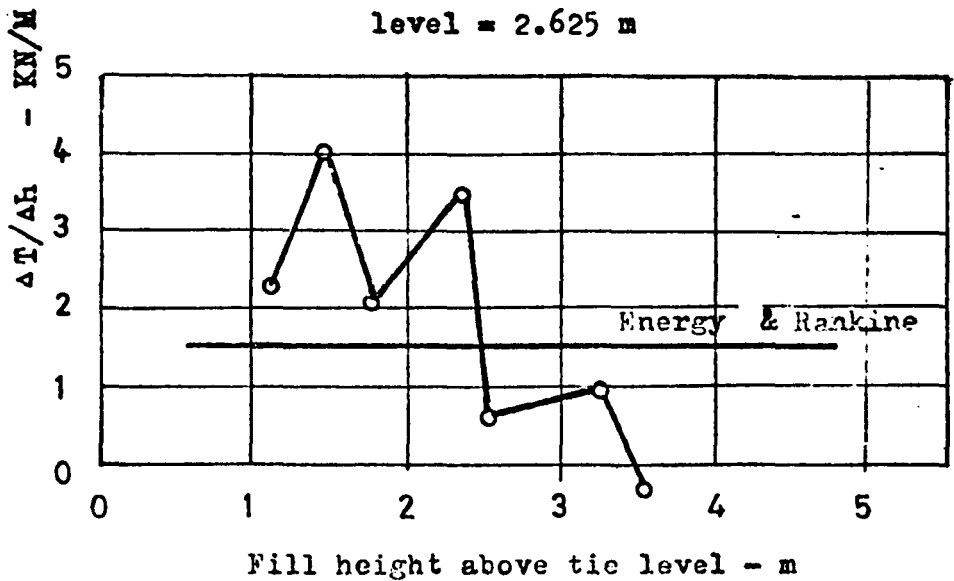
(b)

Fig. 6.3 Experimental & theoretical ΔT/Δh V fill height

above tie level curves.

the Granton wall.   The pattern of $\frac{\Delta T}{\Delta h}$ variation with
increasing fill height above a tie level, shows that the
compaction effect on the tie tension diminishes with increasing
fill height.

In the following section an attempt will be made to
account theoretically for the observed variation in $\frac{\Delta T}{\Delta h}$ with
fill height, by means of a simplified theoretical approach.

6.2.1.c   Theoretical analysis of compaction stresses

As pointed out by Aggour and Brown[1] a rigorous analysis
of the compaction pressures requires a knowledge of various
factors, such as the loading and unloading moduli of the earth
fill, the wall flexibility, the number of the roller passes
and the backfill geometry.   Hence it was found rather
difficult to account theoretically for the variation in tie
tension due to compaction stresses.

However, the author has adopted a simplified theoretical
model to study the effect of compaction on the tie tension on
an approximate basis.   In this model the roller was
represented by three point loads and its position was altered
to obtain the maximum horizontal stress on the facing panels.
These calculations were made according to a modified
Boussinesq theory suggested by Spangler,[70] for the analysis
of stresses due to surface concentrated loads on conventional
retaining walls, Appendix (VIIa).   The data pertaining to the
roller are also shown in Appendix (VIIb).

The theoretical $\frac{\Delta T}{\Delta h}$ values computed from the transient
effects of the roller weight were added to the $\frac{\Delta T}{\Delta h}$ values
calculated from the Rankine theory and plotted against fill
height, Fig (6.4).   Also shown on Fig (6.4) are the average
$\frac{\Delta T}{\Delta h}$ values obtained by interpolation from Figs (6.2) and (6.3).

The fact that both the average observed points and the
theoretical curve show a similar trend would seem to indicate
that compaction does influence the build up of tension in the
reinforcing ties.

△ Average observed $\Delta T/\Delta h$ values.

——————Modified Boussinesq + effect of earth pressure.
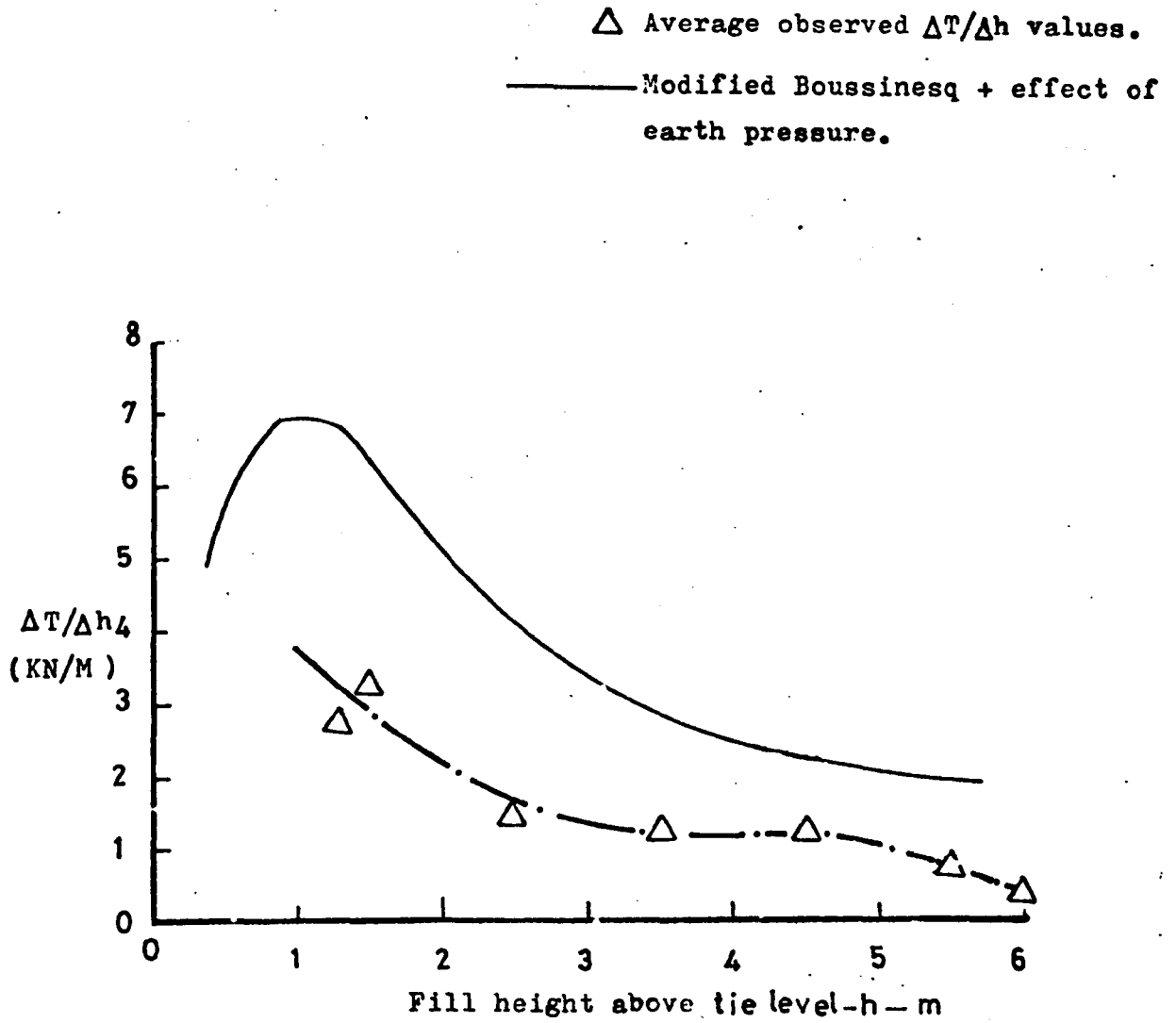
Fig(6.4) Comparison between the observed & the theoretical $\Delta T/\Delta h$ values ,considering transient compaction effects

6.2.2 Comparison between the observed and the theoretical
       maximum tie tension

As shown in Fig (6.5), the maximum tie tensions observed
at the Granton wall, were drawn versus the wall height and
compared with the Energy theory (LO.L.A.) and the Rankine
theory predictions.

The observed maximum tie tension points, generally indicated
an increasing tie tension with wall depth.   The low value of
the observed maximum tie tension near the bottom of the wall,
was probably due to the fixity of the toe of the wall.

For K_a = 0.163, the appropriate value for the fill, the
Energy theory (LO.L.A.) and the Rankine theory predicted
appreciably lower maximum tie tension than the observed
results.   The observed maximum tie tension points were
found to be contained within the Energy theory (LO.L.A.)
curves, evaluated by assuming K = 0.18 and 0.327, Fig (6.5).

This fact seemed to indicate that the compaction
procedure had increased the coefficient of earth pressure in
the scil. to values well above the coefficient of active
earth pressure K_a = 0.163.

To prevent this happening in practice, it is desirable
that the compaction procedure should be controlled during
construction.   This is, in fact, done at present by means
of a specification clause[41] which does not allow rolling
within a distance of two metres from the wall facing.   However,
in practice, it is not always possible to enforce this require-
ment rigidly, as illustrated by the performance of the Granton
wall.[29]

6.2.3 The non-dimensional tension

In an attempt to compare the model wall and field wall
behaviour, the non-dimensional tension $\chi = \dfrac{T_m}{\gamma h \, \Delta H.S}$ was
calculated from the maximum tie tension T_m observed in each
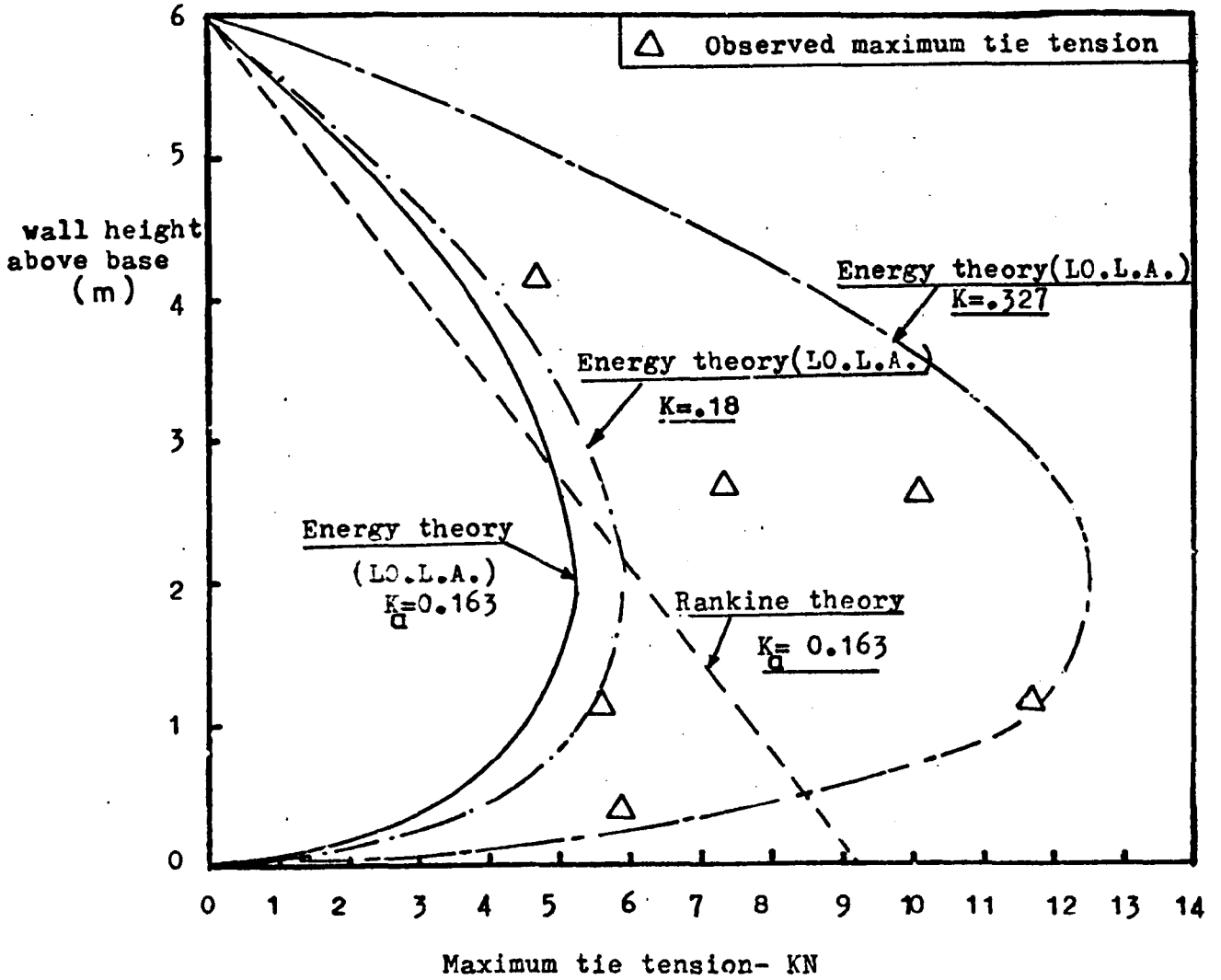
Fig. 6.5 Comparison between the observed & the theoretical maximum tie tension (Granton full scale wall).

level of the Granton wall; T_m being the maximum tension observed when the wall has reached its full height. The observed non-dimensional tensions were plotted against the height of fill above the ties. The results are shown in Fig (6.6). Although the observed non-dimensional tension values were affected by the wall construction procedure, they appeared to indicate a pattern of decreasing non-dimensional tension with increasing fill height above the tie level. This was the general trend of the experimental results observed on the laboratory scale models shown in Fig (5.42) in Chapter Five.

Comparison between the observed and the predicted non-dimensional tension X , Fig (6.6) showed that the energy theory (LO.L.A.) gave a similar pattern to the experimental results. The Rankine and Banerjee methods gave constant values differing from the experimental results.

6.2.4   The internal stability of the Granton wall

The tie tensions in the Granton wall have been found[29] to be affected by the compaction procedure and consequently the safety factors against tie breaking and tie pull out were also affected.

In the present section the safety factors against tie breaking and tie pull out will be evaluated from the observed maximum tie tension and the minimum values of these will be compared with the theoretical values.

6.2.4.a   Safety factor against tie break

The variation in the safety factor against tie break with fill height above the tie level is shown in Fig (6.7). These were evaluated for the cases of four ties from the relationship

$$SF = \frac{\sigma_{y1} \cdot A_r}{T_m}$$

using a yield strength for the stainless steel of 0.49 kN/mm^2.

□ Experimental results.

Non-dimensional tension $\dfrac{Tm}{\gamma h.\Delta H.S}$

Fill height above tie level—m
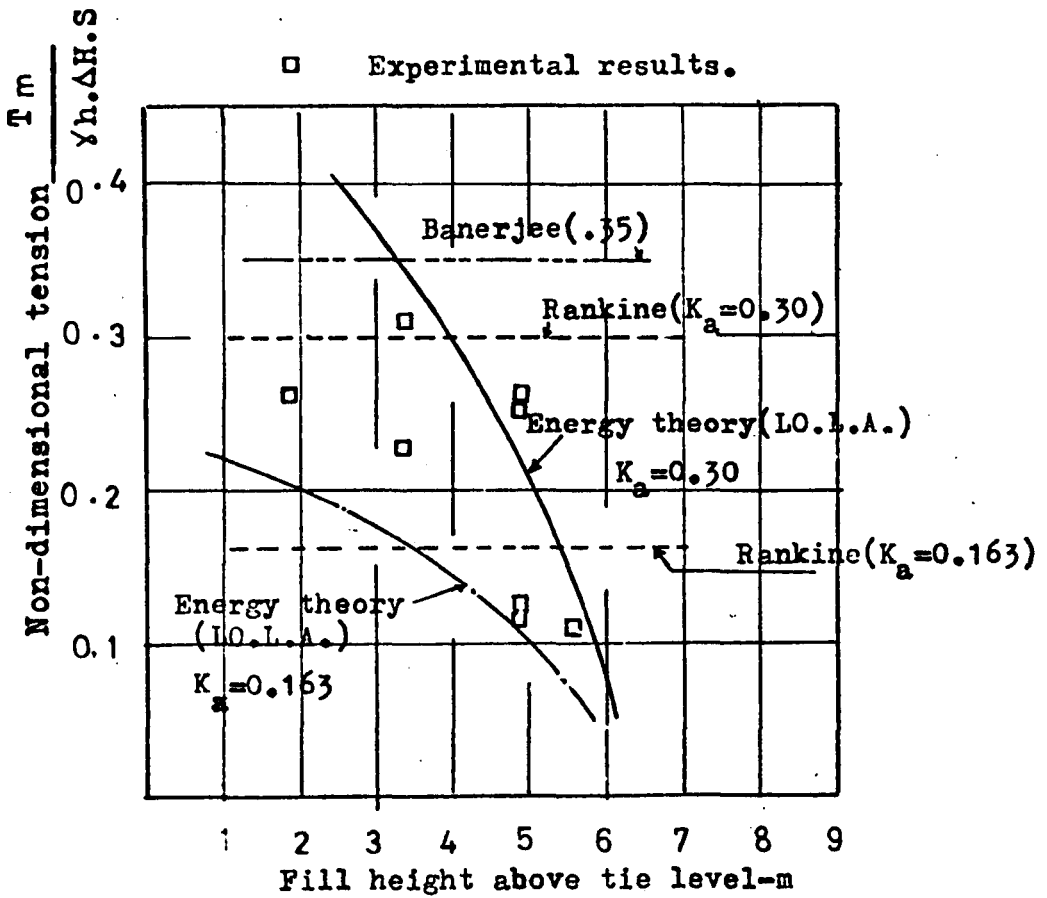
$K_a=0.163$ (Corresponds to the fill condition as placed) ✗

$K_a^{=}030$ (A value assumed in the design of the wall)

Fig. 3.6   Experimental & theoretical non-dimensional
tension Y fill height above tie level

(Cranton reinforced earth wall).

Fig (6.7) shows a sharp decrease in the observed safety factor against tie break, in the first 1.5 metre height of fill above the tie. Probably this was due to the compaction stresses, which were more pronounced at smaller fill heights above the tie level.

The safety factors against tie break of the completed wall were drawn versus wall height and are shown in Fig (6.8). These generally decreased with wall height to a minimum value of 4.93 at a wall level of 2.63 metre above the base of the wall and increased again with wall height.

Table (6.1) shows a comparison between the observed and the theoretical safety factors against tie break, for the completed field wall. All the theories predicted a safety factor against tie break which is higher than the minimum experimental value, but less than the observed maximum value.

The increase in the tie tension by the compaction operation, probably led to a decrease in the experimental safety factor against tie break.

6.2.4.b The safety factor against tie pull out failure

Fig (6.9) shows the variation of the safety factor against tie pull out with fill height above the tie level, for the cases of four ties in the Granton wall. These were calculated using the relationship

$$SF = \frac{2bL\gamma \cdot hf}{T_m}$$

and assuming the total tie length, L, as effective in providing resistance against pull out. The observed maximum tie tension T_m was adopted in these calculations.

The safety factor against tie pull out increased with increasing fill height above the tie level. For the case of tie C_2, Fig (6.9b), the safety factor was less than 1.0, for fill heights less than 1.70 m. As pointed out by Finlay and Sutherland[29] a localized slip might have taken place.
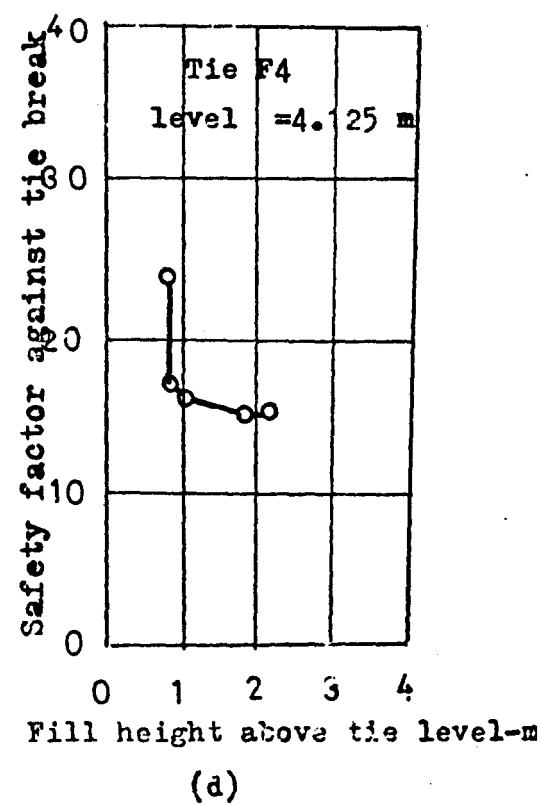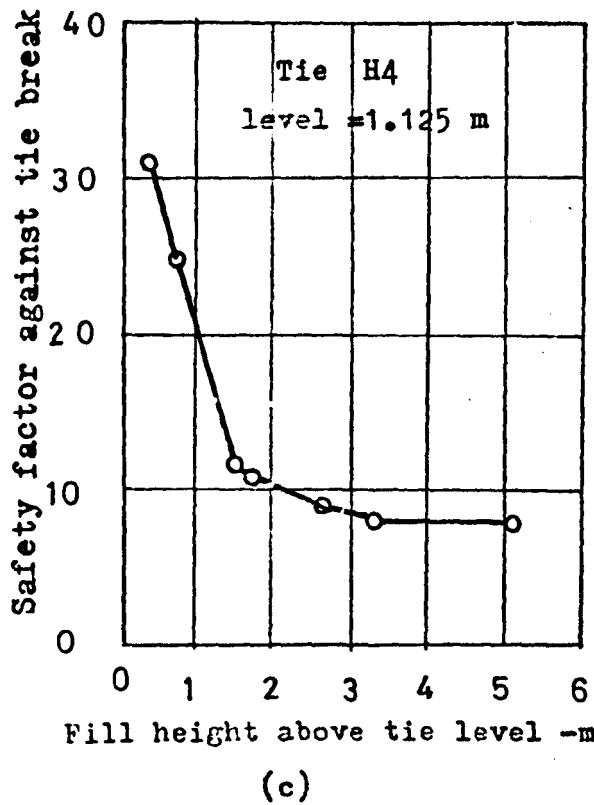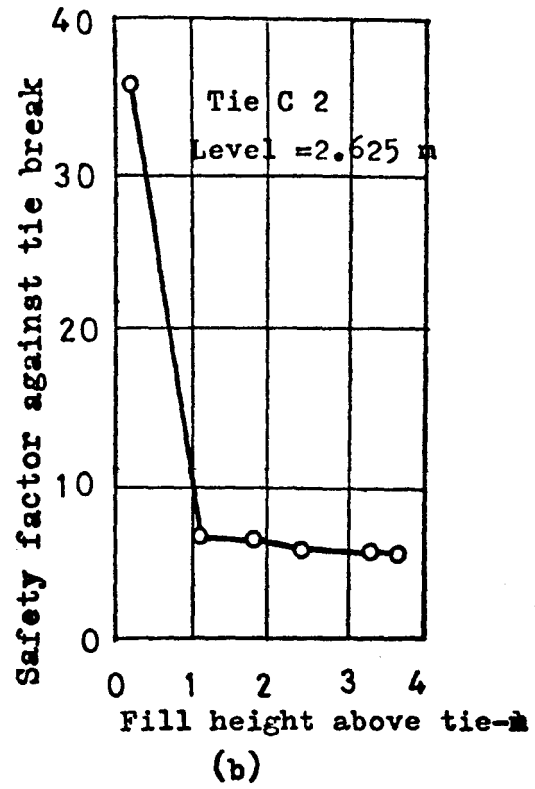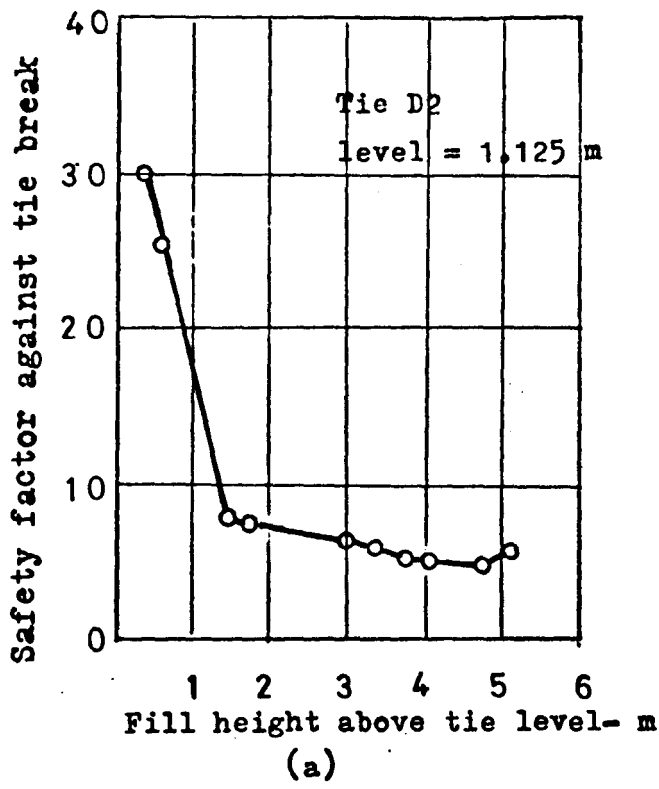
Fig. 6.7 Observed variation in Safety factor against tie break with fill height above tie level(Granton reinforced earth wall).
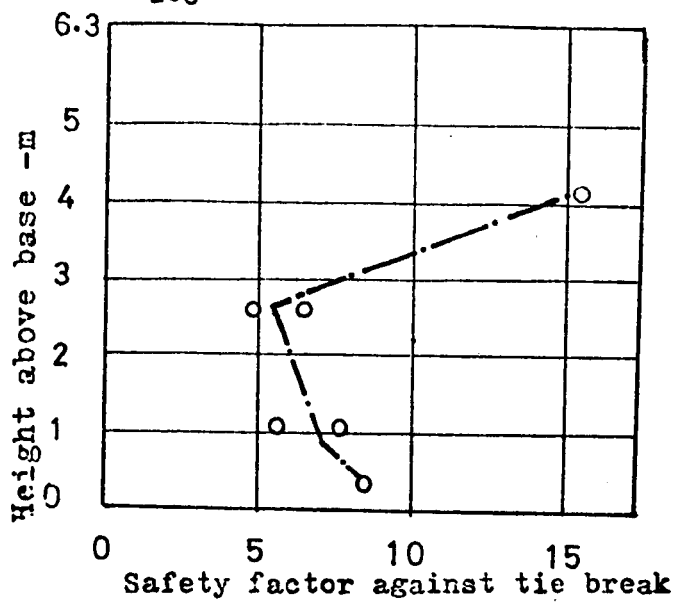
Fig. 6.8 Variation in the observed safety factor against tie breaking failure with wall height(Granton field wall H=6.3 m).

Observed maximum   SF = 15.4
Observed average   SF =   8.2
Observed minimum   SF =   4.93

Wall design parameters	Method	Safety factor against tie break (Theoretical)
σ_{y1} =0.49 kN/mm^2	Rankine	6.1
b = 80mm	Trapezoidal	5.3
t = 1.5mm	Meyerhof	5.8
K_a = .163	Banerjee	6.4
ΔH = 0.75m S = 0.75m	Energy (LO.L.A.)	9.9
γ = 16.65 kN/m^3 H = 6.3m	Energy (T.L.L.A.)	10.1

TABLE (6.1) - Comparison between the observed and the theoretical safety factor against tie break (Granton full scale wall).
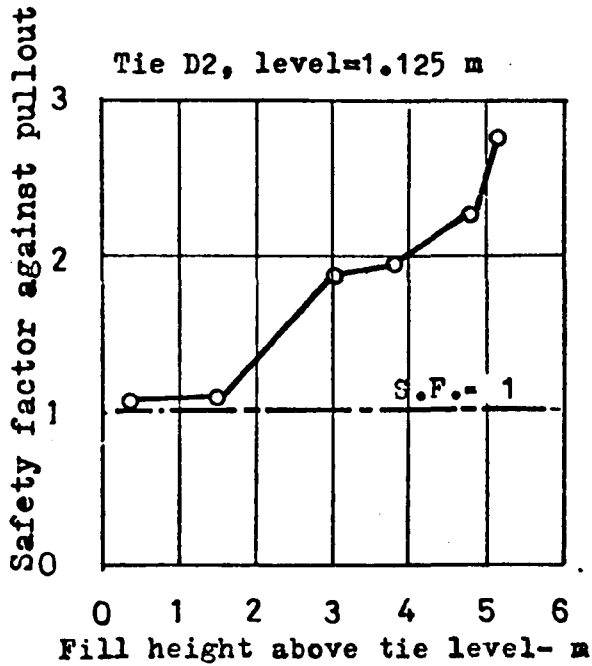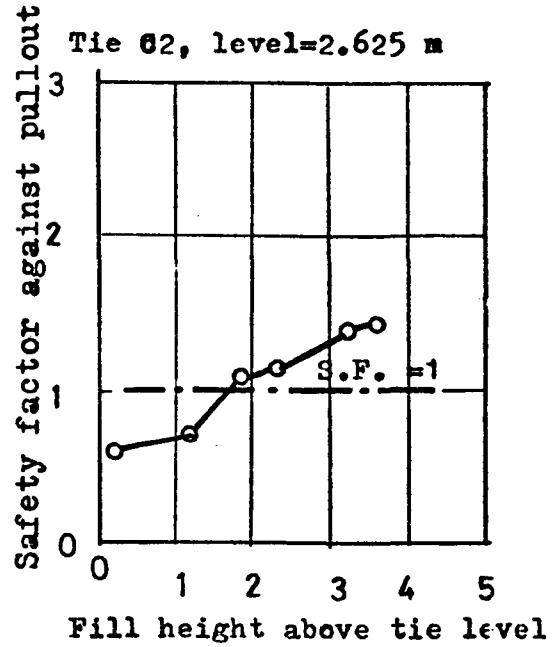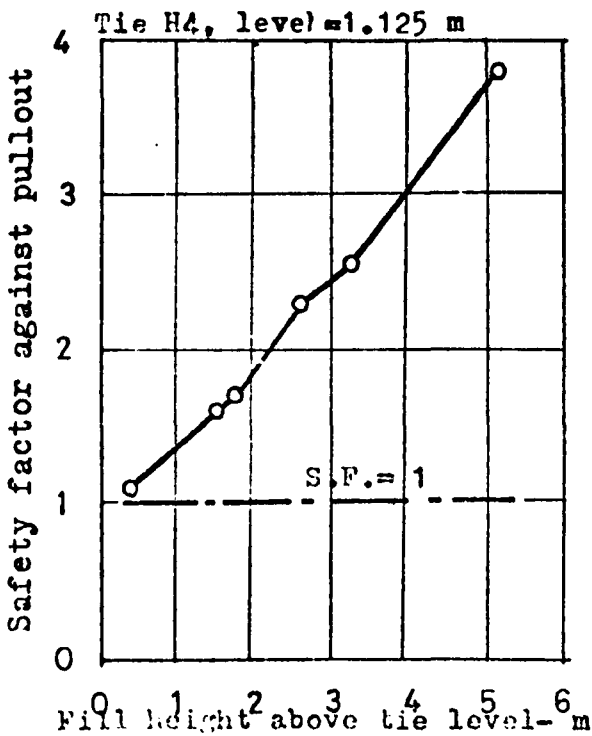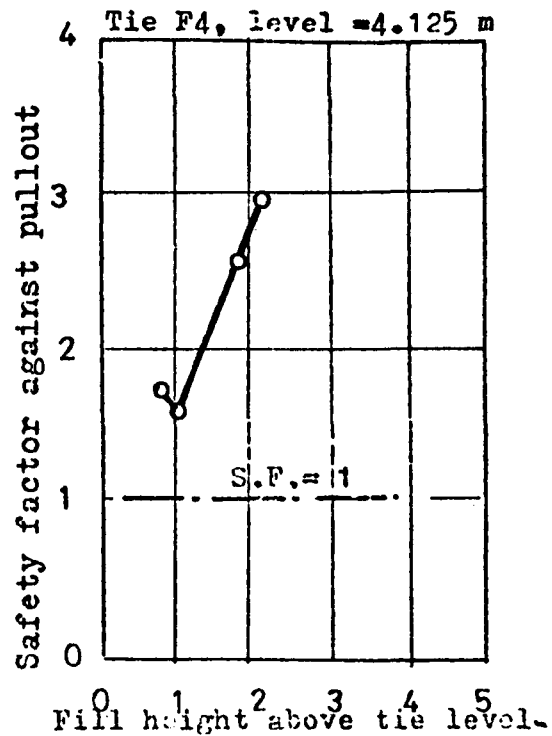
Fig.6.9 Variation in safety factor against pullout with fill height above tie level.

The lowering of the safety factor against pull out to values less than 1.0 could be due to compaction. This may be shown by considering Fig (6.10) in which the safety factor against tie pull out and $\frac{\Delta T}{\Delta h}$ were drawn versus the fill height above the tie level, for the case of tie C_2. When $\frac{\Delta T}{\Delta h}$ values were high, possibly due to compaction stresses, the safety factor against pull out was less than 1.0.

The safety factors against tie pull out of the completed Granton wall are shown in Fig (6.11) versus the wall height. The maximum safety factor against tie pull out was found at the bottom tie level.

Table (6.2) shows a comparison between the observed maximum, average and minimum safety factor against tie pull out and the theoretical minimum values. The actual safety factors of the wall against tie pull out could have been lowered by the construction procedure. For $K_a = 0.163$, corresponding to the state of the fill as placed all the theories predicted higher safety factors against tie pull out, than the observed minimum value of 1.70, but less than the observed maximum value of 4.75, except Banerjee's method which gave appreciably higher safety factor than the observed maximum value.

The Granton wall was found to have a minimum factor of safety against tie break of 4.93 . This is appreciably greater than the minimum factor of safety against tie pull out of 1.70. Therefore the wall is more likely to fail by tie pull out than by tie breaking, as has been pointed out in Chapter Five.

6.2.5 Comparison between model wall and full scale wall

Although the observations made on the Granton wall, have been reported[29] to be affected considerably by the construction technique, some general similarities between the tie tensions measured in the Granton wall and the model walls, were found. These similarities can be summarized in the following points:

(1) The tension distribution along the tie in the Granton
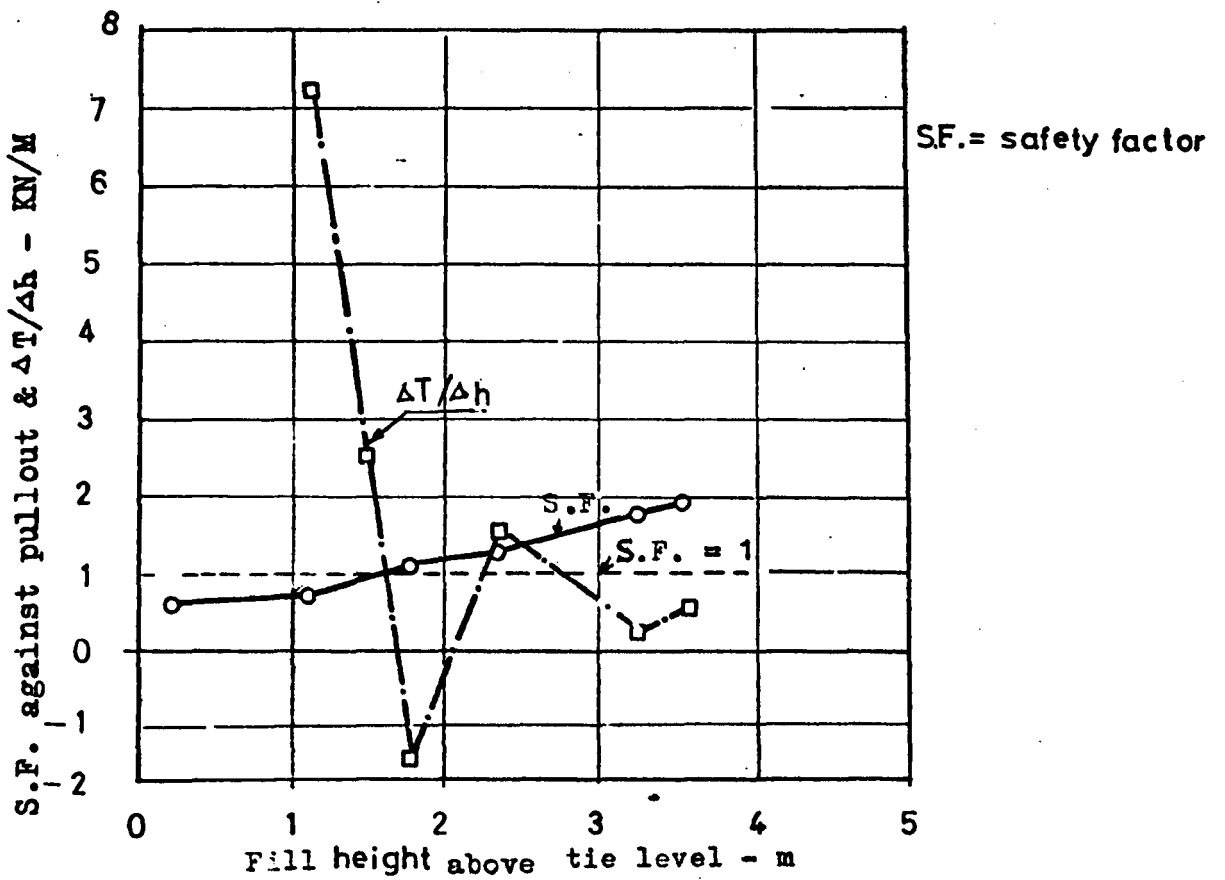
Fig.6.10 Effect of compaction on S.F. against pullout.
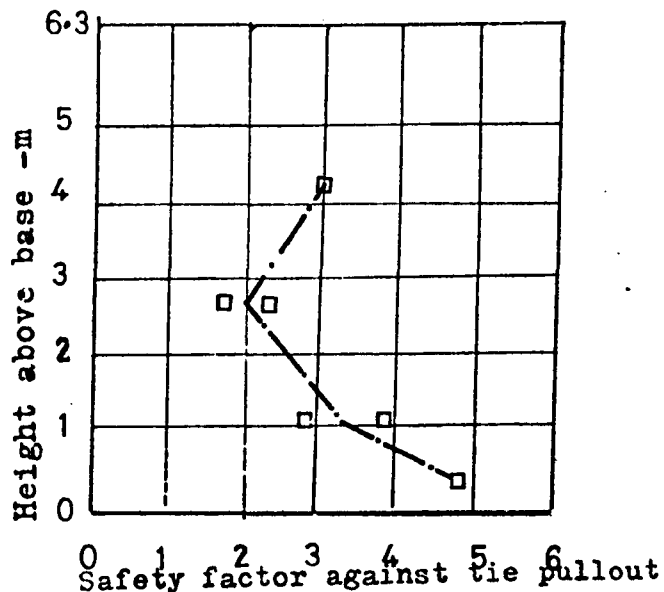
Fig. 6.11 - Variation in the observed safety factor against tie pull out failure with wall height (Granton wall H = 6.3 m)

Observed maximum   SF = 4.75
Observed average   SF = 3.00
Observed minimum   SF = 1.70

Wall design parameters	Method	Safety factor against tie pull out (Theoretical)
b = 80mm L = 6.5 m K_a = 0.163 ΔH = 0.75m S = 0.75m γ = 16.65 KN/m^3 f = 0.32	Rankine (all length effective	3.63
	Rankine (part length effective)	2.50
	Coulomb force	3.2
	Coulomb moment	2.9
	Banerjee	7.5
	Energy (LO.L.A.)	2.66
	Energy (T.L.L.A.)	2.02

TABLE (6.2) - Comparison between the observed and the theoretical safety factor against tie pull out (Granton full scale wall).

wall, was reported[29] to increase from the back of the wall
to a maximum value in the front half of the tie and to decrease
to zero at the free end of the tie.   This observation was
generally applicable to the tie tension distribution observed
in the model walls.

(2)   In the Granton wall the maximum tie tension variation over
the wall height was found to increase with wall depth and to
drop at the tie level just above the base of the wall. This
was also the trend of the tie tension curves observed on the
model walls.

(3)   The non-dimensional tension parameter χ , observed from
Granton wall and the model walls was found to decrease with
increasing fill height above the tie level for both walls.

6.3   Conclusions From a Study on Tie Tension at The Granton Wall

In Sections(6.2.1) to (6.2.5) a study on tie tensions
observed at the Granton full scale wall was presented.
Conclusions reached in this study will now be outlined.

(i)   Effect of compaction on the observed maximum tie tension
was studied by considering the observed maximum tie tension
versus fill height curves.   Probably the compaction operation
increased the tie tension when the fill height above the tie
was small.   The effect of compaction on the observed tie
tension diminished with increasing fill height above the tie
level.   A simplified theoretical model adopted to study the
compaction effect, gave similar trends to the observed
behaviour and indicated most probably that the compaction did
influence the tie tension.

(ii)   In the Granton full scale wall, the observed maximum
tie tension was appreciably higher than the Energy (LO.L.A.)
and the Rankine theory predictions.   This discrepancy can be
attributed probably to the compaction effect.

In practice it is desirable to control the compaction
procedure during the construction of the wall to minimize the

the build up of earth pressures on the wall facing.

(iii)   For the Granton full scale case, the observed non-dimensional tension parameter χ, was found to decrease with increasing fill height above the tie level.   The Energy theory (LO.L.A.) gave a similar mode of variation to the observed results.   The Rankine and Banerjee approaches gave constant values of χ , which were different from the observed results.

(iv)   The safety factor against tie break, was found to decrease sharply with increasing fill height above the tie level, in the first 1.5 m fill height and then remained almost constant.   The initial drop in the safety factor was attributed probably to compaction.   The completed wall had a minimum factor of safety against tie break of 4.93, which was less than the prediction of all the existing theories.

(v)   The safety factor against tie pull out was found to increase with increasing fill height above the tie level. The results indicated probable slipping of the ties due to compaction at fill height of less than 1.7 m.

The completed wall had an adequate factor of safety against tie pull out, with a minimum value of 1.70.   This is less than the minimum safety factor against tie break of 4.93 . Therefore the wall is more likely to fail by tie pull out than by tie break.   All the theories predicted higher safety factors against tie pull out than the minimum observed value.

(vi)   Althoughthe tie tensions observed in the Granton wall were affected by the construction procedure, some similarities in the mode of variation of tie tension over the tie length and with wall depth and in the non-dimensional tension variation with fill height were noted to exist between the model wall and the Granton full scale wall.

CHAPTER SEVEN

FINITE ELEMENT ANALYSIS OF MODEL AND FIELD

REINFORCED EARTH RETAINING WALLS

7.1 Introduction

7.1.1 General

The finite element approach has been widely and success-fully used in the solution of geotechnical engineering problems[20,24,25], including analysis of conventional retaining walls.[19]

The main difficulty in applying this method in the solution of soil mechanics problems arises from the complexity inherent in the stress-strain relationships of soils. Despite this shortcoming the finite element method proves useful and gives satisfactory engineering solutions even when relatively simple forms of soil idealization are adopted, e.g. Penman et al[51].

In Chapter Two mention has been made of the use of the finite element method in France[21,76,81] for the analysis of reinforced earth retaining walls. This analysis idealized the wall as a plane strain problem and used quadrilateral and bar elements to represent the soil and ties respectively. Reinforcement by sheet and perfect bond at the tie/soil interface were assumed.

The results of this study indicated a tie tension distribution along the tie length which was at a maximum near the wall face and decreased towards the free end of the tie. The results from this analysis were not compared by the authors with any observed data.

Banerjee[5] analysed reinforced earth walls in service conditions using a plane strain finite element programme in which the soil and ties were represented by triangular and bar elements respectively. The soil modulus of elasticity was assumed either constant or linearly increasing with wall

depth.   In the first case the nondimensional tension
$\chi = \dfrac{T}{\gamma h. \Delta H.S}$ was found to vary parabolically over the
tie length having a maximum value at the middle of the tie
equal to 0.35.   This value was seen to vary over a range
of $\pm$ 10% in the case where the elasticity modulus was
assumed linearly increasing with wall depth.

Finlay & Sutherland[29]   compared Banerjee's non-
dimensional tension with test results obtained at Granton.
The experimental non-dimensional tension values were found
to range between 0.26 - 0.80 with an average of 0.40.

More recently, Romstad et al[54]   and Chih-Kang Shen
et al[18]   adopted a composite material approach in
deriving the stress-strain relationships of a reinforced
earth mass.   This was incorporated in a finite element
programme, originally developed at the University of
California, U.S.A.   .

The reinforced earth mass was theoretically sub-
divided into "Unit Cells"; a "Unit cell" comprising a tie
bounded by centrelines of horizontal and vertical tie
spacings.   The equivalent composite material properties
were calculated for each "unit cell".

In forming the stress-strain matrix of the composite
material it was assumed that the composite stress-strain
state in a direction perpendicular to the tie was equal
to the soil stress-strain state, the strain in the composite
material parallel to the centreline of the tie was equal to
the strain in the soil and the soil/tie interface was in
perfect bond.

The first assumption made in deriving the composite
material properties is valid where the percentage by volume[38]
of the ties to the reinforced earth mass is small,
which is the usual case in reinforced earth walls (e.g.
$\doteq$ 0.023% for the Granton wall).   The assumption of perfect
bond at the soil/tie interface, made in the finite element
analyses, is doubtful especially for low fill heights above
the tie level[29]   .

This programme was used to analyse Los Angeles County wall in California[14] , U.S.A. The results of the theoretical analysis were compared with the observed data. Good agreement was noted between the computed and the observed soil stresses and horizontal wall movements. The computed stresses in the ties were appreciably greater than the measured stresses, although the computed stress distribution along the tie length, was generally similar to the observed distribution.

The disagreement between the observed and computed results was mainly attributed to the plane strain assumption used in the programme, since the real wall was a three dimensional problem. The stresses in the ties continued to change with time. The programme does not take the time factor into consideration. The construction of the wall was almost continuous. In the programme, only a finite number of construction increments is specified.

This programme will be adopted in this chapter for the analyses of model and field walls.

7.1.2 Objectives of the present study

In the model tests presented in Chapter Five the following parameters were measured:

    (i)   The forces in the ties.
   (ii)   The horizontal and vertical strains in the reinforced earth wall backfill.
 (iii)   The vertical stress distribution near the bottom of the wall.
  (iv)   The horizontal wall deflection.

Although these constitute most of the important parameters needed to study the performance of a reinforced earth fill, there are some variables which were not observed, nor could be calculated from the observed data. These are:

    (i)   The shear stresses in the soil.
   (ii)   The shear strains in the soil.
 (iii)   The principal stresses and the angle of orientation of the major principal stress with the horizontal.

The present finite element analyses is carried out to compare the theoretical values with the experimentally observed results and to obtain a more complete picture of the stresses and strains in the reinforced earth fill.

The field wall behaviour could also be affected by the presence of cohesion in the soil backfill, compaction, the foundation flexibility and the rigidity of the facing panels. The finite element analysis can help to study these factors.

In this chapter the main features of the finite element programme adopted here will be given, the limitations of the programme will be outlined and the results of the analyses will be presented and compared with the model and field wall behaviour. The results of the finite element approach will be compared with predictions from reinforced earth design methods.

Conclusions will be drawn at the end of this chapter.

7.2 General Features of the Finite Element Programme used in this Investigation

The listing and manual of the programme used in the present study are given in a report by Chang[14] . The main features of this programme can be summarized as follows:

(1) It is a plane strain finite element programme which uses quadrilateral, triangular and bar (bending) elements.

(2) The quadrilateral element was developed by Herrmann[33] and was shown to be more accurate than the previous simple elements.

(3) The programme has two options to represent the non-linear, overburden dependent soil behaviour:

(i) By providing a table of soil stiffness and Poisson's ratio at corresponding wall levels, the programme will interpolate the values of Young's modulus and Poisson's ratio at the centre of each element at a given wall depth.

(ii) The empirical hyperbolic model first suggested by Kondner[40] for representing the stress-strain curve of soil can be used.

(4)   The programme has self generation procedures for
      locating the coordinates of the nodal points, specify-
      ing the element connection data and the boundary
      conditions.

(5)   External, internal and pressure loads can be applied
      to any node at any construction increment.   The self
      weight of the soil is automatically calculated by the
      programme and applied at each nodal point.

(6)   The programme takes into account incremental wall
      construction.

7.3   Scope of the Finite Element Programme

7.3.1   Input data

Details of this were given by Chang et al[14]
A brief summary is presented in Table (7.1).

7.3.2   Output data

This was described by Chang[14].   The programme
mainly gives a print out of the input data, the stresses
and strains in the soil, the axial force and moment in the
ties and the stresses and strains in the skin elements. The
programme also gives the displacements of various nodal
points, from which the wall deflection can be obtained.

7.4   Limitations of the Finite Element Programme used in this Study

In the introduction to this chapter it was stated that
the accuracy of the finite element results depend to a large
extent on the properties of the soil.   Although a non-
linear overburden dependent model was used to represent the
soil behaviour in this programme, a more realistic inelastic
and orthotropic soil behaviour has to be incorporated in
order to achieve a better accuracy.   In addition, the
accuracy of the results can be affected by the finite number
of construction increments, the two dimensional idealization
of the reinforced earth wall, the simplifying assumptions
used in obtaining the stress-strain relationships of the
reinforced earth composite, and the presence of failure

TABLE (7.1)   Summary of Input Data

Information	Details
Title	General title of the problem to be analysed
Construction Increments	The total number of construction increments used in the analysis. Each construction increment resembles a stage reached in the construction of the wall.
Material properties	The materials which may be used are: (i) Isotropic material (ii) Orthotropic material (iii) Reinforced earth material (iv) Strip plate (beam) material For each the appropriate elastic constants must be given. For the reinforced earth material additional information regarding tie spacings and elastic constants must be given.
Nodal point coordinate information	Using the self generation options of the programme or otherwise, all the nodal points coordinates have to be specified.
Element connection data	Using the self generation options of the programme or otherwise, all the element connection information, the material type of each element and the construction increment in which a particular element becomes part of the structure has to be specified.
The Boundary Conditions	The known displacements and forces at the appropriate construction increments must be given.
Miscellaneous	The half-band width of the structural material must be checked not to exceed 56. If it exceeds 56, then a new nodal numbering has to be tried.

zones in the backfill of reinforced earth wall which might develop near the wall face.

7.5 Reinforced Earth Walls analysed by the Programme

The series E laboratory tests and the Granton full scale wall previously described in Chapters Five and Six respectively, were analysed using the programme.

The series E walls used perspex ties and were mainly intended to study reinforced earth wall behaviour by observing the stresses and strains in the soil and the ties and the wall deflections. Various tie spacings used in building these walls are shown in Table (7.2).

The Granton reinforced earth wall was constructed using concrete panels as skin element and stainless steel for the ties. Tie spacing adopted is shown in Table (7.2).

7.6 Details of the Data Used in the Finite Element Programme

A summary of the finite element runs and the meshes used for the analyses of model and field walls are shown in Table (7.2) and Figs (7.1) to (7.3), respectively. The properties of the different materials used in the finite element analyses will be described in this section.

7.6.1 Properties of soils

It is important to establish the stress-strain characteristics of soil to be used in the programme.

It has been mentioned in Section (7.2) that the present programme uses two options to account for the nonlinear overburden dependent soil behaviour. In the first option the tangent elastic modulus and the corresponding wall levels are fed into the programme. The second option uses equation (VIII-1) shown in Appendix(VIII) for the tangent modulus of the soil. The derivation of this equation was based on the empirical hyperbolic model suggested by Kondner,[40] to represent the stres-strain relationship of

TABLE (7.2) - Details of the Finite Element runs on the Model and Field Reinforced Earth Retaining Walls

Run No.	Type of Structure	Vertical Tie Spacing ΔHmm	Horizontal Tie Spacing S mm	Foundation Condition	Skin elements condition	Number of materials	Number of construction increments	Mesh No.	Number of elements	Number of nodal points	Time of the run (secs)
1	Model E	250	100	Rigid	No effect	2	10	1	80	99	39
2	Model E	83.3	100	Rigid	No effect	2	10	1	80	99	39
3	Model E	83.3	150	Rigid	No effect	2	10	1	80	99	38
4	Model E	83.3	300	Rigid	No effect	2	10	1	80	99	38.7
5	Model E	100	150	Rigid	No effect	2	10	1	80	99	38.55
6	Field Wall	750	750	Rigid	No effect	3	4	2	56	75	20
7	Field Wall	750	750	Rigid	Rigid	4	4	2	60	75	20.5
8	Field Wall	750	750	Flexible	No effect	4	4	3	84	109	27
9	Field Wall	750	750	Flexible	Rigid	5	4	3	88	109	27.5
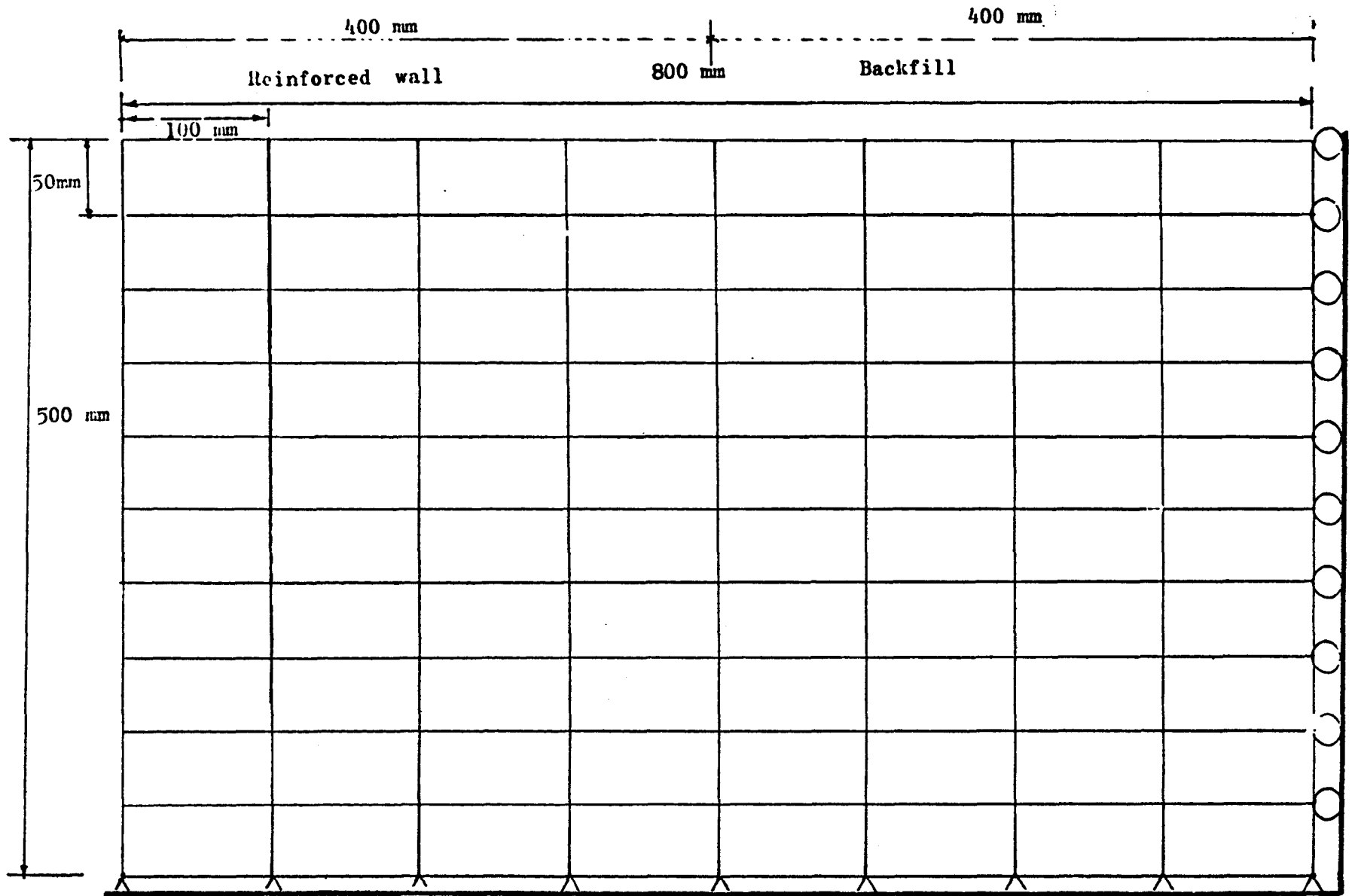
Fig.7·1 Finite element mesh of the model reinforced earth walls
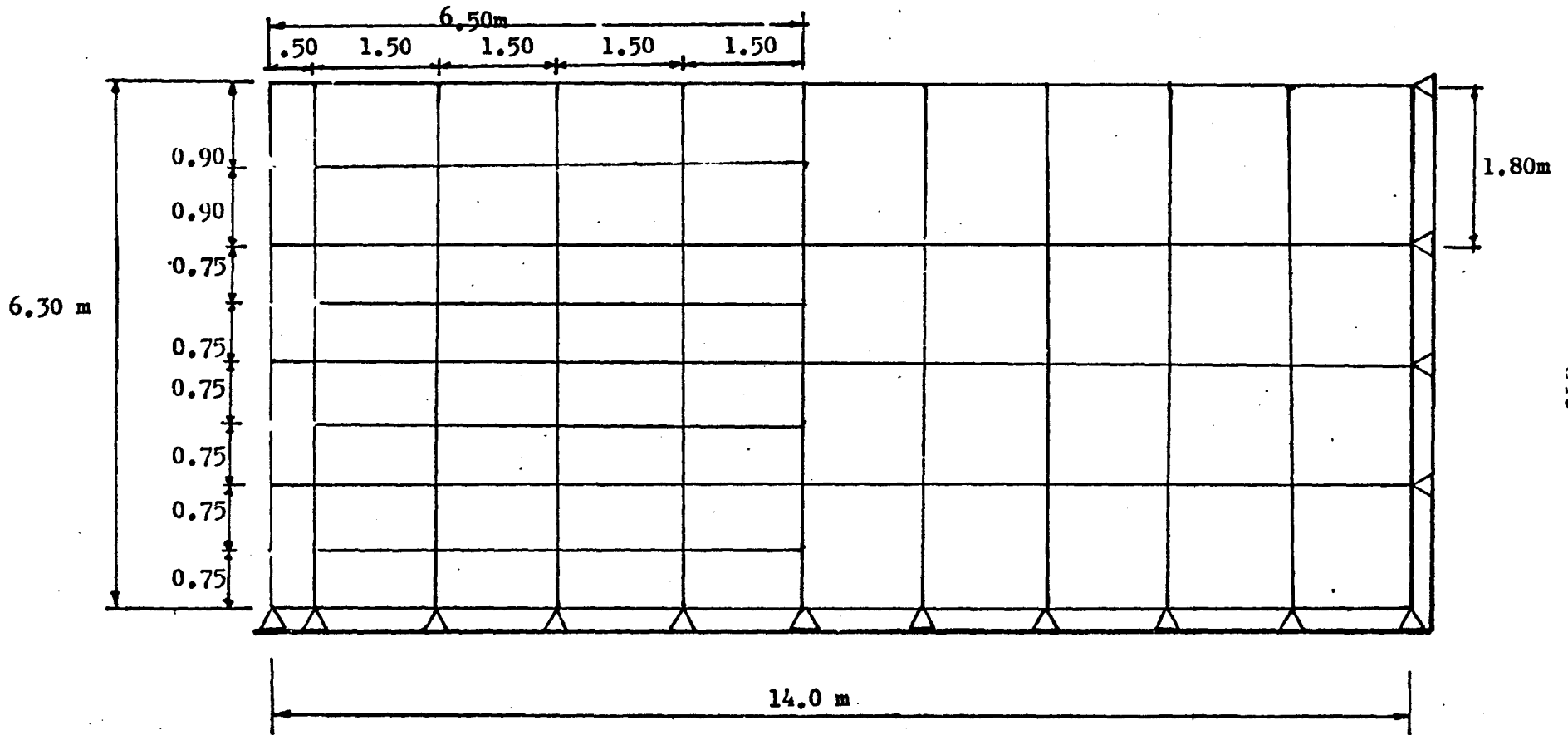
Fig. 7.2 Finite element mesh-2 of Granton reinforced earth wall(without considering found. flexibility)
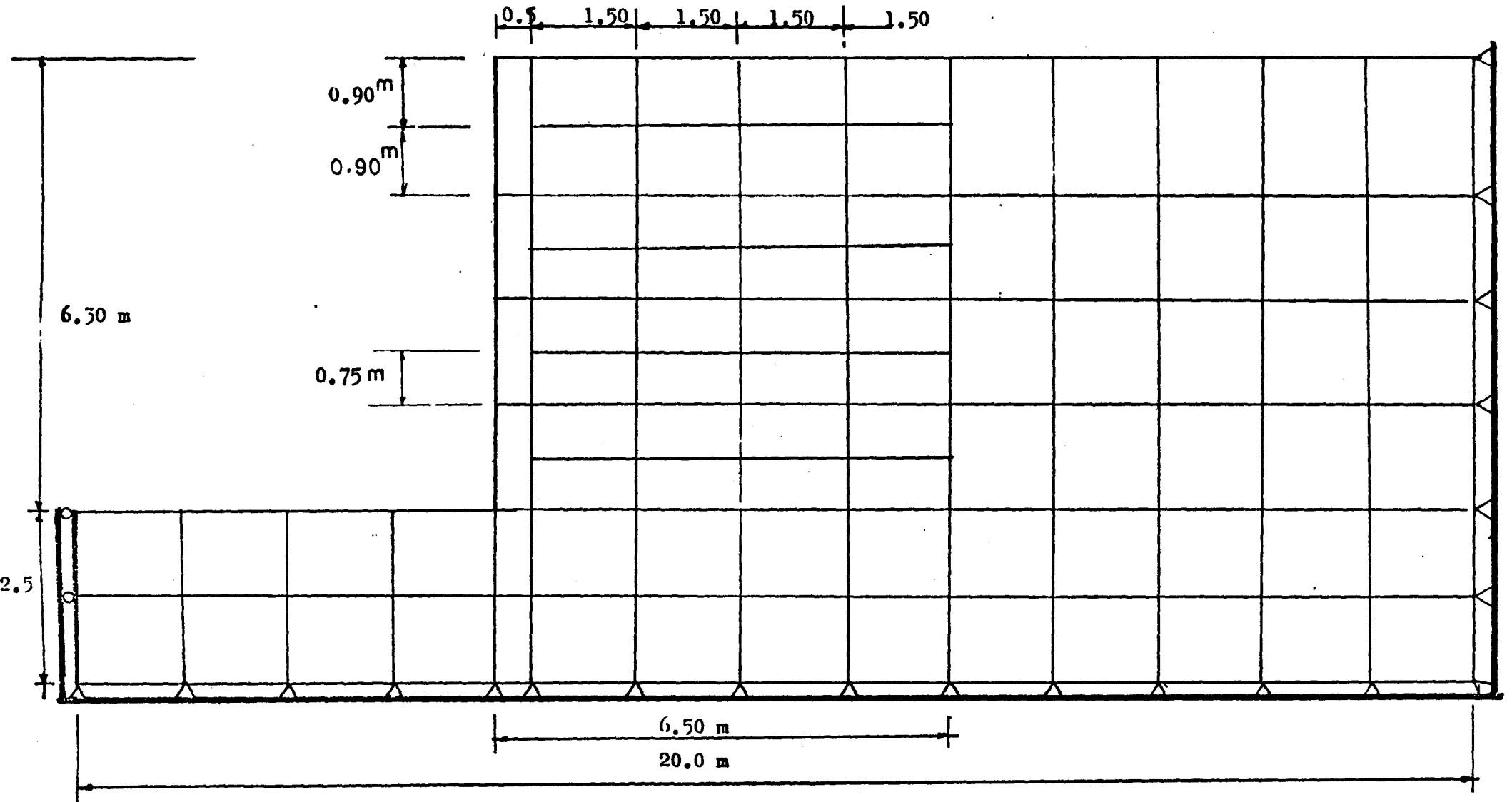
Fig. 7.3 Finite element mesh-3 of Granton reinforced earth wall (Found. flexibility is considered)

soils.   This option was adopted in the present study, since the hyperbolic model was found [26]   to approximate very closely the stress-strain curves of soils.

The soil parameters used in this empirical relation-ship are shown in Table (7.3).   These were determined from triaxial tests carried on 100 mm diameter sand and the burnt oil shale (blaes) samples.

The Poisson's ratio v values for the sand were calculated from the axial and volumetric strains observed in the triaxial tests, using the equation

$$v = \frac{\Delta\epsilon_1 - \Delta\epsilon_v}{2\Delta\epsilon_1}$$ .... (7.1)

The triaxial test results gave Poisson's ratio of 0.39 initially, increasing with increasing deviator stress to 0.72.   Previous investigators[26]   noted this kind of variation in v , but with smaller values, e.g. Duncan et al[26]   obtained a range of 0.11 to 0.65 for a sand tested in a dense state and a range of 0.11 to 0.40 for a sand tested in a loose state.   The increase in v values with increasing stress level was attributed by Duncan et al[26] to dilatancy effect.   High values of v obtained in the present tests may have been due to inaccuracies in measuring volume changes which occurred, using available laboratory equipment.

An approximate procedure used by Penman et al[51] for determining v for the condition of small lateral deformation was adopted.   This procedure requires a knowledge of K_o which may be obtained from the empirical relationship suggested by Jaky[36]   and lately verified by Bishop[8]   and Brooker et al[11]   .   The value of v calculated in this way was equal to 0.263.

Poisson's ratio of the blaes was determined from the axial and volumetric strains observed in the triaxial test using equation (7.1).   A representative value of v was taken as 0.31, Appendix (VIII-c)

7.6.2 Properties of ties

The properties and dimensions of ties used in the model and field walls are shown in Table (7.4).

The elastic modulus of the perspex was taken from the technical service note, published by I.C.I.[34] Plastic Division, at a temperature of $20^{\circ}C$ equal to the mean laboratory temperatutre. Laboratory tests on the tie material at this temperature gave values within $\pm$ 4% of the I.C.I. value.

The elastic modulus of the stainless steel ties, used in the Granton field wall, was determined from a laboratory test and is shown in Table (7.4).

7.6.3 Properties of foundation material

The model walls were assumed to rest on an infinitely rigid foundation.

The Granton wall was analysed assuming a rigid foundation and flexible foundation conditions. In the latter case the 2.50 m deep soft clay layer was modelled by assuming it as an isotropic material and nominal values of E and v were assigned to represent soft clay   and no volume change conditions respectively as shown in Table (7.5).

7.6.4 Properties of skin elements and stone pitching

In the model tests, the effect of the skin elements on the internal stability of the walls was neglected and the skin elements were designed to rotate freely on each other to simulate the full scale panel behaviour. In the present finite element analysis, the stiffness of the model skin elements was assumed not to affect the theoretical wall behaviour.

For the Granton wall, nominal concrete elastic properties and density were assigned for the skin elements as shown in Table (7.6). The stone pitching at the back of the field wall was assumed to have identical elastic properties and density to the concrete.

TABLE (7.3)   The Soil Properties

The soil parameter	SAND used in model tests	BLAES used in the Granton wall
Angle of internal Friction $\emptyset$	40°	46°
Cohesion c	O	41.37 kN/m^2
Density γ	$1.587 \times \frac{-5}{10} \text{ N/mm}^3$	16.65 kN/m^3
Poisson's ratio ν	0.263	0.310
Intercept $\bar{a}$	2.12 N/mm^2	$1.39 \times 10^4 \text{ kN/m}^2$
Slope $\bar{b}$	1.549×10^3	223

where $\bar{a}$ and $\bar{b}$ are the intercepts and slope of the initial tangent modulus E_i $\underline{v}$ the confining prssure σ_3 curve

Equation (7.2)

$$E_i = \bar{a} + \bar{b} \cdot \sigma_3 \quad \dots\dots\dots\dots\dots\dots \quad (7.2)$$

Method of determining the constants $\bar{a}, \bar{b}$ for the sand and the blaes is shown in Appendix (VIII), Sections (b) and (c) respectively.

TABLE (7.4) Properties of Ties

Parameters	Model Walls	Field Wall
Elastic modulus	2896 N/mm^2 @ 20°C	1.965 x 10^8 kN/m^2
Tie Width	22.3 mm	80 mm
Tie Thickness	1.37 mm	1.5 mm
Tie Length	0.40 m	6.50 m
Horizontal tie spacing	100, 150, 300 mm	750 mm
Vertical tie spacing	83.3, 100, 250 mm	750 mm

TABLE (7.5) Properties of Foundation Material

Parameter	Model Walls	Field Wall
Elastic modulus	Rigid foundation	1.20 x 10^4 kN/m^2
Poisson's ratio	"	0.495
Density	"	18.85 kN/m^3

TABLE(7.6)   Properties of Skin Elements

Parameter	The Field Wall Skin Element "Concrete"
Area (unit width)	$0.18m^2$
Moment of inertia (unit width)	$0.486 \times 10^{-3} m^4$
Elasticity modulus	3.00×10^{7} kN/m^2
Poisson's ratio	0.300

7.7 Results of the Finite Element Analysis

In this section the results obtained by idealizing the model and the field wall behaviour will be presented. Further comparison with the observed model and field wall behaviour will be presented in Section (7.8).

7.7.1 Model Walls

From the model wall results the contours of the following parameters were drawn:

- The tie forces
- The non-dimensional tension $\chi = \dfrac{T}{\gamma h \Delta H . S}$

- The theoretical vertical stress σ_y

- The theoretical horizontal stress σ_x

- The stress ratio $\dfrac{\sigma_x}{\sigma_y}$

- The theoretical vertical soil strain ϵ_y

- The theoretical horizontal soil strain ϵ_x
- The theoretical shear stress in the soil τ_{xy}

- The theoretical shear strain in the soil γ_{xy}

7.7.1a The tie forces

Contours of the tie forces predicted by the finite element method for model walls built in series E tests are shown in Figs (7.4) to (7.8).

It can be seen that the patterns of the tie force distribution are similar for the different vertical and horizontal tie spacings. The magnitude of the tie force depends on the tie spacing, and increases with increasing horizontal or vertical tie spacing. The finite element analysis gave a tie tension distribution along horizontal planes in the wall, which is a maximum near the wall face and decreases towards the back of the wall.

7.7.1b The non-dimensional tension

From the predicted tie forces the non-dimensional tension
$\chi = \dfrac{T}{\gamma h.\,\Delta H.S}$ was computed for each tie spacing used in the

Series E tests and the results are shown in Figs (7.9) to (7.13).

The contour maps of the non-dimensional tension χ are practically similar in pattern and identical in magnitude irrespective of the different horizontal and vertical tie spacings used in the walls.

The theoretical non-dimensional tension decreases from a maximum value at the top of the wall to a minimum value at the bottom of the wall and this is in agreement with the observed model and field wall behaviour and the energy theory (LO.L.A.) prediction indicated in Chapters Five and Six, Figs (5.42) and (6.6) respectively.

7.7.1c Stresses in the soil

Contours of the vertical stress σ_y, the horizontal stress σ_x, the stress ratio $\dfrac{\sigma_x}{\sigma_y}$, and the maximum principal

stress σ_1, were drawn for the tie spacing ($\Delta H=100$, $S=150mm$) and are shown in Figs (7.14) to (7.17). Similar patterns of stress distribution can be expected for the rest of series E tests.

The variation in the vertical stress σ_y along horizontal sections in the reinforced earth wall and its backfill are nearly uniform. This indicates that the variation in the vertical stiffnesses of the wall and the backfill almost have no effect on the vertical stress variation.

The contours of horizontal stresses Fig (7.15) showed a large drop at the back of the reinforced earth walls, probably due to the difference in horizontal stiffness of the reinforced earth wall and the soil backfill just behind it. The theoretical horizontal stresses are all compressive as was expected.

The contours of the stress ratio $\frac{\sigma_x}{\sigma_y}$ are shown in Fig (7.16). These have a minimum value of 0.1 in the backfill of the wall and a maximum value of 0.35 in the reinforced earth fill. Comparing these values with the active and at rest coefficients of earth pressure which are 0.22 and 0.36 respectively, it can be seen that the finite element analysis predicts an at rest state of stress in the reinforced earth fill. Values of $\frac{\sigma_x}{\sigma_y}$ less than K_a may indicate the inadequacy of the isotropic assumption of the backfill soil behaviour [18].

Contours of the theoretical maximum principal stress are shown in Fig (7.17). These are generally uniformly distributed over horizontal sections in the reinforced earth fill, and no obvious potential failure surface can be deduced from the graph.

7.7.1.d Strains in the soil

Contours of the vertical and horizontal strains are shown in Figs (7.18) and (7.19) respectively. The contours of the vertical strains are similar to the vertical stress contours and almost regularly spaced over the vertical section. The horizontal strain contours show a large difference between the horizontal strains in the reinforced earth fill and the strains in the backfill. The latter are much larger than the former. The positive sign of these indicates a stretch in the reinforced mass and its backfill. The contours of the lateral strains in the reinforced earth wall generally have a similar pattern to the contours of the tie forces shown in Fig (7.4). Probably this is due to the assumption of perfect bond between the tie and the soil used in the analysis.

The contours of the shear stress and strain in the soil are shown in Figs (7.20), (7.21). The distribution patterns are generally similar and almost symmetrical about the dividing line between the reinforced earth fill and the retained soil behind it.
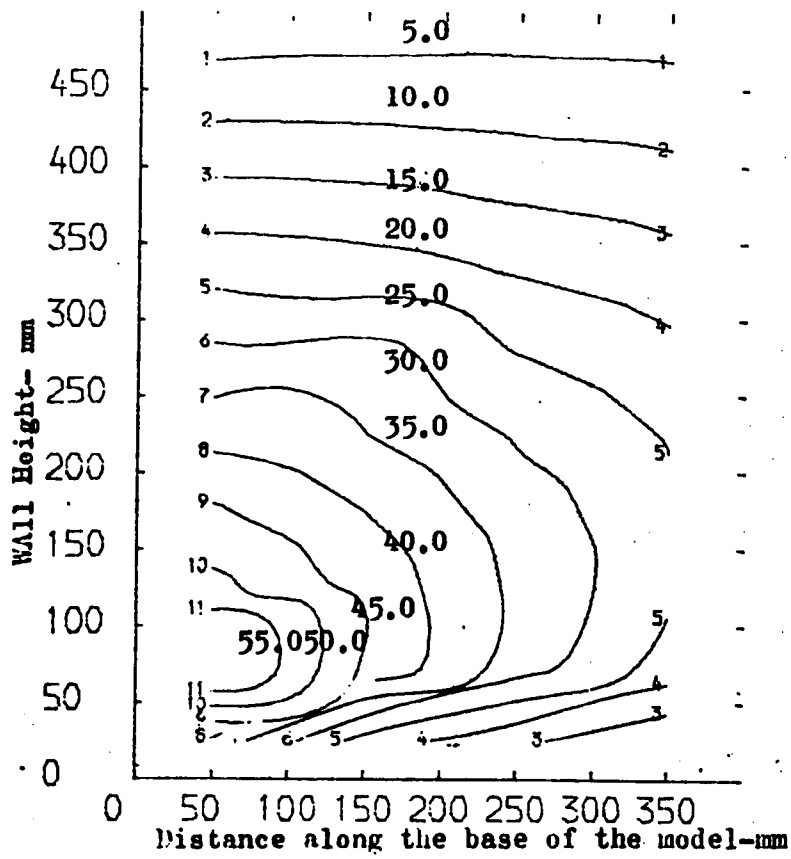
Fig.7.4 Contours of theretical tie forces-N (model walls series E

ΔH= 250 mm, S = 100 mm)
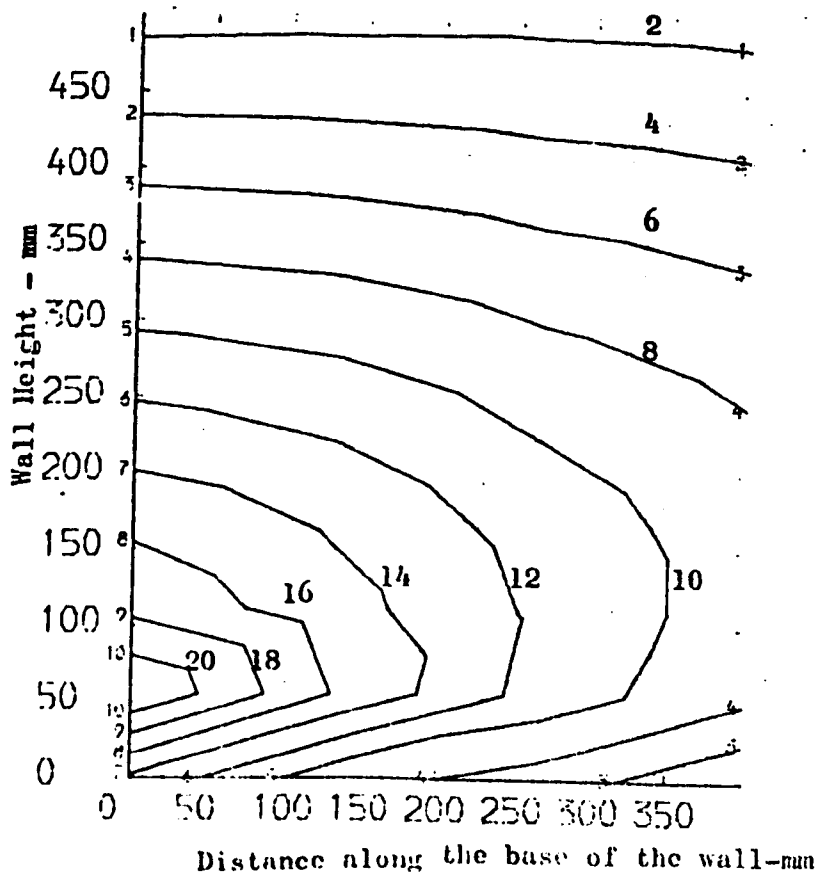
Fig.7.5 Contours of theoretical tie forces-N-(model walls

series E .ΔH=83.3 , S= 100 mm)
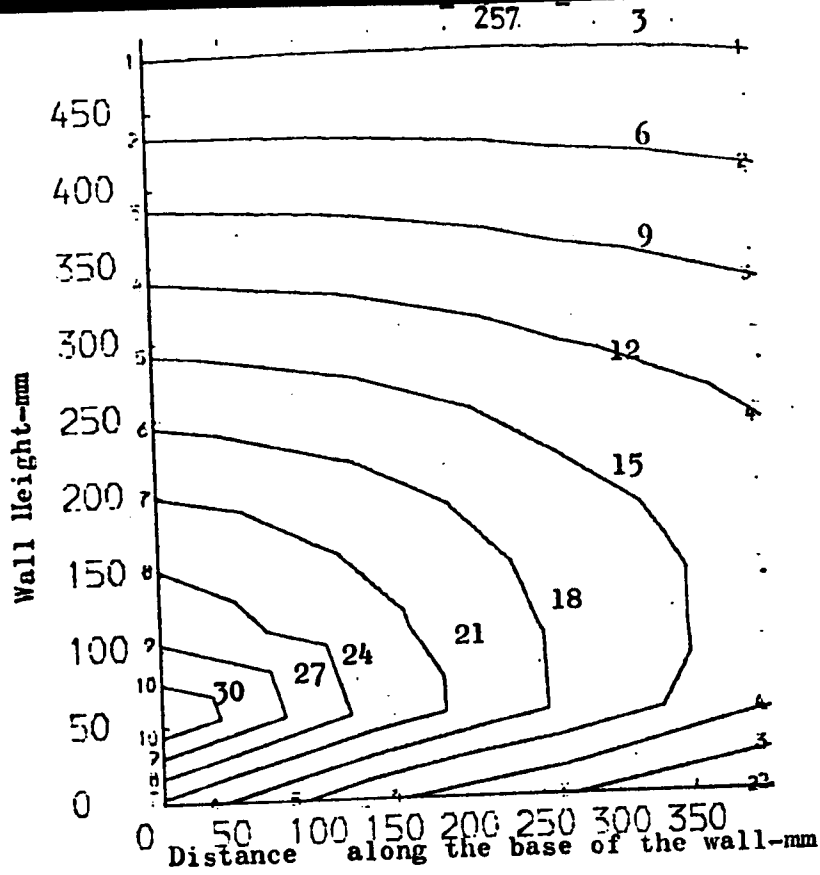
Fig.7.6 Contours of theoretical tie forces-N-(model walls

series E ΔH=83.3 , S=150 mm)
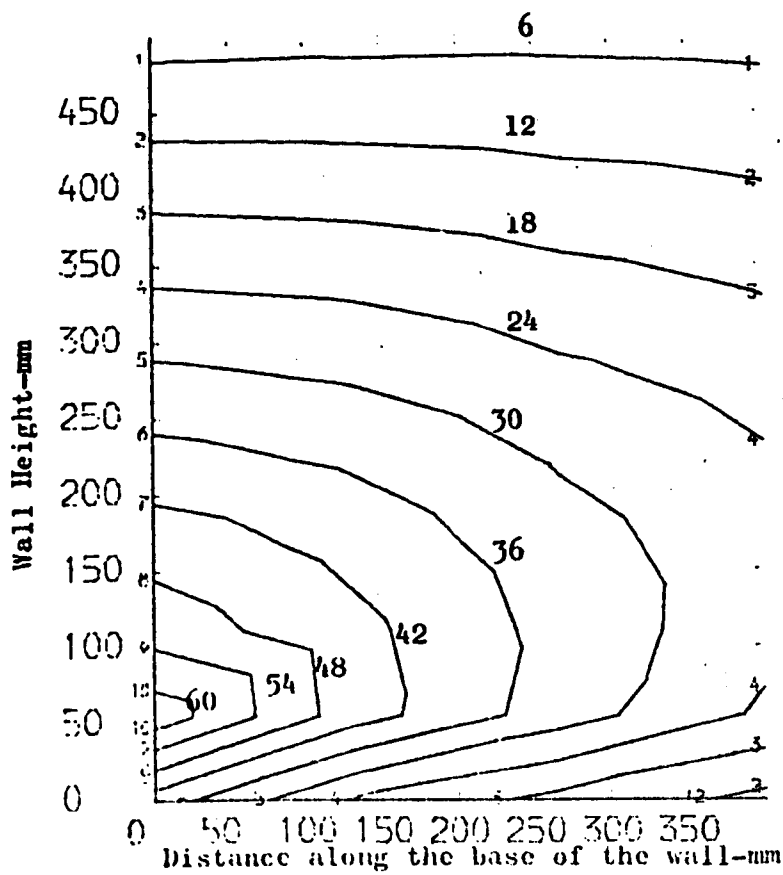
Fig.7.7 Contours of theoretical tie forces-N-(model walls

series E , ΔH=83.3 , S=300 mm)
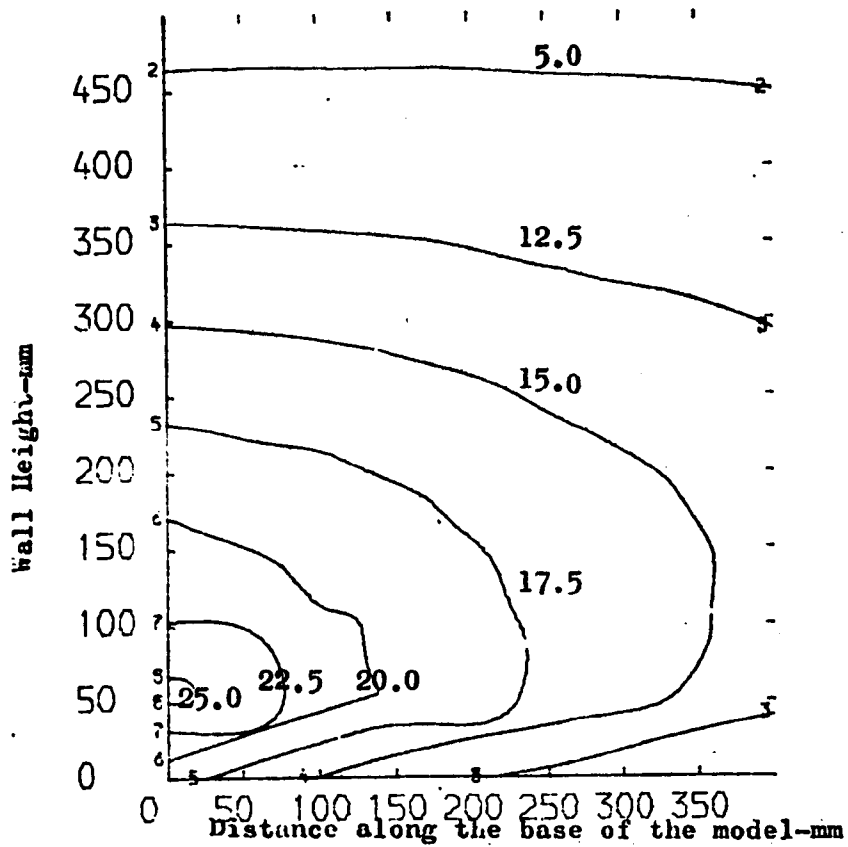
Fig.7·8 Contours of theoretical tie forces -N -(model walls series E

ΔH =150 mm , S = 100 mm)
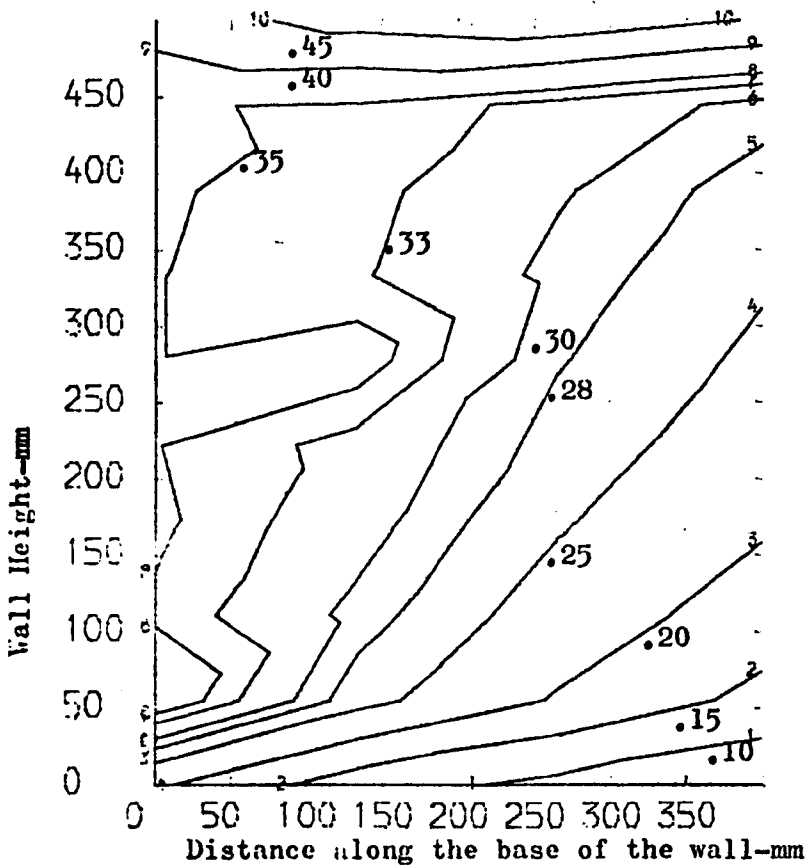
Fig. 7·9 Contours of theoretical non-dimensional tension $\mathfrak{X} = \dfrac{T}{\gamma \cdot h \cdot \Delta H \cdot S}$

(model walls series E , ΔH=250, S=100 mm)
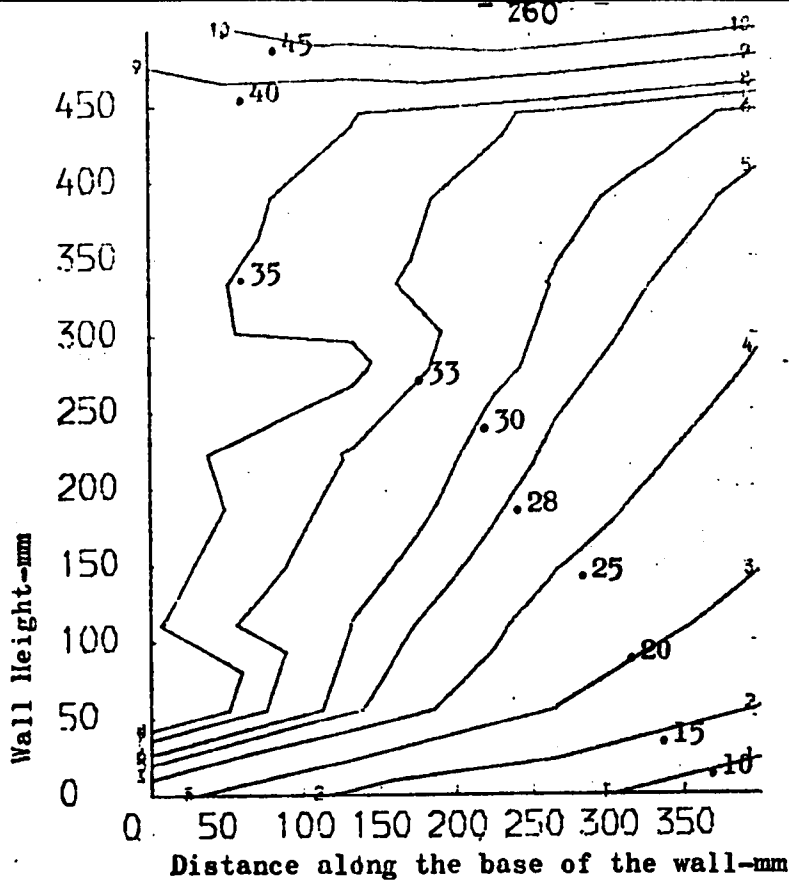
Fig.7.10 Contours of theoretical non-dimensional tension $\mathcal{X} = \dfrac{T}{\gamma.h.\Delta H.S}$

(model walls series E , $\Delta H = 83.3$, S=100 mm)
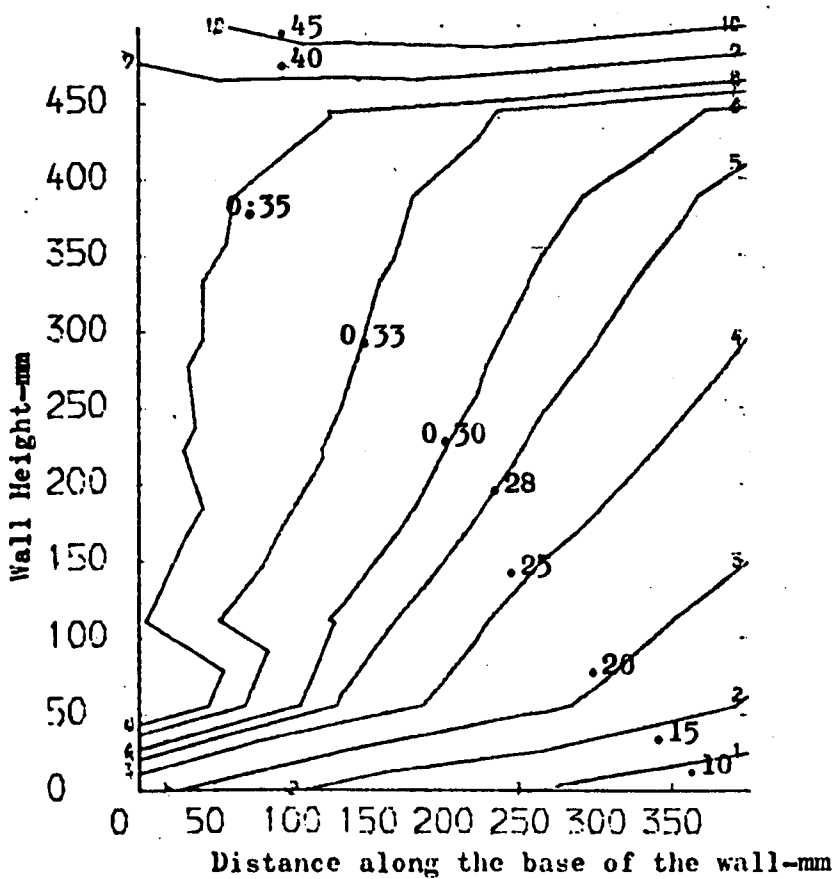
Fig.7.11 Contours of theoretical non-dimensional tension $\mathcal{X} = \dfrac{T}{\gamma.h.\Delta H.S}$

(model walls series E , $\Delta H = 83.3$, S=150 mm)
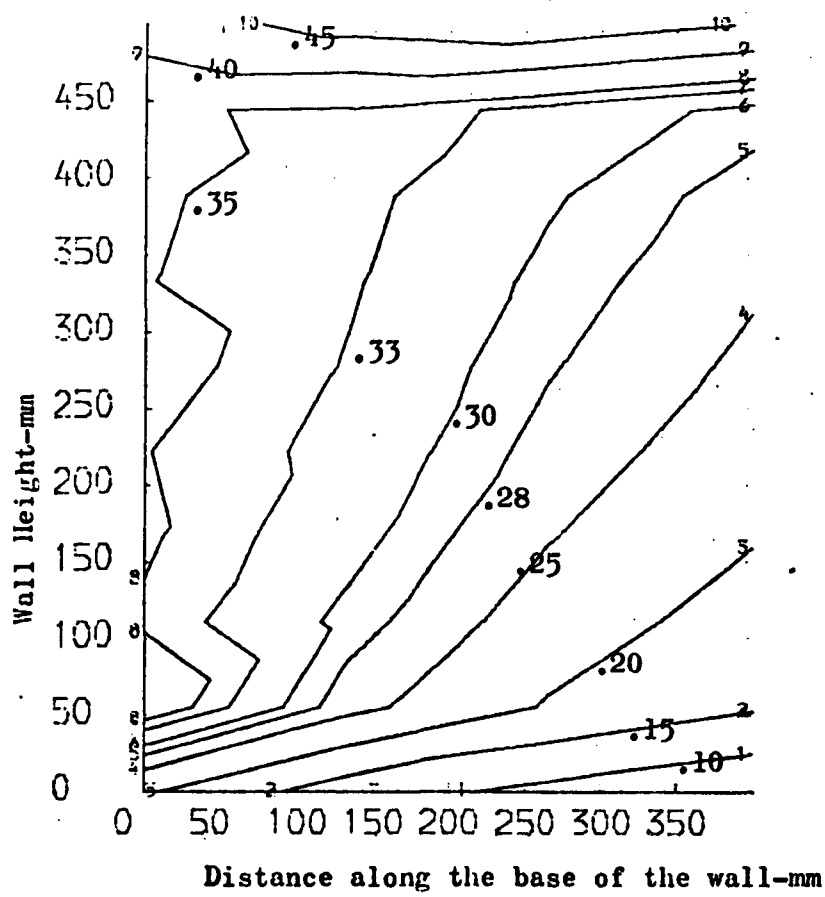
Distance along the base of the wall—mm

Fig.7.12 Contours of theoretical non-dimensional tension $\chi = \dfrac{T}{\gamma \cdot h \cdot \Delta H \cdot S}$

(model walls series E , ΔH=83.3, S=300 mm)

Distance along the base of the wall—mm
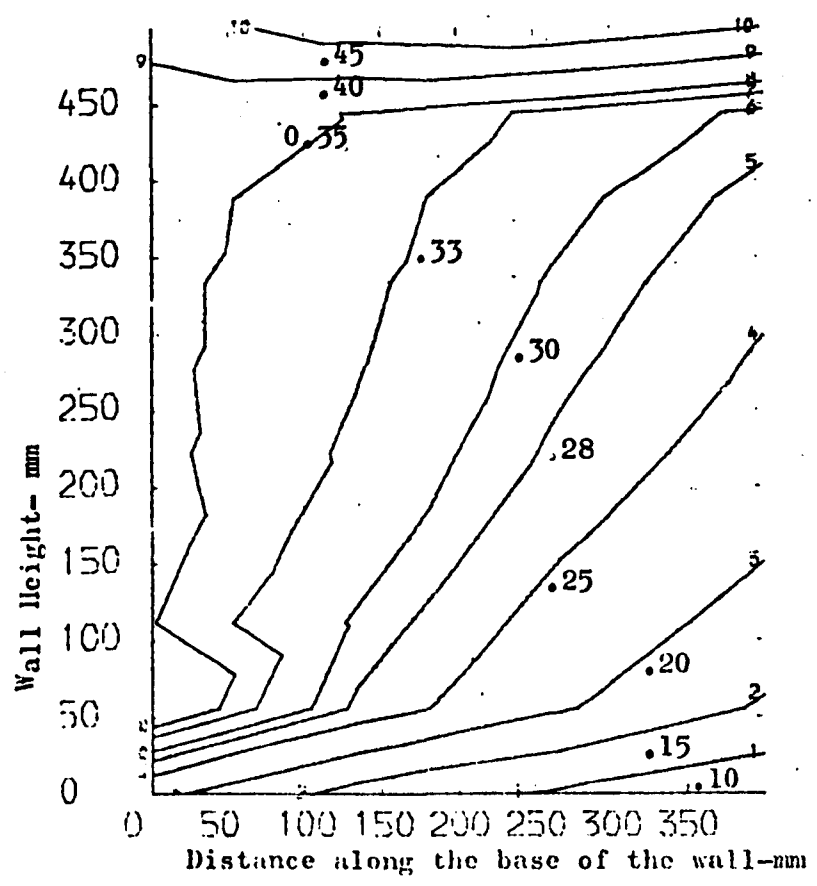
Fig.7.13 Contours of theoretical non-dimensional tension $\chi = \dfrac{T}{\gamma \cdot h \cdot \Delta H \cdot S}$

(model walls series E , ΔH=100 , S=150 mm)
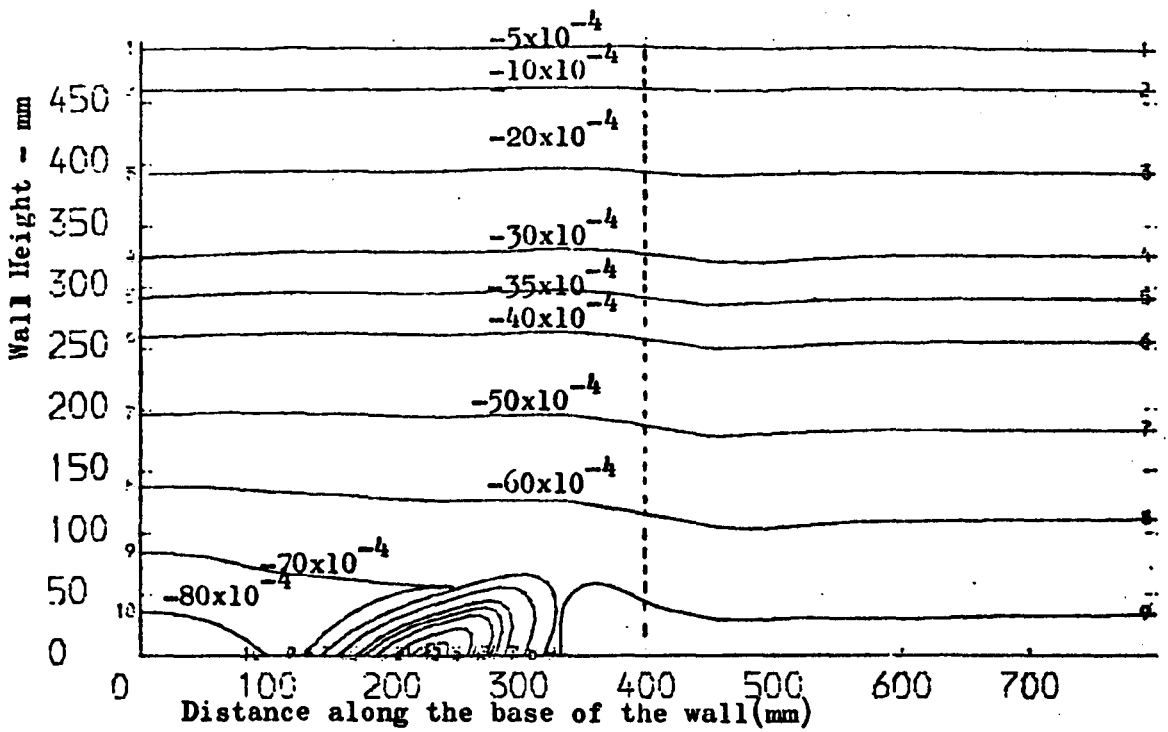
Fig.7.14 Contours of theoretical vertical stresses-N/mm^2(model walls series E

ΔH=100 mm, S=150mm)

— compression

------- Boundary between reinforced earth wall and backfill
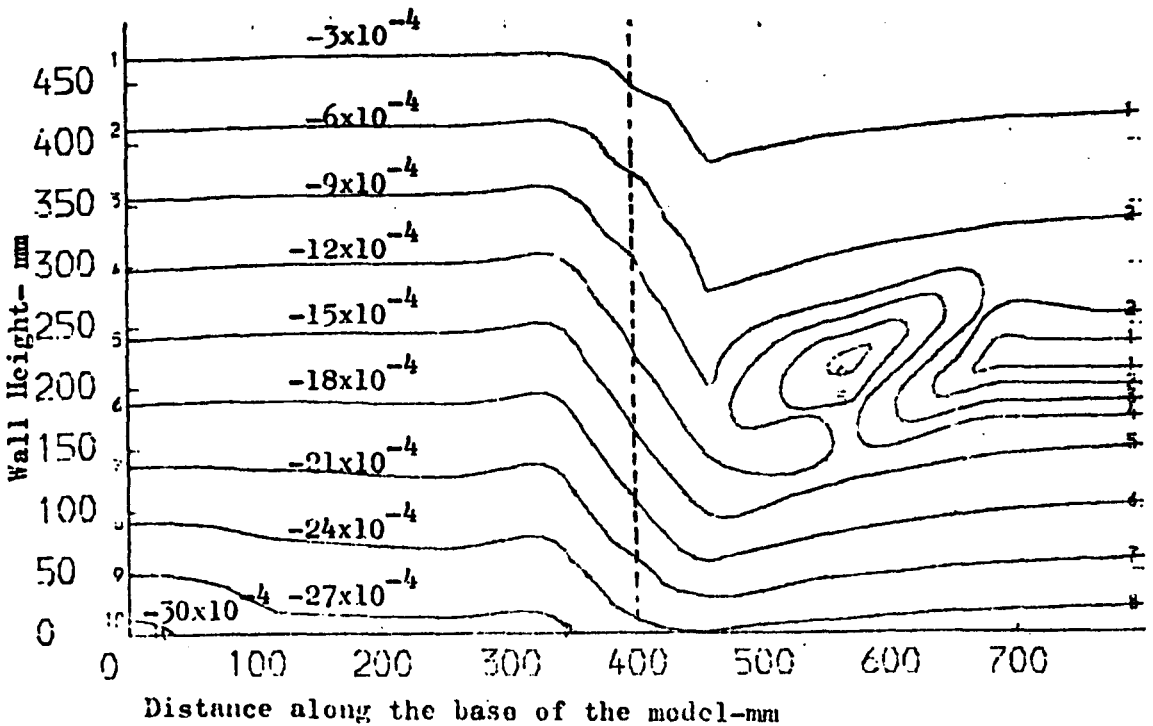
Fig.7.15 Contours of theoretical horizontal stresses-N/mm^2(Model walls series E
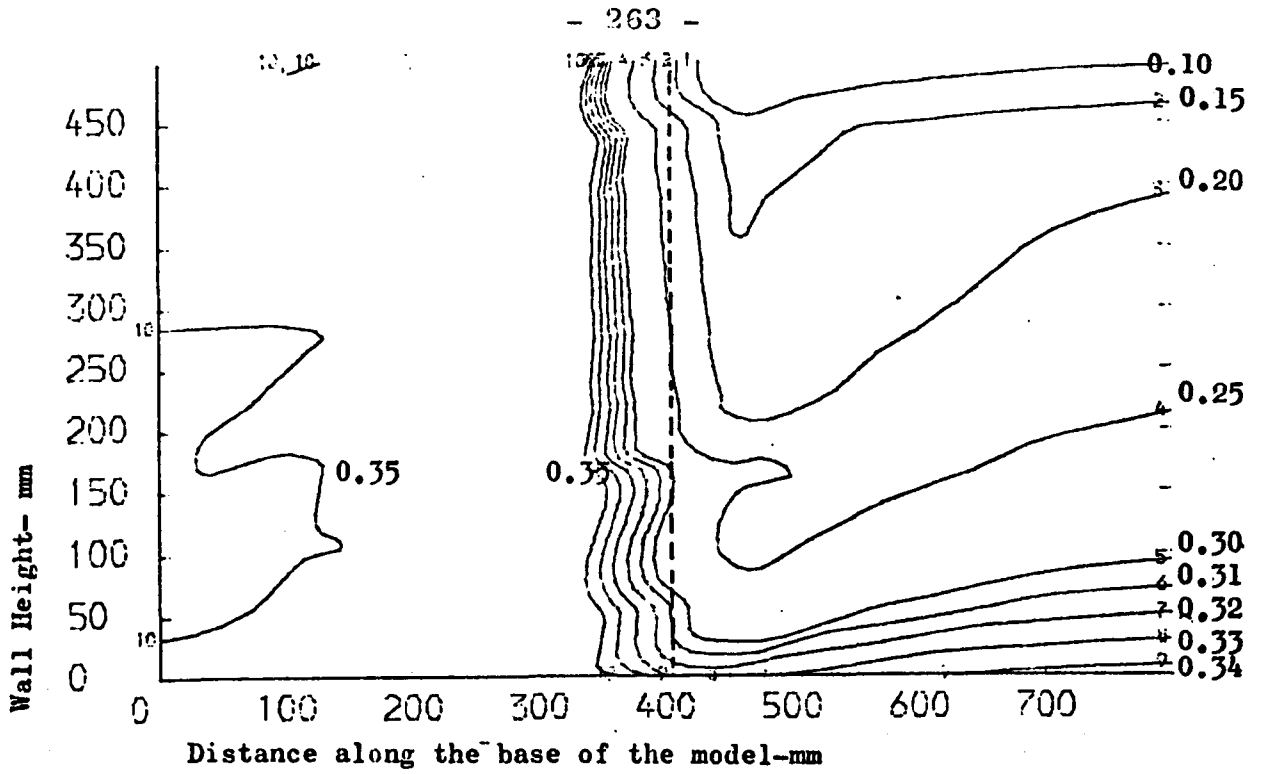
ΔH=100 mm, S=150 mm)

Fig.7.16 Contours of theoretical stress ratio.(model walls series E ,ΔH=100mm
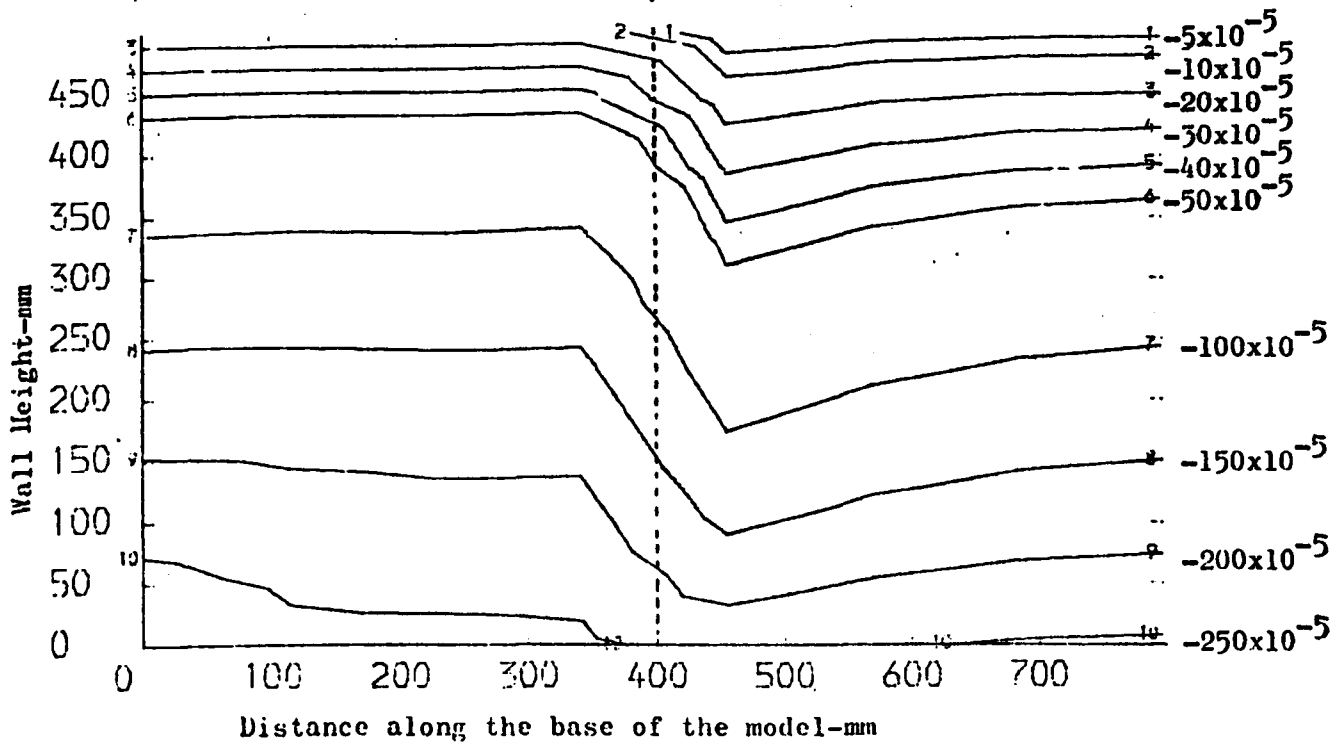
S=150 mm) .

Fig.7.17 Contours of theoretical maximum principal stress -N/mm^2-

(model walls series E, ΔH=100 , S=150 mm)
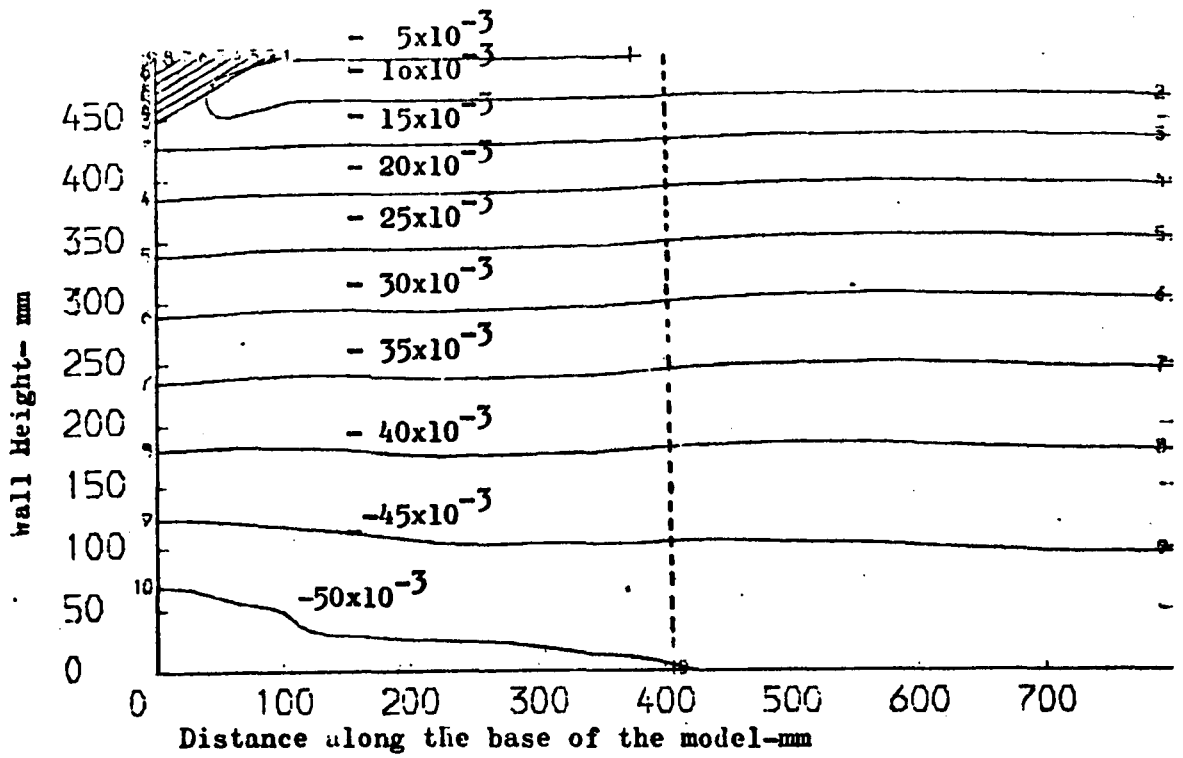
Fig. 7.18 Contours of theoretical vertical strains (model walls series E
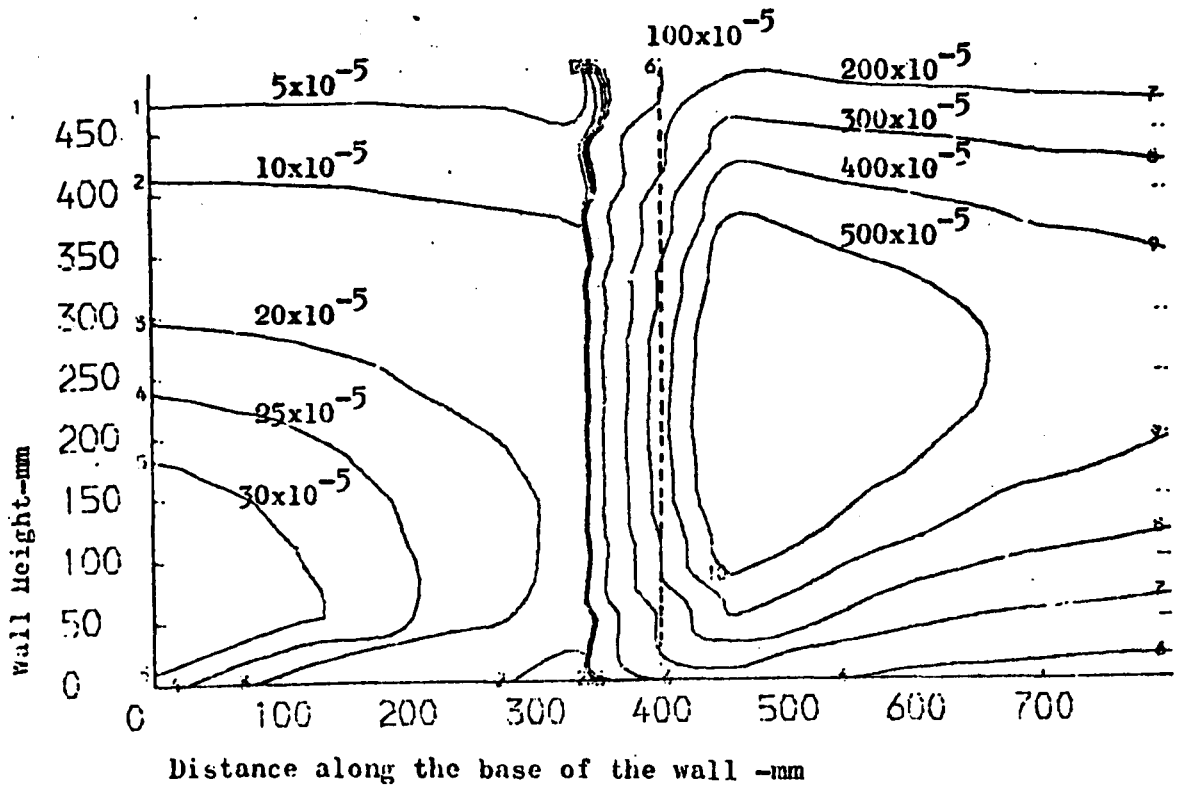
$\Delta H = 100$ mm , $S = 150$ mm)

Fig. 7.19 Contours of theoretical horizontal strains (Model walls series E

$\Delta H = 100$ mm, $S = 150$ mm)
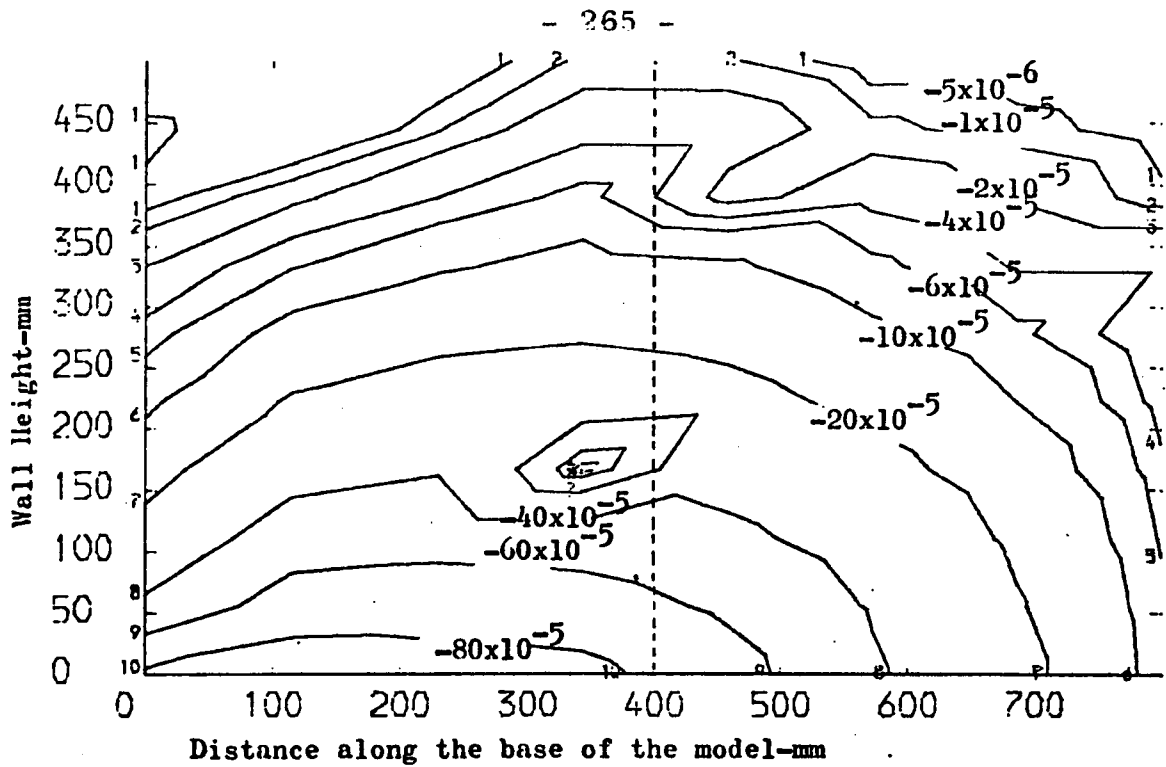
Fig.7.20 Contours of theoretical shear stess in the soil-N/mm^2 (model walls series E , $\triangle$H=100, S=150 mm)
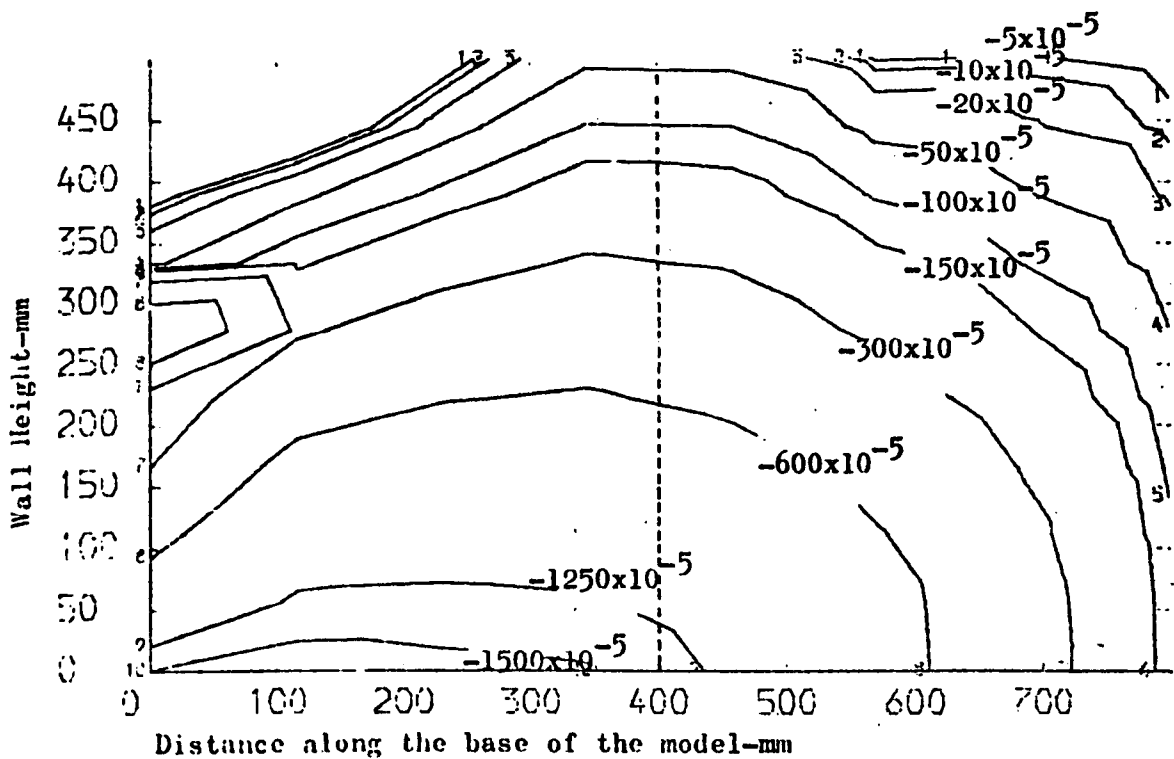
Fig.7.21 Contours of shear strain in the soil (model walls series E $\triangle$H=100, S=150 mm)

7.7.2 Field Wall

In the Granton reinforced earth field wall the tie forces were observed. From the results of the finite element analysis, the theoretical contours of the tie forces and the non-dimensional tension were drawn for four different combinations of foundation and skin element rigidity. The results are shown in Figs (7.22) to (7.29).

The effect of compaction on the reinforced earth wall behaviour was neglected, since a realistic representation requires a knowledge of the unloading modulus of the reinforced earth fill and the fill at the back of the wall.

Therefore the forces developed in the ties are those due to the self weight of the fill, the weight of the spreader beam and the reinforced concrete cope.

7.7.2.a Effect of foundation rigidity on the tie forces

As has been mentioned in Section (6.2d) in Chapter Six, the Granton site was underlain by a rather soft clay stratum 2.50 metre deep, which overlies a gravel layer. To increase the safety factor adopted in designing the foundation of the wall to a value above 2.5, as required by the Edinburgh City Engineer , the whole area under the reinforced earth wall was dug out and replaced with blaes.

Two computer runs were made; one for flexible and the other for rigid foundation behaviour. In the first run the clay stratum was taken as an isotropic material and nominal values of E and v were assumed, as described previously in the material properties. In the second run, the wall was assumed to rest on an undeformable foundation. In both cases the skin elements rigidity was neglected. The results are shown in Figs (7.22) and (7.25). The predicted tie forces were practically similar at the top and middle of the wall. At the wall bottom, however, larger tie forces were induced when a flexible foundation was assumed.

7.7.2.b Effect of skin elements rigidity on the tie forces

In the Granton reinforced earth field wall skin elements used consisted of concrete panels. Finlay and Sutherland[29] pointed out that these elements might have more effect on the wall behaviour than flexible metal skin elements.

In the present programme there is provision for simulating the rigid skin element behaviour by idealizing it as a beam element which has a stiffness and elastic properties corresponding to the actual skin element in the field. The effect of using such an idealization for the skin elements on the tie forces can be seen by comparing Figs (7.22), (7.23) and (7.24). When the skin element rigidity is considered, compressive tie forces are predicted at the top third of the wall for both the rigid and flexible foundation cases. The tie tension magnitude is generally decreased when the skin element rigidity is considered.

7.7.2.c The non-dimensional tension

The contours of the non-dimensional tension for the Granton reinforced earth wall, drawn for the four computer runs are shown in Figs (7.26) to (7.29).

It can be seen that the magnitude and pattern of the non-dimensional tension depend on the conditions of the skin elements and the foundation.

Minimum non-dimensional tension was obtained when the skin element rigidity was taken into account. In this case the non-dimensional tension increased with wall depth, and was different from the theoretical result obtained in the model walls.

When the skin element rigidity was ignored, the theoretical analysis using flexible foundation resulted in slightly higher non-dimensional tension than the analysis in which rigid foundation was adopted.
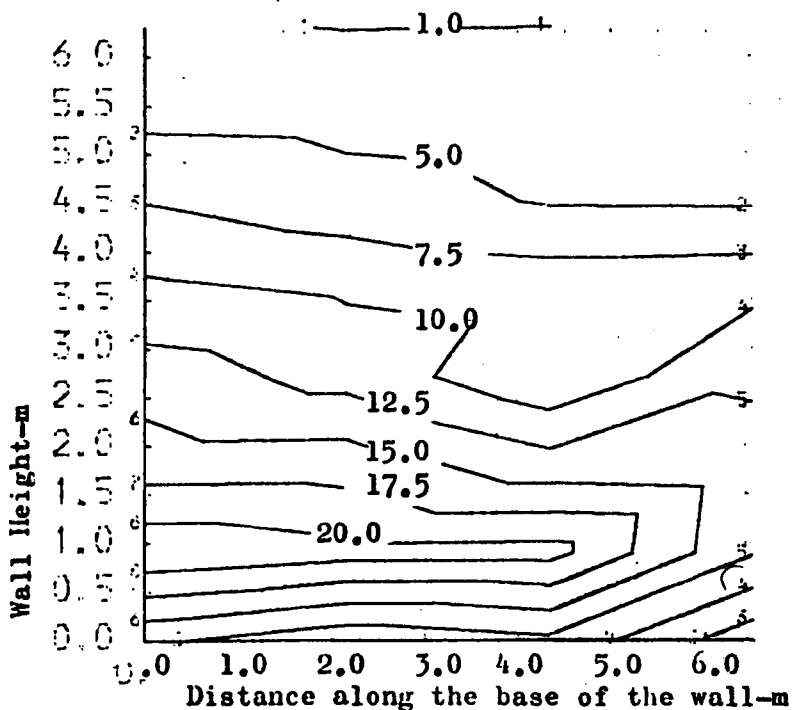
Fig.7.22 Contours of theoretical tie forces in Granton reinforced earth wall
- K N-(assuming a rigid found. & neglecting the skin element rigidity)
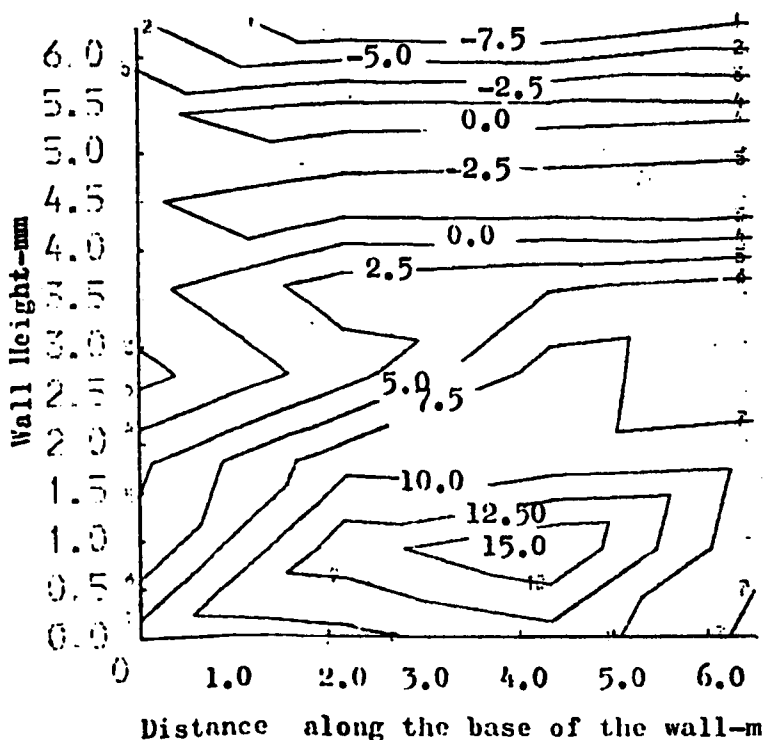
Fig.7.23 Contours of theoretical tie forces in Granton reinforced earth wall
- KN - (assuming rigid found. & rigid skin elements)
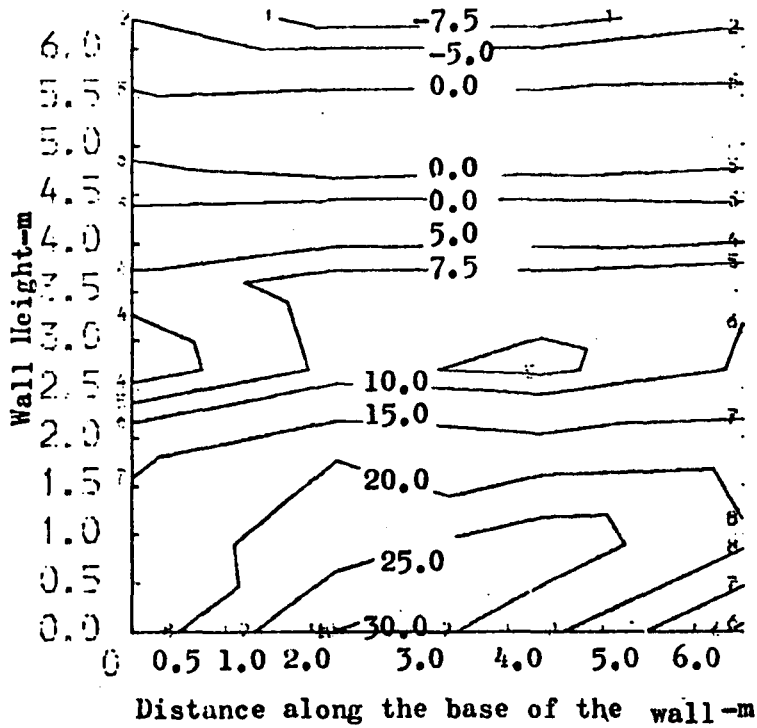
Fig.7.24 Contours of theoretical tie forces in Granton

reinforced earth wall-KN-(assuming flexible found.

&rigid skin elements)
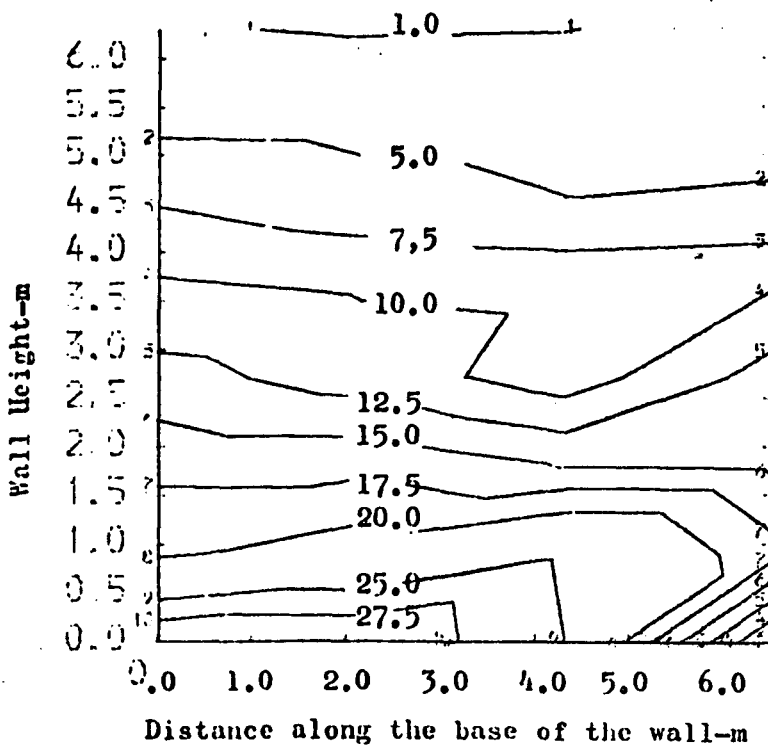
Fig.7.25 Contours of theoretical tie forces in Granton reinforced earth

wall -KN-(assuming flexible found. & neglecting the rigidity of the
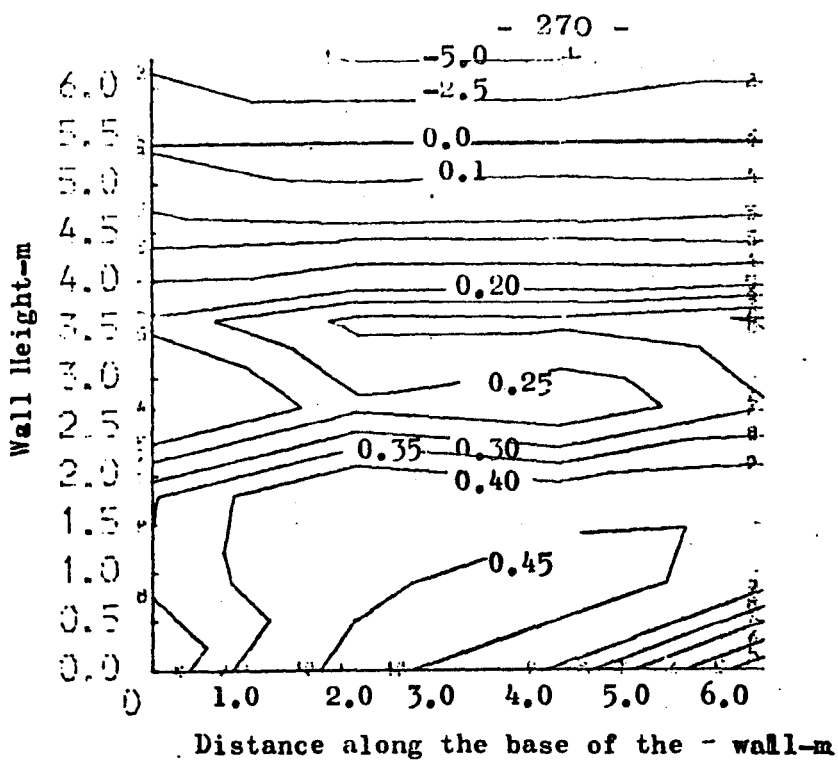
skin elements)

Fig.7·26 Contours of theoretical non-dimensional tension in Granton wall (assuming flexible found. & rigid skin elements)
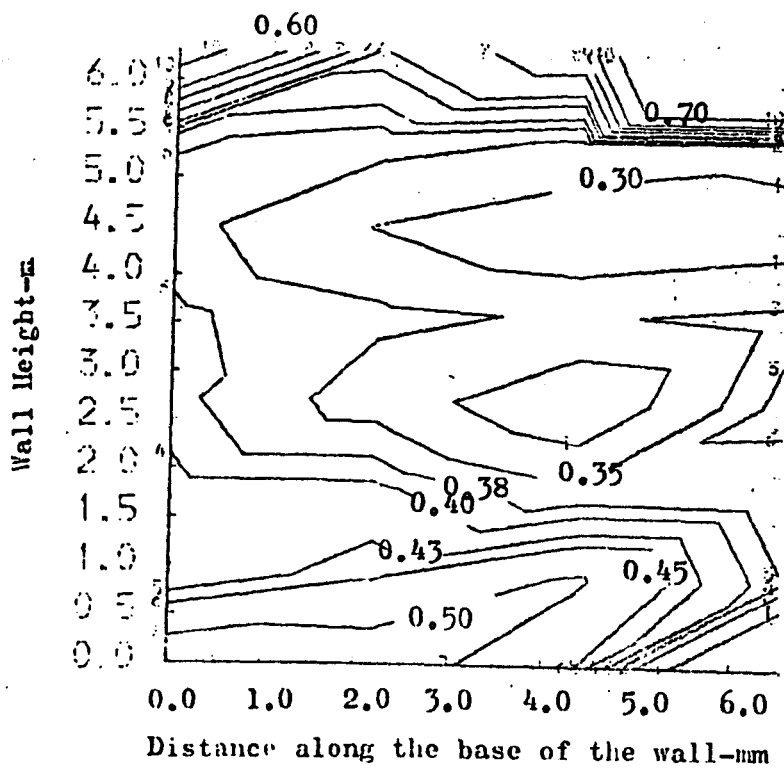
Fig.7·27 Contours of theoretical non-dimensional tension in Granton wall(considering found. flexibility & neglecting the rigidity of the skin elements)
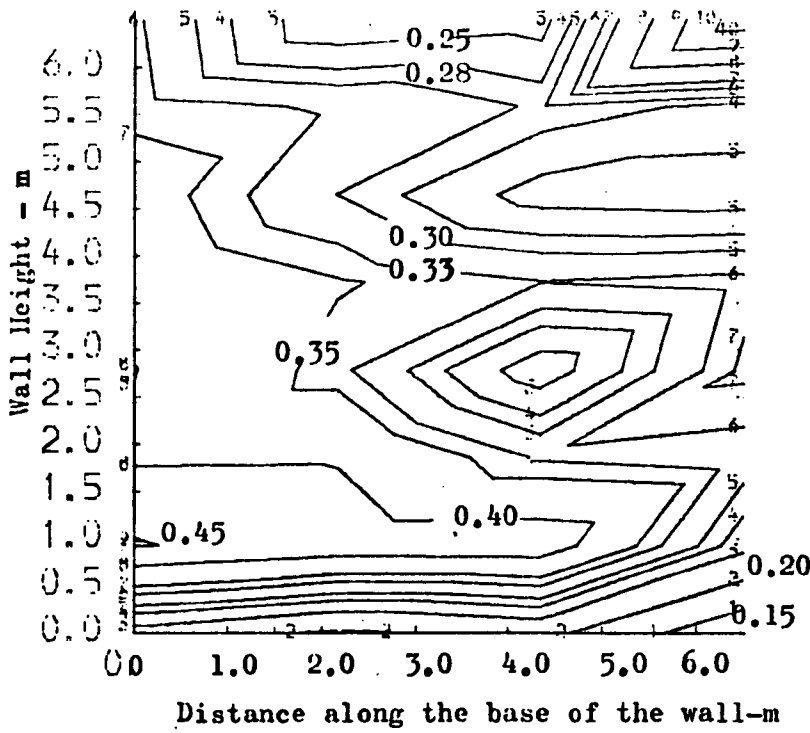
Fig.7.28 Contours of theoretical non-dimensional tension in Granton
wall(Considering a rigid found.& neglecting skin stiffness)
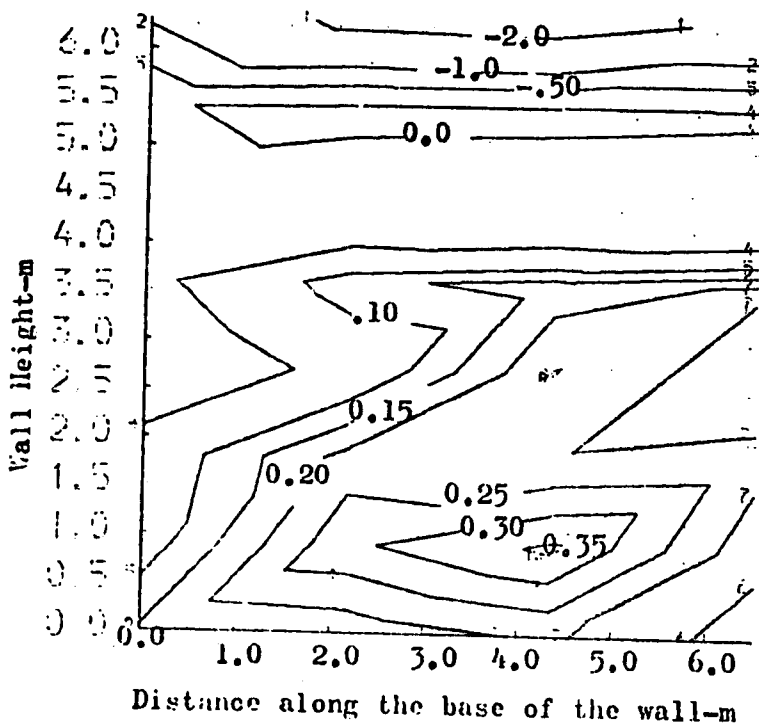
Fig.7.29 Contours of theoretical non-dimensional tension in Granton
Wall(Considering skin elements rigidity & assuming a rigid found.)

7.8 Comparison between the Observed and Predicted Reinforced Earth Wall Behaviour

7.8.1 Model Walls

7.8.1.a Tie forces

The observed tie forces in the reinforced earth model walls and the predicted tie forces by the programme are shown in Figs (7.30) to (7.34). The predicted tie forces are appreciably larger than the observed tie forces and have a different mode of variation. The large discrepancy in the values of the observed and the predicted tie forces is probably due to the limitations of the present finite element programme, outlined in Section (7.4). In addition, the stiffness of the model skin elements was neglected in the theoretical analysis. Consideration of the skin element stiffness results in decreasing the magnitude of the tie forces, as will be shown in the Granton field wall analysis.

7.8.1.b Vertical stresses in the soil

Comparison between the observed and the theoretical vertical soil stresses are shown in Figs (7.35) and (7.36). The predicted vertical soil stress lay very near to the theoretical overburden pressure $\gamma.h$.

In Fig (7.35) the measured vertical stresses in sections 50 and 250 mm from the wall face, are nearly twice the theoretical values, which could be due to an instrumentation error. The measured vertical stress distribution shown in Fig (7.36) is in reasonable agreement with the predicted vertical stress.

7.8.1.c Strains in the soil

7.8.1.c.1 Horizontal strains

The horizontal strains observed at three vertical sections in the model reinforced earth walls and the corresponding theoretical horizontal strains are shown in Tables (7.7) and (7.8).

The observed horizontal soil strains are substantially larger than the predicted horizontal strains. This difference may be attributed to:

(i) The theoretical analysis is based on small strain assumption.

(ii) Only elastic strains were predicted by the programme. The sand in the model was probably in a failure condition especially near the reinforced earth wall face.

(iii) In the programme the horizontal strain of the composite was assumed equal to the strain in the soil. Probably this is not valid for low fill heights, above the tie level since slippage between the ties and the soil might occur.

7.8.1.c.2   The vertical strains

The predicted vertical strains in the soil are appreciably greater than the observed vertical strains as shown in Table (7.9). Most probably the vertical soil stiffness used in the theoretical analysis was larger than the actual stiffness of the soil, since the sand was tested at confining pressures slightly higher than the pressures encountered in the model.

The predicted vertical soil strains are all -ve indicating compression. In some regions of the wall +ve soil strain, indicating expansion were measured. Probably this is due to a dilatancy effect, which is not accounted for in the programme.

7.8.1.d   Horizontal wall deflection

The measured horizontal model wall deflections, using the free field strain coils and the computed wall deflections are shown in Figs (7.37) to (7.39).

The predicted curves are nearly parabolic with the maximum deflection occurring near the midheight of the walls.

Comparison between the experimental and the predicted

wall deflections, showed that the discrepancy between the observed and predicted deflections, probably depends on the number of ties per skin element and the vertical tie spacing ΔH, used in different tests. For the case of one tie per panel and $\Delta H = 100$ mm, Fig (7.37) reasonable agreement was obtained between the observed and predicted values. For the case of three ties per skin element and $\Delta H = 250$ mm Fig (7.38), the observed and predicted wall deflections reasonably agreed at the upper and lower thirds of the wall. At the middle of the wall, the observed deflection was appreciably larger than the predicted deflection, probably due to the large vertical tie spacing of 250 mm adopted in building this wall. For the case of six ties per panel and $\Delta H = 83.3$, Fig (3.39), the observed horizontal wall deflection was smaller than the predicted wall deflection.
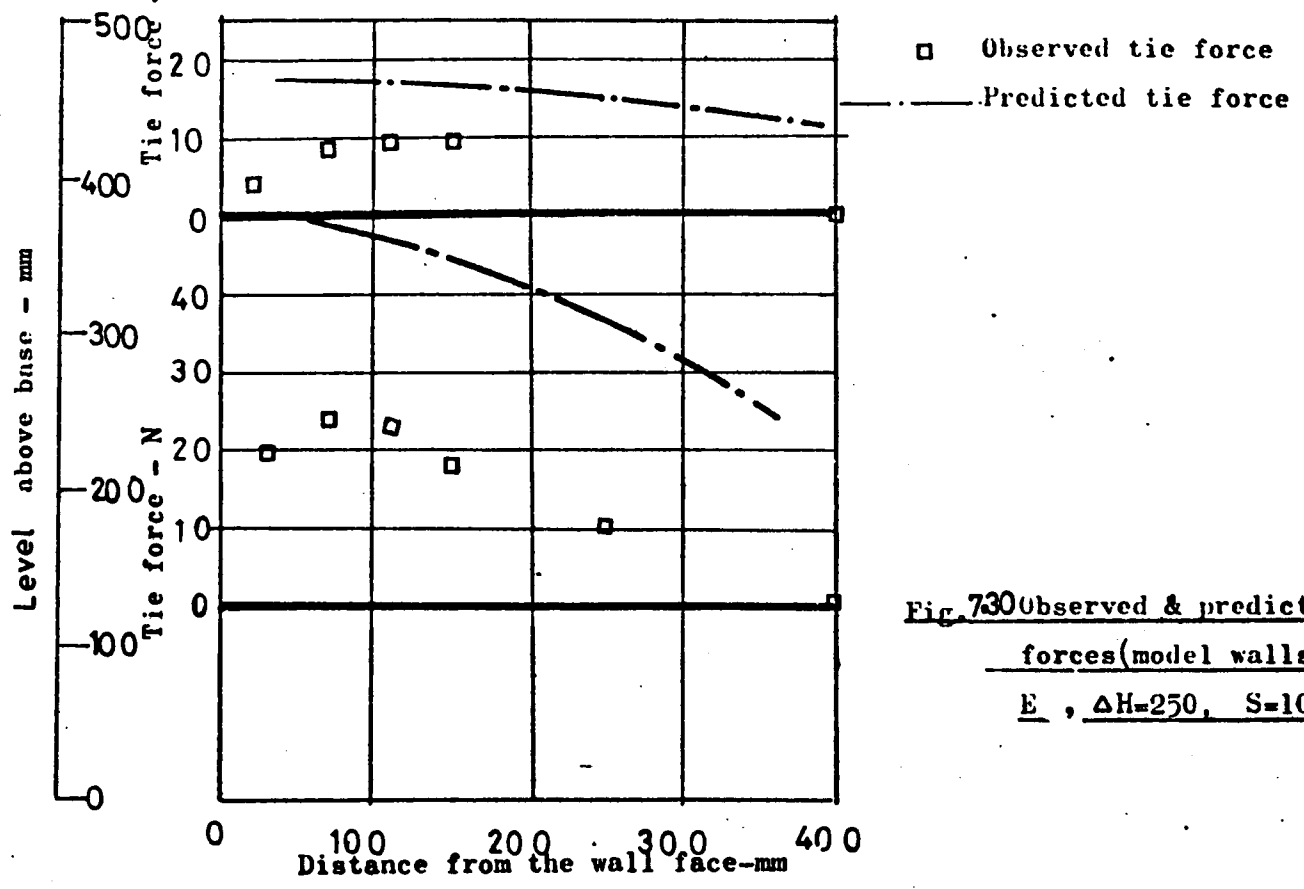
Fig. 7.30 Observed & predicted tie forces (model walls series E , $\Delta H=250$, $S=100$ mm)
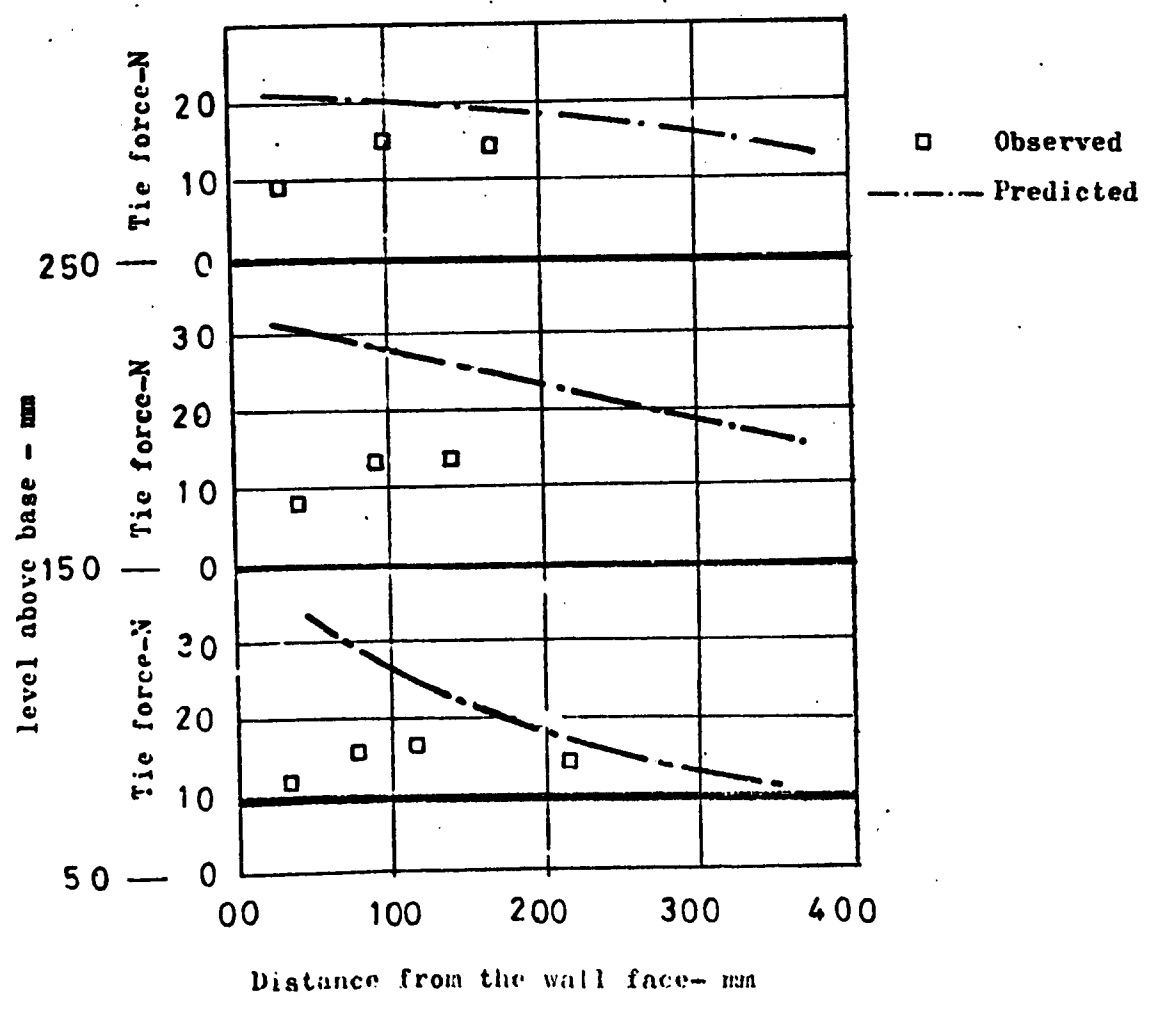
Fig 7.31 Observed and predicted tie forces @ different levels of model reinforced earth wall (series E , $\Delta H=100$, $S=150$mm)
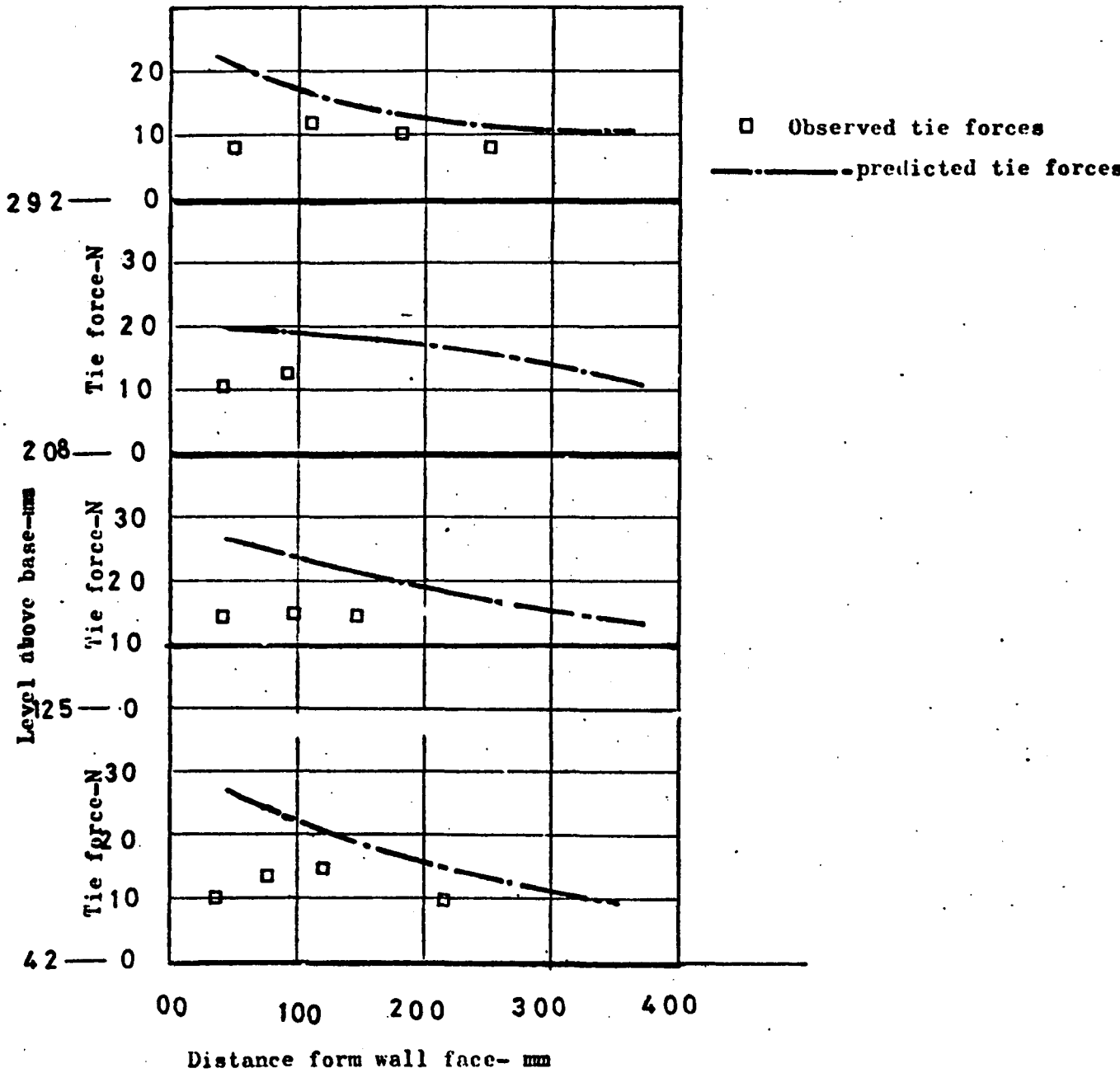
Fig 7.32 Observed & predicted tie forces @ different wall levels
(model wall series E , ΔH≈85.5, S=150 mm)
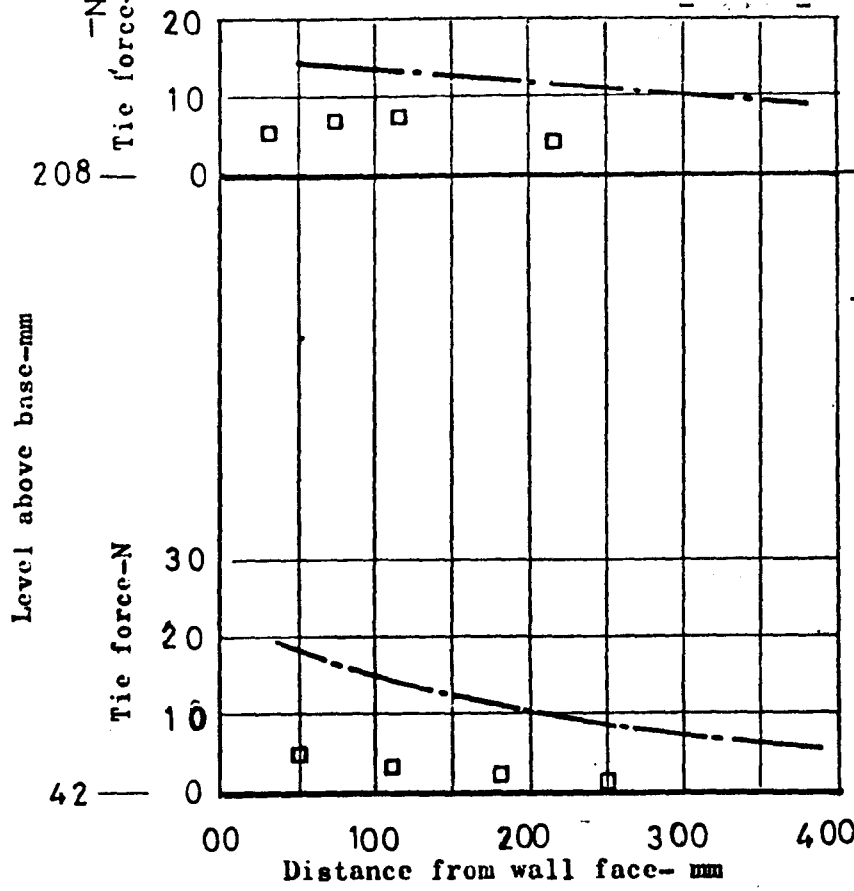
Fig.7.33 Observed & predicted tie forces(model walls series E , ΔH=83.3, S=100 mm)
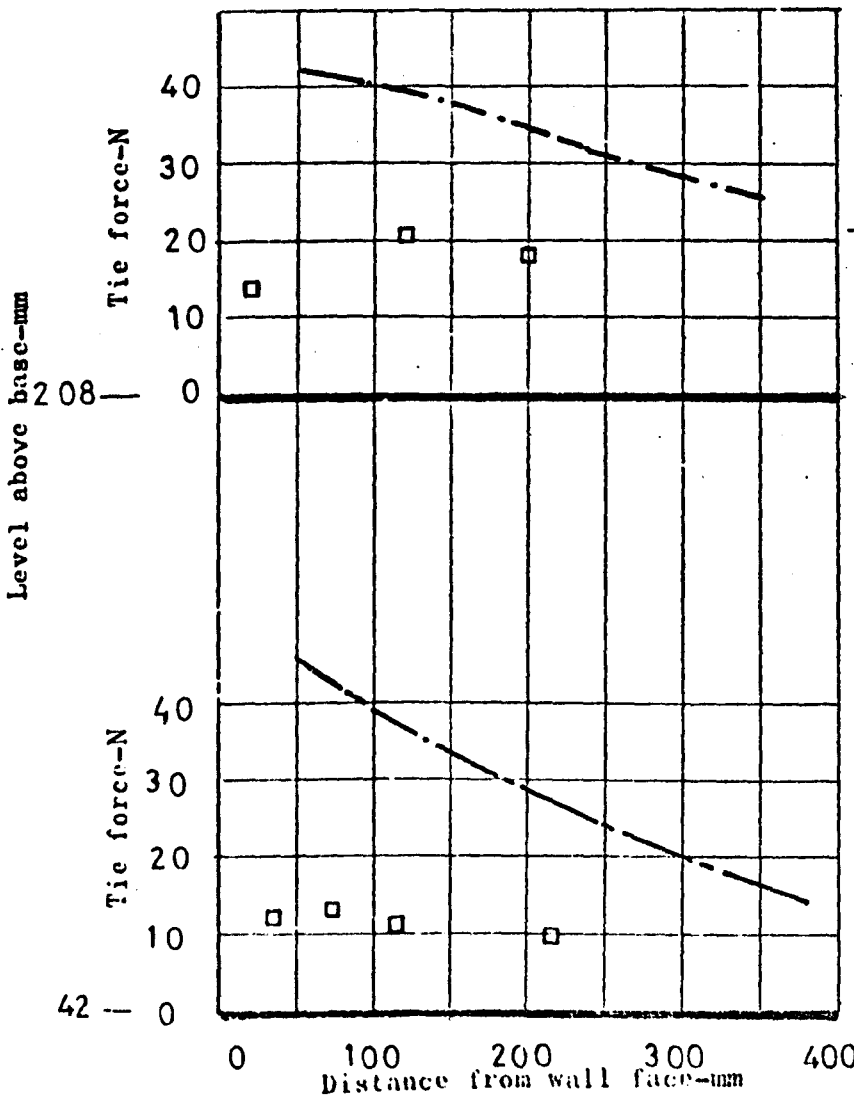
Fig.7.34 Observed & predicted tie forces(model walls series E , ΔH=83.3, S=300 mm)
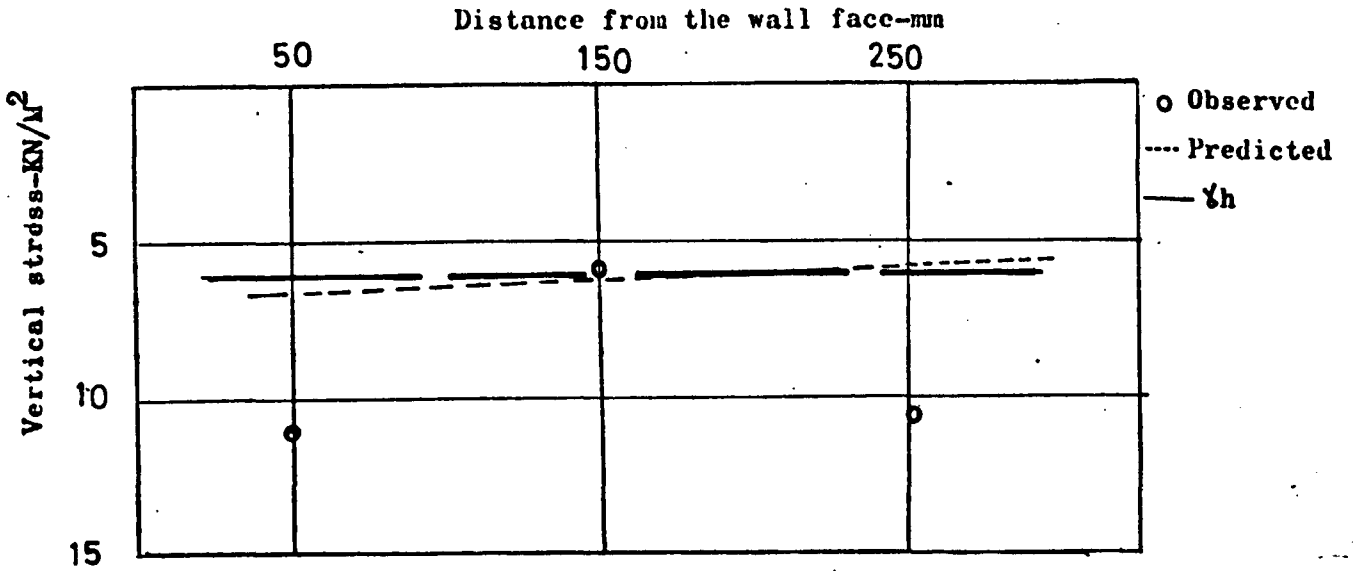
Fig.7.35 Vertical stress distribution @ section 125 mm above the model base
(model wall series E , ΔH=250, S=100 mm wall height=500 mm)
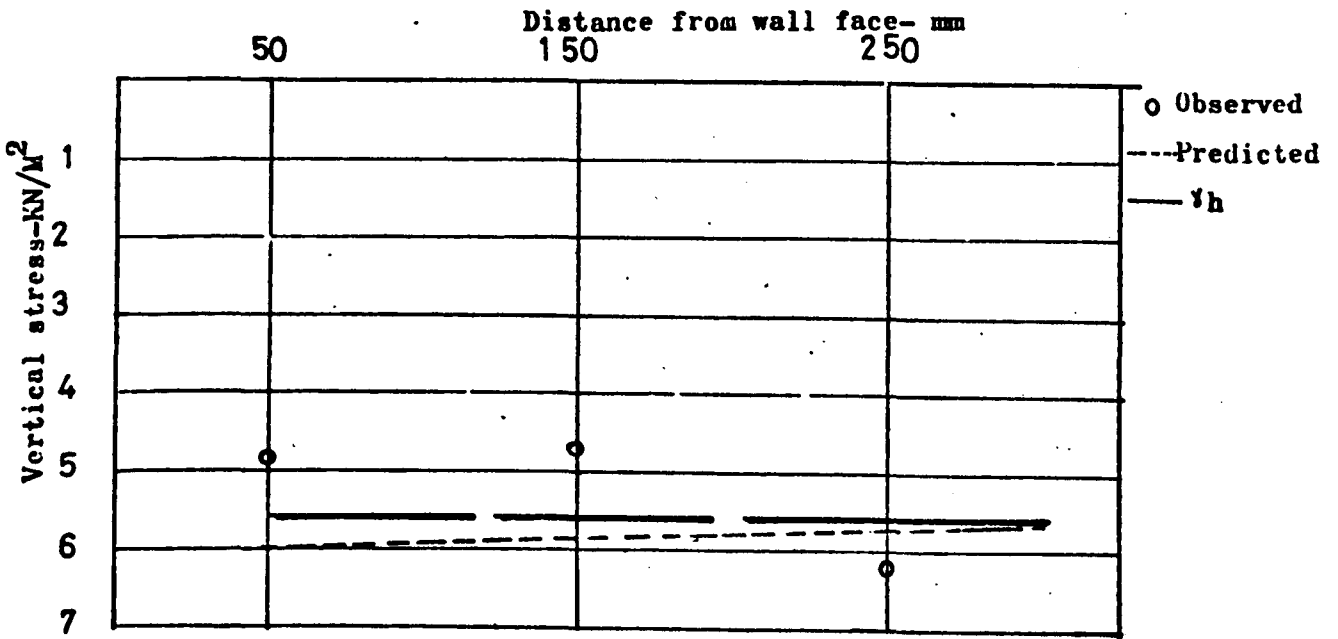
Fig.7.36 Vertical stress distribution @ section 150 mm above the model base
(model walls series E ,ΔH=100 , S=150 mm, wall height =500mm)
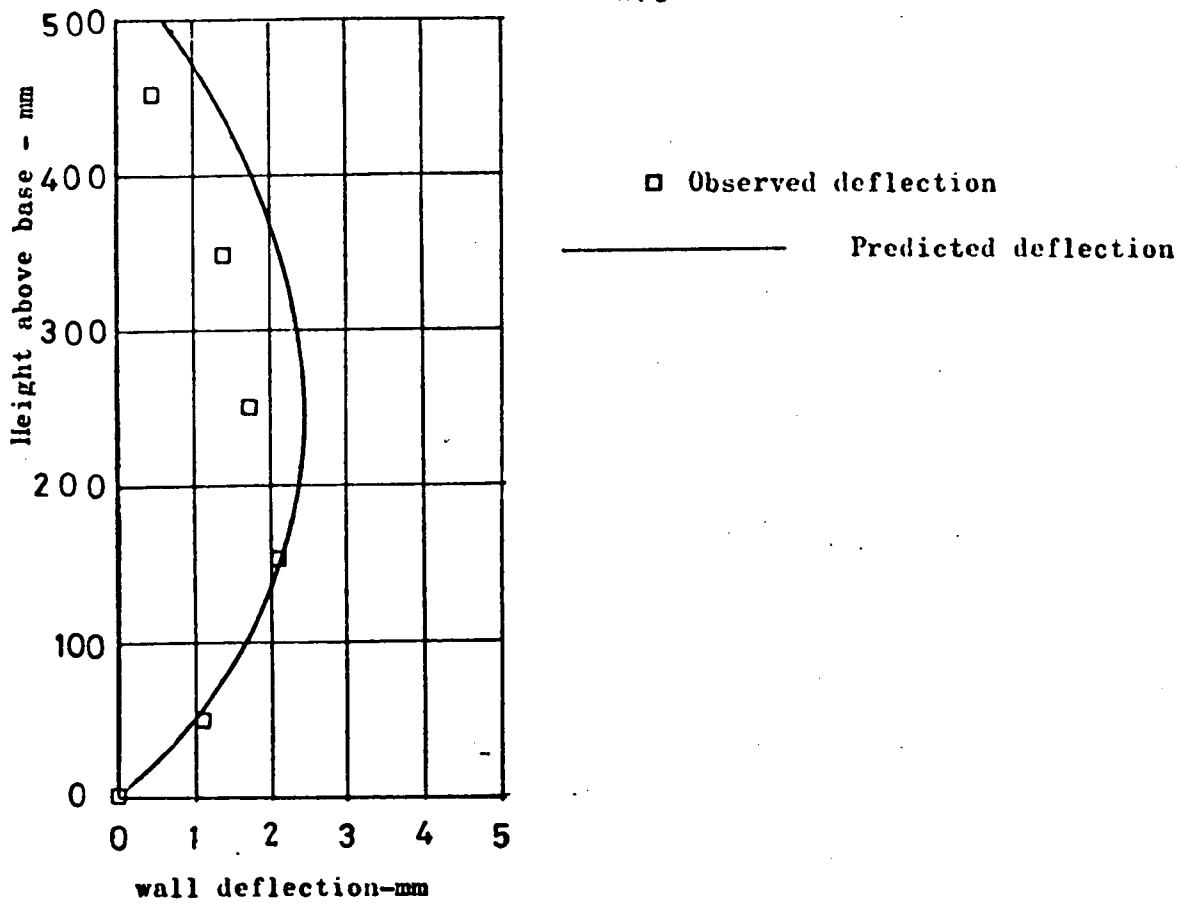
Fig.7·37 Observed & predicted horizontal wall deflection
(model walls series E , △H=100 , S=150 mm , one tie per panel)
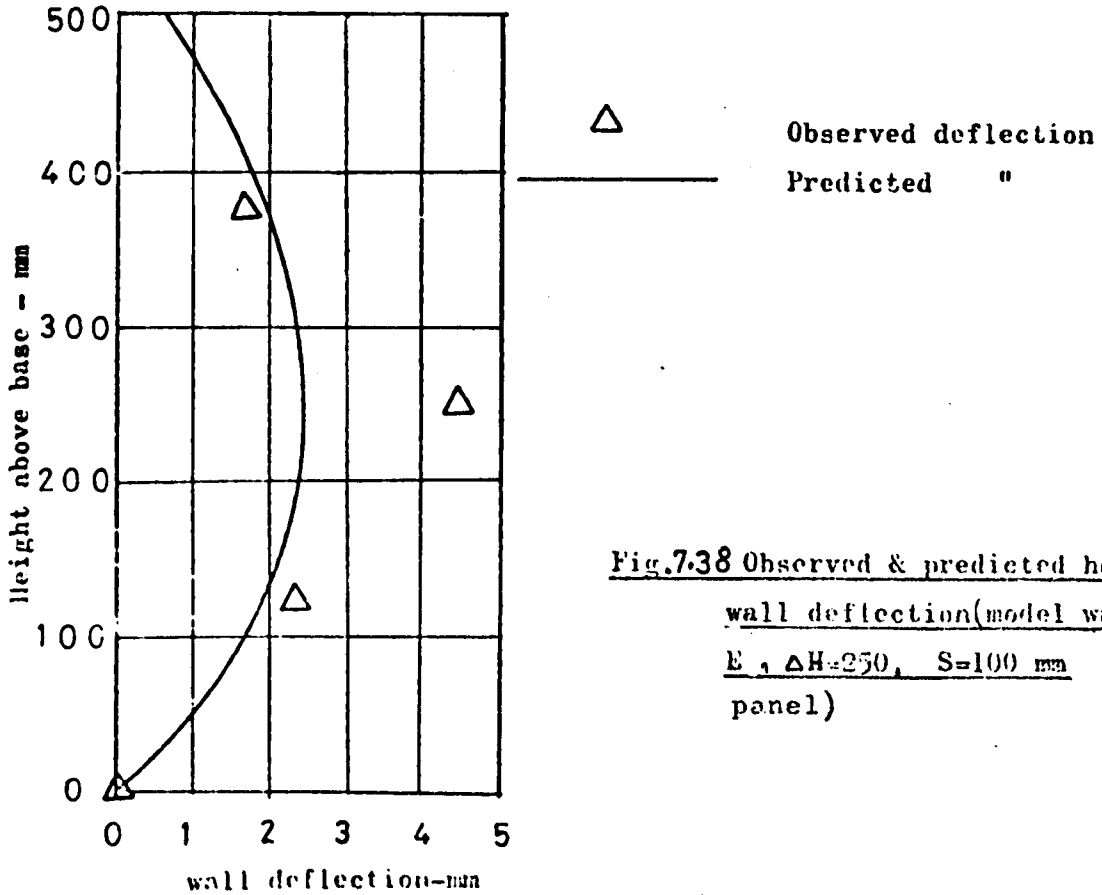
Fig.7.38 Observed & predicted horizontal
wall deflection(model walls series
E , △H=250, S=100 mm 3 ties per
panel)
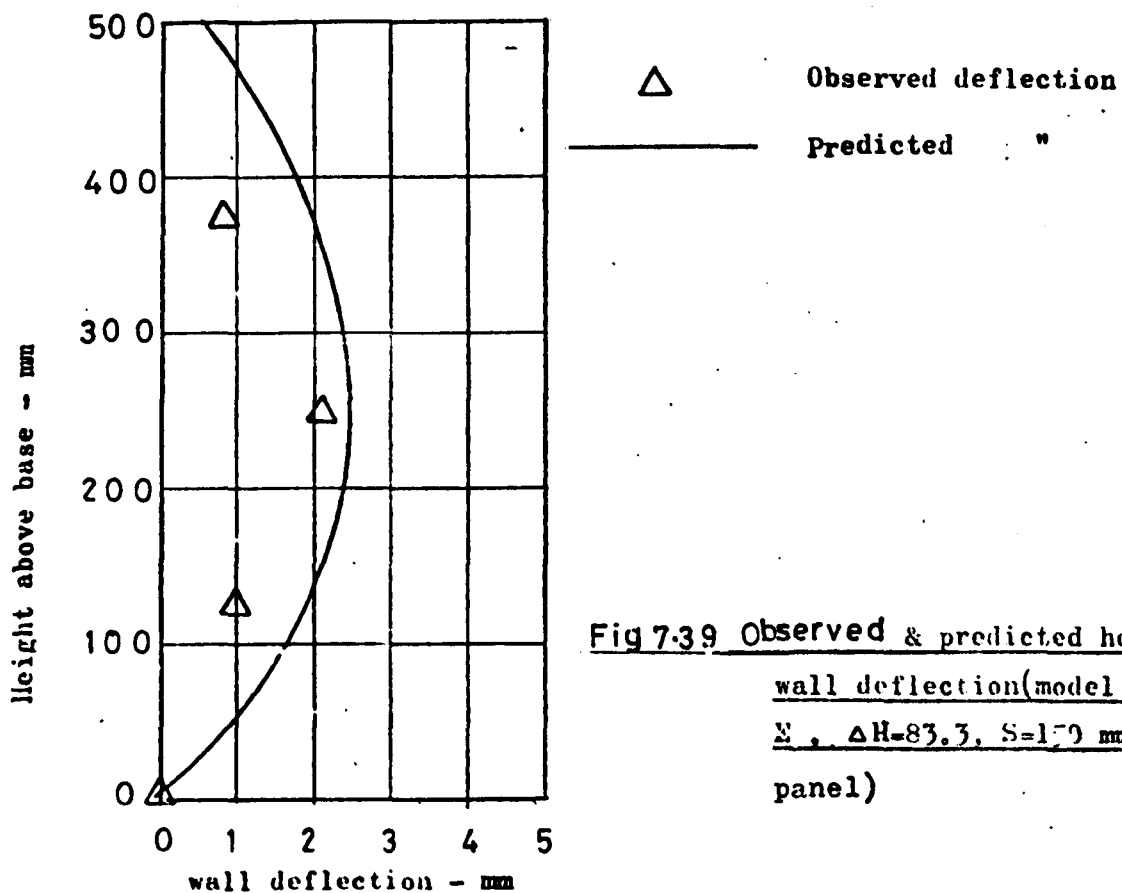
Fig 7.39 Observed & predicted horizontal wall deflection(model walls series Σ , ΔH=83.3, S=1:0 mm , 6 ties per panel)

TABLE (7.7) - Comparison between the observed and predicted
horizontal soil strain (model walls series E,
ΔH = 100 mm, S = 150 mm)

Distance of the vertical section from wall face - mm	Level above base of the model (mm)	Observed horizontal strain ε_x%	Predicted horizontal strain ε_x%
50	50	0.78	0.044
	250	0.83	0.026
	375	0.22	0.015
150	50	0.47	.024
	250	0.74	.021
	375	0.36	.014
250	50	-.128	0.018
	250	0.379	0.019
	375	0.360	0.012

TABLE(7.8) - Comparison between the observed and predicted
horizontal strains in the soil (model walls
series E, ΔH = 250; S = 100 mm)

Distance of the vertical section from wall face - mm	Level above base of the model (mm)	Observed horizontal strain ε_x%	Predicted horizontal strain ε_x%
50	125	1.64	.057
	250	4.8	.035
	375	0.183	.02
150	125	0.23	.04
	250	-2.79	.033
	375	0.157	.017
250	125	0.27	.048
	250	0.21	.039
	375	0.157	.019

TABLE (7.9) - Comparison between observed and predicted vertical strain in the soil (model wall, series E, $\Delta H = 100$, S = 150 mm)

Distance of the horizontal section above the model base mm	Distance from Wall face (mm)	Observed Vertical strain $\varepsilon_y\%$	Predicted Vertical strain $\varepsilon_y\%$
50	50	-.65	-5.4
	150	-	-5.05
	250	-.05	-4.96
150	50	-.058	-4.37
	150	+.15	-4.33
	250	+0.09	-4.25
250	50	-.238	-3.36
	150	+.21	-3.42
	250	+.15	-3.39

-ve   Compression

+ve   Expansion

7.8.2 Field wall

In Section 7.8.1 comparisons were made between the measured and predicted stresses and deformations, in the model wall. Unlike the model wall, the measured stresses and deformations in the Granton field wall were found to be affected considerably by the construction procedure,[29] thus making a direct comparison between the idealized finite element solution and the actual field wall behaviour difficult. However, in this section the stresses and deformations predicted by the finite element approach will be presented together with the actual stresses and deformations observed in the Granton field wall, to find out to what extent the idealized finite element solution can grasp the basic modes of variation of the stresses and deformations measured in the Granton wall.

7.8.2.a The tie forces

Figs (7.40)-(7.41) show the measured and predicted tie forces distribution along the ties. The predicted tie force distribution showed an irregular variation differing from the observed tie force variation.

7.8.2.b Pressure on panels and relative panel tilt

The observed and predicted pressure on the panels and the relative panel tilts are shown in Figs (7.42)-(7.43) respectively. The observed values of the pressure on the panels and relative panel tilts do not coincide with the corresponding predicted values using different assumptions of foundation and skin elements conditions.

Fig. 7.40 Observed & predicted tie forces in Granton field wall
(Assuming flexible found.)

▽ Observed tie force

_ _ _ _ _ _ _ predicted tie force(without considering skin stiffness)

_._._._._ predicted tie force(Taking skin stiffness into account)

distance from wall face - m
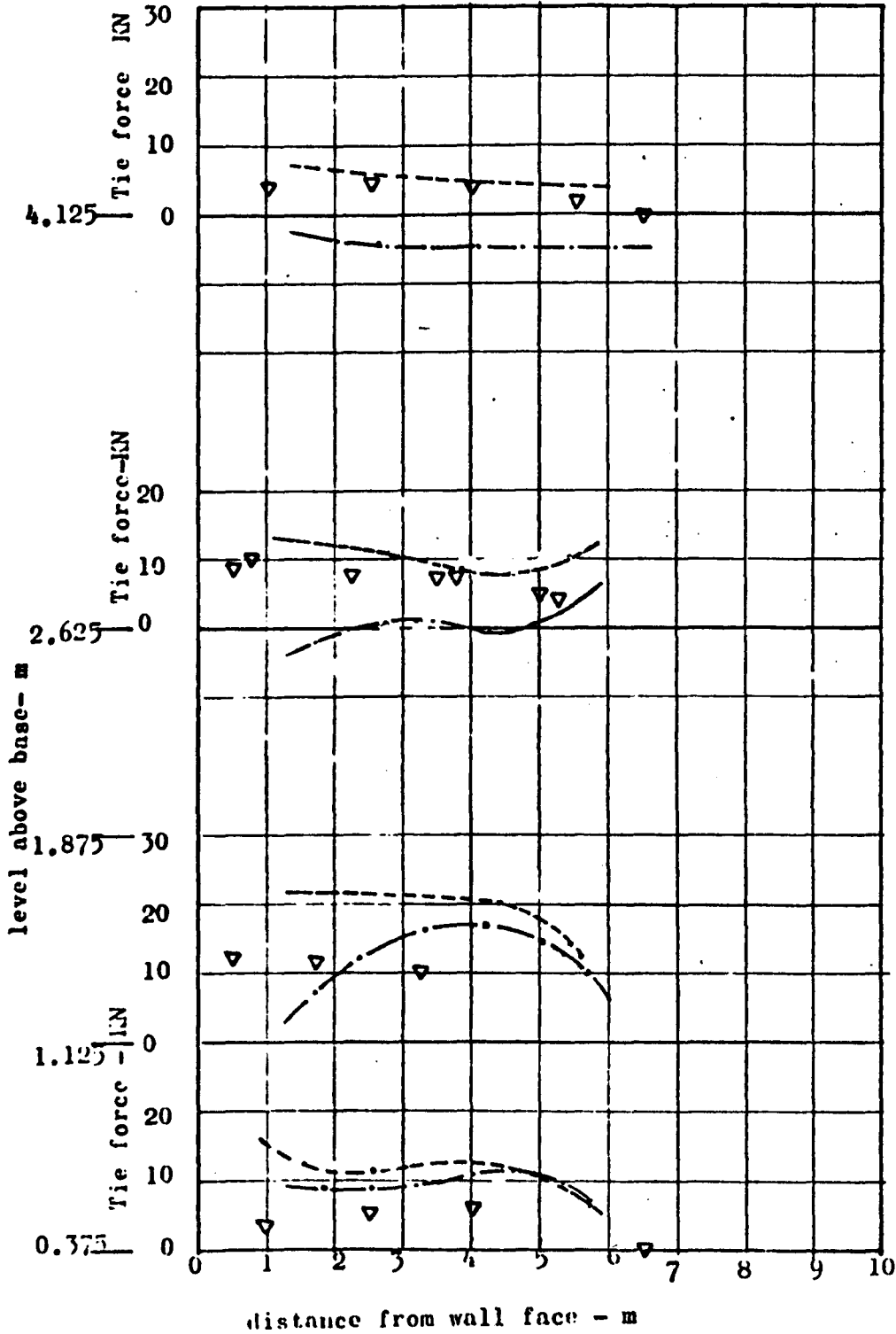
Fig. 7.41 Observed & predicted tie forces in Granton wall

(Assuming rigid found.)

□   Observed earth pressure

1-1   predicted(rigid found. & rigid skin elements)

2-2   "   ("   "   " neglecting skin stiffness)

3-3   "   (Flexible found. & "   "   ")

4-4   "   ("   "   &   rigid skin element)
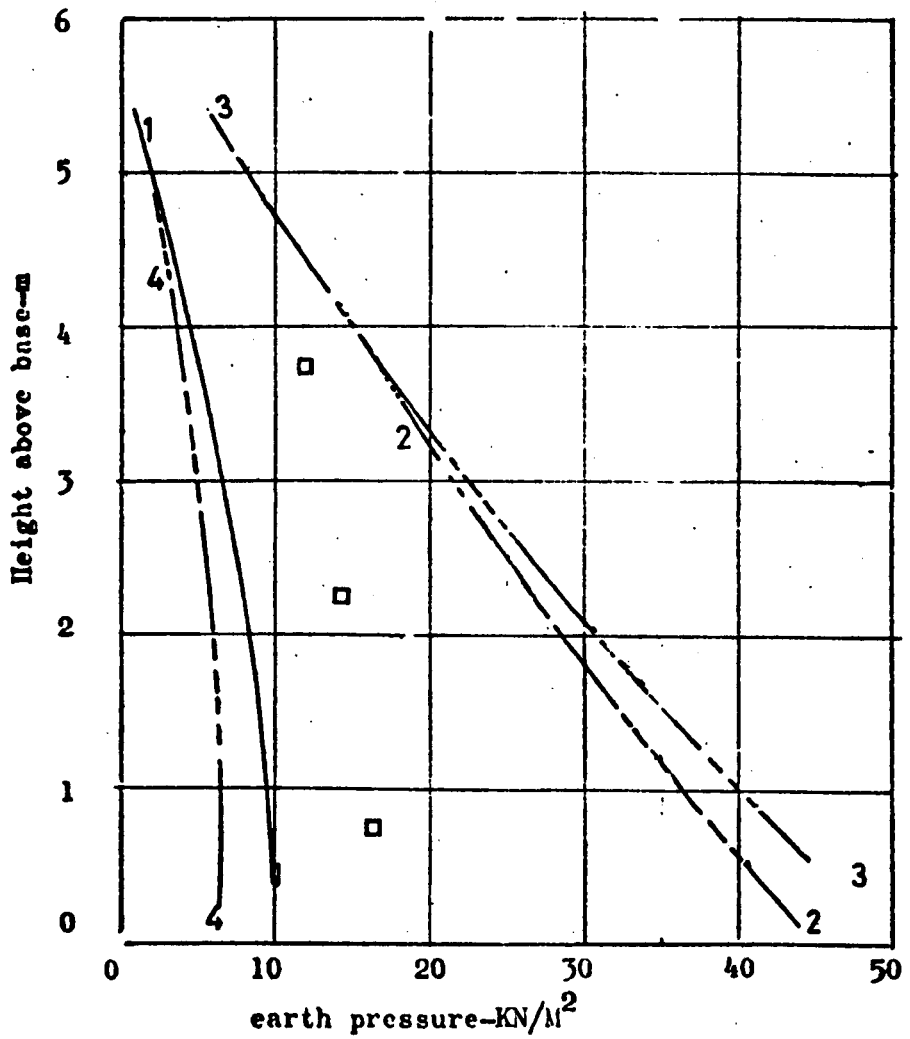
Fig.7.42 Development of earth pressure on Granton wall

■ Observed relative panel tilt
1-1 predicted Deflection(rigid found. & rigid skin,
2-2 " " (" " "neglecting skin
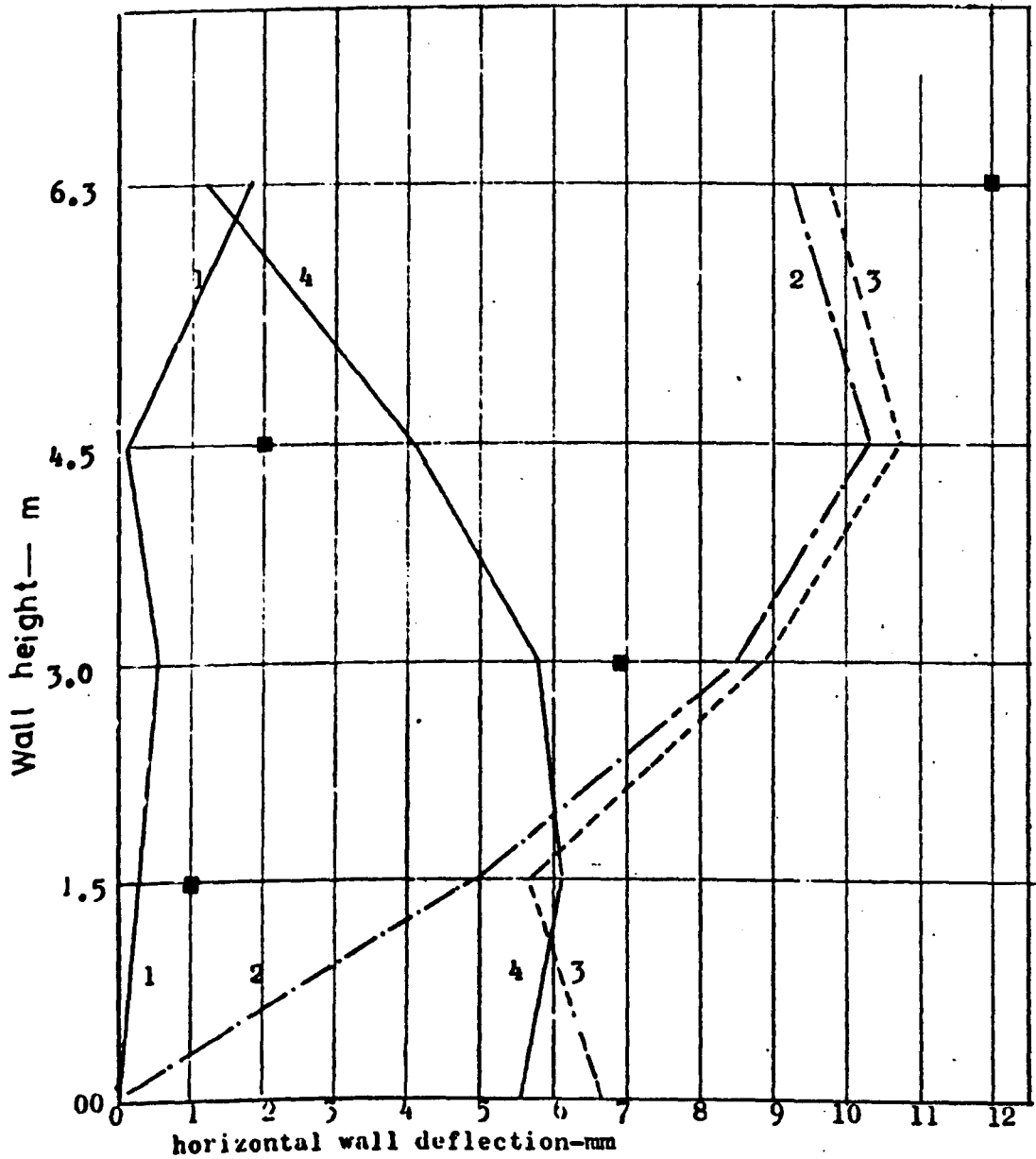
Fig. 7.43 Observed relative panel tilt & predicted wall deflection(Granton field wall)

7.9 Comparison between the finite element method and the Energy and Rankine theories

The maximum tie tension observed in two model walls was compared with the theoretical maximum tie tension envelopes calculated from the energy theory, the Rankine theory and the finite element prediction and are shown in Figs (7.44) and (7.45).

At the top of the wall the theoretical results obtained from the energy theory (LO.L.A.), the Rankine theory using an at rest earth pressure coefficient K_o and the finite element method are coincident.

At the middle and bottom of the walls the finite element method predicted higher tie tension than the observed data.

The general pattern of the tie tension envelope predicted by the finite element method, is similar to the tension envelope predicted by the energy theory (LO.L.A.).
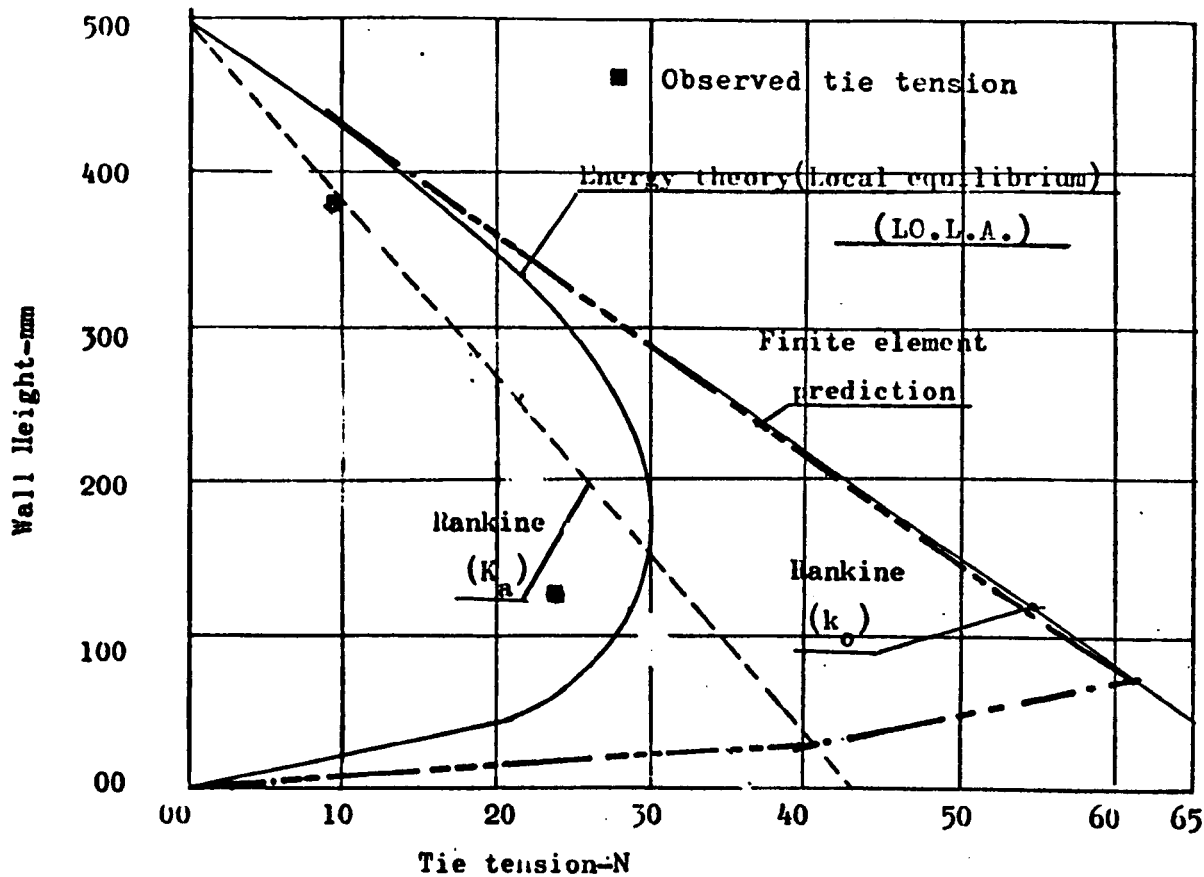
Fig.7.44 Comparison between tension envelopes predicted by the Energy theory, Rankine theory & the finite element method (model walls series E, ΔH=250 mm, S=100 mm)
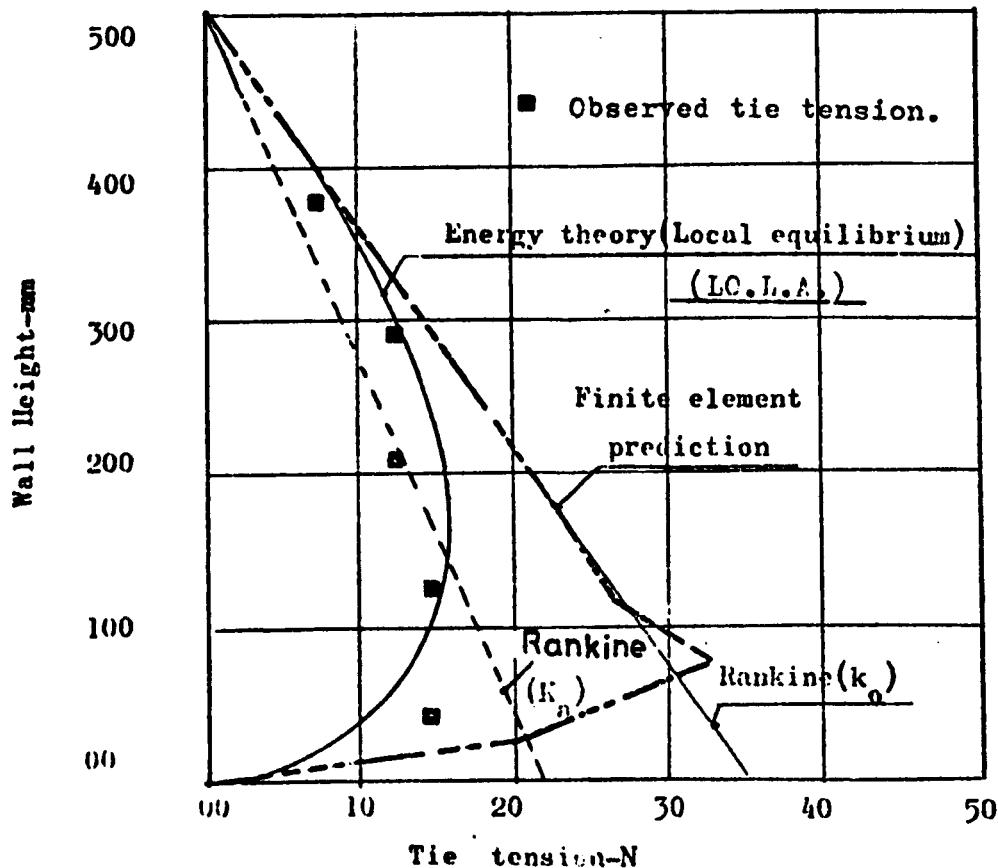
Fig.7.45 Comparison between tension envelopes predicted by Energy theory, Rankine theory & the finite element method, (Model walls series E, ΔH=83.3 mm, S=150 mm)

7.10 Conclusions

In this Chapter the theoretical behaviour of model and field reinforced earth retaining walls was studied using the finite element method. The results from the theoretical analyses were presented and compared with the observed data. The study indicated that the finite element approach, gives a complete theoretical solution for the stresses and strains in a reinforced earth wall. Different parameters influencing reinforced earth wall behaviour, such as skin element and foundation conditions can be varied. In this way the finite element analysis serves as a versatile mathematical tool, which can be used to assess the relative influence of various factors on reinforced earth wall behaviour.

However, from the results of the finite element method and discussions presented in this chapter, several points arose, regarding the model and the Granton field wall behaviour.

In the model the contours of the tie forces were found to be similar in pattern, irrespective of the tie spacing and showed a mode of tie tension variation along horizontal sections in the wall, which is of a maximum at the wall face and decreases towards the back of the wall. Comparison between the results of the finite element analysis and the observed stresses and deformations in the model revealed that the finite element analysis predicted appreciably larger tie forces and vertical soil strains than the observed values. The predicted horizontal soil strains were appreciably lower than the observed values. While the computed horizontal wall deflections did not correspond completely in magnitude with the observed deflections, deflected shape of the wall, given by the computed and observed deflections was similar. The discrepancy in the magnitude of the observed and predicted wall deflections was found to depend on the vertical tie spacing and the number of ties per skin element. For the case of one tie per skin element and $\Delta H = 100$ mm reasonable agreement was noted between the observed and predicted wall

deflections.   The computed vertical stresses lay very near
to the overburden pressure γh.   The pressure cells in some
cases gave an erroneous indication of the vertical stress
and in other cases gave reasonable agreement with the computed
vertical stresses.

The discrepancy between the observed and predicted
stresses and deformations in the model, was probably attributed
to the limitations of the programme outlined in Section(7.4).
In the programme the sand was assumed to be isotropic and to
behave elastically.   It has been reported [26]   that the
behaviour of materials which dilate, such as the sand used
in the present model, cannot be characterized accurately by
a single value of Poisson's ratio ν .   The stiffness of
the skin element was neglected in the theoretical analysis
of the model walls, and this may also have had an effect in
the deviation noted between the observed and predicted
values.

For the full scale situation, the finite element method
helped to study the relative effects of the skin element and
foundation conditions on the Granton field wall.   The
actual stresses and deformations developed in the Granton
wall, have been found[29]   to be affected by the wall
construction procedure, and these were presented together
with the idealized finite element solution.   The finite
element results showed some similarities in modes of varia-
tion with the observed field wall data, but the magnitudes
were different.

Comparison between the finite element solutions,
the Energy and the Rankine theories, for cases of two model
walls, revealed that the finite element prediction coincided
with the energy theory (LO.L.A.) and the Rankine theory
using an at rest coefficient of earth pressure K_o, at the
top of the wall, although the finite element method
appreciably overestimated the stresses in the ties near the
middle and bottom of the walls.

For the application of the finite element method in the
design of full scale reinforced earth walls, the effects of

various aspects such as compaction stresses, skin element
stiffness and foundation conditions have to be accurately
modelled in the analysis.   If the backfill material is
expected to dilate or contract,such as sand in dense and
loose states respectively, procedures which reflect the
effect of the shear stresses on the volume change
have to be incorporated in the finite element analysis.
Generally the use of the finite element in the design is
costly in terms of preparation time and computer facilities.

CHAPTER EIGHT

CONCLUSIONS

Detailed conclusions of the studies carried out on the reinforced earth retaining walls in this thesis have been recorded at the end of each chapter. Conclusions based on all the studies presented in the preceding chapters will only be outlined in this concluding chapter.

With reference to the existing theories applied to reinforced earth retaining walls, rectangular in cross-section and using a cohesionless material as backfill, the following conclusions were reached:

(1) For walls consisting of a large number of layers and having a smooth back the Rankine and the Coulomb theories predict identical values of tie tension.

(2) The Trapezoidal and Meyerhof vertical stress distributions resulted in higher tie tensions than the Rankine theory, depending on the $\frac{H}{L}$ ratio of the wall and $\emptyset$ value of the backfill material. In most cases in practice, where $\frac{H}{L} \doteq 1$ and $\emptyset$ is relatively high, the Trapezoidal method predicts higher tie tensions than Meyerhof method and the difference between the tie tension predicted by the Trapezoidal and the Rankine methods is about 25 per cent or less compared to the Rankine values.

(3) The Rankine theory, being the main theory currently used in the design of reinforced earth walls is based on the simplifying assumption that the vertical direction is principal for the vertical stress. This gives a linear tie tension distribution with wall depth and implies a maximum tie tension at the face of the wall.

(4) None of the above theories takes into account a nonlinear tie tension variation over the tie length. All the above theories predict a maximum tie tension at the bottom of the wall.

With reference to the Energy theory developed in the present study the following conclusion was reached:

(5)   This theory can take into account non-linear tension distribution both over the tie length and over the wall depth, the effect of the tie length on the tie tension, and the deflected shape of the wall.

With reference to the model test results, and their comparison with design predictions, the following conclusions were reached:

(6)   The observed critical heights of walls failing by tie breaking were appreciably higher than the theoretical values predicted by the Rankine, the Trapezoidal, Meyerhof and Banerjee methods.   The various Energy theory expressions (LO.L.A., LO.L.D., T.L.L.A., T.L.L.D. and T.P.P.D.) each predicted different critical heights but all the results from the Energy theories were closer to the observed values than the predictions from the existing theories.

(7)   Comparison between the experimental and the theoretical adherence lengths, indicated that generally all theories overestimated considerably the adherence length.   The Energy theory (LO.L.A.) predicted shorter ties than any of the existing theories.

(8)   Measurements of the tie tension in the model reinforced earth walls indicated that the tie tension increases from the face of the wall to a maximum in the front half of the tie and decreases to zero at the free end of the tie.   For ties near the bottom of the wall the maximum tie tension generally lies near the wall face.

(9)   The observed maximum tie tension was found to decrease with increasing tie length.   The Energy theory expressions (T.L.D. and T.P.D.) predicted nearly similar trends and magnitudes to the observed values, although the Energy theory (LO.L.A.) gave higher magnitudes but with similar trend. The Rankine theory predicted a constant value of tie tension which was independent of the tie length.   The Trapezoidal and Meyerhof methods predicted a decreasing tie tension with increasing tie length which approached the Rankine values when the tie length L was large.   The Rankine, the

Trapezoidal and Meyerhof methods predicted higher magnitudes of tie tension than the observed values.

(10) The observed maximum tie tension was found to increase with increasing wall depth but a decrease in the value of the observed maximum tie tension was noted at bottom tie level. The Energy theory (LO.L.A.) gave a similar mode of variation to the experimental results. This method predicted larger tie tensions for walls built with relatively large tie spacings, and the difference was found to decrease with decreasing tie spacing. The Energy theory (T.L.L.D.) gave a maximum underestimate of the observed tie tension of about 25 per cent of the observed value. The Rankine theory gave a maximum underestimate of the observed tie tension, at the top of the wall, of about 28 per cent and minimum over-estimate of 37 per cent of the observed tie tension at the bottom of the wall.

(11) The non-dimensional tension factor $X = \dfrac{T_m}{\gamma h \, \Delta HS}$
for model walls built to a maximum height of 500 mm, was found to be a maximum at the top of the wall ($\doteq 0.40$) and decreased to a minimum value at the bottom of the wall ($\doteq 0.075$). The Energy theory (LO.L.A.) gave a similar pattern to the observed results. The Trapezoidal and Meyerhof methods predicted an increasing non-dimensional tension factor with fill height which was different in magnitude and pattern from the observed non-dimensional tension factor X. The Rankine and Banerjee methods gave constant values of the non-dimensional tension equal to 0.22 and 0.35 respectively which were also different from the observed values.

(12) For a rectangular reinforced earth wall with uniform tie distribution, the safety factor against tie break was a maximum at the top of the wall and decreased towards the bottom of the wall. The safety factor against tie pull out calculated on the basis of various assumptions of tie tension (maximum or average) and the tie length (all or part effective),

was a minimum at the top of the wall and increased towards
the bottom of the wall.

(13) The Energy theory (LO.L.A.) appeared to give a lower
limit of the observed safety factor against tie break. The
Energy theory (T.L.L.D.) and the Rankine theory predicted
higher safety factors against tie break in some cases.

(14) Comparison between the experimental and the theoretical
safety factors against tie pull out, indicated that none
of the existing methods suggested by the previous investigators
for calculation of the safety factor against tie pull out,
completely agree with the experimental results.

The Energy theory (LO.L.A.) appeared to predict the
general trend of the experimental results, although it did
not correspond completely in magnitude with the experimental
values. The Energy theory (T.L.L.D.) predicted higher
magnitudes and a different pattern from the experimental
results.

(15) Measurements of the horizontal strains in the soil,
showed maximum positive strains indicating expansion, near
the wall face and negative strains indicating compression
at sections lying furthest from the wall face. From these
strain measurements, it was concluded that the state of stress
in the soil near the wall face was probably tending towards
an active state of stress and the soil furthest from the
wall face was probably tending towards a passive state of
stress.

(16) The wall deflections calculated from the observed
horizontal strains in the soil, were found to lie close to
the directly measured horizontal wall deflections, indicating
compatibility between the observed horizontal soil strains
and the measured wall deflections.

(17) The pattern of the vertical soil strain appeared to
indicate the effect of the horizontal thrust at the back of

the wall. The pattern of the vertical soil stress did not show such an effect. These two measurements do not appear to be compatible and were attributed probably to inconsistent pressure cell behaviour with particular regard to their calibration factors.

From analysis of tie tension at the Granton full scale wall the following conclusions have been reached:

(18) A study of the maximum observed tie tension versus fill height curves indicated that compaction stresses affect the observed tie tension for low ($\doteq$ 1.50m) fill heights above the tie level, and that the compaction effect diminishes with increasing fill height above the tie level. A simplified theoretical analysis showed a similar effect and supported the supposition that the large increases in tie tension at relatively low fill heights above the tie was due to the compaction operation.

(19) The plots of the observed maximum tie tensions with wall height along with predictions from the corresponding Energy theory (LO.L.A.) and the Rankine theory indicated that both theories appreciably underestimated the observed maximum tie tension. The Energy theory (LO.L.A.) was found to predict a pattern of tie tension distribution which is similar to the general pattern of the observed tie tension. The observed maximum tie tension points were found to lie within the theoretical curves calculated from the Energy theory for K $=$ 0.18 and 0.327. Therefore, compaction probably resulted in increasing the K value of the backfill. To prevent this happening in practice it is desirable that compaction procedure should be controlled.

(20) The non-dimensional tension factor χ, evaluated from the observed maximum tie tension, was found to be a maximum at the top of the wall ($\doteq$ 0.30) and decreased towards the the bottom of the wall ($\doteq$ 0.1). This behaviour was predicted by the Energy theory (LO.L.A.). Banerjee and Rankine gave constant non-dimensional tension factors which were different from the observed results.

(21)   The construction procedure appeared to lower the
actual safety factors of the wall against tie break and
tie pull out.   Localized slippage of the ties was possible
when the fill heights above the tie level were less than
1.70m.   The completed full scale wall had a large safety
factor against tie break having a minimum value of 4.93 and a
smaller safety factor against tie pull out and its minimum
value was equal 1.70.   Hence a full scale wall is more
likely to fail by tie pull out than by tie break.

(22)   Some similarities in behaviour were noted between the
Granton full scale wall and model walls regarding the tie
tension distribution along a tie length and with wall height,
and also with the variation in the non-dimensional tension
factor with fill height above a tie level.

From theoretical studies on the model walls based on
a plane strain finite element programme, the following
conclusions have been reached:

(23)   The plane strain finite element analysis predicted a
maximum tie tension at the wall face decreasing towards the
back of the wall.

(24)   The non-dimensional tension factor X , predicted by
the finite element analysis was found to range between 0.45
at the top of the wall to 0.10 at the bottom of the wall.
This range was slightly higher than the observed range of
the non-dimensional tension factor, which was found to lie
between 0.40 at the top of the wall to 0.075 at the bottom
of the wall.

(25)   The finite element analysis predicted generally
appreciably higher magnitudes of tie tensions and vertical
strains in the soil than the observed values.   The predicted
horizontal strains in the soil were appreciably lower than
the observed values.   The analysis predicted similar patterns
of wall deflections to the observed results and the
magnitudes of the two sets of results seemed to correspond

with each other in some cases. The discrepancy between the
observed and the predicted values was attributed probably to
the limitations of the finite element programme, with
particular regard to the idealization of the sand as an
elastic material.

From the analysis of the Granton field wall, based on
the finite element approach, the following conclusions were
reached:

(26)   The observed wall behaviour was found to be affected
by the construction procedure.   The finite element analysis
indicated that the theoretical wall behaviour was also
affected by the foundation and the skin element conditions.

(27)   The finite element analysis predicted some similarities
in mode of variation of the observed tie tensions, although
the magnitudes were different.   No agreement was reached
between the observed relative panel tilts and pressure on
the panels and the corresponding theoretical values.

(28)   For the use of the finite element method in the design
of full scale wall, additional factors such as compaction,
foundations and skin elements have to be taken into account.
If the backfill material is expected to dilate under the
shear stresses, procedures which reflect the changes in
volume under shear stresses would have to be incorporated
in the finite element analysis.

Concluding Remark

The present study aimed at investigating the behaviour
of reinforced earth walls, rectangular in cross-section with
cohesionless backfill and built on rigid foundation, on an
experimental and theoretical basis.

From the observations on model walls, a design procedure
founded on an energy approach has been developed. Comparisons
with experimental results obtained from laboratory scale

model walls indicated closer agreement with the Energy
theory (LO.L.A.) than the existing theories.

The Energy theory was further applied for a full scale
wall case and it was found to predict smaller tie stresses
than the observed values.   This was attributed to the
construction procedure which appeared to have an effect on
the full scale wall behaviour.

Recommendations for further studies on reinforced earth
walls will be outlined in the following section.

Future Work

The following recommendations are made for further
studies on reinforced earth retaining walls:

(1)   The Energy theory proposed by the author for the design
of reinforced earth walls can be further extended to take
account of the foundation flexibility, the skin element
stiffness and the compaction stresses.

In this theory various modes of wall deflection, earth
pressure distribution and tension variation over the tie
length may be incorporated in the analysis.   The results
may be compared with model test results.

(2)   The model studies conducted by the author were limited
to rectangular walls.   From the Energy theory it was shown
that there may be an advantage in building walls of different
shapes to reach a nearly optimum design.

(3)   Study of model walls under different types of surcharge
loadings is also recommended.

(4)   Full scale wall behaviour may be affected by different
factors such as:
     (a)   The residual compaction stresses.
     (b)   The stiffness of the skin elements.
     (c)   The flexibility of the foundation.

(d)   The presence of clay fraction in the wall back
fill. This affects the soil-tie coefficient of
friction and the internal stability of the wall.

These aspects may be studied on laboratory scale models.
Points a ,b , c   and   d can also be studied on an analytical
basis.

(5)   Study of suitable tie materials to be used in full scale
reinforced earth structures. At present stainless steel and
aluminium are mainly used.   Plastics and certain fabrics
may be considered as other alternatives.

(6)   Study of corrosion of metal ties.

(7)   The finite element analysis could be further developed to:

(i)   Account for inelastic and anisotropic soil
behaviour.

(ii)   Represent the soil as a no-tension material.

(iii) Allow for slip between the soil and the ties
and the development of plastic zones near the wall face.

(iv) Account for volume changes in the soil and the
subsequent changes in their elastic properties.

APPENDIX I

Relationship between the non-dimensional tension factor χ and the angle β of inclination of the failure plane with the vertical

The relationship between the non-dimensional tension factor χ and the angle β, of inclination of the failure wedge with the vertical, Fig (3.6) was tested by calculating the numerical values of χ and β from equation (3.14), using values of safety factors ranging from 2 to 8 and angles of internal friction of soil $\emptyset$, from 25° to 50°. The β values were varied from 10° to 80° and the corresponding χ values were calculated. Results of calculations for a cohesionless material are shown in Table (I.1). It can be seen from Table (I.1) that χ values increase with increasing β values, up to a maximum and then decrease.

Similar behaviour of the relationship between χ and β was noted for the case of a backfill material with some cohesion.

Angle of failure wedge with the vertical-β	The non-dimensional tension factor - χ															
	Safety factor 'SF = 2'				Safety factor 'SF - 4'				Safety factor 'SF = 6'				Safety factor 'SF = 8'			
	ϕ=25°	ϕ=30°	ϕ=35°	ϕ=40°	ϕ=25°	ϕ=30°	ϕ=35°	ϕ=40°	ϕ=25°	ϕ=30°	ϕ=35°	ϕ=40°	ϕ=25°	ϕ=30°	ϕ=35°	ϕ=40°
10	0.526	0.444	0.378	0.322	1.075	0.912	0.780	0.669	1.624	1.380	1.184	1.016	2.173	1.848	1.585	1.364
20	.802	0.692	0.597	0.513	1.679	1.465	1.281	1.118	2.556	2.239	1.965	1.723	3.433	3.012	2.649	2.328
30	0.958	0.833	0.721	0.618	2.064	1.833	1.625	1.433	3.170	2.833	2.529	2.248	4.277	3.833	3.436	3.063
40	1.0341	0.898	0.770	0.648	2.320	2.083	1.860	1.648	3.605	3.267	2.950	2.648	4.891	4.452	4.041	3.648
50	1.0381	0.884	0.734	0.587	2.476	2.231	1.994	1.761	3.913	3.578	3.254	2.934	5.351	4.926	4.514	4.108
60	0.9392	0.75	0.561	0.368	2.515	2.250	1.985	1.716	4.091	3.75	3.409	3.063	5.667	5.250	4.833	4.410
70	0.615	0.342	0.061	-.234	2.324	1.995	1.655	1.298	4.034	3.647	3.248	2.830	5.744	5.300	4.842	4.362
80	-.596	-1.157	-1.754	-2.403	1.253	0.659	.0257	-0.661	3.101	2.474	1.806	1.0813	4.949	4.289	3.586	2.823

TABLE (I-1) - Values of the non-dimensional tension χ, corresponding to the angle of inclination of the failure wedge with the vertical calculated from Equation (3.14) for different values of SF and ϕ (cohesionless material $\chi_0 = 0$)

APPENDIX II

Equation of strain energy stored in a tie
due to normal loads
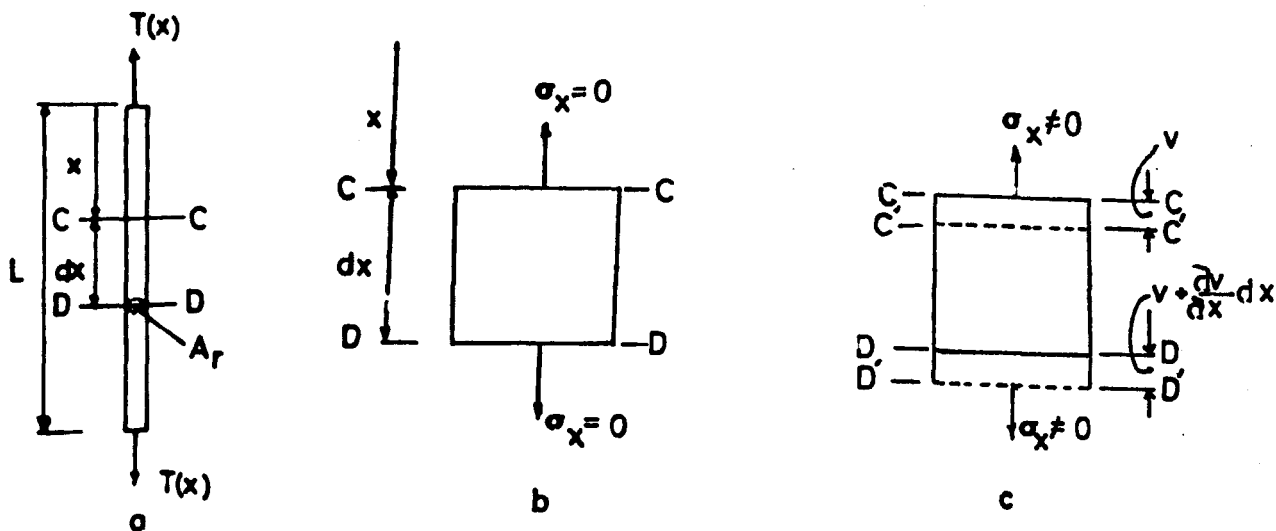
Fig II-1

In order to calculate the strain energy stored in a
tie only axial stresses were assumed to be acting on a tie.
As shown in Fig (II.1) the elastic strain energy due to an
external load T(x) can be calculated by the principle of
strain energy described by standard text books on the
theory of structures, e.g. Borg et al.[10]

The tensile strain $\varepsilon_x = ((v + \frac{\partial v}{\partial x} dx) - v)/dx$

$$\varepsilon_x = \frac{\partial v}{\partial x}$$

As the displacement of Section C-C, Fig (II.1.a) changes by
an amount dv, the displacement of section D-D changes by an
amount $d (v + \frac{\partial v}{\partial x} dx)$ and σ_x changes by $d\sigma_x$.

Consider the work done by external force T(x) and
neglecting higher order terms.

Work done $- A_r \cdot \sigma_x \cdot d(v + \frac{\partial v}{\partial x}) - A_r \, \sigma_x \cdot dv$

$$- A_r \cdot \sigma_x \, d(\frac{\partial v}{\partial x}) \, dx$$

Work done (Tie length dx) $= dU_i = \int_0^{\sigma_x} A_r \cdot \sigma_x \cdot d(\frac{\partial v}{\partial x}) \, dx$

or $dU_i = \int_0^{\sigma_x} A_r \cdot \sigma_x \cdot d\varepsilon_x \cdot dx$

substituting $\varepsilon_x = \frac{\sigma_x}{E_r}$ (Hooke's Law)

$\therefore$ Total work done $= U_i = \int_0^L \int_0^{\sigma_x} A_r \cdot \frac{\sigma_x}{E_r} \, dx \cdot d\sigma_x$

$$U_i = \int_0^L \frac{A_r \cdot \sigma_x^2}{2E_r} \cdot dx$$

or $U_i = \int_0^L \frac{T^2(x)}{2A_r \cdot E_r} \cdot dx$ ....(II.1)

APPENDIX III

Calculation of strain energy stored in a tie

For the assumed linear and parabolic tie tension distribution shown in Fig (3.11), the strain energy stored in a tie can be calculated as follows.

From the assumed linear tie tension distribution along the tie, Fig (3.11.a) the total strain energy U_1, stored in a tie can be calculated from equation (II.1).

$$U_1 = \frac{Tm^2 \cdot L(1 - \hat{\beta})}{6 A_r E_r} + \frac{Tm^2 (1 - \hat{\alpha})^2 \hat{\beta} L}{6 A_r E_r} + \frac{\hat{\alpha}^2 Tm^2 \hat{\beta} \cdot L}{2 A_r E_r}$$

$$U_1 = \frac{Tm^2 L}{6 A_r E_r} (1 + 2 \hat{\alpha} \cdot \hat{\beta} (2 \hat{\alpha} - 1)) \quad \ldots\ldots\ldots (III.1)$$

The value of U_1 depends on $\hat{\alpha}$ and $\hat{\beta}$. For the case when the maximum tie tension lies at the wall face, or when the ratio of the tension at the wall face to the maximum tie tension = 0.5, U_1 is maximum and is given by:

$$U_1 = \frac{Tm^2 L}{6 A_r E_r} \quad \ldots\ldots\ldots\ldots\ldots\ldots (III.2)$$

For the case when a parabolic tie tension distribution over the tie length was assumed Fig (3.11.b) the equation of the curve can be written as:

$$T(x) = ax^2 + bx + c$$

where x is the distance along the tie and a, b, c are constants and their values can be evaluated from the boundary conditions:

(i) $\dfrac{dT(x)}{dx} = 0$; at $x = \hat{\beta} L$

(ii) $Tm = a(\hat{\beta}L)^2 + b(\hat{\beta}L) + c$

(iii) $0 = aL^2 + bL + c$

From which the general equation for the curve can be obtained as:

$$T(x) = \frac{Tm}{(1-\hat{\beta})^2 L^2} (-x^2 + 2\hat{\beta}Lx + (1 - 2\hat{\beta})L^2)$$

The strain energy stored can be calculated from equation (II-1) as:

$$U_i = \frac{Tm^2 L}{30 A_r E_r (1 - \hat{\beta})^4} (20\hat{\beta}^2 - 25\hat{\beta} + 8) \quad \ldots\ldots (III.3)$$

when the maximum tie tension lies at the face of the wall or at the middle of the tie, $\hat{\beta} = 0$ and 0.5 respectively, the strain energy is

$$U_i = \frac{4}{15} \cdot \frac{Tm^2 \cdot L}{A_r E_r} \quad \ldots\ldots\ldots\ldots\ldots\ldots (III.4)$$

For values of $\hat{\beta}$ lying between 0 and 0.5, U_i increases or decreases slightly.

APPENDIX IV

Series D test results

The results of tie tension measurements from the Series D tests are presented in Tables (IV.1) to (IV.4).   In this series 22 walls were built, using perspex ties 22.7 mm wide and of varying lengths.   The soil/tie coefficient of friction was 0.398.   The results of walls No. 3 and 19 are not included in these tables, since wall No. 3 was not instrumented and wall No. 19 failed earlier than was expected. The tie tensions in the walls shown in Tables (IV.3)and (IV.4), were measured at position (i) shown in Fig (IV.1). In these tables also h and T denote the fill height above the tie level and the tie tension respectively.

	(i)	(ii)	(iii)	(iv)	Tie
	30	180	330	480	

distance from centre of strain gauge to wall face

wall face

	(i)	(ii)	(iii)	(v)
	30	180	330	460

distance from centre of strain gauge to wall face - mm
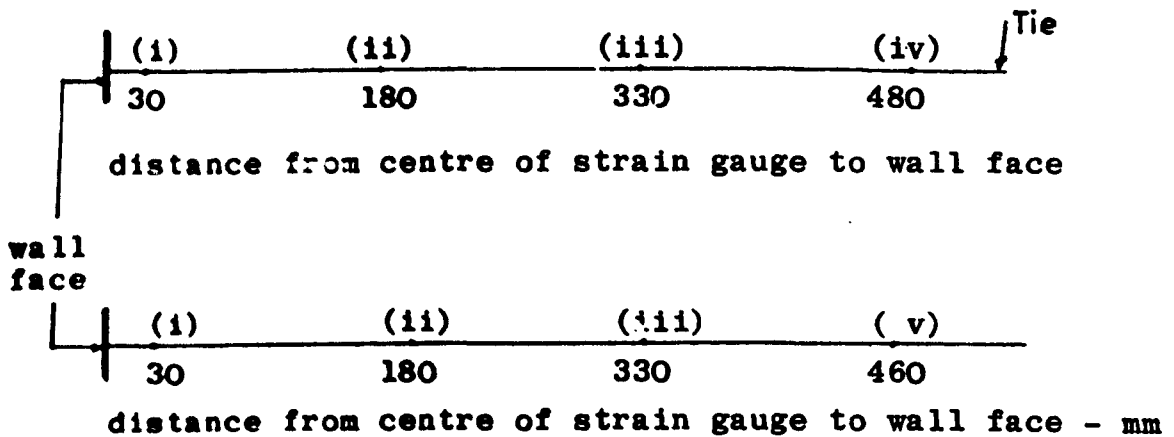
Fig (IV.1) - Positions of strain gauges on ties (Series D tests)

Information about the test	Fill height above tie level h (mm)	Measured tie tension - N - at positions on tie shown in Fig (IV.1)			
		(i)	(ii)	(iii)	(iv)
Test No. 1 L - 500 mm ΔH- 250 mm S - 300 mm Υ - 1.610 gm/cm³ H$_c$ - 440 mm	75	15.05	9.96	8.53	1.5
	100	17.4	12.52	9.4	1.8
	125	24.4	17.31	12.4	2.6
	195	31.3	23.45	17.37	4.6
	210	35.0	27.06	19.8	5.3
	250	43.3	33.4	22.7	6.23
	285	53.1	40.78	27.66	7.7
	315	55.86	-	-	-
		(i)	(ii)	(iii)	(v)
Test No. 2 L - 480 mm ΔH - 250 mm S · 300 mm Υ - 1.610 gm/cm³ H$_c$ - 365 mm	70	9.8	7.7	3.87	0.82
	125	16.0	13.8	6.84	0.96
	175	25.2	21.6	11.4	2.18
	225	30.3	26.9	15.1	2.93
	250	39.2	35.0	19.8	4.4

TABLE (IV.1) - Results of tie tension measurements in Series D tests

Information about the test	Fill height above tie level h (mm)	Measured tie tension - N - at positions on tie shown in Fig (IV.1)			
		(i)	(ii)	(iii)	(iv)
Test No. 5(D)	75	3.50	4.4	4.24	
L = 460 mm	125	13.40	12.30	7.31	
ΔH = 250 mm	145	16.90	14.48	9.45	
S = 300 mm	175	20.90	18.40	11.78	
γ = 1.610 gm/cm^3	190	26.0	21.8	13.15	
H$_c$ = 330 mm					
Test No.14(D)		(i)	(ii)		
L = 250 mm	70	2.4	2.3		
ΔH = 250 mm	113	9.8	4.9		
S = 150 mm	160	12.5	6.72		
γ = 1.6010gm/cm^3	200	16.6	6.72		
H$_c$ = 330 mm					
Test No.15(D)		(i)	(ii)		
L = 250 mm	80	4.63	–		
ΔH = 250 mm	120	10.9	5.52		
S = 150 mm	185	14.7	7.2		
γ = 1.622 gm/cm^3	230	21.0	–		
H$_c$= 357.5 mm					

TABLE (IV.2) - Results of tie tension measurements in Series D tests

h = height of fill above tie level

T = Tie tension

Test No. 4(D) — Information about the test: $L = 480$, $H_c = 365$, $\gamma = 1.610$ gm/cm³, $\Delta H = 250$ mm, $S = 300$ mm

h - mm	75	115	132	195	240
T - N	6.85	16.4	20.4	26.4	31.1

Test No. 6(D) — Information about the test: $L = 490$ mm, $H_c = 410$ mm, $\gamma = 1.610$ gm/cm³, $\Delta H = 250$ mm, $S = 300$ mm

h - mm	100	125	180	235	270	285
T - N	10.8	16.64	22.46	31.4	39.16	36.79

Test No. 7(D) — Information about the test: $L = 470$ mm, $H_c = 340$ mm, $\Delta H = 250$ mm, $S = 300$ mm, $\gamma = 1.610$ gm/cm³

h - mm	85	122	180	215
T - N	9.66	16.41	23.8	28.1

Test No. 8(D) — Information about the test: $L = 460$ mm, $H_c = 350$ mm, $\Delta H = 250$ mm, $S = 300$ mm, $\gamma = 1.617$ gm/cm³

h - mm	110	125	165	190	205	225
T - N	9.8	14.95	20.46	24.11	29.90	32.1

Test No. 9(D) — Information about the test: $L = 500$ mm, $H_c = 360$ mm, $\Delta H = 250$ mm, $S = 300$ mm, $\gamma = 1.622$ gm/cm³

h - mm	110	165	205	235
T - N	17.5	24.4	30.1	31.89

Test No. 10(D) — Information about the test: $L = 500$ mm, $H_c = 465$ mm, $\Delta H = 250$ mm, $S = 300$ mm, $\gamma = 1.6146$ gm/cm³

h - mm	100	121	175	235	285	330	340
T - N	2.14	10.2	20.2	29.7	36.21	40.4	47.4

Test No. 11(D) — Information about the test: $L = 450$ mm, $H_c = 310$ mm, $\Delta H = 250$ mm, $S = 300$ mm, $\gamma = 1.615$ gm/cm³

h - mm	90	135	165	185
T - N	10.36	14.77	19.62	22.3

TABLE (IV.3) - Results of tie tension measurements in Series D Tests

h = height of fill above tie level

T = Tie tension

Test No.	Information about the test	$L = 440$ mm, $H_c = 320$ mm, $\Delta H = 250$ mm $S = 300$ mm, $\gamma = 1.6150$ gm/cm^3				
12 (D)	h – mm	118		128		195
	T – N	8		13.2		27.2
13 (D)	Information about the test	$L = 440$ mm, $H_c = 278$ mm, $\Delta H = 250$ mm $S = 300$ mm, $\gamma = 1.603$ gm/cm^3				
	h – mm	110		125		153
	T – N	13.66		19.1		19.1
16 (D)	Information about the test	$L = 250$ mm, $H_c = 350$ mm, $\Delta H = 250$ mm $S = 150$ mm, $\gamma = 1.589$ gm/cm^3				
	h – mm	85	130	185	205	225
	T – N	7.07	11.8	16.0	17.7	19.3
17 (D)	Information about the test	$L = 240$ mm, $H_c = 305$ mm, $\Delta H = 250$ mm $S = 150$ mm, $\gamma = 1.5960$ gm/cm^3				
	h – mm	85		130		180
	T – N	7.3		10.76		15.84
18 (D)	Information about the test	$L = 170$ mm, $H_c = 310$ mm, $\Delta H = 250$ mm $S = 100$ mm, $\gamma = 1.615$ gm/cm^3				
	h – mm	80		130		185
	T – N	5.65		8.63		10.20
20 (D)	Information about the test	$L = 250$ mm, $H_c = 265$ mm, $\Delta H = 125$ mm $S = 300$ mm, $\gamma = 1.610$ gm/cm^3				
	h – mm	80		125		188
	T – N	3.20		13.74		20.0
21 (D)	Information about the test	$L = 170$ mm, $H_c = 350$ mm, $\Delta H = 250$ mm $S = 100$ mm, $\gamma = 1.617$ gm/cm^3				
	h – mm	85	130	175	205	225
	T – N	3.7	7.5	9.85	11.90	14.60
22 (D)	Information about the test	$L = 167$ mm, $H_c = 340$ mm, $\Delta H = 250$ mm $S = 100$ mm, $\gamma = 1.595$ gm/cm^3				
	h – mm	130		175		215
	T – N	6.94		8.72		11.8

TABLE (IV.4) – Results of tie tension measurements in Series D tests

APPENDIX (V)

Series E Test Results

A summary of the tie tensions measured in the Series E tests is presented in Tables (V.1) to (V.5). The tie tensions in this series were measured at different positions on ties shown in Fig (V.1). These positions are designated consecutively from (a) to (u) and are entered in Tables (V.1) to (V.5).

The observations of the horizontal and the vertical strain in the soil and the vertical stress in the soil, were made at vertical sections in the wall lying at 50 mm, 150 mm and 250 mm from the wall face. These three positions, Fig V.2 are indicated as (i), (ii) and (iii) respectively and entered in Tables (V.6) to (V.9) in which these observations are summarized.

A summary of the horizontal wall deflection measured in the Series E tests is shown in Table (V.10). The numbers in the table refer to the positions of the strain coils on the face of the wall as shown in Fig (V.3).

Distances in mm from centre of stain gauge to the inside of wall face
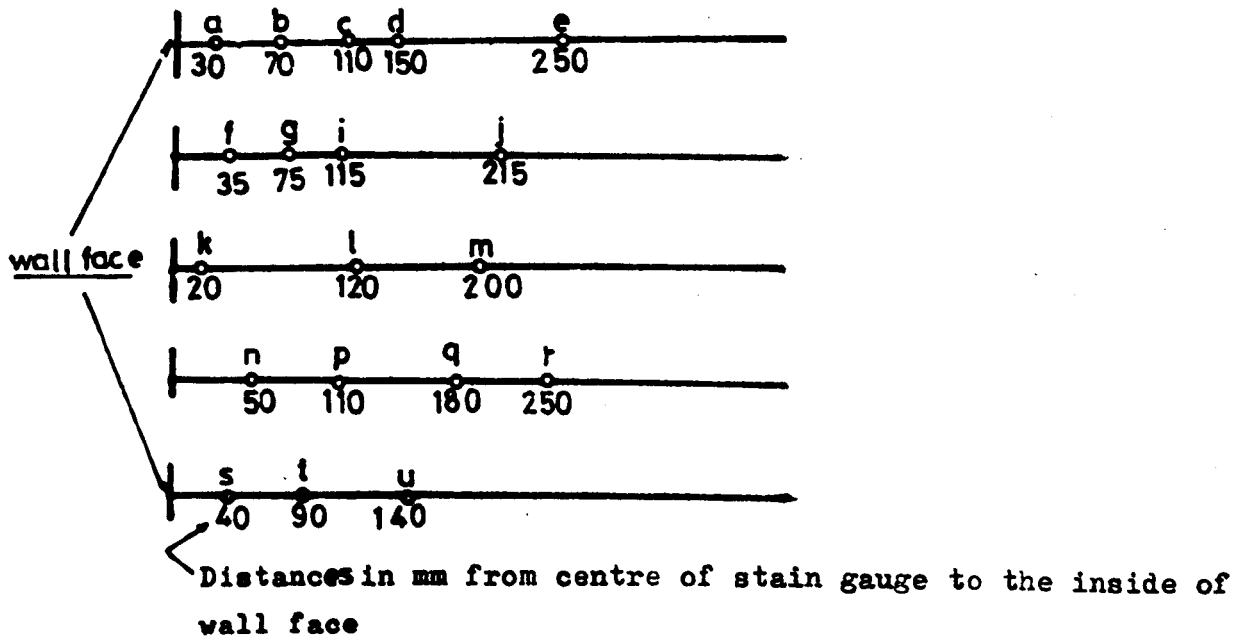
Fig (V.1) - Positions of strain gauges on ties for the measurement of tie tension (Series E tests)
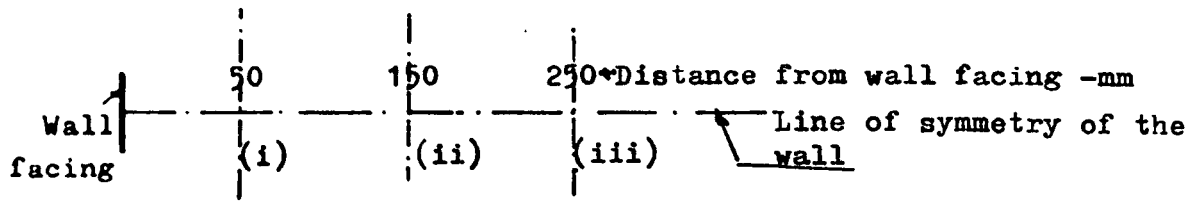
Fig(V.2) -Positions of transducers for measuring stresses & strains in the soil from the facing of the wall
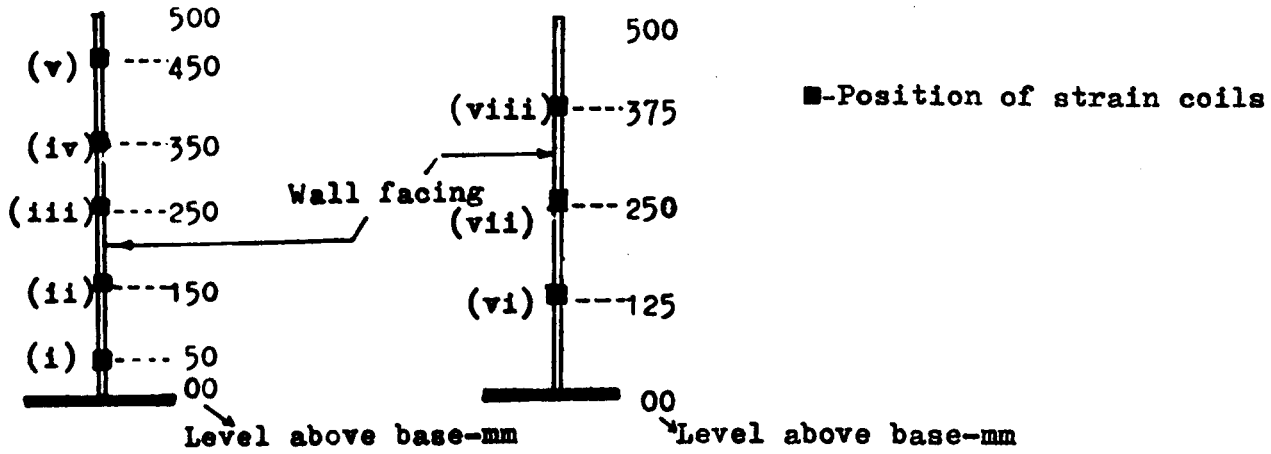
Fig (V.3) - Positions of strain coils on the wall facing.

Tie level above base of model mm	Fill height above tie level h – mm	Measured tie tension – N – observed at positions on tie shown in Fig (V.1)				
		a	b	c	d	e
125	125	6.4	7.1	6.3	5.5	3.8
	250	15.3	17.3	15.7	12.0	6.9
	375	19.5	23.9	23.1	17.7	10.1
375	125	4.34	5.42	9.51	9.41	–

TABLE (V.1) - Results of tie tension measurements in the Series E tests ($\Delta H = 250$ mm, S = 100 mm)

Tie level above base of the model mm	Fill height above tie level mm	Tie tension - N - observed at positions on tie shown in Fig (V.1)			
		f	g	i	j
50	150	2.4	3.2	3.9	3.6
	350	9.9	12.8	12.9	10.8
	450	12.0	16.3	16.10	14.1
150		s	t	u	
	100	1.68	3.5	3.9	
	250	5.4	9.5	9.7	
	350	8.0	13.6	14.1	
250		n	p	q	
	50	1.5	2.6	1.9	
	150	6.4	9.5	8.0	
	250	9.2	14.9	14.4	
350		k	l	m	
	50	1.0	1.3	1.8	
	150	5.4	9.4	10.1	

TABLE (V.2) - Results of tie tension measurements in the
Series E tests (ΔH = 100 mm, S = 150 mm).

Tie level above base of the model mm	Fill height above tie level – mm	Tie tension – N – observed at positions on tie shown in Fig (V.1)			
		f	g	i	j
42	83	1.53	1.53	0.96	0
	166	1.55	1.91	0.51	0
	208	2.20	2.38	1.21	0
	250	2.30	2.38	1.21	0
	333	3.14	3.61	1.99	0
	416	4.30	4.16	2.4	0.62
	458	4.6	3.72	2.4	0.62
208	42	1.36	1.58	1.76	2.2
	167	5.00	5.00	5.30	3.76
	250	4.84	4.60	6.00	3.76
	292	5.23	6.50	6.71	4.46
		n	p	q	r
292	83	2.50	2.10	2.4	2.0
	166	5.2	7.3	5.6	5.0
	208	7.0	9.9	8.9	7.30
375	83	1.62	2.83	2.3	2.9
	125	5.02	6.6	6.0	5.7

TABLE (V.3) – Results of tie tension measurements in the
Series E tests ($\Delta H = 83.3$, S = 100 mm)

Tie level above base of the model mm	Fill height above tie level - mm	Tie tension - N - observed at position on tie shown in Fig (V.1)			
		f	g	i	j
42	250	5.8	7.1	7.8	7.1
	333	7.9	9.7	10.4	7.1
	458	10.2	13.5	14.7	9.9
125		s	t	u	
	167	6.3	4.5	5.4	-
	250	10.0	8.7	8.4	-
	375	14.9	14.7	14.5	-
208	84	6.12	5.4	-	-
	167	7.20	6.3	-	-
	292	11.70	12.6	-	-
292		n	p	q	r
	83	2.7	4.4	3.6	3.9
	208	8.8	12.3	10.4	8.3
375		k	l	m	
	83	1.5	3.7	3.1	-
	125	4.3	7.1	5.9	-

TABLE (V.4) - Results of tie tension measurements in the Series E tests ($\Delta H = 83.3$ mm, S = 150 mm)

Tie level above base of the model mm	Fill height above tie level – mm	Tie tension – N – observed at position on tie shown in Fig (V.1)			
		f	g	i	j
42	166	5.5	4.9	4.7	4.5
	208	8.6	8.7	6.1	5.6
	333	10.5	10.4	8.4	7.6
	458	12.1	13.4	11.2	10.2
125	83	2.5	4.0	3.4	2.6
	167	10.7	13.8	12.7	8.5
	250	13.4	18.8	18.0	12.4
	375	19.3	26.8	25.0	15.9
208		k	l	m	
	84	7.7	8.0	8.6	
	167	9.9	13.5	12.6	
	292	14.0	20.7	17.8	
292		n	p	q	r
	83	1.7	3.5	3.5	2.7
	208	6.7	11.3	11.0	9.9
375		k	l	m	
	83	2.7	3.3	4.4	
	125	6.1	9.8	10.9	

TABLE (V.5) – Results of tie tension measurements in the Series E tests (ΔH = 83.3 mm, S = 300 mm)

+ve Expansion

-v Compression

Tie Spacing	Instrument-ation level above base of model (mm)	Fill height above instru-mentation level (mm)	Horizontal strain in sand ε_x% observed at positions i, ii, iii (Fig (V.2)		
			i– ε_x%	ii– ε_x%	iii– ε_x%
ΔH – 100 mm S – 150 mm	50	50	0.055	–	–
		150	0.108	0.0554	-0.0665
		200	0.172	0.0724	-0.0665
		250	0.397	0.258	-0.223
		350	0.621	0.406	-0.258
		450	0.783	0.467	-0.128
	250	50	0.145	0.105	0.11
		150	0.693	0.623	0.334
		250	0.832	0.761	0.379
	350	50	–	–	-0.021
		150	0.22	0.360	0.361
ΔH – 250 mm S – 100 mm	125	125	0.34	0.022	0.090
		250	1.41	0.160	0.175
		375	1.64	0.270	0.230
	250	40	1.8	0.340	-0.600
		125	3.06	0.520	-0.500
		250	3.8	0.710	-0.400
	250	125	1.91	0.230	-3.140
		250	4.8	0.210	-2.790
	375	125	0.183	0.157	0.157

TABLE (V.6) – Results of horizontal soil strain measurements in the Series E tests

+ ve Expansion
- ve Compression

Tie Spacing	Instrumentation level above base of model (mm)	Fill height above instrumentation level (mm)	Horizontal strain in sand ε% observed at positions i, ii, iii shown in Fig (V.2)		
			i— ε_x%	ii— ε_x%	iii— ε_x%
ΔH = 83.3 mm S = 100 mm	42	83	0.057	0.010	0.050
		125	0.108	0.070	0.120
		167	0.22	0.146	0.190
		270	0.26	0.195	0.200
		333	0.110	0.052	0.020
		375	0.190	0.067	0.039
	208	84	0.223	0.108	0.0702
		187	0.379	0.112	0.0234
		250	0.147	−0.121	−0.243
		292	0.180	−0.095	−0.205
ΔH = 83.3 mm S = 150 mm	42	166	0.057	0.010	0.050
		208	0.108	0.070	0.120
		250	0.220	0.146	0.191
		416	0.110	0.005	0.0196
		458	0.190	0.067	0.039
	250	125	0.298	0.137	0.076
		208	0.330	0.155	0.057
		250	0.447	0.175	0.119

TABLE (V.7) – Results of horizontal soil strain measurements in the Series E tests

+ve Expansion
-ve Compression

Tie Spacing (mm)	Instrumentation level above base of model (mm)	Fill height above instrumentation level (mm)	Vertical strain in sand $\varepsilon_y\%$ observed at positions i,ii,iii shown in Fig (V.2)		
			i— $\varepsilon_y\%$	ii— $\varepsilon_y\%$	iii— $\varepsilon_y\%$
ΔH - 100 mm S - 150 mm	50	50	-0.25	-0.04	-0.048
		100	-0.31	-	-0.22
		250	-0.474	-	-0.363
		350	-0.503	-	-0.347
		450	-0.508	-	-0.500
	50	50	-0.286	-	-0.122
		150	-0.633	-	0.016
		250	-0.534	-	0.091
		350	-0.624	-	0.038
		450	-0.650	-	-0.050
	150	150	0.042	0.124	0.099
		250	0.029	0.164	0.079
		350	-0.058	0.153	0.090
	250	150	-0.164	0.0816	0.089
		250	-0.238	-	0.150

TABLE (V.8) - Results of vertical soil strain measurements in the Series E tests

Tie Spacing (mm)	Instrumentation level above base of model (mm)	Fill height above instrumentation level (mm)	Vertical soil stress σ_y KN/m^2 observed at positions i, ii, iii, shown in Fig (V.2)		
			i	ii	iii
$\Delta H = 100$ mm S = 150 mm	50	50	0.20	–	0.79
		150	1.30	–	2.60
		250	2.20	–	3.70
		350	3.50	–	5.10
		450	4.50	–	6.50
	150	50	0.62	0.285	0.68
		150	2.5	2.36	2.91
		250	3.63	3.32	4.35
		350	4.80	4.69	6.19
$\Delta H = 250$ mm S = 100 mm	125	125	5.22	1.59	4.54
		250	8.62	3.52	7.82
		375	11.16	5.93	10.80

TABLE (V.9) - Results of vertical soil stress measurements
in the Series E tests

Tie Spacing (mm)	Total fill height (mm)	Observed horizontal wall deflections mm – at positions shown in Fig (V.3)				
		i	ii	iii	iv	v
ΔH = 100 mm S = 150 mm	100	0.488				
	150	0.63	0.804			
	300	1.23	1.67	1.087		
	400	0.94	1.79	0.83	0.54	
	500	1.13	2.04	1.07	1.44	0.50
ΔH = 100 mm S = 150 mm	150	0.973				
	200	0.32	0.11			
	300	0.20	0.624	0.463		
	500	1.81	1.98	1.18	1.024	0.170

Tie Spacing (mm)	Total fill height (mm)	vi	vii	viii
ΔH = 83.3 mm S = 150 mm	125	0.31	0.38	
	208	0.44	0.686	
	250	0.73	1.521	
	270	0.750	1.515	0.18
	458	0.921	1.96	0.25
	500	0.99	2.081	0.76
ΔH = 83.3 mm S = 100 mm	125	0.189		
	208	0.33		
	292	0.704		
	355	0.820		
	500	0.960		
ΔH = 250 mm S = 100 mm	125	0.820	0.311	
	250	1.21	1.23	
	375	1.93	3.547	0.581
	500	2.31	4.382	1.650

TABLE(V.10) – Results of horizontal wall deflections in the Series E tests

APPENDIX VI

Method of evaluating the experimental
safety factors against tie pull out

A computer programme was developed by the author and the main purpose was to calculate the experimental factor of safety against tie pull out from the tie tension distribution along the tie length curves.   This programme also calculates the experimental safety factors against tie pull out using the maximum tension in the tie and assuming either all the tie length or only the tie length beyond the maximum tension position as effective against tie pull out failure.   An experimental safety factor against tie pull out is also cal-culated by the programme from the average tie tension and assuming all the tie length as effective against pull out.

For the calculation of the experimental safety factor against tie pull out from the slope of the observed tie tension distribution along the tie, a smooth curve of the degree n (n - number of observations) is passed through the observed points.   The slope of the tie tension curve is calculated at predetermined intervals along the tie, from the difference in tie tension ΔT between adjacent points and the corresponding increment of tie length ΔL.   The programme evaluates the safety factor against tie pull out at each interval along the tie using equation (5.5) . An average safety factor is then calculated from the safety factors evaluated at discrete localities over the tie length.

Features of the programme

The programme consists of the main calling programme and the subroutine INTERP, which is based on the Lagrange inter-polation polynomial.

Symbols used in the programme

NUMPR   - number of problems to be analysed

WIDTH   - width of reinforcing tie

LENGTH   - length of reinforcing tie

GAMA   = Backfill density

TANU   = coefficients of friction between soil and tie

H   = fill height above tie level

NI   = number of observations of tie tension along a tie

X(I)   = positions along a tie at which tie tension was
             observed

FX(I)   = observed values of tie tension along a tie

FPHI   = tie resistance against   pull out.

Programme Listing

A listing of the computer programme, used for the

evaluation of the experimental safety factors against

tie pull out   is   given in the following pages.

```
C       OSMAN    NEW-ENG
C       PROGRAM USE LAGRANGE INTERPOLATION FORMULA.
C       TO CALCULATE INTERMEDIATE VALUES OF FUNCTION X
C       TABULATED FOR EQUAL OR UNEQUAL INTERVALS

C       XI =ARRAY OF GIVEN V ALES OF X
C       FX = ARRAY OF FUNCTION
        DIMENSION X(20),FX(20),Z(50),T(50)
        DIMENSION ZZ(50),TT(50)
        DIMENSION TITLE(20)
        DIMENSION DT(50),DL(50),SFC(50),DFPHI(50)
        REAL LENGTH
100     FORMAT(20A4)
101     FORMAT(F5.2)
102     FORMAT(/,T5,'OBSERVED TIE TENSION',///,16,'X-COORD',T28,
       *'TIE TENSION',//,T6,'CMS',T33,'N',//(F10.2,15X,F10.2),/)
103     FORMAT(1H1,8X,20A4,///)
130     FORMAT(I5)
140     FORMAT(I5)
150     FORMAT('1',//,T5,'DIST. ALNG. TIE',I29,'DL',T42,'TENSION',
       * T62,'DT',T72,'PULL RESIST.',T90,'SAFE FACT.',//,
       *T12,'CMS',T29,'CMS',T45,'N',T62,'N',T78,'N',//,6(6X,F10.4))
151     FORMAT(6X,F10.4,22X,F10.4)
200     FORMAT(F10.2)
203     FORMAT(//,T5,'S.F. FROM AVERAGE TENSION =',F10.4)
204     FORMAT(//,T5,'WIDTH =',F10.2,/,T5,'LENGTH =',F10.2,/
       *,T5,'DENSITY =',
       11PE11.4,/,T5,'HEIGHT ABOVE TIE = ',
       *0PF10.2,/,T5,'COEF. OF FRICTION = ',F10.4)
205     FORMAT(//,T5,'MAX. TIE RESIST. AGAINST PULLOUT=',F10.4)
206     FORMAT(2F10.2,E11.4,F10.4)
207     FORMAT(//,T6,'THE AVR. SF CAL. FROM T-CURVE SLOPE =',F10.4)
208     FORMAT(//,T5,'TIE RESIS. L-EFFECTIVE BEYOND T-PEAK =',F10.4)
209     FORMAT(//,T5,'SF ASSUM. ALL L-EFFECTIVE =',F10.4, //,
       *T5,'SF ASSUM. L-AFTER T-PEAK EFFCV. =',F10.4)
        READ(5,140)NUMPR
        READ(5,206)WIDTH,LENGTH,GAMA,TANU
        KOUNT=0
120     CONTINUE
        KOUNT=KOUNT+1
        READ(5,100,END=700) TITLE
        READ(5,200)H
        READ(5,130)N1
        READ(5,101)(X(I),I=1,N1)
        READ(5,101)(FX(I),I=1,N1)
        FPHI=2*WIDTH*LENGTH*GAMA*H*TANU
        WRITE(6,103)TITLE
        WRITE(6,102)(X(I),FX(I),I=1,N1)
        WRITE(6,204)WIDTH,LENGTH,GAMA,H,TANU
        WRITE(6,205)FPHI
        NN=10
        BIG=FX(1)
        IBIG=1
        DO111JJ=2,N1
        IF(BIG.LT.FX(JJ))GO TO 112
        GO TO 111
```

```
112     BIG=FX(JJ)
        IBIG=JJ
111     CONTINUE
        LFCTV=LENGTH-X(IBIG)*10
        FPHI2=2*WIDTH*LFCTV*GAMA*H*TANU
        WRITE(6,208)FPHI2
        SF1=FPHI/FX(IBIG)
        SF2=FPHI2/FX(IBIG)
        WRITE(6,209)SF1,SF2
C       *********************
C       *********************
C       PREPEAK INTERPOL. AND SAFETY FACT. CALCULATION
C       *********************
C       *********************
C
        N=IBIG
        IF(N.EQ.1)GO TO 30
        AINC=X(IBIG)/NN
        Z(1)=AINC/2.0
        DO78L=2,NN
        Z(L)=     Z(1)+AINC*(L-1)
78      CONTINUE
        CALL INTERP(X,FX,N,Z,NN,T)
        M1=NN
        DO303IX=1,M1
        ZZ(IX)=Z(IX)
        TT(IX)=T(IX)
303     CONTINUE
C       *********************
C       THE POST PEAK INTERPOLATION AND SAFETY FACTOR CAL.
C       *********************
C
        NN=3*NN
        N=N1+1-IBIG
        AINC=(X(N1)-X(IBIG))/NN
        Z(1)=X(IBIG)+AINC/2.
        DO 10 L=2,NN
        Z(L)=Z(1)+AINC*(L-1)
10      CONTINUE
        X(1)=X(IBIG)
        FX(1)=FX(IBIG)
        IK=N-1
        DO5II=1,IK
        X(II+1)=X(IBIG+II)
        FX(II+1)=FX(IBIG+II)
5       CONTINUE
        CALL INTERP(X,FX,N,Z,NN,T)
        M2=NN
        M=M1+M2
        SUMT=0.0
         DO 202 ID =1,N1
202     SUMT=SUMT+FX(ID)
        TAV=SUMT/N1
        SF=FPHI/TAV
        WRITE(6,203)SF
        DO301 IX=1,M2
        TT(IX+M1)=T(IX)
        ZZ(IX+M1)=Z(IX)
```

```
 301      CONTINUE
          NM=M-1
          DO260JJ=1,NM
          DT(JJ)=TT(JJ)-TT(JJ+1)
          DL(JJ)=ZZ(JJ+1)-ZZ(JJ)
          DFPHI(JJ)=2*WIDTH*DL(JJ)*GAMA*H*TANU*10
          SFC(JJ)=DFPHI(JJ)/DT(JJ)
 260      CONTINUE
          WRITE(6,150)(ZZ(L),DL(L),TT(L),DT(L),DFPHI(L),SFC(L),L=1,NM)
          WRITE(6,151)ZZ(M),TT(M)
          SUMSF=0.0
          DO 11 K=11,39
  11      SUMSF=SUMSF+SFC(K)
          SFAV=SUMSF/29.
          WRITE(6,207)SFAV
 999      IF(KOUNT-NUMPR)120,700,700
  30      CONTINUE
          WRITE(6,102)(X(I),FX(I),I=1,N1)
          N=N1
          NN=40
          AINC=X(N1)/NN
          Z(1)=AINC/2.0
          DO 40 IIB=2,NN
  40      Z(IIB) = Z(1)+AINC*(IIB-1)
          CALL INTERP(X,FX,N,Z,NN,T)
          NM=NN-1
          DO299JI=1,NM
          DFPHI(JI)=2*WIDTH*DL(JI)*GAMA*H*TANU*10
          DT(JI)=T(JI)-T(JI+1)
          DL(JI)=Z(JI+1)-Z(JI)
          SFC(JI)=DFPHI(JI)/DT(JI)
 299      CONTINUE
          WRITE(6,150)(Z(L),DL(L),T(L),DT(L),DFPHI(L),SFC(L),L=1,NM)
          WRITE(6,151)Z(NN),T(NN)
          SUMSF=0.0
          DO 55 IK=1,39
  55      SUMSF=SUMSF+SFC(IK)
          SFAV=SUMSF/39.
          WRITE(6,207)SFAV
          GO TO 999
 700      STOP
          END
```

```
      SUBROUTINE INTERP(X,FX,N,Z,NN,T)
      DIMENSION X(20),FX(20),RX(50),ANUM(50),DNUM(50),AL(50),
     *Z(50),T(50)
      DO 888L=1,NN
C     ***********************
C
C     TO CALCULATE QX
C     ***********************
      QX=1.0
      DO 300 I=1,N
      RX(I)=ABS(Z(L)-X(I))
      QX=QX*RX(I)
300   CONTINUE
C     ***********************
C     TO CALCULATE NUMERATOR
C     ***********************
      DO 33 I=1,N
      ANUM(I)=ABS(QX/RX(I))
33    CONTINUE
C     ***********************
C     TOCALCULATE THE DENUMERATOR
C     ***********************
      DO 500 I=1,N
500   DNUM(I)=1.0
      DO 600 I=1,N
      DO 600 J=1,N
      IF(I .NE. J) DNUM(I)  = ABS(DNUM(I)*(X(I)-X(J)))
600   CONTINUE
      DO 800 I=1,N
800   AL(I)=ANUM(I)/DNUM(I)
C     ***********************
C     TO DETERMINE THE SIGN OF AL
C     ***********************
      KK=0
      DO 900 I=1,N
      IF(Z(L) .GT. X(I))  KK=KK+1
900   CONTINUE
      IZ=KK+2
      DO 1 LL=IZ,N,2
1     AL(LL)=-AL(LL)
      DO 66 I=1,KK,2
      IR=KK-I
      IF(IR .GT. 0) AL(IR)=-AL(IR)
66    CONTINUE
      T(L)=0.0
      DO 4000 I=1,N
4000  T(L)=T(L)+AL(I)*FX(I)
888   CONTINUE
      RETURN
      END
```

APPENDIX VII

(a)   Stresses due to concentrated surface loads

Spangeler[70]   gave the following formula for the calculation of the horizontal stresses due to concentrated surface loadings acting on a conventional retaining wall:

$$p = P_w \frac{x^2 \cdot z}{R_o^5} \quad \ldots \ldots \ldots \ldots \ldots (VII-1)$$

where p = horizontal unit pressure at any point on the wall

P_w = applied wheel load

X = horizontal distance from load to point on the wall

Y = lateral distance from load to point on wall

Z = vertical distance from load to point on wall

R_o = $\sqrt{x^2 + y^2 + z^2}$

This formula was based on a modified Boussinesq theory.

(b)   Specifications of the roller used in the Granton wall

Type 10-Ton smooth-wheeled roller

Basic weight	=	106.3 KN
Water ballasted weight	=	122.3 KN
Weight of front wheel	=	37.17 KN
Weight of rear wheels	=	69.12 KN
Pressure front wheel	=	1372 KN/m^2
Pressure rear wheels	=	2234 KN/m^2
Front wheel diameter	=	1.22 m
Rear wheel diameter	=	1.52 m
Rear wheel width	=	0.61 m
Overall length of roller	=	4.57 m
Overall rolling width	=	1.88 m

APPENDIX VIII

(a) Tangent modulus of soil used in the programme

The overburden dependence of soil modulus E_t is modelled in the programme by the following equation

$$E_t = E_i \left(1 - \frac{\gamma h (1-\sin\emptyset)\sin\emptyset}{2c \cos\emptyset + 2 \sin\emptyset \left(\frac{\gamma h}{N_\emptyset} - \frac{2c}{N_\emptyset^2}\right)}\right)^2 \quad \ldots . (VIII.1)$$

where $N_\emptyset = \tan^2(45 + \frac{\emptyset}{2})$

$E_i = \bar{a} + \bar{b}\,\sigma_3 = \bar{a} + \bar{b}\,(1-\sin\emptyset)\gamma h$

γ = density

c = cohesion

$\emptyset$ = angle of internal friction

h = overburden height

(b) Determination of E_i for the sand

The stress-strain curves obtained for the sand from a series of triaxial tests, e.g. Fig(VIII.1), were approximated by a hyperbolic relationship originally advanced by Kondner[40] which is of the form:

$$(\sigma_1 - \sigma_3) = \frac{\epsilon}{q + r\epsilon} \quad \ldots\ldots\ldots\ldots\ldots\ldots (VIII.2)$$

σ_1 and σ_3 are the major and the minor principal stresses respectively

q = reciprocal of the initial tangent modulus, E_i

r = reciprocal of the asymptotic value of the deviator stress

The values of q and r were determined from the triaxial test results, using Equation (VIII.2) and transforming the hyperbolae into straight lines as shown in Fig (VIII.2). This was done for each case of pressure cell σ_3 and the corresponding initial tangent modulus was determined for each case.

A straight line was assumed for the relationship between σ_3 and E_i. The constants $\bar{a}$ and $\bar{b}$ were determined using regression analysis as shown in Fig (VIII.3).

(c)   Determination of E_i and ν for the blaes

In order to determine the initial tangent modulus E_i of the blaes, the stress-strain curves obtained from a series of triaxial tests were approximated by Equation (VIII.2). The experimental results were found as not completely fitting into the hyperbolic model given by Equation (VIII.2). The initial tangent moduli were then determined directly from the stress-strain curves of the blaes as shown in Fig (VIII.4).

The values of the initial tangent moduli were plotted against the cell pressure σ_3 and a straight line relationship was assumed, Fig (VIII.5), from which the values of $\bar{a}$ and $\bar{b}$ were determined.

The Poisson's ratio of the blaes was determined from the triaxial test results in the manner described in Section (7.6.1). The results of the measurements are shown in Fig (VIII.6).
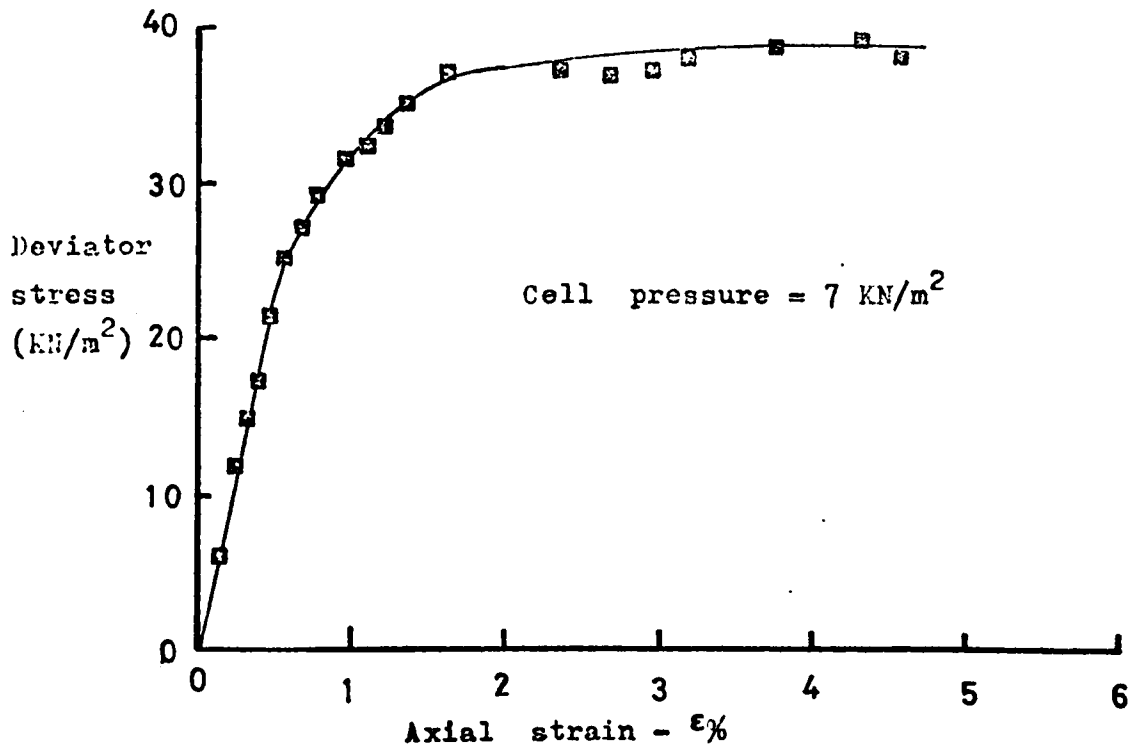
Fig.VIII-1   Stress-strain curve of dry sand: triaxial test .
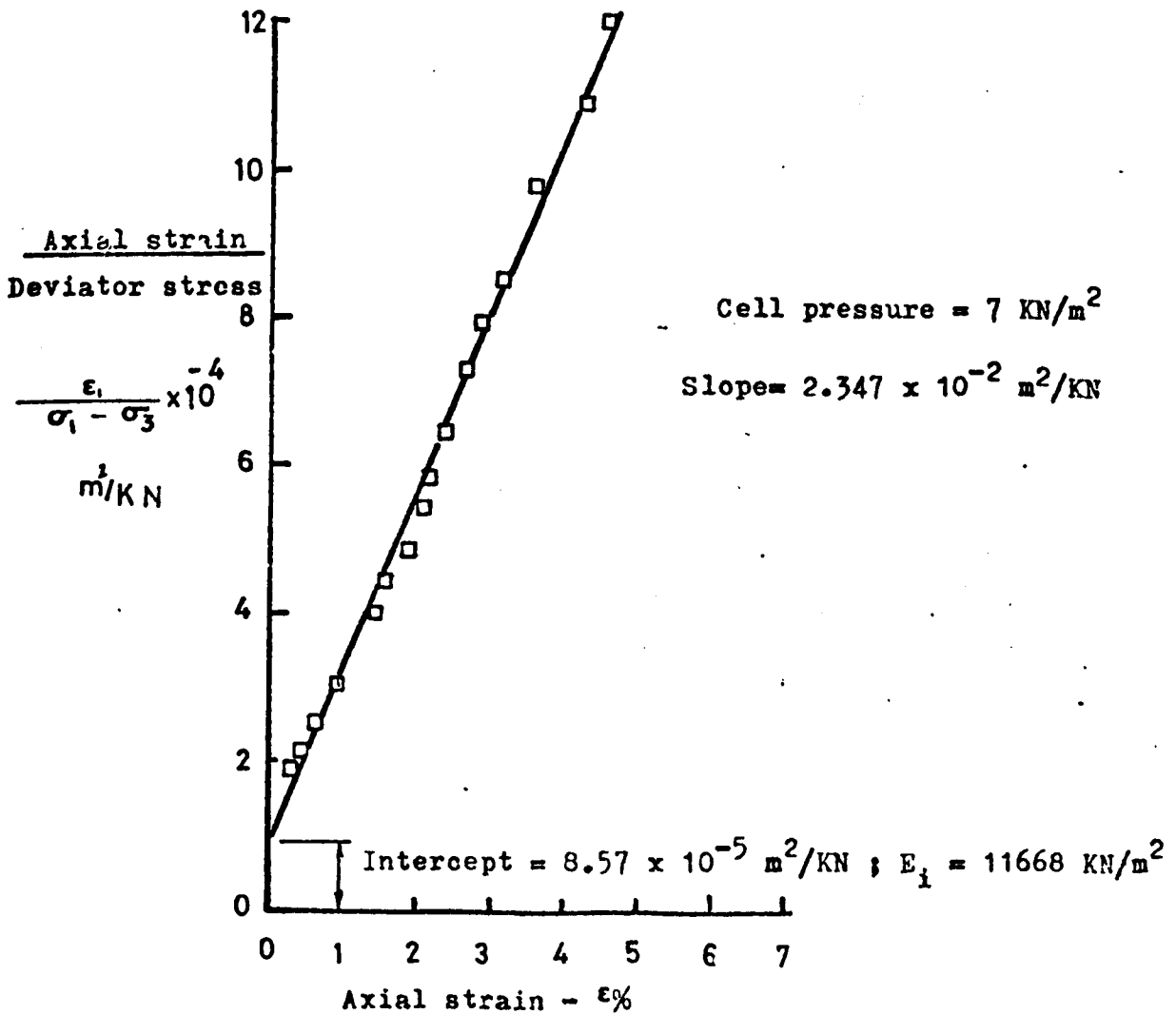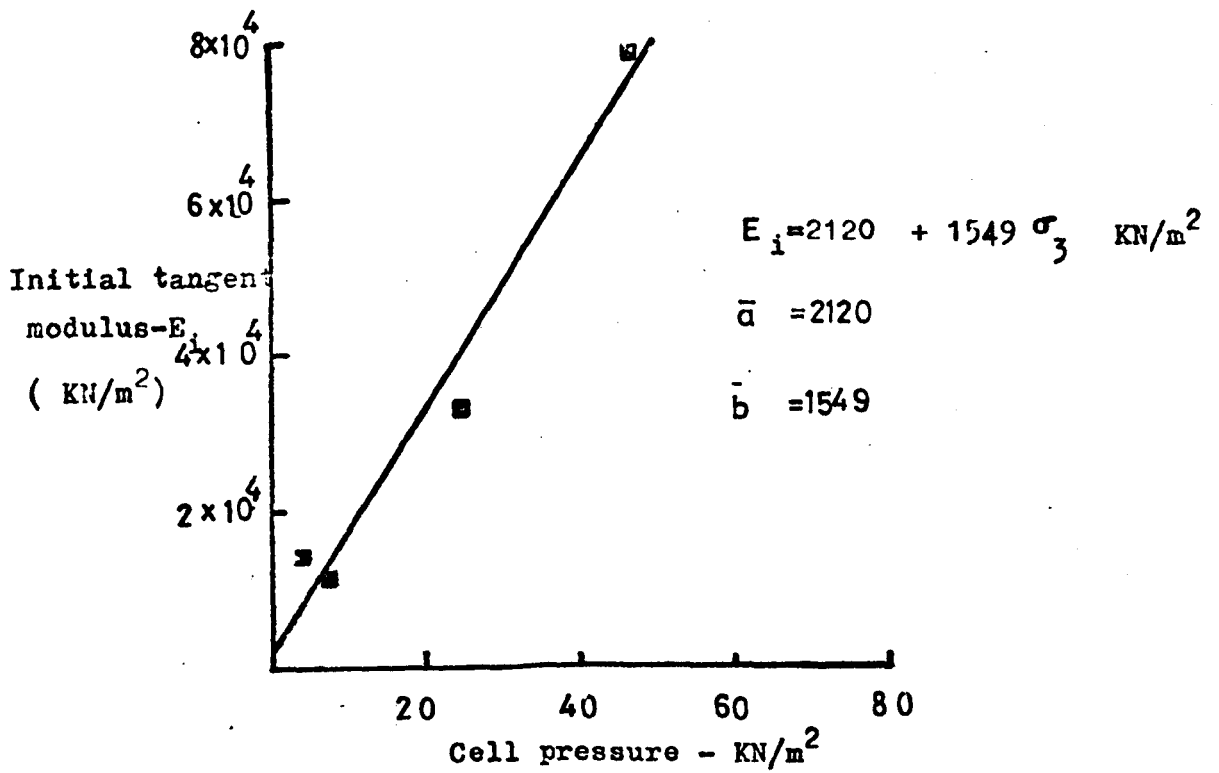
Fig. VIII-3 Variation in the initial tangent modulus
with cell pressure for dry sand tested in a
triaxial condition.
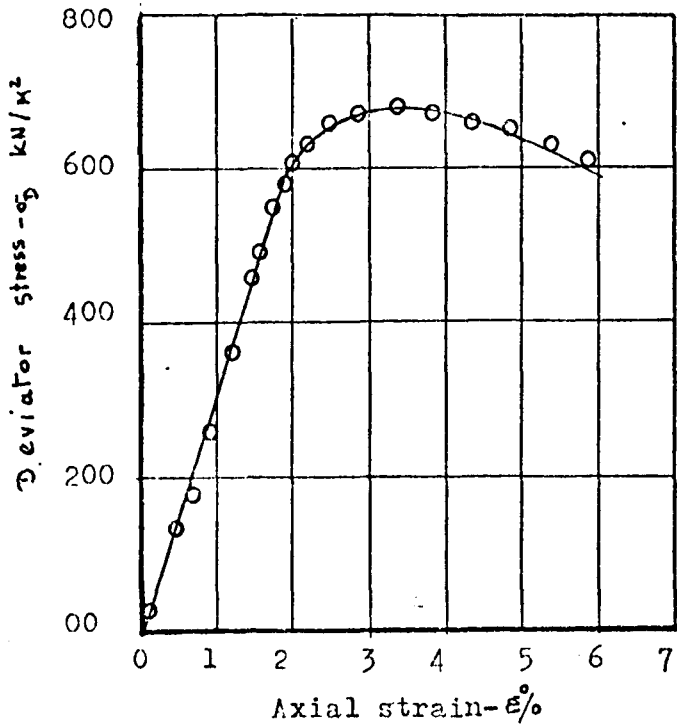
cell pressure=69 KN/m^2
E$_i$ =3.10x10^{4}KN/m^2

(a)
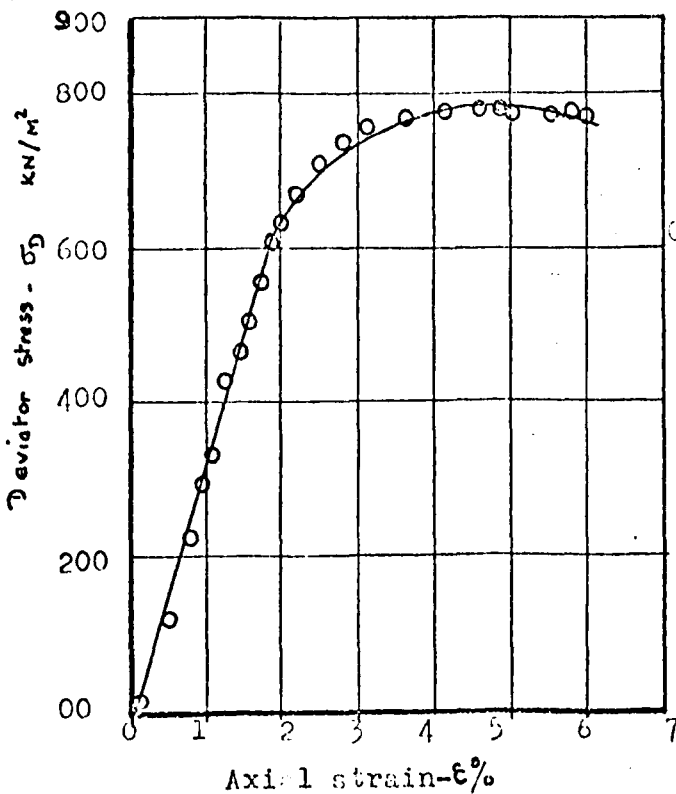
Cell pressure =105 KN/m^2
E$_i$ =3.25x10^4 KN/m^2

(b)

Fig VIII-4 Stress strain curves of blaes(Undrained triaxial test)
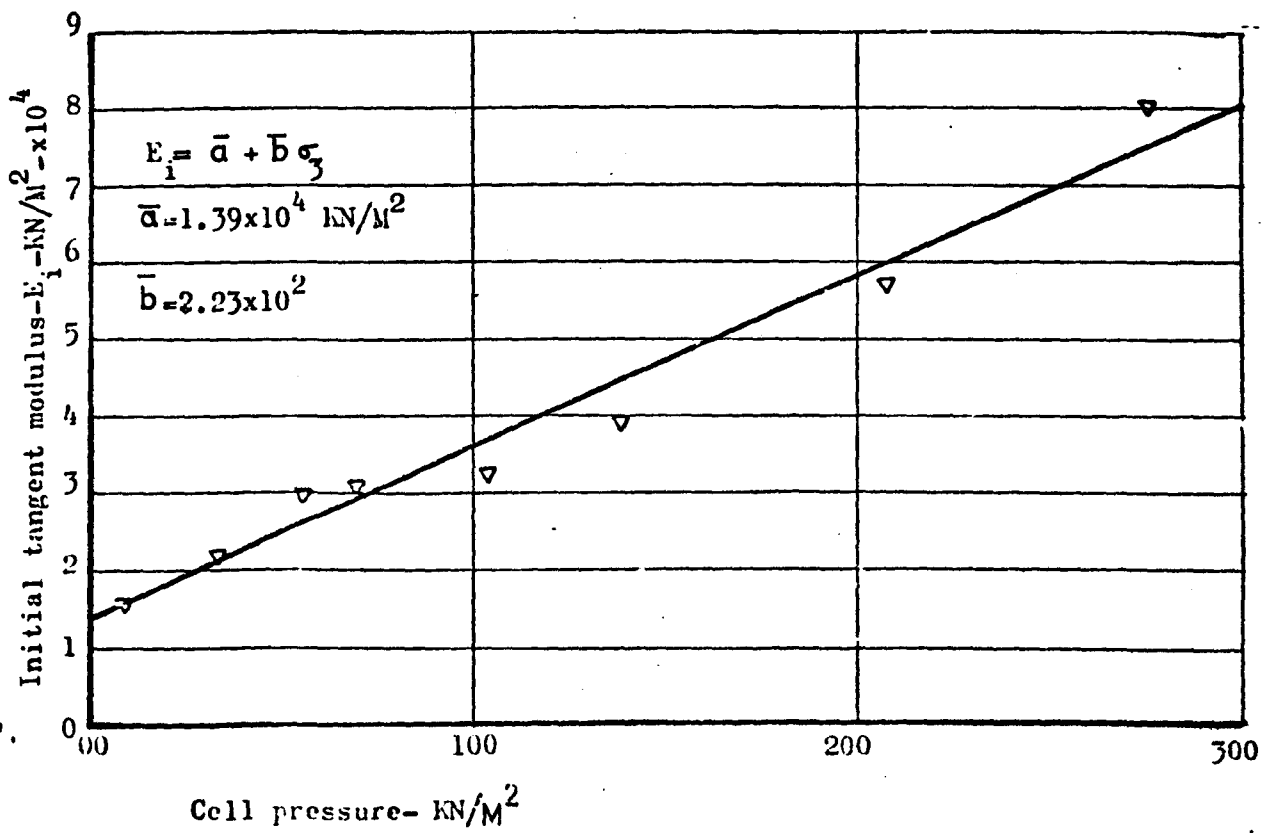
Fig VIII-5   Initial tangent modulus V   cell pressure [B laes   ]
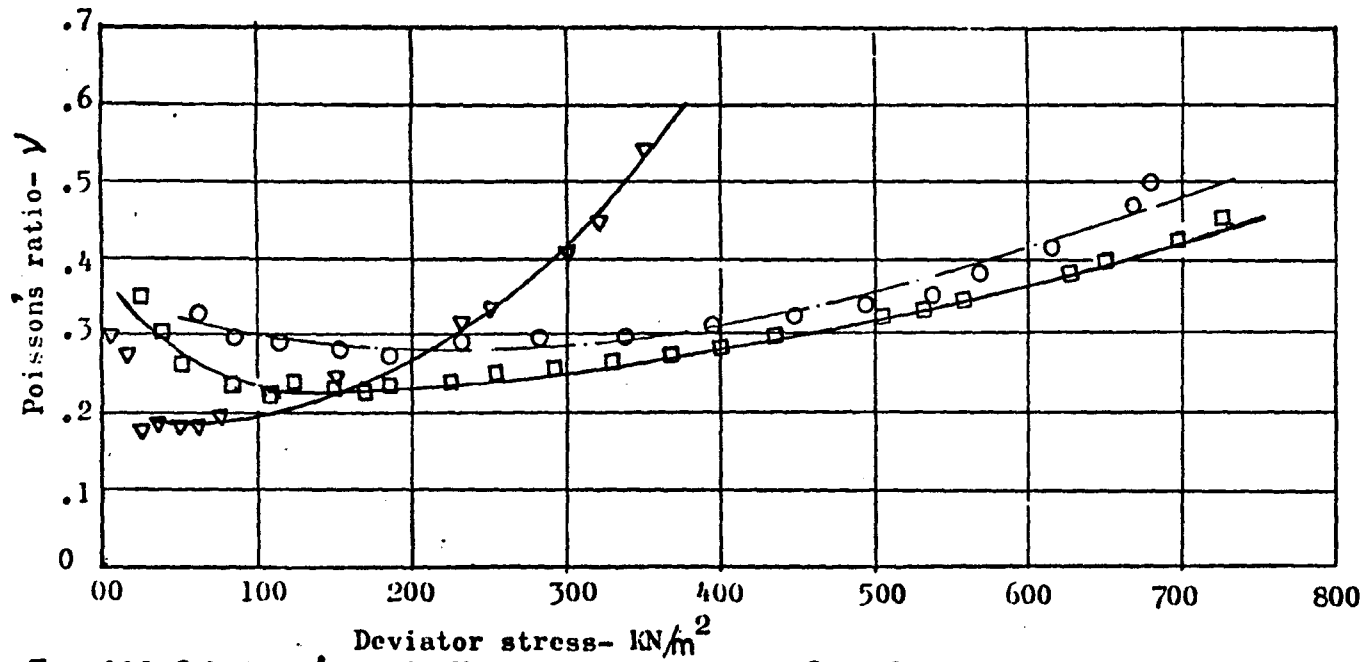
cell pressure=7 KN/m²
cell pressure=55KN/m²
cell pressure=103 KN/m²

Poissons ratio- ν

Deviator stress- KN/m²

Fig. VIII·6 Poisson's ratio ν deviator stress (Blaes)

REFERENCES

(1) Aggour, M.S. & Brown, C.B. (1974). "The Prediction of
     Earth Pressure on Retaining Walls due to Compaction"
     Géotechnique, London, Vol 24, No.4,pp.489-502.

(2) Arthur, J.R.F. & Roscoe, K.H. (1965). "An Examination
     of the Edge Effects in Plane strain Model Earth
     Pressure Tests". Proceedings, Sixth International
     Conference on Soil Mechanics and Foundations Engineering ,
     Montreal, Vol.2, pp.363-367.

(3) Bacot, J. (1974). "Étude Théorique et Expérimentale de
     Soutenements Realises en Terre Armée". Ph.D. Thesis,
     Présentée Devant L'universite Claude Bernard-Lyon,
     France, 209pp.

(4) Baguelin, F. & Bustamante, M. (1971). "Conception et
     Étude de Stabilité des Ouvrages en Terre Armée",
     Bulletin de Liaison des Laboratoire des Ponts et
     Chaussées, Numéro spécial"Autoroute de Menton", France.
     pp.101-108.

(5) Banerjee, P.K. (1975). "Principles of Analysis and
     Design of Reinforced Earth Retaining Walls", The
     Highway Engineer, Journal of the institution of
     Highway Engineers, London, Vol. 22, No. 1, pp.13-18.

(6) Barclay, M. (1972). "Reinforced Earth: Back to the
     Grass Roots", New Civil Engineer, Part No. 15, pp.18-19.

(7) Binquet, J. & Carlier, C. (1973). "Étude Experimentale
     de la Rupture du Murs en Terre Armée Sur Modele
     Tridimensionnel", Rapport Interne Du Laboratorie
     Central Des Ponts et chaussées, France. 165 pp.

(8) Bishop, A.W. (1958). "Test Equipments for Measuring the
     Coefficient of Earth Pressure at Rest", Proceedings
     Brussels conference on Earth Pressure Problems, Brussels,
     Vol. 1, pp.2-14.

(9)   Bonfante, B. & Vaubourg, P. (1972). "Murs Rectangulaires Armes de Facon Non Uniforme", Rapport Interne, Ecole Central de Lyon, France, 47pp.

(10)   Borg, S.F. & Gennaro, J.J. (1966). "Advanced structural Analysis", D. Van Nostrand Company Inc., Affiliated East-West Press PVT Ltd., New Delhi. 368 pp.

(11)   Brooker, E.W. & Ireland, H.O. (1965). "Earth Pressure at rest Related to stress History". Canadian Geotechnical Journal, Vol. 2, No.1, pp.1-15.

(12)   Butterfield, R. & Andrawes, K.Z. (1971). "The Visualization of Planar Displacement Fields". Stress-strain behaviour of soils. Proceedings of the Roscoe Memorial Symposium, Cambridge University, pp.467-475, Edited by Parry, R.H.G.

(13)   Casagrande, L. (1973) "Comments on Conventional Design of Retaining Structures". Journal of the Soil Mechanics and Foundations Division, Proceedings of The American Society of Civil Engineers, Vol. 99, No. SM2, pp.181-198.

(14)   Chang, J.C. (1974). "Earthwork Reinforcement Techniques", Research Report, California Division of Highways Transportation Laboratory, 301p.

(15)   Chang, J.C., Forsyth, R.A. & Beaton, J.L. (1974). "Performance of a Reinforced Earth Fill", Report of the State of California Department of Transportation Laboratory, presented at the 53rd Annual Meeting of the Highways Research Board, 27pp.

(16)   Chang, J.C., Forsyth, R.A. & Smith, T. (1972). "Reinforced Earth Highway Embankment - Road 39", Highway Focus, Vol.4, No.1, pp.15-35. U.S. Department of Transportation, Federal Highway Administration.

(17)   Chapuis, R. & Pringuet, P. (1971). "Terre Armeé Étude sur Modèles Reduits", Rapport Interne, Ecole Central de Lyon, France, 45pp.

(18)   Chih-Kang Shen, Romstad, K.M. & Herrmann, L.R. (1976).
        "Integrated study of Reinforced Earth - II: Behaviour
        and Design", Journal of the Geotechnical Engineering
        Division, Proceedings of the American Society of Civil
        Engineers, Vol. 102, No. GT6, pp.577-590.

(19)   Clough, G.W. & Duncan, J.M. (1971). "Finite Element
        analysis of Retaining Wall Behaviour", Journal of
        the Soil Mechanics and Foundations Division,
        Proceedings of the American Society of Civil Engineers,
        Vol. 97, No. SM12, pp.1657-1673.

(20)   Clough, R.W. & Woodward, R.J. (1967). "Analysis of
        Embankment Stresses and Deformations", Journal of
        the Soil Mechanics and Foundations Division, Proceedings
        of the American Society of Civil Engineers, Vol.93,
        No SM4, pp.529-549.

(21)   Corte, J.F. & Payen, G. (1974). "Étude d'un Mur en
        Terre Armée par la Methode des Éléments Finis",
        Rapport Interne, Laboratoire Central des Ponts et
        Chaussées, France, 94pp.

(22)   D'Appolonia, D.J., Whitman, R.V. & D'Appolonia, E. (1969).
        "Sand Compaction with Vibratory Rollers", Journal of
        the Soil Mechanics and Foundations Division, Proceedings
        of The American Society of Civil Engineers, Vol. 95,
        No. SM1, pp.263-311.

(23)   Darbin, M. (1970). "La Terre Armée dan la Construction
        des Routes et Autoroutes". Revue Généralle des Routes
        et Aérodromes. No. 457, pp.122-127, France.

(24)   Desai, C.S. (1974). "Theory and Applications of the
        Finite Element Method in Geotechnical Engineering".
        Proceedings of the Symposium on the Applications of
        the Finite Element Method in Geotechnical Engineering,
        U.S. Army Engineer Waterways Experiment Station Corps
        of Engineers, Vicksburg, Mississippi, pp.3-90,
        Edited by Desai, C.S.

(25)   Duncan, J.M. (1972). "Finite Element Analysis of
        Stresses and Movements in Dams, Excavations and
        Slopes". Proceedings of the Symposium on the
        Applications of the Finite Element Method in
        Geotechnical Engineering, U.S. Army Engineer
        Waterways Experiment Station Corps of Engineers,
        Vicksburg, Mississippi, pp.267-324, edited by
        Desai, C.S.

(26)   Duncan, J.M. & Chin-Yung Chang (1970). "Nonlinear
        Analysis of Stress and Strain in Soils", Journal of
        the Soil Mechanics and Foundations Division,
        Proceedings of the American Society of Civil Engineers,
        Vol. 96, No. SM5, pp.1629-1653.

(27)   Endicott, L.J. (1974). "The Determination of Stress
        Fields from Plane Strain Data", Géotechnique, London,
        Vol.24, No. 4, pp.517-530.

(28)   Finlay, T.W. (1959). "Behaviour of Pressure Cells"
        Personal Research Record.

(29)   Finlay, T.W. & Sutherland, H.B. (1977). "Field
        Measurements on a Reinforced Earth Wall at Granton".
        Proceedings Ninth International Conference on Soil
        Mechanics and Foundations Engineering, Tokyo.

(30)   Gedney, D.S. & McKittrick, D.P. (1975). "Reinforced
        Earth : A New Alternative for Earth-retention structures"
        Civil Engineering, A.S.C.E., Vol.10, pp.58-61.

(31)   Hadala, P.F. (1967). "The Effect of Placement Method
        on the Response of Soil Stress Gauges", Proceedings,
        International symposium on Wave Propagation and
        Dynamic Properties of Earth Materials, University of
        New Mexico, Albuqerque, pp.255-263.

(32)   Harrison, W.J. & Gerrard, C.M. (1972). "Elastic Theory
        Applied to Reinforced Earth". Journal of the Soil
        Mechanics and Foundations Division, Proceedings of the
        American Society of Civil Engineers, Vol.98, No. SM12,
        pp.1325-1345.

(33) Herrmann, L.R. (1973). "Efficiency Evaluation of a
      Two-dimensional Incompatible Finite Element",
      Computers and Structures, Vol 3, pp.1377-1395

(34) ICI (1973). "Perspex Arcylic Sheet". Technical
      Service Note, PX122, Sheet Group ICI, Plastics
      Division, Welwyn Garden City, Herts.

(35) Jakobson, B. (1958). "On the Influence of Wall Movement
      on Earth Pressure". Proceedings Brussels Conference
      on Earth Pressure Problems, Brussels, Vol.1, pp.105-
      115.

(36) Jaky, J. (1948). "Pressure in Silos", Proceedings
      Second International Conference on Soil Mechanics and
      Foundations Engineering, Rotterdam, Vol.1, pp.103-107.

(37) James, R.G. (1971). "Some Aspects of Soil Mechanics
      Model Testing". Stress-strain behaviour of soils.
      Proceedings of the Roscoe Memorial Symposium,
      Cambridge University, pp.417-440, edited by Parry,R.H.G.

(38) Jones, R.M. (1975). "Mechanics of Composite Materials"
      McGraw-Hill Book Company.

(39) Kolbuszewski, J.J. (1948). "An Experimental Study of
      the Maximum and Minimum porosities of Sands".
      Proceedings Second International Conference on Soil
      Mechanics and Foundations Engineering, Rotterdam,
      Vol. 1, pp.158-165.

(40) Kondner, R.L. (1963). "Hyperbolic Stress-Strain Response:
      Cohesive Soils". Journal of the Soil Mechanics and
      Foundations Division. Proceedings of the American
      Society of Civil Engineers, Vol. 89, No. SM1,
      pp.115-143.

(41) Laboratoire Central des Ponts et Chaussées (1976).
      "Reinforced Earth". Technical Information Note,
      prepared under leadership of Schlosser, F., 23pp.

(42) Lareal, P. & Bacot, J. (1973). "Etude sur Modeles
        Reduits Tridimensionnels de la Rupture de Massifs
        en Terre Armée". Revenue Travaux, pp46-52, France.

(43) Lazebnik, G.E. & Chernysheva, E.I. (1968), "Certain
        Errors in Experimental Determination of Earth
        Pressure on Models of Retaining Walls".
        Hydrotechnical Construction, Vol.4, pp.333-339

(44) Lee, K.L., Adams, B.D. & Vagneron, J.M.J. (1972).
        "Reinforced Earth Walls", Report to the National
        Science Foundation, University of California,
        Los Angeles, California 90024.

(45) Lee, K.L., Adams, B.D. & Vagneron, J.M.J. (1973).
        "Reinforced Earth Retaining Walls", Journal of the
        Soil Mechanics and Foundations Division, Proceedings
        of the American Society of Civil Engineers, Vol.99,
        No. SM10, pp.745-764.

(46) Levadoux, J. & Viou, J. (1973). "Terre Armée Etude
        sur Modèles Tridimensionnels", Rapport Interne,
        Ecole Centrale de Lyon, France, 54pp.

(47) Long, N.T., Schlosser, F., Guegan, Y. & Legeay, G. (1972).
        "Étude des Murs en Terre Armée sur Modeles Reduis
        Bidimensionnels", Rapport de Recherche No. 30,
        Laboratoires des Ponts et Chaussées, 63pp.

(48) Marec, M., Baguelin, F. & Vincentelli, A. (1971).
        Donnees sur les Murs en Terre Armée Construits sur
        l'autoroute de Menton", Bulletin de Liaison des
        Laboratoires Central des Ponts et Chaussées, Numero
        Special, "Autoroute de Menton", pp.109-114.

(49) Morgan, J.R. & Gerrard, C.M. (1968). "Free Field
        Measurements of Stresses and Strains in Soils".
        Proceedings of the Fourth Conference of the
        Australian Road Research Board, Melbourne, Vol.4,
        Part No.2., pp.1743-1760.

(50) Neale, D.F. (1966). "Penetration Characteristics of
      Cohesionless Soils". Ph.D. Thesis, Glasgow University,
      Civil Engineering Department.

(51) Penman, A.D.M., Burland, J.B. & Charles, J.A. (1971).
      "Observed and Predicted Deformations in a Large
      Embankment Dam During Construction". Building
      Research Station Current Paper, CP18/71, Garston,
      Watford, U.K.

(52) Price, D.I. (1975). "Reinforced Earth", Ground
      Engineering, London, Vol. 8, No. 2, pp.19-24.

(53) Rocha, M. (1957). "The Possibility of Solving Soil
      Mechanics Problems by the use of Models". Proceedings
      Fourth International Conference on Soil Mechanics and
      Foundations Engineering, Vol.1, pp.183-188.

(54) Romstad, K.M., Herrmann, L.R. & Chih-Kang shen (1976)
      "Integrated Study of Reinforced Earth - 1: Theoretical
      Formulation". Journal of the Geotechnical Engineering
      Division, Proceedings of the American Society of Civil
      Engineers, Vol.102, No. GT5, pp457-471.

(55) Roscoe, K.H. (1970). "The Influence of Strains in
      Soil Mechanics", 10th Rankine Lecture, Geotechnique,
      London, Vol.20, No.2, pp.129-170.

(56) Roscoe, K.H. (1968). "Soils and Model Tests", Journal
      of Strain Analysis, Vol.3, No.1, pp.57-64.

(57) Roscoe, K.H., Arthur, J.R.F. & James, R.G. (1963). "The
      Determination of Strains in Soils by an X-Ray Method",
      Part I, Civil Engineering and Public Works Review,
      Vol. 58, No. 684, pp.873-876.

(58) Rowe, P.W. (1971). "Large Scale Laboratory Model
      Retaining Wall Apparatus", stress-strain behaviour
      of soils. Proceedings of the Roscoe Memorial Symposium,
      Cambridge University, pp.441-449, Edited by Parry,R.H.G.

(59)   Scala, A.J. (1968). "A study of Pressures Generated
       by Vibrating Rollers", Proceedings of the Fourth
       Conference of the Australian Road Research Board,
       Melbourne, Vol.4, Part No.2, pp.1260-1273.

(60)   Schlosser, F. (1972). "La Terre Armée dans l'Échangeur
       de Sète", Revue Générale des Routes et des Aerodromes,
       No. 480, France.

(61)   Schlosser, F. (1972). "La Terre Armée: Recherches
       et Réalisations". La Technique Routière, Vol.17,
       No.3, pp.15-45, France.

(62)   Schlosser, F. (1970). "Mur Expérimental en Terre Armée
       d'Incarville", Bulletin de Liaison des Laboratoire
       des Ponts et Chaussées, No. 33, France.

(63)   Schlosser, F. & Long, N.T. (1974). "Recent Results in
       French Research on Reinforced Earth", Journal of the
       Construction Division, Proceedings of the American
       Society of Civil Engineers, Vol.100, No.CO3, pp.
       223-237.

(64)   Schlosser, F. & Long, N.T. (1973). Étude du
       Comportement du Matériau Terre Armée", Annales
       de l'Institut Technique due Bâtiment et des Travaux
       Publics, pp.102-119, France.

(65)   Schlosser, F. & Long, N.T. (1972). "Comportement de la
       Terre Armeé dans les Ouvrages de Soutènement",
       Proceedings Fifth European Conference on Soil Mechanics
       and Foundations Engineering, Madrid, Vol.1, pp.299-306.

(66)   Schlosser, F., Long, N.T. & Sevestre, F. (1973).
       "Ouvrages en Terre Armée sur sols de Faible Portance",
       Proceedings Eighth International Conference on Soil
       Mechanics and Foundations Engineering, Moscow, Vol.2,
       No.2, pp.201-205.

(67)   Schlosser, F. & Vidal, H. (1969). "Reinforced Earth",
       Bulletin de Liaison des Laboratoires Routier des
       Ponts et Chaussées, No.41, 44pp, France. (Translation
       from French).

(68)   Selig, E.T. (1964). "A Review of Stress and Strain
       Measurement in Soil", Proceedings of the Symposium
       On Soil-Structure Interaction University of Arizona,
       Tucson, Arizona, pp.172-186.

(69)   Sowers, G.F., Robb, A.D., Mullis, C.H. & Glenn, A.J.
       (1957). "The Residual Lateral Pressures Produced
       by Compacting Soils", Proceedings, Fourth International
       Conference on Soil Mechanics and Foundations
       Engineering, London, Vol.2, pp.243-247.

(70)   Spangler, M.G. (1960). "Engineering Characteristics
       of Soils and Soil Testing". Highway Engineering
       Handbook, McGraw-Hill Book Company, Section 8,
       pp.6-63, Chief Editor Woods, K.B.

(71)   Sutherland, H.B. (1965). "Model studies for Shaft
       Raising through Cohesionless Soils", Proceedings
       Sixth International Conference on Soil Mechanics
       and Foundations Engineering, Montreal, Vol.2, pp.
       410-413.

(72)   Symons, I.F. (1973). "Reinforced Earth Retaining Walls".
       Highways and Road Construction, Vol.41, No.1766,
       pp.10-14.

(73)   Terzaghi, K. (1934). "Large Retaining Wall Tests: 1
       Pressure of Dry Sand", Engineering News - Record,
       Vol.112, pp.136-140.

(74)   Truesdale, W.B. & Anderson, M.E. (1964). "A New
       Device for Soil Strain Measurement", Proceedings
       of the Symposium on Soil-Structure Interaction,
       University of Arizona, Tucson, Arizona, pp.124-137.

(75)   Uesawa, H. (1968). "A Conception and Basic Experiment
       on Reinforced Earth Method", Japanese Publication,
       Japanese National Railways Research Institute,
       pp.206-212 (cited Lee et al (1973)).

(76) Vauloup, L. (1973). "Étude de la Terre Armée par la Methode des Elements finis". Rapport Interne due laboratoire central des Ponts et chaussées, 132pp, France.

(77) Vidal, H. (1967). "Patent specification No. 1069361, Improvement in Constructional Works", The Patent Office, London. 16 pps.

(78) Vidal, H. (1966). "La Terre Armée, Annales de l'Institut Technique du Bâtiment et des Travaux Publics, France, No. 223-224, pp.887-938.

(79) Vidal, H. (1969). "The Principle of Reinforced Earth", Highway Research Record, Washington, No. 282, pp.1-16.

(80) Vidal, H. (1970). "Reinforced Earth - steel Retaining Wall". Civil Engineering, A.S.C.E., Vol.40, No.2, pp.72-73.

(81) Yziquel, A. (1974). "Étude de la Terre Armée par la Méthode des Éléments Finis", Rapport Interne du laboratoire Central des Ponts et Chaussées. 45pp.